Microfluidics Studies of the Regulation of Myoblast Migration

by

Ziba Rovei Miab

A Thesis submitted to the Faculty of Graduate Studies of
The University of Manitoba
in partial fulfilment of the requirements of the degree of

DOCTOR OF PHILOSOPHY

Department of Biological Sciences
University of Manitoba
Winnipeg

Table of Contents

Acknowledgements

I would like to say a very special thank you to my special supervisor, mentor, friend, and hero of my life ***Dr. Judy Anderson****. Her support, guidance and overall insights in science have made this an inspiring and unforgettable experience in my life. It is a genuine pleasure to express my sense of thanks to Dr. Francis Lin for his support and guidance.*

I am deeply grateful to my amazing partner (J Horton) for his patience, his endless support, and understanding to make this journey more enjoyable for me.

I am forever indebted to my beautiful and supportive parents for giving me the opportunities and courage that have made me who I am. They selflessly encouraged me to explore and seek new directions in life, gain more knowledge, and find my destiny. They supported me and generously thought me to be creative, love life, fight for what I deserve, and never give up. This journey would not have been possible if not for them, and I proudly dedicate this milestone to them.

Last not the least, I would like to say thank you to my committee members and my lab mates for their unlimited support and encouragements.

List of Abbreviations:

=, uniform

∇, gradient

2D, two-dimensional

3D, three-dimensional

ANOVA, analysis of variance

BSA, bovine serum albumin

C2C12, murine myoblast cell line

CN, collagen

D3 chip, triple-docking device

ECM, extracellular matrix

EGF, epidermal growth factor

FITC, fluorescein isothiocyanate

FN, fibronectin

HGF, hepatocyte growth factor

HT plot, Histogram-by-Time plot

PBS, phosphate-buffered saline

PDMS, polydimethylsiloxane

Rho/ROCK, Rho-associated coiled coil-forming protein kinase

SEM, standard error of the mean

Sema3A, Semaphorin 3A

SF, shape factor

TTP, time-to-peak

RGD, (Arg-Gly-Asp) peptide

Anti-Intg, anti-Integrin

FAK, focal adhesion kinase or PTK2

CS1, connecting segment 1

List of Figures

List of Tables

Abstract

Cell migration is an essential process in which cells move from one location to another using different mechanisms. Migration occurs during development, and in the maintenance of multicellular organisms during wound healing, tissue regeneration, and immune and pathophysiological responses. In skeletal muscle, satellite cells with dual roles as muscle precursors and self-renewing unipotent adult stem cells, are resident on muscle fibers and normally mitotically inactive. Their activation and subsequent migration critically mediate muscle repair. While early literature suggested satellite cells could demonstrate multipotency (giving rise to bone or adipose cells, this has not held up to scrutiny[1]. In this three-part thesis research, C2C12 mouse myoblast morphology and migration were first studied using a microfluidic platform under a range of chemo- and hapto-taxis conditions. The haptotaxis substrate was found to modify myoblast chemotaxis. Since cultured cells and tissues produce a natural extracellular matrix (ECM) which is pivotal in cell migration behavior, a second set of experiments was designed to study the haptotaxis effect of a natural substrate produced by one set of differentiated myoblasts on the migration behavior of a second set of myoblasts. Cell behavior was examined in four microfluidic devices with pillars in the migration channel. Results showed that more myotubes would align and form in the device (device 1) with offset rows of pillars. Differences in flow rate and velocity significantly affected migration patterns. Fibronectin (FN) in an applied substrate also shortened the time to confluency. Considering the effects of ECM and FN on myoblast behavior, a final set of experiments explored the interaction between FN and integrin, the FN receptors. Four inhibitors were applied to interrupt this interaction in device 1. Anti-Integrin antibody had the strongest inhibitory effect, followed by in order by focal adhesion kinase, CS1, and RGD peptides. The capability of microfluidic devices is advantageous for controlling cellular microenvironments, and thus offers a valuable approach for quantitative studies of cell migration *in vitro*. Devices can be designed to incorporate conditions that mimic what is known of normal physiology and control microenvironmental changes that model particular situations of disease or tissue injury. Further research to identify a device that promotes muscle fiber growth and enable longer-term studies of myoblast behavior toward muscle tissue engineering and regeneration, can now utilize the results of these novel experiments showing the potent impact on myoblast migration and alignment of combined haptotaxis and chemotaxis stimuli, microfluidic device design, and the different interaction of the receptor, integrin with an applied FN substrate vs. a natural ECM.

Summary

In this literature review, I will first outline skeletal muscle development and regeneration *in vivo*, highlighting aspects of cell signaling and migration *in vivo*. I will then review the current literature on *in vitro* studies of myogenesis and migration before reviewing approaches used in the literature to study cell migration and behavior. I then discuss approaches to engineering skeletal muscle tissue, and the many challenges associated with this goal. The organization of this review is based on stepwise understanding of muscle formation and repair, specifically as modelled in microfluidic devices, the approach used in my experimental chapters. Sections of this review make use of my review article[2] on use of microfluidics for studying muscle cell migration and there is reference to parts of my published research paper[3] which forms the first results chapter.

1. Introduction

1.1 Muscle cell migration

All three types of muscle including, cardiac, skeletal, and smooth muscle cells migrate in general and specific tissue needs. The basic functioning of muscles is contraction or movement which occurs via coordinated motions. Cell migration is fundamental in embryogenesis, often by collective movement of a homogeneous cell population[4]. Migration is also a key feature that can underpin homeostasis and regulatory functions in adult organisms. For example, neural crest cells migrate into many tissues in developing brain, limb, and skin, and help regulate function of many other cell types in many organs [4]. Neural crest cells arise from the embryonic ectoderm, and give rise to several non-neuronal cells, including pigment cells in skin, cartilage, bone, and pericytes, and some have self-renewal capability [5,6].

Somatic stromal or stem cells play a critical role in muscle development and regeneration. Skeletal muscle stem (satellite) cells also serve as a vehicle in gene-delivery technologies and cell therapy [7]. Deficient expression of Pax7, a gene product critical to myogenesis, and its paralog Pax3, impair stem cell migration during development [8]. Muscle cell migration contributes from the earliest stages of development, including gastrulation when cells migrate collectively as a sheet in forming three germ layers[9] and in predictable patterns toward a target region before differentiating into a particular tissue. Cell migration an important aspect of immune protection, such as when leukocytes move to the site of infection to clear invading microorganisms. Cell

migration also contributes in pathologies of injury and repair, vascular disease, osteoporosis, inflammation, cancer, and malformations[9].

For single cells, migration begins with cell polarization in response to a promigratory agent. Cell protrusions extend along the direction of migration, driven by actin polymerization and are stabilized by attachment to extracellular matrix (ECM) proteins on the surrounding substrate. These adhesions act as tracking locators that let cells move forward over them, detaching when they disassemble at the rear of the cell [10].

This cycle can be a singular or ongoing response in a larger developmental or pathological process. Migration has different modes: ameboid, mesenchymal, and collective, each specific to cell type, cell number, and the substrate environment (Figure. 1). Cells can move individually or collectively, depending on multiple environmental and internal factors, including the type of substratum, adhesion strength, extrinsic signals, dimensionality, mechanical elasticity, and cytoskeletal organization. Interactions between cell-intrinsic factors and the environment will promote a particular migratory mode. For example, immune cells with a nimble, fast-moving and fast-turning behavior, do not adhere strongly to the substrate as they lack a cytoskeleton organized for attachment; their movement is amoeboid. Movement by extension of membrane blebs, protrusion of the cell's plasma membrane, occurs in some tumor cells that lack a highly organized actin cytoskeleton. Mesenchymal migration occurs with cell polarization as the cell follows its leading edge of lamellipodia. This mode varies in speed: epithelial cells and fibroblasts move more slowly than other types of cells, despite a complex cytoskeleton. Some cell types, depending on their environment, will switch between ameboid and mesenchymal modes of migration. Cells also move as collective groups in chains and layers, as in development [4,11].

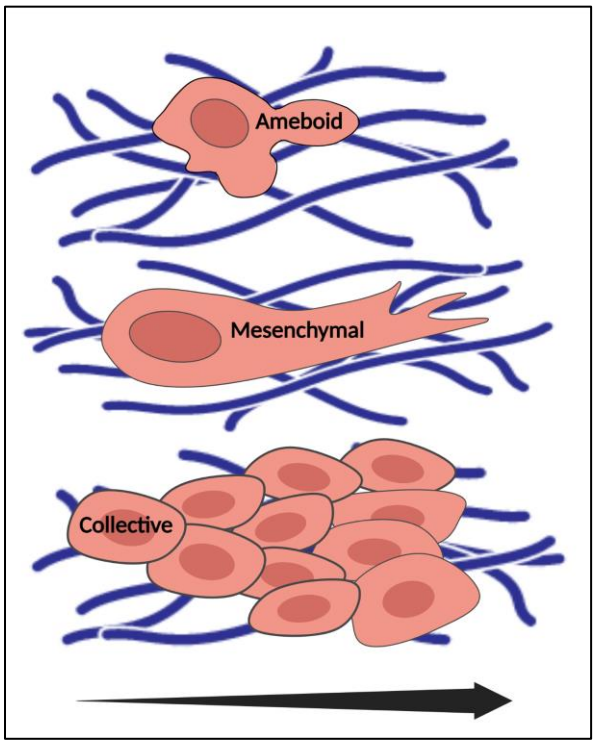

Figure 1. The modes of cell migration. Cells demonstrate different modes of migration, based on the cell type and the substrate in or on which they are migrating; the cells show different morphologies when they engage in different ameboid, mesenchymal, and collective migration. (figure modified after Roveimiab et al.)[2,4].

Cell movement also includes polarization, protrusions, cell body translocation, and retraction of a following edge. Such processes are organized by signaling networks, often with the same effectors, despite differences in cell type and migration mode [4].

Cells migrating in one direction show distinct polarity. The leading or advancing edge form flat, thin knobs-like extensions called filopodia during actin polymerization. Integrin, the FN receptors, on their membranes allow cell attachment to integrin proteins in the ECM. At the following aspect of the cell, actin microfilaments, called stress fibers, depolymerize and shorten; this lets the cell detach from the back and move forward. Therefore, a retraction force is required to translocate the cell body during migration. This force is mainly produced by myosin motors sliding on actin filaments inside the cell; the net difference between contraction and adhesion forces is the basis of cell movement. Actomyosin contraction, cytoskeletal disassembly, and

retraction force are essential for cell movement, including during cytokinesis in cell proliferation [12,13].

Adhesive forces in attachment vary between cell types and near the edges of a cell used to form cell protrusions by actin polymerization, while the remaining force is applied in actin network flow. Actin filaments can be in a direction opposite to that of cell movement, as the leading edge moves forward [12].

1.2 The role of actin in cell movement

The cytoskeleton provides a structural scaffold and plays important role for cell movement (Figure. 2) by using three protein filaments: actin, intermediate filaments, and microtubules, which differ in size and composition. Microtubules, 25 nm in diameter, are composed of tubulins alpha and beta, two subunits that bind into long-strand protofilaments. Thirteen protofilaments form a microtubule. Microtubules extend from the cell centrosome and shape cytoplasmic structure. Intermediate filaments are 10 nm diameter; in contrast to homogeneous microtubules and actin filaments, they are composed of tissue-specific subunit proteins and are less dynamic. However, microtubule strength and supporting functions both depend on the intermediate filaments found in every cell type. For instance, desmin filaments are in muscle cells, neurofilaments are restricted to neurons, and keratins are localized in epithelial cells. In addition, intermediate filaments are not polar like tubulin in microtubules and actin filaments [14].

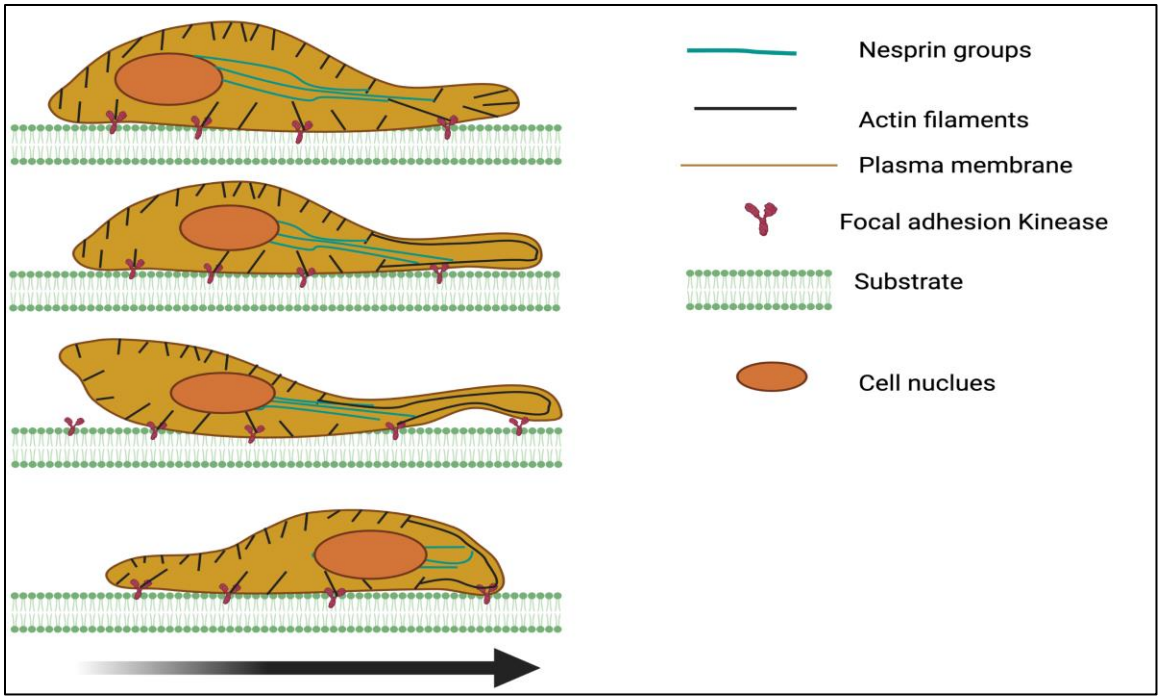

Figure 2. A schematic of cell movement. Actomyosin-mediated contraction pushes the cell body to move forward from the adhesive parts (focal adhesion kinase). The cell tail detaches from the substrate, and protease enzymes that are released by migratory cells into the ECM digest the proteins connecting the cell and its underlying substratum, and allow the cell to move forward [15]. In addition, nesprin proteins are thought to help position the nuclei, and coordinate and stabilize nuclear mobility inside the cell through interactions with the cell cytoskeleton as the cell moves forward ECM, extracellular matrix (modified after Roveimiab et al.)[2].

Actin monomers polymerize with a 166° rotation between nearest neighbors by head-to-tail interactions of the polarized molecule to form thin and flexible microfilaments 7 nm in diameter. Actin-binding proteins localize along the filaments and ‘‘manage’’ activities such as crosslinking into actin bundles and networks, and interactions with other filaments and organelles. Actin filaments are typically at highest density in the cell cortex, just beneath the plasma membrane, particularly in motile cells. In striated muscle, actin filaments are also organized internally into bundles within sarcomeres, the unit of striated muscle contractility. Actin filaments have critical roles in mechanical support, changes in cell shape, movement of the cell surface across the cytoplasm, migration on a substrate, and proliferation; the configuration and role of actin filaments depend on the particular activities of a cell at a given time. *In vitro* assembly of

actin filaments is regulated by the ionic strength of actin in solution. At low concentration, actin filaments depolymerize to monomers; at higher ionic strength, monomers will polymerize. Typically, monomers are added more rapidly to the fast-growing end (called the plus or positive end) of an actin filament. Although ATP is not required for polymerization, it plays an important role in slowing monomer binding and filament dissociation at the end where ATP is bound as ATP-actin. The helical structure of actin filaments results in repeating cycles of polymerization and depolymerization, depending on internal ionic strength of the cell matrix. The above process, called treadmilling, is associated with the dynamic behavior contributed by different monomer concentrations at minus and plus ends of actin filaments. Treadmilling requires ATP and influences filament assembly and disassembly during changes in movement and cell [16]. However, the role of treadmilling in cell movement is still not clear[17].

1.3 Muscle cell migration and regeneration

Migration by force-generating cells in smooth muscle is modulated by ECM components, peptide growth factors, cytokines, and drugs. Promigratory stimuli activate signal transduction cascades, which induce cytoskeletal remodeling and changes in cell adhesion to the ECM and activate (phosphorylate) motor proteins that contribute to movement. Myosin is a common molecular motor, converting ATP to ADP by myosin ATPases during force production. This conversion of chemical into mechanical energy acts on actin filaments. Contributions of actin polymerization and work by molecular motors lead to actin flow, the continuous movement of peripheral actin networks, in cell motility. Remodeling of actin filaments, molecular motors, and focal cell contacts with the ECM are organized to mediate cell migration toward or away from chemical-gradient cues, by changes in matrix adhesiveness, composition, or stiffness [12,18,19].

1.4 Skeletal muscle precursor cell migration and tissue regeneration

In general, muscle satellite cells are transcriptionally almost inactive and mitotically quiescent in residence on healthy muscle fibers. Evidence for a very low rate of transcriptional activity (making mRNA) comes from work by van Velthoven[20] and deductions from observing that transgenic manipulation of gene expression by satellite cells using Pax7CreER to delete genes in adult SCs, relies on there being active transcription of those deleted loci to yield phenotypes. Muscle satellite cells function as self-renewing stem cells and muscle precursors for growth, regeneration, and adaptation. Activation and subsequent migration of satellite cells critically mediate muscle repair since nuclei inside muscle fibers are postmitotic; only the fusion of satellite-

cell progeny (myoblasts) to fibers can add nuclei. Muscle adaptation by forming new fibers in injury-repair depends on satellite cell mobility after activation [21]. Anderson and collaborators showed that nitric oxide (NO) and hepatocyte growth factor (HGF) are important chemical signaling factors that activate satellite cells; they are released from skeletal muscle during contraction or stretching. Inhibiting the enzyme that makes NO (NO synthase) blocks the immediate injury-induced activation of satellite cells and delays and impairs regeneration [22-24]. The protein HGF is also called scatter factor; HGF promotes cell motility as seen in metastasis of cancer cells, and the migration of muscle cells in culture, on muscle fibers, and *in vivo* [25]. M2 macrophages in an area of muscle inflammation produce HGF which induces myoblasts to secrete Semaphorin 3A (Sema3A) [26], a protein that is implicated in restoring the nerve and blood supplies to skeletal muscle during repair from injury [26-28].

Myoblasts demonstrate a dose-dependent response to HGF [29], and HGF increases the speed of their migration on cultured fibers and induces a more unidirectional movement [28]. *In vivo*, HGF originates from two sources: the cylinder of ECM where it is stored around fibers and single myoblasts (more of a point source) and macrophages. Thus, the structure of skeletal muscle tissue means that cells are responding to complex HGF gradients within the mixture of adhesive, stabilizing matrix proteins, including fibronectin and collagen. In trials of myoblast transplantation to promote muscle repair, cells essentially migrate only 200 μm before differentiating [30]; this explains the need for multivariable approaches to myoblast transplantation and wound repair by tissue engineering that is more complex than initially envisioned in the late 1980s.

After fiber injury, tissue-resident macrophages and neutrophils are activated and release high concentration of growth factors, including HGF, chemokines, and cytokines, which attract in-migration of immune cells that interact with myoblasts and further promote repair. Growth factors released by T cells, interleukin-2, insulin-like growth factor I, interferon gamma, and amphiregulin also impact migration and proliferation by myoblasts [23]. Satellite cell populations and their responsiveness to activating stimuli both decrease with age [22], and immune factors released from muscle also change with age.

Macrophages also express and release HGF, and synthesize nitric oxide after injury in skeletal muscle or epithelial tissues [24]. The microenvironment of old muscle could be modified by regulating such immune factors to improve myoblast migration, increase muscle growth, and improve function[23]. Matrix metalloproteases (MMPs) also help regulate myoblast migration,

differentiation, and tissue repair as MMPs digest ECM components. The out-migration of activated satellite cells from fibers and their movement toward other myoblasts to fuse and form new fibers require their migration across the basement membrane that is remodeled during inflammation and regeneration. MMP degradation of the ECM thus has a critical role in satellite cell migration and differentiation[31]. Myoblasts can move significant distances, suggesting they are in a state of constant, variable-speed movement within the basement membrane on fibers especially after fiber damage, although in many of the published studies of myoblast movement, cells are completely separated from the basal lamina context as they are *in vitro*, in dispersed-cell cultures. By contrast, the cell bodies of quiescent satellite cells do not move *in vivo* [27,32] or in vitro, in single fiber cultures prepared by the method that retains their quiescence[33,34]. Even a very focal injury induces satellite cell migration toward the damage, although the migration between separate muscles is limited by connective tissues [27,35].

Activated satellite cells and myoblasts can migrate relatively large distances as shown by Allen and colleagues, using a high-resolution SPECT instrument (single-photon emission computed tomography) to follow movement by myoblasts injected into the systemic circulation as they ‘‘home’’ to regenerating muscle [32]. A repeat of that study in a sheep tested long-distance migration after bupivacaine injury to semitendinosus muscle. Myoblasts labeled with a lentiviral vector tagged with a green fluorescent protein (GFP) were injected 5cm distal to the injury and 8 days later, GFP+ cells were observed in sections of the injured muscle (R.E. Allen, pers. comm.).

1.5 Engineering skeletal muscle tissue

Tissue engineering of skeletal muscle has great promise for treating diseases of muscle wasting and major trauma (e.g., warfare injuries) that require significant muscle replacement to reconstruct a body segment. Tissue transplantation itself causes functional loss and volume deficiency [36-38]; therefore, new methods to improve the success and efficiency of tissue engineering to produce large volumes of skeletal muscle composed of bundles of well aligned myofibers are critical in a modern approach to therapeutics.

To have a significantly large mass of engineered muscle tissue, a large volume of myoblasts must be produced by amplification in culture from an original sample without limiting the migration or differentiation capabilities of those cells. Induced pluripotent stem cells (iPSCs) could be used to form skeletal myoblasts that, similar to cells of a murine derived C2C12 cell line, would have an acceptable rate of differentiation and a very low chance of tumorigenesis [39,40]. To improve

prospects for engineering skeletal muscle tissue for therapeutic use, molecular mechanisms underlying muscle development; myoblast migration, fusion, and differentiation; and cell-cycling processes must be clearly understood, from transcription factors that ‘‘tune’’ the balance between growth by proliferation and myoblast differentiation to muscle that could become functional through innervation[41,42].

Other factors, including mechanical and electrical stimulation, as well as ECM are all critical to myoblast activities, including migration during muscle formation. Directed mechanical tension can mediate myoblasts to form new fibers that align exquisitely to the long axis of a muscle during contraction or passive movement; tension also influences cell number, fiber diameter, and muscle biochemistry. Electrical stimulation underlies voluntary control of skeletal muscle function; it promotes nerve regeneration during muscle repair as well as myogenesis and angiogenesis in skeletal muscle tissue [43].

1.6 Conventional cell migration assay

Studies of cell migration utilize a variety of *in vivo* and *in vitro* approaches, including changes in cell position and shape, using a variety of microscopy techniques. For example, different aspects of cell behavior during migration and cellular responses to stimuli are often imaged with fluorescence or phase-contrast microscopy before analysis with computer software, such as NIH ImageJ. Approaches to the study of directed and spontaneous cell migration are exemplified by studies of leukocyte migration in which cells migrate from wells punched into a layer of agarose gel, into the surrounding agarose layer; this is a better approach for studying directed and random migration than the Boyden chamber, since cell migration is measured as the distance cells move from the edge of the well toward an applied chemotactic factor. A chemotactic index of migration is calculated at a microscopic scale with higher resolution, and the measurement of migration distance is standardized against migration toward a control medium[44]. An Optimax image analyzer can be used to automate measures of cell migration. [45] A capillary chamber migration assay is similar to the Boyden chamber assay.[46] A high-throughput study of migration using the now classic *in vitro* ‘‘scratch assay’’ was established to reveal potential toxicities that affect development of human neural crest tissue. The analysis was at the level of individual cells, typically tracked by time-lapse microscopy over time, using automated Introtox software for image processing.[47] The scratch or *in vitro* wound-healing assay is inexpensive and relatively easy to conduct; it is often used to study cell migration in 2D. The scratch assay is conducted by scraping

a line or area into a monolayer of cultured cells; the scratch simulates a tissue wound and a simulated healing response can be visualized in real time by tracking cells microscopically as they move from the intact area toward and into the scratch-injured part of the culture. An alternative approach applies electrical stimuli to injure cultured cells; this approach is recommended by researchers as it is considered to be a more physiological injury than a scratch. The "Tscratch" automated software program can be applied to analyze the pattern and speed of cell migration in such an approach. *In vivo* migration assays of mesenchymal stromal cells (often called stem cells in the literature) were conducted in mice subjected to a chronic wound that was not allowed to heal[46,48,49].

An option that avoids these disruptive methods utilizes a "cell-exclusion zone" in a culture or tissue which prevents cell growth into that area; later, the barrier is removed, and cells are allowed to migrate inward to fill the gap. An advanced version of this approach is called a fence assay, which allows the rate of movement to be measured using automated digital-image analyzers. The microcarrier bead assay cultures cells onto beads and then beads are transferred to a 2D culture area. Cells that migrate from the beads onto the culture dish are then incubated and beads are removed by suction. Cell migration in these approaches is monitored by light microscopy. The spheroid migration assay[50] uses a combination of 3D and 2D microfluidic technologies to study cancer cells. This assay is similar to that using cell grown on beads, with the movement of cells off the 3D spheroid onto a 2D substrate being monitored under a microscope. Both assays simulate the close cell–cell contact observed in cell migration studies.

1.7 Chemotaxis studies

Chemotaxis is the motion of cells directed by a soluble chemical gradient. Chemotaxis is typically described in contrast with more random-impact Brownian motion. Chemotactic signals are important for growth, migration, and cell differentiation within a dynamic, 3D microenvironment since gradients provide critical influence on cell responses to processes such as inflammation, wound healing, and cancer. In traditional cell cultures containing medium, it is essentially impossible to generate spatial gradients with reliable control or stability, as isotropic and unbounded diffusion of molecules in solution limits gradient stability in the absence of a reservoir and outflow. Fortunately, microfluidic technology can manufacture a wide variety of remarkably complex devices that help route fluids accurately over micron-scale dimensions; such

devices also deliver the capability to create gradients based on fluid flow at a scale appropriate for studying cell migration in real time.[51]

1.8 Traditional chemotaxis assays and HGF

Traditional chemotaxis assays generate gradients *in vitro*; their application has instrumentally shaped our current understanding of gradient signaling, although they can barely produce stable, and well-defined gradients with reliable spatial and temporal profiles.[51] The Boyden chamber, developed in 1962, is used for Transwell migration assays and has greatly advanced our understanding of chemotaxis. Migration is quantified as cells respond to chemokines over a range of concentrations. The Boyden chamber has two sections separated by a membrane or filter (pore size typically 2–12 μm). A putative chemoattractant or chemorepellent solution is placed in the lower chamber and cells are incubated in the upper chamber. The motion of cells migrating through the porous membrane simulates the movement of cells through the interstitial space and the ECM, and between other cells *in vivo*. In some studies of leukocytes, endothelial cells are grown on the upper surface of the membrane and cells migrate in response to the differential gradient generated between two types of cells on either side of the membrane. For analysis, cells are fixed, stained, and counted. The Boyden chamber assay is easy to use and enables observations and analysis of chemokine effects on cells that are more accessible to study than in a typical culture dish.[52]

Use of a Boyden chamber or Transwell assay is limited by the difficulty of sustaining a chemokine gradient in the chamber for more than a few hours due to diffusion, and challenges of visualizing cells in real time as they pass through the membrane. It is also impossible to study the integrated response to multiple gradient signals. Also, the effects of shear stress on the cells, for example, from fluid movements while the cells are migrating, cannot be distinguished from chemokinetic effects on the cells.[51,53]

Modern applications such as "IncuCyte" for live cell imaging during chemotaxis address some of these limitations. Biological hydrogels of collagen, fibrin, or agarose can be manipulated to establish *in vitro* gradients around cells. Cells or tissue explants can be cultured on a gel surface or mixed within a liquid hydrogel solution before it gels. A gradient of one or more biomolecules can be formed in two ways in this assay: either by co-culturing test cells or tissue with a second cellular source of a putative or known chemokine, or by molding the gel or making holes in it that

can be filled with a soluble form of one or more potentially active molecules. Hydrogel modifications thus enable real-time observation of cells responding to one or multiple chemokines.

Recent advances generated biological hydrogel gradients by spacing lines or drops of a biomolecule on the surface of a gel, so it diffuses into the gel matrix. The droplets are placed by pump or inkjet printing and form a concentration gradient by diffusing in space and time, out from the source and into the gel where the cells are cultured. Advantages include the ease of making these gels that better resemble *in vivo* tissue than cells in conventional 2D culture dishes. Chemokine movement in a biological hydrogel is based on free diffusion, unaffected by bulk movement, so it is feasible to control the position of a biomolecular source. However, several drawbacks interfere with use of this method, including endogenous secretion of biomolecules, (possibly the same as that under study), by the cells themselves.

As it is technically challenging to detect nanomolar concentrations, the concentration-dependent response to a given biologically active molecule is not easily detected by protein assays of the gel. The porosity and polymer chemistry of the gel network also reduce the ability to control the gradient patterns, and once a biomolecule is loaded into a source cavity, concentration, shape, and diffusion of the gradient cannot be modified. This adds between-experiment variability as cells and biomolecule source compartments are established manually. Finally, single-cell responses are not easily visualized due to the 3D architecture of the culture system and gel itself, due to the optical properties of some gels (e.g., containing refractile collagen fibrils) that obscure cells in phase-contrast microscopy. Therefore, cells in hydrogels have to be tracked using Z-series image stacks by confocal imaging or 3D-tracking algorithms. Overall, biological hydrogels have advantages over Boyden chamber assays: they are easy to use without complex equipment, and produce reasonably controllable gradients of more than one biomolecule.[51]

Micropipette-generated gradients use glass micropipettes to generate biomolecular gradients. A fine glass tip with an internal diameter 1 mm or less is pulled from a heated glass capillary tube. A biomolecule solution is suctioned into the tip which is then placed at a known distance from cells of interest using a manipulator under a microscope. The solution is released in proximity to the cells using a pump to control the volume and frequency of ejections that generates a gradient.[54] A variant of the micropipette method uses pneumatically ejected biomolecules that diffuse passively from a micropipette tip and induce cellular responses, for example, by primary neurons and neutrophils.[55,56]

In contrast to cells on or within biological hydrogels, single-cell responses to chemokine gradients at a known distance or direction can be measured since cells can be visually distinguished from the background. The method can create multifactor gradients by adjusting multiple micropipettes around a cell of interest. However, these micropipette-generated gradients are not particularly controllable between experiments due to changes in the free solution that generates the biomolecule gradients, thermal variation and evaporation of the solution, and variations in the size and shape of the micropipette tips. Commercial tips are pulled under well-controlled conditions, but still show geometric differences that will generate variation among gradients under the same experimental conditions.

The three-dimensional gradients described above also require confocal microscopy and fluorometric dyes for quantification during an experiment, and careful positioning of the micropipette tip or tips relative to a cell, on a crowded microscope platform with equipment to control humidity, carbon dioxide, and temperature. Therefore, complex on-stage environmental controls are typically most feasible in such experiments on nonmammalian cells that do not require 37°C or cells that respond fairly quickly to a gradient (within 1–2 h). Despite these limitations, the micropipette method is well suited to studying single-cell responses, although less suitable for measuring cell responses to multiple gradients.[51]

The Zigmond chamber was developed in 1977 to study neutrophil chemotaxis, as it allows direct visualization of cells. The device is made up of a glass slide with a central 1-mm wide ridge that divides it into two sides and forms two weakly confined channels in the glass; the channels are deeper than the ridge is tall, so an overlying coverslip floating on the medium and span from the whole slide, will create two channels bridged by a thinner layer of medium in a 3-10 μm gap above the ridge. By filling one channel with plain medium and the other with medium containing a chemokine, diffusion across the gap forms a gradient. Cells are plated on the coverslip and observed near the ridge are observed using a microscope. The precise geometry of the Zigmond chamber can produce a uniform, linear, uniaxial gradient, which can be studied in detail over time. The important drawback is that the gradient has only a short lifetime (stable for 1 h), so the Zigmond chamber device is used to study only fast-responding cells such as sperm and neutrophils. A further limitation is that the fluid under the coverslip can evaporate; this can affect the fluid flow that generates the gradient and protects cell viability. However, the Zigmond device is useful for

studying cell migration under a gradient that is reliable for up to 1 h and the gradient can be monitored with fluorometric dyes.[51]

The Dunn chamber is similar to a Zigmond chamber, but less sensitive to evaporation. Source and sink chambers in the Dunn device are made of concentric circles and cover slipped to avoid evaporation. Limitations and strengths of this device are generally similar to those of a Zigmond chamber, and a multifactor gradient can be generated only in one axis, similar to Boyden and Zigmond chambers. While the Dunn chamber is geometrically symmetrical, evaluation of cell responses in a radial direction is difficult.[51]

Proteins such as myokines that are produced by skeletal muscle during contraction may have local influences on muscle and non-muscle cells. Some of the myokines that are upregulated in resistance exercise are: leukemia inhibitory factor (LIF), interleukins, decorin, and irisin. These myokines can promote muscle growth. There are also other growth factors that release during exercise, beside hepatocyte growth factor (HGF) such as insulin like growth factor (IGF-1), and nitric oxide (NO). Both NO and HGF have the ability to activate satellite cells and induce the muscle growth. It was also shown that NO can upregulate myokines such as interleukine-6 (IL-6), one of the main myokines. IL-6 increases after exercise and is also able to upregulate muscle hypertrophy signaling factors, activate, and induce satellite cells growth and proliferation[57].

1.9 Haptotaxis studies (cell-ECM interaction)

Cell adhesion, the interaction between cells or with an ECM, is a broad topic of biological study due to its functional importance. Interactions inherent in cell adhesion sustain normal cell physiology and behavior and influence development of pathology, wound repair, and tissue engineering. Ultimately, advanced tissue engineering will only be achieved when cells can attach, grow, and be viable on biological substrates during synthesis of implantable tissues. The extracellular matrix (ECM) has a dynamic composition and is continually remodeled by proteases. ECM also has a critical role in development and pathological process. General structure of ECM is composed of two domains: the first is a condensed matrix layer, which is close to epithelial cell and other sheets, including mesothelium, meningothelium, and synovia. It also includes muscle, Schwann cells, and adipocytes. The second domain of ECM is the basement membrane, which has similar structure to first domain as they both have collagen in their structure even though the collagens differ in the two domains[58,59]. Laminin, tenascin, and proteoglycans as adhesive glycoproteins attach to the scaffold and interact with the cells in and out of the matrix. This

interaction happens through receptors which Integrins are one of them. More than 20 types of collagen have been identified and they have critical role in the structure of vertebrates and many other organisms[58,59].

In tissues with more mechanical stress such as tendons, bone, cartilage, and skin, collagen is formed as fibrils that can supply tensile strength. Of the 28 isoforms of collagen, only type I, II, III, V, and XI can self-assemble into fibrils. Each fibril is composed of 3 collagen molecules that are wrapped in a triple helix structure that has 300 nm length and 1.5 nm diameter. Collagen types IV, VIII, and X form network like basement membrane.

Laminin 1 was discovered 40 years ago, and different laminin homologues have been identified since that time. Across 12 different isoforms of laminin, all have certain structural features in common. Epidermal growth factor-like domain is common to all laminin isoforms which host nidogen and binds laminin to collagen type IV. The laminin α chain has a C-terminal domain that hosts an integrin binding site. All epithelial cells, most smooth, skeletal, and cardiac muscle cells, bone marrow cells, nerves, and cells in the neuroretina synthetize laminin. Laminin also has an important role in cell adhesion, migration and differentiation procedures[58,59].

The first member of the tenascin family of proteins, tenascin-cytotactin (TN-C) was discovered 35 years ago. TN-C forms a hexamer structure. Other TN family members have TA (tenascin assembly) domain that form trimers. This complex structure makes it easier for tenascin proteins to interact with other extracellular matrix proteins. The expression patterns of tenascins are complex and does not occur in normal adult tissue except under pathological conditions. Tenascin family members have a critical role in cell proliferation, differentiation, cell migration and apoptosis[58].

Integrin is present in all animal species and has a αβ heterodimeric structure, although the number of the αβ is different in different organisms. The subfamily of integrin that recognizes fibronectin, collagen, and laminin is a β_1-dimer. Integrins function through extracellular or intracellular adhesion molecules which provides the mechanical strength between the inside and outside of the cell. Integrin's cytoplasmic domain binds to actin microfilaments in cytoskeleton. This binding happens through various proteins, including talin, α-actinin, vinculin, and paxillin. Integrin-ligand interaction impacts on signal transduction pathway and effect on cell structure, viability, proliferation, and motility[58,59].

Extracellular matrix proteins are either the structural elements and act as scaffolds like collagen or glue, like laminin and integrin. Proteoglycans with their protein core and attached to glycosaminoglycan chain can be grouped to several families. First family is composed of lecticans and the side chain from chondroitin sulphate and keratan sulphate. Members of this family, including aggrecan, versican, neurocan, and brevican provide structural support in the ECM. Versican can also stimulate fibroblast proliferation. In second family their side chains are made of chondroitin, dermatan sulphate or keratan. Their family members such as decorin, biglycan, fibromodulin, and keratocan in general, organize collagen networks, and decorin is involved in differentiation of epithelial and endothelial cells[58,59].

Matrix metalloproteinases (MMPs) in the ECM have critical role in ECM degradation. They are calcium dependent and zinc containing endopeptidases. They belong to a bigger family which is called metzincin. More than 20 mammalian MMPs have been discovered, and each is capable of degrading different ECM proteins. MMPs can be produced with majority of cells, including epithelial, fibroblast, myofibroblast, chondrocyte, etc. Besides their ability to degrade the ECM, they can also regulate mechanical resistance during cell migration[58].

Fibronectin (FN) is one of the main fibrous proteins in the ECM and has a critical role in interstitial ECM organization, cell function and attachment. Fibronectin is a glycoprotein with high molecular weight which can be stretched more than its resting length. The structure of fibronectin is a dimeric glycoprotein with two similar subunits. In each subunit there are 3 different types of fibronectin[59,60]. Stretching capability of FN especially after binding to integrin gives fibronectin the ability to regulate mechanical forces. Fibronectin interacts with cell-surface receptors and creates a fibrillar network on the cell surface; this formation is important in cell adhesion, growth, development, differentiation, and migration.

To investigate the structure and behavior of extracellular matrix proteins and cell adhesion, a microfluidic device can be used to model the *in vivo* movement of cells and study the regulation of cell adhesion behavior by a small number of cells. A typical microfluidic device uses passive fluid pumping, where liquid is pumped indirectly through a microchannel between the inlet and outlet ports due to the surface tension of a small drop of liquid (cell medium or a potential cytokine solution); this reduces the wasted volume of cytokine. Also, by applying an oscillatory flow through channels, we are able to mimic normal physiological conditions (e.g., in the cardiovascular system) by providing the stimulus of pulsatile mechanical shear stress to a cell population[61]. The

directional motility of cells or parts of cells (e.g., axonal outgrowth from a neuron) is usually toward a gradient of cell adhesion sites or substrate-bound molecules that chemoattract the cell. Such gradients in the ECM also operate during angiogenesis; gradients can be artificially placed on a biomaterial substrate by controlling the concentration of a particular protein on the polymer surface.

Cells may sense and respond to cell-adhesive and/or chemoattractant substrates. Responses recognized by changes in cell morphology, migration speed, cell–cell interactions, or even a "memory effect" by which some cells will migrate back to their starting point. The ECM is also continuously remodeled since cells in any tissue produce ECM molecules over time. This dynamic feature of tissue formation rearranges cells and/or the matrix components in a tissue and is a critical aspect of embryonic development and tissue repair. The ECM provides stability and mechanical support to cells and contributes important biological signals that impact cell cycling, motility, and other behaviors. The majority of cardiac ECM are collagens type I and III that are remodeled by cardiomyocytes in response to physiological and pathological stimuli, including infarction, pressure and/or volume overload, and inflammation.[62]

The prototypical ECM protein, tenascin (TN-C), is expressed in the early stages of inflammation, wound healing, tissue remodeling, and embryogenesis. TN-C has a notable anti adhesion property that can destroy cellular interaction with fibronectin in the ECM and result in loss of focal adhesion sites.[62]

1.10 Microfluidic devices for studies of muscle cell migration

Microfluidic studies of muscle cell behavior have recently been used to study contractility and migration with applications in cancer therapy, drug delivery, and the development of" organ-on a-chip" models. In general, a microfluidic chip is about the size of a universal serial bus (USB) drive and consists of micrometer-scale channels to study cell behavior under conditions that mimic one or more aspects of physiology.[63]

By contrast to a flow-based microfluidic gradient device, 3D gel-based microfluidic devices better mimic the physiological ECM and maintain a stable, somewhat less-controlled gradient. For example, a large source and sink in the device will create a stable linear concentration gradient in a small hydrogel-filled channel at the equilibrium state of mixing. This approach is useful for studying directed cell migration in a controlled 3D microenvironment. One example of a 3D microfluidic device is presented in Figure 3, below.

Microfluidic devices have also revealed the migratory behavior of endothelial cells under a VEGF gradient, while in co-culture with smooth muscle or cancer cells within a collagen-gel scaffold. Importantly, both the gradient of growth factor and the substrate condition (i.e., the stiffness of the collagen gel) influenced cell movement. Microfluidic devices can be used to generate gradients in the substrate as well, for use in studying other mechanisms of cellular movement, including actin filament movement on myosin heads on a substrate surface, without interference from bulk flow that would produce larger-scale disturbances and obscure very fine-scale movements of myosin–actin interactions.[64]

One such microfluidic device is shown in Figure 3. This device is made of an air-permeable polymer polydimethylsiloxane (PDMS), and has two fluidically isolated compartment, proximal and distal. The two compartments are connected by microgrooves that facilitate observation of axonal growth during neuromuscular interaction. It is necessary to apply an appropriate ratio of neuronal and muscle cells to respective proximal and distal compartments, in order to avoid blockage of the microgrooves[65-67].

Many microfluidic devices are designed to generate controllable chemical gradients that comprise putative stimuli for cells of interest. Their flow-based mechanisms can generate stable gradients, the shape of which can be manipulated due to the device design. Typically, the gradients are uniaxial and cells in the device channels are subject to shear stress. Using this type of microfluidic gradient device, our lab demonstrated the influence of a gradient of epidermal growth factor on the growth and migration of adult rat adipose derived stem cells.[68]

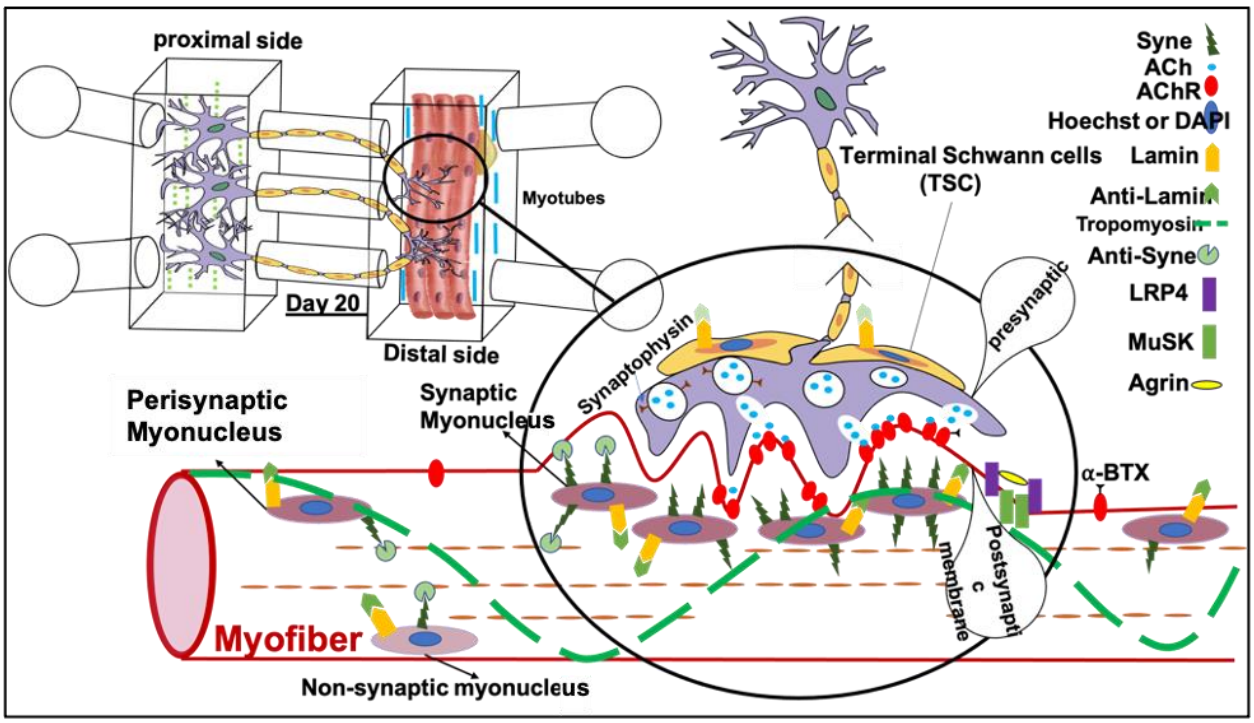

Figure 3. Modelling the formation of neuromuscular junctions in a microfluidic device. A sterile Xona Laboratories microfluidic device with 450 nm microgrooves would be coated with poly-L-laminin in the proximal compartment and laminin or collagen in the distal compartment and incubated overnight. After removing the substrate and 2 hours before adding neurons, proximal chambers would be filled with neuron initial medium, and incubated and observed daily to follow axonal growth into the distal compartment. At day 14, muscle cells would be added to the distal compartment. After 4-6 days incubation to allow for muscle-cell differentiation into myotubes in low serum medium, AchRs would be stained 15-30 mins before fixation and immunostaining for other proteins of interest[67,69]. Original artwork by Z. Rovei Miab, 2021.

1.11 Skeletal muscle cell culture and migration using microfluidics

C2C12 cells of a murine skeletal muscle cell line derived from satellite cells, are commonly used in studying myogenic differentiation. C2C12 myoblasts express unambiguous markers of skeletal myocyte differentiation, and have been used in various 2D and 3D culture configurations.[70] C2C12 myoblasts in culture fuse to form multinucleate syncytia, called myotubes, an *in vitro* form that displays many of the morpho-functional features of typical multinucleated muscle fibers found *in vivo*, including contractile sarcomeres, and adaptation to regulatory influences such as neural and hormonal signals.[71] Endothelial cells and skeletal

myoblasts respond to mechanotaxis by distinctive changes in cell alignment and migration, depending on dynamic and static cues that modify mobility, proliferation, differentiation, and cell spreading on the substrate.[72]

Similarly, cell-strain experiments without a microfluidic device showed differential responses in cell dimensions by primary fetal rabbit myoblasts, lung type-II alveolar cells, and bone cells subjected to cyclical stretch and release.[73] A microdevice of a biocompatible polymer, poly (lactic co- glycolic acid) melt-casted from PDMS mold, was used to form microgrooves of various depths to culture C2C12 cells and study their migration and proliferation.[74] Cell alignment responded to the dimensions of the grooves by increasing expression of filamentous actin, and migration by pseudopodia responded to groove depth.[74] The 3D microgrooves also induced cell proliferation, consistent with observations that a smooth substrate reduced cycling, possibly by reducing adhesion. The 3D configuration of the ECM, cell alignment, and tissue architecture are all important influences on skeletal myoblast proliferation and migration, and are modified by mechanical stretching.[75]

Microfluidic devices have been used to study combinations of mechanical stretching, shear forces of fluid movement, and cell alignment on geometrically patterned substrates, including alignment of C2C12 cells.[76] While reports relevant to muscle cell behavior and migration are not always consistent due to the variety of substrate configurations and properties,[76] the control of such features can be facilitated by the use of microfluidic devices. The responses of C2C12 cells among others were studied using a microfluidic device after cells were plated on different ECM substrates; cell growth and motility responses to mechanical stimuli were tracked.[77]

Isotropically-modified substrates patterned by microgrooves, lanes, and aligned electrospun nanofibers in the device facilitated cell alignment after plating; subsequent protocols stretched cells or subjected them to shear forces from flow within the device. The evolution of intracellular calcium concentrations, expression of phosphorylated (activated) focal adhesion kinase, and visualization of cell orientation were used as direct measures of cellular responses to shear and stretch. C2C12 cells oriented themselves perpendicular to the stretch direction on a nonpatterned surface, but showed irregular orientation or realigned in parallel to a micropatterned fibronectin substrate.[77]

The contraction of muscle cells during culture may also be studied using microfluidic devices. A PDMS-based microfluidic device was constructed by soft lithography and C2C12

myoblasts were seeded in collagen inside microchannels and cultured for a week to study the contraction of the differentiated myotubes that model fibers. Myotubes demonstrated contraction by internal structural displacements upon electrical stimulation, and by their expression of a actinin in sarcomeres of stimulated cells.[78]

Another microfluidic culture system allowed study of skeletal muscle myoblast contractility after electrical stimulation; muscle cells were co-cultured with non-excitable cells such as monocytes. In such cultures, both cell types are influenced by myokines, proteins released from contracting muscle that promote muscle cell movement. C2C12 cells were cultured around a conductive polymer wire composed of poly(3,4-ethylenedioxythiophene) and polyurethane; the wire was attached to the PDMS chamber containing cell medium. This approach was able to regulate muscle cell contraction during culture using controlled ionic currents generated by depolarization.[79]

In laboratory of Dr. Lin (University of Manitoba), microfluidic experiments were used to investigate how an HGF gradient regulates myoblast migration and differentiation under the influence of various substrates, alone or in combination; the substrates are also established in a gradient pattern across the migration channels of triple docking devices[3,80], and other novel 2D or 3D devices, as represented by examples in Figure. 4. These studies are aimed to help improve methods of engineering skeletal muscle tissue to grow ‘‘bulk muscle grafts’’ that would be able to replace large volumes of muscle lost through trauma or other injuries.

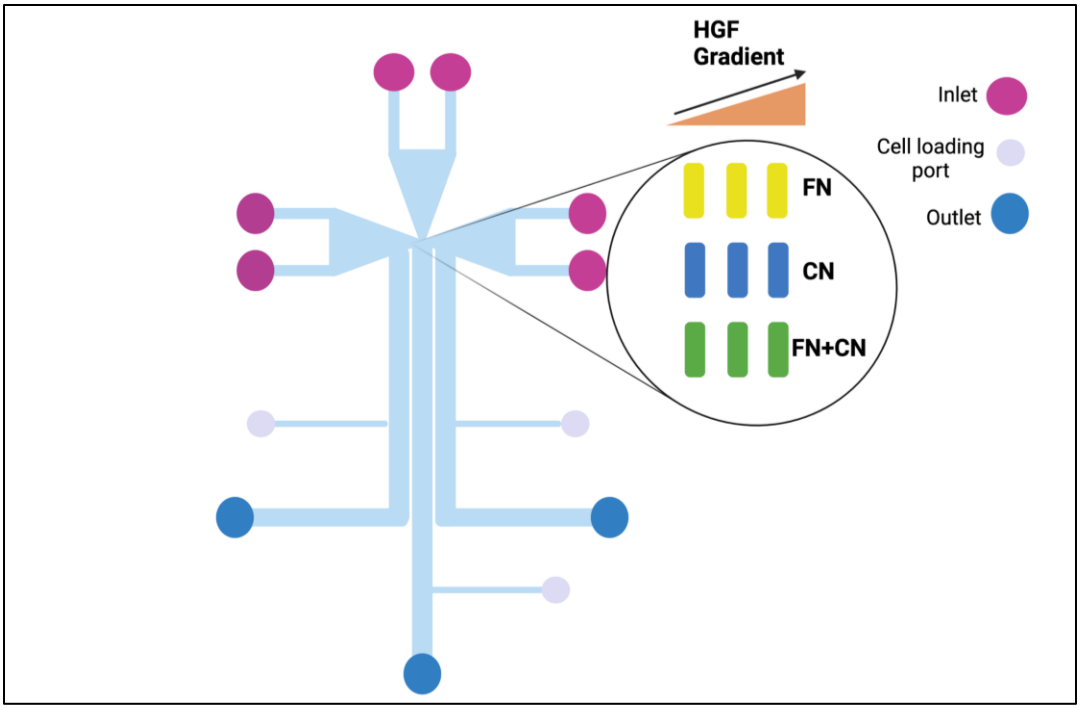

Figure 4. Triple-docking microfluidic device. This microfluidic device (left) is designed to enable investigation of the effects of a gradient of HGF (depicted as a triangle in the upper middle of the panel) in combination with 2D gradients of the substrate (middle). Cells are introduced into the device at cell-loading ports (shown in green on the left, with one loading port per channel [81]) inside the device. Channels are prepared with or without an HGF gradient after they are coated with a substrate of fibronectin, collagen, or fibronectin plus collagen (shown in the middle part of the figure, representing the three channels coated under various conditions). Migration by cells in the experimental channels (measured in conditions with a particular substrate coating and/or an HGF gradient) is compared to cell migration in control channels without a substrate coating and/or HGF (modified after Roveimiab et al.)[2,3,82].

Another study used a microfluidic device to estimate cell responses to different modes of delivering culture medium in long-term culture experiments. The PDMS based microfluidic device was composed of five parallel channels connected to tubing to allow repeated refreshment of medium inside channels. Such lengthy cultures will be the basis of developing future tissue-on-a-chip technologies that can reproduce the biology and physiology of normal tissue and could be used to promote functional repair of muscle. Since continuous flow provides more cell heterogeneity in cells cultured in a device, over the longer term, such cultures result in abnormal

cell morphologies and vesicle formation in the cytoplasm. These findings suggested fluid delivery should be pulsatile in such devices, a feature that was achieved by pumping medium at a specified rate to maintain normal cell morphology and viability[82]. A different microfluidic device for long-term culture of C2C12 myoblasts was used to investigate cell proliferation without medium exchange.[83,84]

A PDMS-based device was fabricated to form multiple channels in elastic silicone rubber; channels varied in thickness and had extended cell cultivation channels and two cell-seeding ports. This microfluidic device was combined with a so-called ‘‘Braille display,’’ a level surface with a grid of over 300 vertically moving pins; the pins were used to power an integrated system of pumps and valves and induce local deformations of the channel networks. A transparent heater was used to maintain temperature outside the incubator and avoid changing the culture medium, so cell responses could be studied with finely controlled fluid movement patterns. These two reports revealed an exciting new possibility for portable cell-culture systems that could be visualized in long-term time-lapse studies, while maintaining healthy cells with minimal medium. A later study on spatial differentiation of C2C12 skeletal myoblasts discovered the effects of culturing in medium with a linear gradient of two bone morphogenetic proteins, BMP-2 and BMP-7. A microfluidic device fabricated as layer-by layer films of poly(l-lysine) and hyaluronan was used to bind layers of film and generate a matrix-bound gradient of growth factors including the BMPs, and then the microfluidic device was removed.[85]

A micro-bioreactor array was developed to cultivate two different cell lines together, including C2C12 myoblasts and nondifferentiated human embryonic stem cells (hESCs), in different configurations of flow. In this study, a PDMS based microfluidic device was fabricated with 12 culture wells connected to the main channels. After binding to a glass slide, coating with fibronectin, and seeding with cells, the device was covered with a thin layer of PDMS. Inlets and outlets were connected to a syringe and filled with cold medium, and the whole device was placed in an incubator. Cell type-specific comparisons spurred interest in understanding the more complex regulatory pathways of hESCs as they grow and differentiate in culture. For comparison, C2C12 myoblasts and rat cardiac myocytes were also cultivated and examined by automated image analysis in situ in the microfluidic device, to investigate the expression of genes that are used to mark the progression of cell differentiation.[70]

Microfluidic devices have thus proven to be valuable tools in research on cardiac, smooth, and skeletal muscle. Their use has fostered major advances in our understanding of the migration behavior of fast-responding cells, including immune cells, and cells that seem to respond more slowly. In turn, ongoing refinement of microfluidic devices designed specifically for testing individual hypotheses encourages further exploration of mechanisms underlying the many types of differential response patterns even among the three types of muscle cells. Additional enhancements to make multigradient devices have more recently enabled even more in-depth studies of proliferation, migration, and differentiation of several cell types under a wide range of culture conditions.[51,80]

Features of skeletal myoblast differentiation, clustering, alignment, and fusion into myotubes *in vivo* in development and regeneration,[86,87] and in culture,[88] can therefore be modeled in the channels and on the patterned substrates of a variety of PDMS-based microfluidic devices.[89] Findings that myoblasts migrate to regions of high myoblast density in culture and toward fused myotubes[90] are consistent with observations that small muscle wounds heal quickly in comparison to large-volume injuries.

An important gap in our understanding is identifying how a differentiated myotube by itself can slow or sufficiently overwhelm the migration of a myoblast to trigger the return of the myoblast to the quiescent state as a stem cell on a newly repaired fiber in a muscle *in vivo*, after injury.

1.12 Designing new microfluidic devices

In this research project, I addressed this gap by developing newly designed microfluidic devices to load C2C12 cells in two waves; the idea is to have the first set of cells induced to differentiate into myotubes before the device channels are reseeded with a second set of myoblasts. That second wave could then be examined for their movement and differentiation behavior[91]. Figure 5 provides a schematic of potential experiments, envisioned in writing our recent review paper[80].

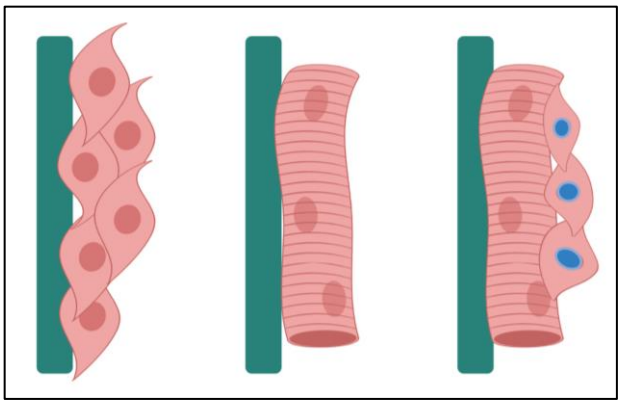

Figure 5. Future application of microfluidics to study myoblast migration on myotubes. Future application of microfluidic technology to study myoblast migration on myotubes. A novel design for a triple-docking device will enable time-lapse observations of myoblasts under controlled conditions for investigation of the initial cell differentiation into myotubes, and the behavior of a second wave of myoblasts that is introduced into channels containing the myotubes. Preliminary results suggest cell–cell communication by myoblasts during migration is highly attuned to the substrate composition and the state differentiation in neighboring myoblasts (modified after Roveimiab et al.)[2,82].

The use of D^3 chips[3] to study cell behavior under the influence of gradients in the substrate and/or the medium surrounding cells had two significant limitations. First, the docking channel essentially fills with cells during an experiment and prevents the loading of any further cells from the inlet of the device. Second, in the D^3 chip, cells could be loaded through the outlet port into the migration channels, but cells would flow away too quickly once the direction of flow was restored, since there was no way to slow that flow. Thus, in order to investigate the formation of myotubes within a device, and how a more naturally produced substrate made by those differentiated myotubes might affect migration and haptotaxis behavior of a second set of cells loaded into the device, the new devices were designed.

Previous literature suggests that it is possible to use pillars within channels of a microfluidic device as a way to anchor muscle strips so they can provide force and lead to the growth of neurons toward muscle developing in the device. A 3D compartment allowed the co-culture of motor neurons derived from mouse embryonic stem cells (mESCs) together with mouse skeletal muscle cells within an ECM substrate. This system facilitated the observation of 3D axonal

outgrowth and NMJ formation. In that research by the Kamm laboratory, the device was composed of a reservoir, a gel filling port, gel region, and a channel for the medium that was surrounded with a vacuum channel with a vacuum inlet. Pillars were stablished in the opposite side of the gel chamber in another layer placed between the microfluidic layer and a coverslip[92].

Current research is now exploring avenues for muscle-tissue engineering to establish ways to treat large-volume (volumetric) muscle injury or muscle dysfunction[93]. There is still a need for an *in vitro* model that can generate physiologically aligned myofibers. For example, a micropatterned PDMS membrane with parallel microgrooves was fabricated to investigate the effects of microgrooves in muscle cell fusion and muscle cell organization[94]. In that device, f-actin assembly was very organized due to the inclusion of directional microgrooves. In the stage during cell cycling, regulator proteins, such as P21 interaction with cell-cell adhesion protein, N-cadherins, is thought to be responsible for myotube formation between the microgrooves. The aligned myotubes that developed in that device were proposed to be transferable to biodegradable hydrogels for use in tissue engineering and muscle regeneration applications[94].

In the Folch laboratory, C2C12 cells were cultured on microtracks that were surrounded with a protein-repellent coating in a microfluidic device. Myoblasts only adhere to adhesive parts and align along the microtracks. This device was made with standard photolithography and soft-lithographic methods and fabrication includes two devices, one with micropatterned and the other one for long-term perfusion. This device was composed of 3 inlets that joined the main channel. The main channel was patterned with microtracks configured as two longitudinal flow channels that crossed the middle of main channel. Laminar streams were applied to stimulate subdomains of single myoblasts. Narrow streams of agrin were also applied over the micropatterned myotubes to help promote clustering of acetylcholine receptors in areas that were in contact with agrin[95]. Ultimately, whatever the design of a device to study myotube formation and cell migration after the initial migration of myoblasts, is to improve upon the specificity of myotube formation compared to what occurs in a simple tissue culture dish. In typical cultures, myotubes simply form everywhere in the dish, based on cell-cell contact and the level of confluence reached by cells in the dish (which differs from location to location across the surface). The aim for microfluidics approaches is to be able to control the pattern and alignment of cells during myotube formation through specific device designs[95]. For the current investigation, an understanding of myogenesis is essential.

1.13 Myogenesis in development

Myogenesis, or the process of generating muscle, is divided to different phases in embryonic myogenesis. Firstly, muscle fibers will be generated by mesoderm derived structures, and then additional muscle fibers will be generated subsequently. Muscle progenitor cells will proliferate as long as the muscle gets mature, and then progenitor cells will go to quiescent stage. When a muscle is damaged, myogenesis will continue by differentiating the cells, and the muscle will reach homeostasis[96].

Skeletal muscles form 40% of the human body mass and are critical in controlling the body posture, movement, breathing, and also metabolism. Myofibres together form the skeletal muscle tissue along with other connective tissues, such as blood vessels, stem cells and nerves. Development of muscle is controlled by the regulatory networks, including signaling and transcription factors. Dermomyotome cells, the dorsal part of the somite, express myogenesis regulatory factors including Pax 3 and Pax 7. Wnt/ß-catenin signaling pathway regulates multi steps of myogenesis via step-specific targets. *In vitro* and embryo myogenesis regulation is also controlled by muscle specific transcription factors such as MyoD, Myf5, and myogenin which are critical in the terminal differentiation, whereas MRF4 is critical in differentiation and myotube specific gene expression processes[97]. It was shown that exclusive expression of MRF4 induced the differentiation of cultured skeletal muscle cells. Therefore, these transcription factors are important in skeletal muscle development[98].

Myogenic regulatory factors (MRFs family) which are divided to primary including MyoD and Myf-5 are necessary for skeletal myoblast determinations and the secondary MRFs, including myogenin and MRF4 act later to induce the differentiation (Figure 6). Any mutation in these genes can show the role of MRFs family in myogenesis[98].

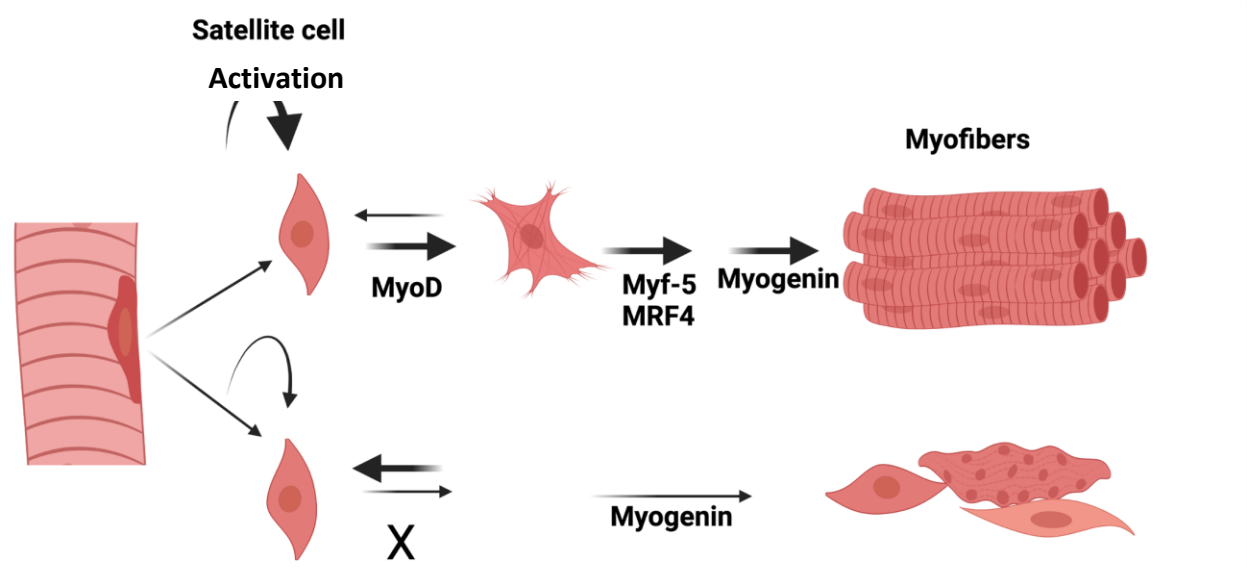

Figure 6. The role of MRFs family in myogenesis; MyoD and Myf-5 contribute with MRF4 and myogenin to induce myoblast differentiation[99]. Differentiation and fusion of myoblasts are critical in muscle recovery for muscle dystrophy/atrophy. Cellular mechanism of myoblast fusion is also important. Fusion in myoblast is cadherin, cytoskeleton, and membrane dependent. Myomaker and Myomixer, muscle-specific membrane micropipettes, are critical in myoblast fusion, non-muscle cell fusion to myoblast is induced by myomaker and is upregulated by co-expression of Myomixer. Bubbling blebs that were mentioned in the section on cell migration, were shown to have an important role in cell fusion. Membrane protrusion or bleb formation, is caused by the detachment of membrane from the underlying actin cytoskeleton in the cortical region of the cell, called the actin cortex. It was shown that phosphatidylinositol-4,5-bisphosphate (PIP2) directs actin regulators and is involved in bleb formation. Lian et al. 2020 showed that phosphatidylinositol-3,4,5-trisphosphate (PIP3) in membrane besides blebs are critical in myogenesis by rescuing differentiation defects rhabdomyosarcoma[100]. Original artwork by Z. Rovei Miab, 2021.

Extracellular matrix proteins and their signaling behavior, other than giving structural support to the cells are all important in cell behavior such as myoblast differentiation and myogenesis. Fibronectin has been established to have a more significant role in myoblast alignment and differentiation compared to other extracellular matrix proteins such as laminin and gelatin. Fibronectin effects on muscle cell development were shown in embryogenic myogenesis and muscle regeneration. Fibronectin binding effects and fibronectin expression occur through the

expression of RGD-binding integrins on myoblasts. Integrins are critical in cell migration and differentiation. In cell-cell contacts N- and M-cadherins are also critical in regard to myoblasts finding each other and fusing to form myotubes and then muscle fibers[94,100].

1.14 Myogenesis in tissue repair

In tissue repair, myogenesis starts with myogenic precursor cells (MPCs) that give rise to satellite cells. When satellite cells are activated and differentiate , they undergo processes similar to those in embryonic myogenesis[101].

Activation and proliferation of muscle progenitor cells during injury, and differentiation to myotubes to from a new muscle tissue are both critical in the muscle regeneration process. During embryogenesis Wnt signaling is important in muscle formation. This signaling pathway is also critical in myogenic differentiation and myogenic stem cell fate. It was shown the transition from Notch activation to Wnt activation is important in muscle cell regeneration. Notch signaling pathway is essential in cell-cell communication and differentiation[102]. We also know that migration of macrophages and fibroblasts to injured area, and their growth factor secretion are required in tissue repair and muscle regeneration, and this occurs in parallel with angiogenesis. From a tissue-engineering perspective, gene transfection approaches can be helpful to promote myogenesis and have now been applied in clinical treatments of peripheral limb injury and myocardial ischemia. In general, clinical gene delivery requires several factors: using an appropriate gene, an optimized matrix, and transfection within an appropriate environment are critical. The environment is established to include fibroblasts and macrophages in the injured area[103]. Transcription factors and signaling molecules involved in muscle regeneration are similar, although not identical to those which control embryonic myogenesis[96].

1.15 Transcription factors in myogenesis

Myogenic regulatory factors (MRFs) including MyoD, Myf5, myogenin, and MRF4 are basic helix-loop-helix molecules, and regulate myogenesis and control myocyte proliferation, differentiation, and sarcomere assembly during embryogenesis and postnatal myogenesis[104]. MyoD was discovered as the first muscle-specification protein in the MRF family and its discovery was important in leading to our current understanding of the differentiation process in skeletal muscle[104,105]. Embryogenesis shapes the basic structure of skeletal muscle. MRFs, especially MyoD, are now established as essential factors in muscle development, since over expression of MyoD could induce non-muscle cells to turn to muscle like cells. Skeletal muscle development

occurs by direct binding of MRFs to DNA. Embryonic myogenic progenitors are characterized by expression of key regulators of myogenesis such as Pax3 and Pax7, where Pax 3 has a critical role in early muscle formation in the embryo and Pax7 is critical in postnatal formation and muscle regeneration[105]. Expression of MyoD is induced by FoxO3, Six1/4 and Pax3 and Pax7 during myoblast proliferation. During the differentiation process when MyoD is expressed, it further induces myogenin expression and with that, Myf5 is downregulated which leads to differentiation. Expression of myogenin also downregulates expression of Pax7, which leads to specification of the cell as muscle. These activities of MyoD and myogenin also induce the expression of MRF-4 and other genes that are used in research to denote muscle differentiation, including myofilament genes such as myosin and actin. While other MRF-gene expression is downregulated, MRF-4 expression continues until muscle fibers mature[104-106].

1.16 Cell fusion and myotube formation

Skeletal muscle cells, called myoblasts, fuse to each other and form multinucleated myofibers which have their myonuclei positioned at the fiber periphery[107]. Cell membrane modification is critical in myoblast fusion, and it involves different steps, including adhesion, membrane opposition, hemi-fusion, pore formation, cytoplasmic mixing, and then the myofiber formation and myonuclear addition. There are lipid regulators and key proteins which are proven to be involved in certain steps; some steps need further investigation to prove that the proteins are engaged. In myoblast fusion stage, in the adhesion and membrane opposition phase, proteins and lipids consisting of cadherin, myomaker, Bai3, stabilin, phosphatidylserine, graf1, and ferlins are involved[108]. Actin polymerization during membrane opposition involves the following proteins and lipids: Rac, Dock, Elmo, Srf, and N-WASp. In the hemi-fusion step, myomaker, annexins, and phosphatidylserine, are engaged. In the next step, which is pore formation, myomerger and dynamin proteins are involved. Once the pore opens, the cytoplasm of the two cells becomes mixed, reflecting the “single cell” nature of a new bi-nucleated myotube[107,108].

Myofiber formation can be symmetric or asymmetric, during surgery and exercise by stimulating the muscle stem cell and activating it an asymmetric fusion of myonuclei occurs. Both myomaker and myomerger proteins cooperate in symmetric myofiber formation. During the addition of myonuclei to an existing myofiber, the activation of myomaker and myomerger is required in the myocyte, but it’s not clear if the two proteins are active on the myofiber yet[108,109].

In vertebrate animals, myoblasts fuse together to form the multinucleated muscle cell, which is a syncytial cell, called the muscle fiber. This formation would not be possible in the absence of myomaker, a skeletal muscle transmembrane protein. In fibroblasts induced to express myomerger, a second muscle-specific fusion protein, cells do not fuse; however, co-expression of myomaker will lead to the fusion[108,109]. Thus, myomaker is sufficient and essential for cell fusion. These factors are both critical to forming muscle, and act independently, as demonstrated in research on zebrafish and chick muscle. Actin polymerization is another key protein in the cell cytoskeleton during the myoblast fusion, since inhibition of actin polymerization will inhibit both myomaker and myomerger activities during myoblast fusion[108].

In an embryo, mesodermal precursor cells divide and give rise to myoblasts which proliferate further. Those cells also migrate to a specific location, before they exit the cell cycle and fuse to each other to form the multinucleated muscle fibers under the regulation of MRF-gene expression. In tissue culture, proliferating myoblasts that are switched from high-serum to low-serum culture medium will be stimulated into fusion. Another factor that stimulates myoblast differentiation *in vitro* is cell-cell contact[110].

Myotube formation occurs in two different stages *in vivo*: the first wave of myoblast fusion forms the first set of myotubes which mature into small fibers. The non-fused myoblasts remaining outside the myotube membranes lie close to the surface of primary myotubes. After a temporary delay, many of the unfused myoblasts proceed to form a second set of myotubes that mature into secondary fibers. The primary myotubes do not have satellite cells initially, and express embryonic myosin heavy chain in their initial sarcomere formation. Later, a small portion of the remaining myoblasts become satellite cells by becoming quiescent, non-cycling cells within the basal lamina surrounding both primary and secondary myofibers. The pattern of MRF expression also differs between primary and secondary myotubes in developing embryos, and myosin expression begins with the developmental myosin heavy chain isoform. While the secondary myotubes are forming, the primary myotubes will grow larger. Primary myotubes enlarge further by addition of new myoblasts and their nuclei to the fiber ends later during postnatal growth[111].

1.17 Cell cytoskeleton changes during myotube formation

The cell cytoskeleton provides strength and flexibility to cells. Striated skeletal muscle is composed of extrafibrillar, intrafibrillar, and microtubules that they all together help to the contractility and flexibility of the muscle[112]. The smallest contractile section of the muscle is the

sarcomere, which is composed of myosin and actin filaments. Boundaries of the sarcomere are called Z-disc, and I-bands are on the either side of the Z-disc which encompass the myosin thick filaments, or A-band. Therefore, actin thin and thick filaments and titin are the existing filaments in non-static sarcomere structure and have a critical role in muscle contraction[113].

Myotube formation requires a complex cytoskeletal rearrangement from the very beginning of the process which includes myoblast migration, elongation, target recognition, and fusion, and attachment to myotubes. The actin cytoskeleton has a critical role in myotube formation and attachment to locate the precise and accurate attachment site for that particular myotube. Furthermore, microtubules (MTs) showed their criteria in elongation of the myotubes during cell development in cytoskeleton. Actin and MTs coordination during the myotube formation while myotube is extending by actin-cytoskeleton in filopodia and recognizing the proper site, fusion is still happening to enlarge the myofiber with the help of MTs[114]. Elongation of myotubes might be due to MT and myotube attachments that are directed by actin filaments in filopodia. The crosstalk between actin and MTs occurs because of proteins such as myosin II, APC2, and formin proteins. An actin binding protein, RacGAP binds to anillin, an F-actin binding protein, to create the linkage between the central spindle of microtubules and the actomyosin contractile ring during cleavage-furrow formation during cell division during drosophila embryos[114].

Drosophila proteins such as PAK (family of kinases), PIX (PAK interacting exchange factor), and dGIT (drosophila homologue of GIT-1 like proteins) have a critical role in actin cytoskeleton remodeling during morphogenesis, cell migration, and cell-cell communication. As well, dGIT and PAK in a complex function, regulate muscle morphogenesis. Mutation in dGIT showed an attachment deficiency when myotubes reached the target site. It has been thought that myotubes find their target through the same actin-based mechanism. Actin-rich cell filopodia that form at the ends of actin cytoskeleton are helpful for this navigation and target reaching. Most of the genes that are critical in myoblast fusion and attachment, also regulate the actin cytoskeleton in some manner. Proteins such as Robo and Drl work together to remodel actin networks for motility and attachment at the edges of the myotubes[114].

During cell fusion, both actin filaments and MTs re-arrange, and actin molecules organize like a mixed-polarity sheet about 50 μm thick, directly under the plasma membrane. Proteins such as integrins, cadherins, and the dedicator of cytokinesis protein 1 (DOCK1) trigger the changes in

actin cytoskeleton arrangement. All three of these proteins influence on actin organization via a pattern of Rac activation that differs slightly among the three. Integrins activate Rac at the sites of cell attachment, cadherin works by activating Rac-1 through the Rho-GEF Trio when myoblasts adhere and during cell fusion. DOCK-1 influences actin rearrangement directly through Rac activation[115].

1.18 Muscle-cell differentiation and nerve dependency

In general, in order for any intact muscles to function properly, they need to be innervated and contract. A neuromuscular junction (NMJ) or synapse forms between a motor neuron and each skeletal myofiber; this connection controls voluntary muscle contraction[69,116]. Signaling molecules released from either muscle or neuron have a critical role in NMJ formation and maintenance.

Acetylcholine (ACh), one of the signaling molecules released from axon terminals in the pre-synaptic compartment of a NMJ, is a fundamental neurotransmitter. It binds to nicotinic ACh receptors (nAChRs) to initiate NMJ formation during myogenesis, and also to stimulate muscle contraction by the muscle fiber. In parallel with AChR activation by ACh binding, the roles of other signaling molecules and receptors such as agrin, LRP4, and MuSK are essential to NMJ formation, but their mechanism is not completely understood, even to this day [65-67,117].

Electrical signals carried from the motor neurons, are subsequently converted to action potential on the adjacent muscle through a series of steps including: the clustering of AChRs on a muscle fiber membrane, and secretion of ACh molecules from the motor axon terminals into the synaptic area[69,117]. The binding of ACh to the AChRs on the post-synaptic membrane changes the voltage at the sodium-potassium channels on the membrane and lets sodium enter and potassium to leave the fiber. This ion movement depolarizes the membrane and creates an action potential in the sarcolemma. This voltage change leads to calcium ion release from sarcoplasmic reticulum. Calcium binds to troponin on the actin filaments of sarcomeres, and this induces a relocation of tropomyosin molecules, which in turn causes cross-bridge formation between actin and myosin filaments. Cross-bridge formation leads to muscle contraction and force generation. This action continues until troponin and calcium release from one another, and the inhibitory effect of tropomyosin is released[69].

Components of the basal lamina and the cytoplasmic proteins inside a muscle fiber are important in AChR clustering during postsynaptic differentiation and NMJ development. Agrin, a major signaling protein in the basal lamina, is secreted from motor neurons and has a critical role

in NMJ formation, as it activates MuSK-LRP4 receptors and leads to higher AChR density on the myofiber surface[107,118]. MuSK, a member of receptor tyrosine kinase (RTK) family, binds to agrin via an intermediate protein or co-receptor (LRP4). LPR4, a single-spanning transmembrane protein, is connected to agrin via multiple hydrogen bonds and is also important in AChR clustering as it induces the interaction of MuSK and agrin[69,117].

Nuclear positioning is critical in cell proliferation, migration, differentiation and NMJ formation. A related process involves regulation of nuclear anchoring by nesprin protein cooperation with other proteins, since this process provides plasticity or flexibility of positioning for the already-anchored nuclei in a myotube. It occurs with the help of cytoskeletal elements such as microtubules, actin, and intermediate filaments and their networking with the nuclear envelope. There are five different types of nuclear positioning and movement in muscle formation, as part of the process before nuclei reach the myofiber periphery at the end of muscle fiber differentiation. The 5 types include nuclear centration, alignment, spreading, dispersion, and nuclear anchoring or clustering. Nuclear clustering is observed beneath the NMJ and may be related to the metabolic activity at the synapses or the mRNAs expressed in the region of NMJs[107]. The NMJ protein called spectrin-repeat segment of the nuclear envelope protein-1 (also called Syne-1) is concentrated in synaptic nuclei. Syne-1 is more highly expressed in synaptic nuclei than other parts of myotube. Syne-MuSK (nesprin) interactions are also involved in anchoring the nuclei beneath synaptic area. Nuclei positioning is a multi-step procedure and can be Syne-1 independent, while ANC-1 is required in positioning both mitochondria and nuclei, and in anchoring those organelles in place. However, it is still not clear if nuclei aggregation has a critical role in maintenance and maturation of NMJ formation[119].

In addition, nesprin cooperation with other proteins provides plasticity for anchored nuclei[107,118]. Nesprin in mammals can bind to MTs, actin, and intermediate filaments; this binding is one of the reasons that nesprin is involved in nuclei plasticity, positioning, and movement. Also, dynein, one of the cytoskeletal motor proteins, can bind to nuclear envelope through nesprin. In cell, dynein moves along MTs, and all these forces will be transferred to the nuclear envelope, which in the end leads to nuclear motility[107]. The alignment of nuclei occurs on a single plane in a mammalian myotube which is the first type of nuclear movement in muscle. Nesprin 1-alpha and pericentriolar material-1 (PCM-1) are also critical in nuclear alignment. These two proteins engage the centrosomal proteins to the nuclear envelope including, Cep135, the dynein-dynactin complex

and kinesin motor proteins. PCM-1 and Nesprin-1 have almost the same role in anchoring motor proteins in the nuclear envelope in myotubes. And nesprin acts at the very early stages of cell differentiation by engaging pericentriolar proteins in nuclear envelope. In nuclear spreading during myotube formation, nesprin-1 and nesprin-2 anchor with kinesin. This complex translocates the nuclei through the cytoplasm of the myotube. In nuclear anchoring, the role of nesprin is through engagement of MTs to form astral structural caging for each nucleus in its place[118].

Many modern models for studying protein-protein interaction, employ *in vivo* studies in knockout mice. *In vitro* studies, such as those involving central nervous system (CNS) neurons as they grow and polarize in a microfluidic system with a fluidically isolated environment without neurotrophins, has also been used to study particular protein-protein interactions. The culture model can simulate CNS axonal injury by applying localized treatment and/or stimulation in the culture environment[65]. Another model mimics the circuit between a lower motor neuron from the spinal cord, and an NMJ, using microfluidic devices by co-culturing motor neurons, spinal glial cells, and muscle cells[66]. An alternative model simulated the NMJ region of a muscle cell by placing motor neurons and muscle cells together in a microfluidic chamber and studying the pre- and post-synaptic domains of the newly formed NMJ regions and the role of glial-derived neurotropic factor in the co culture system[67].

One of the concerns regarding these studies is the lack of a suitable *in vitro* mammalian model to study the nuclear positioning process during muscle maturation. The role of neuron-muscle interaction in degenerative muscle disease such as muscle atrophy is complex and still an active area for research, so modeling this interaction using in an *in vitro* research tool needs further investigation and development[65-67].

Indeed, probing the detailed interaction between spinal cord neurons and skeletal muscle is hindered by a lack of an appropriate *in vitro* model to monitor that interaction in NMJs. In conventional neuron and muscle co-cultures, a basic NMJ can be formed; but, to probe more physiologically relevant questions, the complexity of NMJs must be formed in that model so that cellular and molecular interactions can be fully examined[120-123]. Culturing neurons and muscle cells separately to study the effect of exposure to external factors in each compartment through distinct and separate flows, is really important for studying NMJ formation in greater detail.

1.19 Fibronectin-integrin binding and inhibitors

Fibronectin has a minimum of ten integrin, the FN receptors which help most cells to adhere to a FN-coated surface. These interactions make FN, a key substrate protein. Cell interaction with adhesion proteins in the ECM will influence the migration, morphology, and viability of cells as well as their gene expression. Cell adhesion proteins are structurally diverse, large, and multifunctional[124]. Fibronectin is an example of a mosaic protein that is composed of three types of amino acid segments, in addition to the V-segment which has more complex connection patterns. The short hinge areas between FN domains, allow the molecule to form different shapes. The two areas in FN that control cell binding activity are: III9-10 and III14-V. The RGD sequence is one of the amino acid sequences with an adhesive motif and is placed in III10. The III9 region which cooperates with RGD, has the fewest amino acid sequences, is named the synergy peptide, PHSRN. In addition, the III14-V area is composed of two integrin, the FN receptors, each of which has three binding sites including: CS1, CS5, and H1 sequences. The affinity of the CS1 site for integrins is 20-fold higher than at the two other sites. As well, CS1 and CS5 are only present in some FN molecules, whereas the H1 site is present in many kinds of protein (Figure 7)[124].

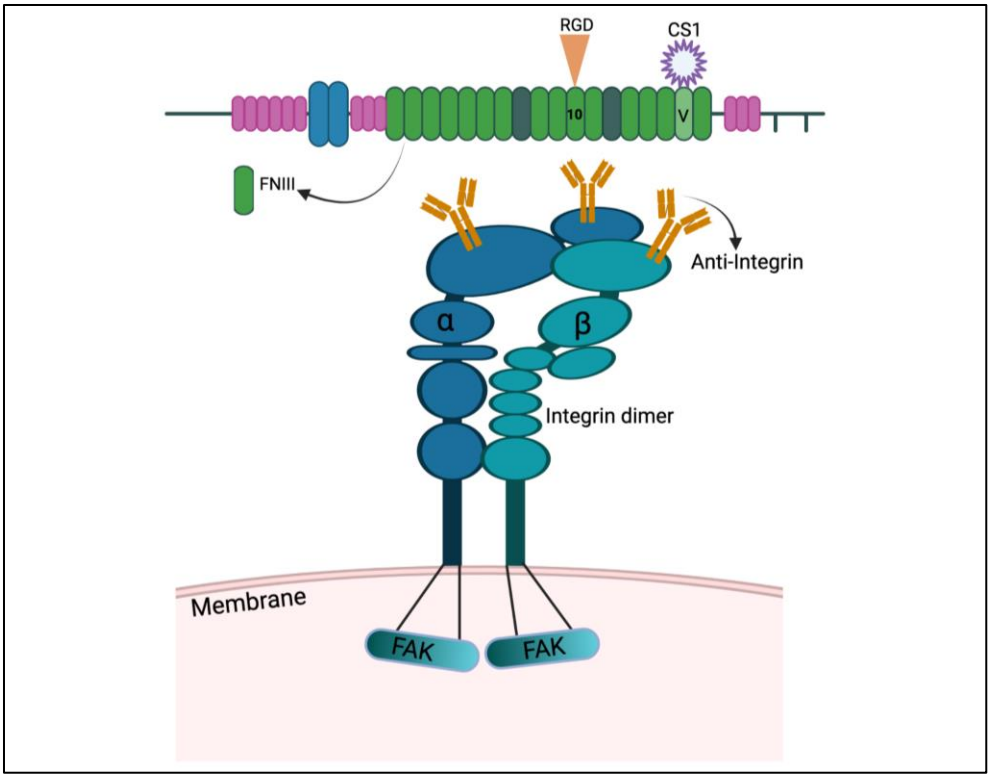

Figure 7. Fibronectin-integrin binding molecular structure. FN-Intg binding segments in the ECM can be inhibited through interfering with the ligand, by using either a fibronectin fragment (RGD peptide) or a fibronectin CS1 peptide, or by interfering with the receptor activity by blocking the binding domain of integrin dimers or inhibiting focal adhesion kinase (FAK)[125]. Original artwork by Z. Rovei Miab, 2021

My main focus is skeletal muscle cells, which are always in contact with variety of cells, although this does not exclude other cell types. In an injured muscle region, beside myoblast and expressed gene and growth factors, macrophages, peripheral blood cells, fibroblast, endothelial cells, etc. are interacting even after the complete healing process. The interaction between lymphocyte and high endothelial cell (HEC), was inhibited by the blockage of CS1and RGD peptides[126]. It is known that two ß1-integrin, the FN receptors, including α4ß1 and α5ß1are expressed in peripheral blood lymphocytes can recognize adhesion domains in FN. It was shown that migration of lymphocytes can be regulated by the selective expression of ß1-integrins[126]. Cell migration can be directed in higher level with α5ß1, by showing that in α5 subunits replacement, cells could still attach but not migrate, even though the ß1 subunit didn't change[127]. It was shown

that FN segments can link to the growth factors, direct the epithelial to mesenchymal transition, impact on stem cell differentiation which makes FN an important protein in wound healing and tissue engineering[127].

In regenerating muscle, loss of FN can reduce the muscle stem cells function via protein tyrosine kinase 2 (PTK2 or FAK) pathway by affecting on integrin signaling[128]. Aging in muscle can downregulate the FAK expression and reduce the adhesion. FAK can be activated with FN through integrins bindings. FN also improved the attachment of aged muscle stem cells compare to the collagen and laminin[128]. In this study, adhesion capacity of aged muscle stem cells was examined by loading cells on CN and FN in presence of FAK inhibitor. Compared to the control sample, the number of the attached young muscle stem cells to each substrate was low in presence of FAK inhibitor. In addition, responsiveness of aged cells cultured on CN to FAK inhibitor was lower than aged cells loaded on FN. This agrees with the fact that activity of FAK is lost in aged muscle cells and can be upregulated by presence of FN[128].

FAK an important attachment site between ECM and cells were inhibited in bone cells to investigate whether or not they can moderate the mechano-transduction with two different methods: MC3T3-E1 osteoblast cells were cultured on a soluble without integrin binding sites like bovine serum albumin (BSA), or after culturing cells on FN blocking the FN-I binding sites with Arg-Gly-Asp-Ser (RGDS) peptides[129]. After treatments, they exposed the cells to fluid shear stress and measured the cyclooxygenase 2 (COX-2) and prostaglandin E2 (PEG2) pathways which are critical in bone formation with mechanical induction. In cells treated with RGDS, both COX-2 and PGE2 were reduced compared to the control. But FN was secreted from cells cultured on BSA and FAK formation increased over time in these cells and induced COX in response to fluid shear stress. FN can induce FAK and that can moderate PGE and COX-2 in osteoblast cells[129].

The current deficiency in our understanding of the migratory behavior of myoblasts and their interaction with ECM proteins limits the application of tissue engineering approaches to solving broader issues of how to promote muscle regeneration. Addressing that gap requires highly controllable experiments that simulate potentially therapeutic microenvironments. Such a microenvironment can be investigated through novel designs and experimental protocols using microfluidic devices.

2. Rationale and hypothesis

Effective muscle repair relies on myoblasts and local chemical and fixed gradients. Muscle stem cells (myoblasts) are activated by hepatocyte growth factor (HGF) before they can migrate and fuse into myotubes (new muscle fibers). Since C2C12 cells behave as myoblasts that move and fuse in culture, they are useful for exploring how soluble HGF and fixed collagen (CN) or fibronectin (FN) cues regulate migration. Microfluidic devices allow exquisite regulation of conditions where cells move. Controlling chemical gradients in such devices is much improved over traditional studies of chemotaxis, cells responding to soluble cues. Fine-scale substrate deposition in the cell-migration channel can also model extracellular matrix (ECM) proteins (CN, FN) where cells move. Best of all, a chemical gradient can be presented above a substrate to find their combined impact on migration.

Myoblast migration depends on the dose of HGF which makes movement faster and straighter. Since both myoblasts and the ECM around fibers release HGF, regenerating muscle is a complex mixture of HGF and ECM gradients, both influence myoblast responses and impact repair. In testing myoblast transplantation to promote muscle repair, cells migrated only 200μm; these early trials failed as the importance of cell migration in cell-based therapies was obvious 50 years ago. However, the hierarchy of haptotactic-ECM and chemotactic-HGF gradients in regulating myoblast migration is unknown. Proposed research aims to understand HGF gradient interactions with ECM composition during myoblast migration, the effects of naturally produced substrate on myoblast behavior, and the potency of interrupting FN-I binding interactions on myoblast behavior and migration during myotube formation.

The first hypothesis of this PhD project was that myoblasts respond differently to a uniform HGF than to a formed gradient HGF in D3 chip and their migratory behavior is influenced by underlying substrate configuration, either in a gradient or as a uniform substrate. Experiments related to this hypothesis are presented in the section titled Results chapter 1, now published.

The second hypothesis of this PhD dissertation has two parts: a) that normal extracellular matrix (ECM) made by myotubes formed by C2C12 myoblasts and fused C2C12-cell myotubes after fusion in a microfluidic device, would modify myoblast migration differently than an artificial or applied ECM substrate; and b) that one or more of my four new microfluidic devices would better promote myoblast fusion in a migration channel. In order to test these ideas, I designed experiments in which a second set of pre-labelled myoblasts could be seeded on top of

an initial set of differentiated myoblasts, and their migration behaviour tracked to determine their preference for a natural substrate produced by the differentiated cells and the influence of an applied fibronectin substrate. Experiments allowed the study of time- and myotube-dependent changes in myoblast migration behaviour and shape. Experiments related to this hypothesis are presented in the section titled: Results chapter 2.

The third hypothesis was that inhibition of FN and its binding integrin receptors on cell membranes, would impact myoblasts and myotube signaling that promotes fusion. Experiments were designed to investigate how the FN binding and inhibitors would influence the behavior of a second set of cells in interactions with a first set of cells that was seeded and then differentiated over a naturally produced substrate or a substrate coating of FN applied to the device. These experiments utilized one of the four devices tested in Results chapter 2, as it had best promoted the alignment of set-1 cells and the migration of set-2 cells toward set-1 nuclei, a key component of fusion into myotubes. The influence of four different inhibitors to block FN-integrin interaction, including an inhibitor of focal adhesion kinase (FAK), the kinase, a blocker of the type III connecting segment in the cell attachment domain in FN (CS1), and a blocking antibody of the integrin binding site (anti-integrin). All these peptides were hypothesized to influence the myoblast migratory process. Treatments were applied in a device (previously called Device1 in the earlier experiments described in Results chapter 2) that has offset rows of pillars and showed the largest proportion of set-2 cells closer to the nuclei of set-1 cells than to pillars in the device channel. Experiments related to this hypothesis are presented in the section titled: Results chapter 3.

This project was undertaken to address a major gap in our understanding of myoblast migration as a tool that could be used through tissue engineering approaches, how to use knowledge of myoblast behaviour to promote muscle wound repair. Applications of results to bioengineering and biotechnology fields could help produce large-volume muscle “patches” to treat traumatic wounds or tissue loss.

3. Traction and attraction: Haptotaxis substrates collagen and fibronectin interact with chemotaxis by HGF to regulate myoblast migration in a microfluidic device. Results-1

Roveimiab Z, Lin F, Anderson JE. Am J Physiol Cell Physiol 319: C75–C92, 2020. First published April 29, 2020; doi:10.1152/ajpcell.00417.2019.

For this published paper: FL and JA funded the research; ZR, FL, and JA designed the experiments; ZR conducted the experiments, collected and analyzed the data, and graphed the results; ZR drafted the manuscript; and ZR, FL, and JA edited the manuscript.

3.1 Abstract

Cell migration is central to development, wound healing, tissue regeneration, and immunity. Despite extensive knowledge of muscle regeneration, myoblast migration during regeneration is not well understood. C2C12 mouse myoblast migration and morphology were investigated using a triple-docking polydimethylsiloxane-based microfluidic device in which cells moved under gravity-driven laminar flow on uniform (=) collagen (CN=), fibronectin (FN=), or opposing gradients (CN-FN or FN-CN). In haptotaxis experiments, migration was faster on FN= than on CN=. At 10 hr, cells were more elongated on FN-CN and migration was faster than on the CN-FN substrate. Net migration distance on FN-CN at 10 hr was greater than on CN-FN, as cells rapidly entered the channel as a larger population (bulk-cell movement, wave 1). Hepatocyte growth factor (HGF) stimulated rapid chemotaxis on FN= but not CN=, increasing migration speed at 10 hr early in the channel at low HGF in a steep HGF gradient. HGF accelerated migration on FN= and bulk-cell movement on both uniform substrates. An HGF gradient also slowed cells in wave 2 moving on FN-CN, not CN-FN. Both opposing-gradient substrates affected the shape, speed, and net distance of migrating cells. Gradient and uniform configurations of HGF and substrate differentially influenced migration behavior. Therefore, haptotaxis substrate configuration potently modifies myoblast chemotaxis by HGF. Innovative microfluidic experiments advance our understanding of intricate complexities of myoblast migration. Findings can be leveraged to engineer muscle-tissue volumes for transplantation after serious injury. New analytical approaches may generate broader insights into cell migration.

3.2 Introduction

Successful muscle repair depends on stem cells and the chemical and structural

microenvironment. Muscle stem or satellite cells are activated by injury through a cascade involving nitric oxide, hepatocyte growth factor (HGF) [130-133], and Wnt and Notch-Delta1 signaling [134,135]. The surrounding extracellular matrix (ECM) presents growth factors to cells via components including glycosaminoglycan, proteins and hydroxyapatite [136]. HGF binding to its receptor, c-met, on satellite cells initiates cell cycling and migration [137,138]. In muscle regeneration, satellite cells emerge through the ECM that surrounds fibers, by processes mediated by nitric oxide and Wnt signaling involving changes in cell shape [139].

Myogenesis is often modeled *in vitro* using mouse C2C12 myoblasts, which will migrate, differentiate and fuse similar to activated satellite cells [70,71] during muscle repair *in vivo* [137,138,140]. C2C12 myoblasts respond in culture, to fixed gradients of ECM proteins (haptotaxis) and growth factors [141,142]. HGF or scatter factor, promotes cell migration in cancer metastasis and myoblast motility in cultures of cells and isolated muscle fibers, and *in vivo* [25]. Myoblasts *in vitro* show a dose-dependent migration response to HGF [131]. On cultured fibers, migration by activated satellite cells is faster and more one-directional when stimulated by HGF [138].

HGF is released from 2 sources after muscle damage *in vivo*: the ECM around fibers (a linear or cylindrical source) and single myoblasts (a point source) [130]. Thus, structural features of the local tissue form a complex of HGF gradients overlain on a mixture of adhesive, stabilizing matrix proteins such as fibronectin (FN) and collagen (CN). During regeneration, this pattern of HGF, FN, and CN influences myoblast responses, including their motility. The pivotal role of myoblast migration was shown in early transplantation trials to promote muscle repair: cells migrated only 200μm before differentiating [143], which accounted for the failure of the approach toward repairing muscle wounds or treating disease. Despite this understanding the importance of cell migration in the designing cell-based disease treatments for over 50 years [144], the hierarchical regulation of myoblast migration by interacting gradients of haptotactic ECM and chemotactic HGF is not understood.

Microfluidic devices were previously used in our laboratory to model tissue conditions in which adipose-derived stem cells responded to gradients of epidermal growth factor (EGF). Cells were visualized as they encountered a controllable gradient of EGF, thought to regulate their behavior [68]. Microfluidic devices are manufactured to allow real-time microscopy studies of cell migration [140,145]. Devices typically have inputs for fluids and cells, and importantly include separate "docking" channels from which cells can move into migration (flow) channels containing

a stable chemokine gradient in the presented medium.

The present study explored potential interactions of chemotaxis by HGF and haptotaxis by the ECM substrate composition during myoblast migration. Cell movement and behavior were investigated using a two-dimensional (2D) microfluidic device to test the hypothesis that the behavior of migrating myoblasts responds differently to a gradient of HGF than to uniform HGF and is further influenced by the configuration of CN and/or FN in the underlying substrate.

3.3 Materials and Methods

3.3.1 Cell preparation

C2C12 mouse myoblasts (catalogue# CRL-1772, RRID: CVCL_0188, American Type Culture Collection, Manassas, VA) were cultured in Falcon flasks (50cc, VWR Fisher, Mississauga, ON, Canada) for up to 20 passages in high-glucose growth medium containing Dulbecco's modified Eagle's medium (11965092, ThermoFisher Scientific, Grand Island, NY), 10% fetal bovine serum (SH3039603, ThermoFisher), and 1% penicillin streptomycin (CA45000-652 PS, VWR, South Logan, UT) under 5% CO_2 at 37 °C and 95% relative humidity. Cells were detached from flasks using trypsin and counted. Since cell density influenced morphology and migration behavior (low cell density limited cell-cell contact, essentially prevented mobility, and led to cell detachment), a standard 1000 myoblasts were seeded into each cell-loading port in a microfluidic device.

3.3.2 Preparation of the microfluidic device

A previously developed microfluidic device called a D3 chip [80] was used for experiments on chemotaxis to HGF and haptotaxis to ECM proteins. Standard photolithography and soft-lithography were employed to fabricate the device: two-layer photolithography produced the cell-docking structure as the first layer (10 µm thick) and flow channels as the second layer (60 µm thick), modified from previous reports, to allow movement of the large C2C12 myoblasts. The three microfluidic channels were coated with ECM substrate and C2C12 cells were seeded in the device (10^6 cells/ml of medium), loading 1 µl of cell suspension per port. Devices were placed on the heated stage of an inverted fluorescence confocal Nikon Ti-U microscope (Nikon Canada, Inc., Mississauga, ON, Canada) within a stage chamber (at 5% CO_2, 95% relative humidity, and 37 °C), to maintain culture conditions as above. The three channels in a device were photographed in a single image using a 10X objective lens for phase-contrast optics, every 15 minutes for 24 hours. Images were compiled into 24-hour time-lapse videos for observation. Measurements were taken

on every fourth image (60-min intervals) to track features of cell behavior.

3.3.3 Haptotaxis experiments

Channels were coated uniformly (designated as "=") with either collagen (CN=) or fibronectin (FN=) to generate a solid substrate immediately prior to seeding cells in the device [146]. Rat tail CN type-1 (cat. #5153-1KIT, BioMatrix, San Diego, CA) and human FN (cat. #6221021, Corning, Bedford, MA) were prepared (100 μg/ml) in phosphate-buffered saline (PBS). Migration channels were coated by perfusing through the two loading ports of each channel, with either FN or CN for 1 hour at 4°C. After 1 hour, the inlet supplies of CN or FN were disconnected and bovine serum albumin (0.04% in PBS) was added retrogradely through the outlet ports for 1 hr. at room temperature, to remove excess non-gelled protein. Cells were then injected into the loading ports, from which they moved into the docking areas and then the migration channels and were observed and photographed using phase-contrast optics at 15-min intervals for 24 hrs. in time-lapse mode.

In other experiments, channels were coated with one of two opposing-gradients formed by perfusing the two substrates, FN and CN, through one port each, for the migration channels. Labeled substrates, rhodamine-labeled FN (100μg/ml, FNR01-A, Cytoskeleton, Denver, CO) and fluorescein isothiocyanate (FITC) -conjugated water-soluble CN-1 (100μg/ml, AS-85111, ANASPEC, Fremont, CA), were applied in representative experiments to identify the position of each protein and the interface of the two in ECM-substrate gradients established in two different directions. Starting from their entry into the migration channel, cells encountered an opposing gradient profile that was first CN then FN (denoted CN-FN) or first FN then CN (FN-CN) as they migrated across the channel.

3.3.4 Chemotaxis experiments

Human recombinant HGF (Sigma, H1404, Saint Louis, MO) was used as the chemotaxin. HGF was prepared at 2.5 ng/ml (2.5HGF) or 10 ng/ml (10HGF) in growth medium with plain growth medium serving as a control (0HGF). HGF-containing medium was added to inlets of the device after cells were seeded into the docking channels.

In other experiments, a gradient of HGF (designated in text as "∇" in graphs) was established by gravity flow. HGF was perfused at a particular concentration into one inlet port while control medium (without HGF or 0HGF) was added to the second inlet port for that channel; as the flows from the two inlets met in a cell-migration channel, a gradient was established (e.g.,

2.5∇ denotes a gradient from 0-2.5 ng/ml across the channel from bin 1 (low) to bin 10 (high). To confirm the presence of an HGF gradient, representative experiments were conducted in which the HGF solution was mixed with FITC-conjugated dextran (70 kDa, FD70S-100MG, lot# SLBT8689, Sigma) to enable indirect evaluation of a protein moiety similar in size to HGF. Fluorescence images of the gradient across the cell-migration channel were taken at selected times (every hour from 0-5 hours, and at 10 hours) to minimize damage to cells from repeated exposure to ultraviolet illumination during the longer experiments. Fluorescence intensity across the channel was measured using NIH ImageJ to give the average intensity at each pixel width (0.92 μm) across the channel (normalized as a percentage of the channel width) through a standard area.

3.3.5 Combined effects of HGF chemotaxis and a haptotaxis substrate

In a final set of experiments, device channels were coated with CN= or FN= or one of the two opposing-gradient substrates, CN-FN or FN-CN before cells were introduced in the presence of an HGF supply (2.5HGF=, 2.5HGF∇, or 10HGF∇) or control medium (0HGF) within the coated cell-migration channels. Again, net migration distance was monitored using time-lapse videos captured every 15 min over 0-24 hours by tracking cell position and cell structure.

3.3.6 Cell-tracking analysis

Cells were tracked in each video frame using NIH ImageJ, as they migrated across the 240-μm wide channels of the device. The image of each migration channel was sub-divided into 10 equidistant 24-μm bins. In a given experiment, for each of the 20-300 cells tracked per channel, the cell's distance into the channel and position were recorded using Excel spreadsheets (Microsoft Office). Migration in a channel was tracked over time by two approaches: by measuring the position of the cell nucleus (regardless of cell shape or spread), and in a subset of experiments, by measuring the furthest distance into the channel observed for the cell's leading edge (defined as the most forward position of the longest cellular extension into the migration channel), travelling initially away from the docking area.

A histogram of movements by individual cells over time in an experiment was initially graphed for each bin using Excel to construct a "histogram-by-time" (HT) plot of the frequency distribution of the proportion of cells located in each bin of the 10 bins over time. Secondary analysis of HT plots was used to follow the progress of migration by calculating the migration speed of cells. Plotting the changes in the proportion of cells in the channel that were located in representative bins near the start of migration (bin 2) and in the middle of the migration channel

(bin 6) over time, termed "derivative plots" were used to reveal time-dependent shifts in cells as they moved in the waves observed in HT plots, from each bin into the next bin, stayed in a bin, or moved back toward the loading dock, defined as "directional movement" by cells. The direction of cell movement was only evaluated for movement across the channel (i.e., movement along the channel was not assessed). Derivative plots show the mean times (starting at time=0 hr.) to a peak or valley in the curve; these two points on the curve were identified as times when the derivative of the curve=0: the first wave in forward migration (TTP+, "wave 1 peak") and the minimum value in migration just as the second wave in migration into that bin begins (TTP-, "wave 2 start"), under each condition. TTP+ and TTP- served to represent the migration speed of cells at these two times through two representative bins, bins 2 and 6. Derivative plots for later experiments were derived from data without generating HT plots. Migration speeds at wave-1-peak and wave-2-start times (in text referred to as wave-1 and wave-2 migration speeds) were determined for cells migrating under various conditions of a) chemotaxis by HGF (uniform (=) or as a gradient, ∇, in medium), and b) haptotaxis by CN and FN (uniform coating (=), or in an opposing-gradient as a profile of CN-FN or FN-CN). Migration speeds in chemotaxis experiments on CN=, FN=, CN-FN, and FN-CN were graphed and analyzed at 10 hours (when most but not all conditions resulted in movement through both bins 2 and 6) and at the end of experiments (24 hours). Influences of substrate and/or HGF on cell migration speed across the bins were studied by determining changes in cell migration speed for wave-1 and wave-2 movements in derivative plots over time and among conditions. Migration speed was therefore determined only for cells in two bins at two different times.

The size of the population of cells, termed bulk-cell movement, was determined for cells migrating in bins 2 and 6 at 10 and 24 hrs. Bulk-cell movement was calculated as the proportion of total cells in the migration channel, that were located in a particular bin at the times of TTP+ and TTP- for cells moving in waves 1 and 2, respectively, in the derivative plots for that bin during a migration experiment.

Net migration distance under various conditions was calculated for the bulk-cell movements across bins. This net distance travelled across the channel from bin 1 to bin 10 by each cell in the channel was determined over the first 10 hr. and at the end of 24 hr. of each experiment (net distance =sum of (distance to bin n) X (#cells in bin n) for n=1-10 bins) as cells moved progressively into and across the migration channel. Net migration distance was therefore related to all cells in a channel at a given time.

Observations of cells migrating on opposing-substrate gradients (in the absence of chemotaxis by HGF) suggested that cell morphology changed on that substrate profile as cells moved from one substrate to another. Shape factor (SF) was measured as SF=cell perimeter divided by the square root of cell area, to assess the observation 10 hours into the experiments. By tracing the clearly discernable perimeter of cells, the calculated SF values of cells migrating from CN-FN and FN-CN were compared to evaluate whether there was a potentially significant difference in cell morphology during migration under those two conditions.

3.4 Data analysis

Multiple independent experiments were used to study each condition, since use of the 3 channels of each D3 chip was configured to examine 2 variations plus a control condition in a single experiment. Since inlet and outlet ports of each migration channel were unique, this approach produced data from 2-7 independent experiments for statistical analysis of cell responses to each condition of substrate and/or HGF. Data (reported in text as mean ± standard error of the mean, SEM), were plotted as box-whisker plots showing median, mean, first and third quartile, and maximum and minimum values.

The progression of cells across migration channel was examined by studying changes in the frequency distribution of cells across the 10 evenly-spaced bins of the device channels, represented numerically in HT plots of cell proportion in each bin over time, were evaluated using Chi-squared statistics. Potential changes in migration speed, bulk-cell migration, and net migration distance were evaluated using analysis of variance (ANOVA) with post hoc Tukey's tests for pairwise comparisons, as appropriate. SF data, the time of entry into a bin, and comparisons of two groups were compared by two-tailed t-tests (paired or unpaired, as appropriate). Results were considered significant at a probability of $p<0.05$.

3.5 Results

3.5.1 Haptotaxis on a uniform substrate

Myoblast migratory behavior in the D3 chip for cells moving across a migration channel, varied on the two uniform substrates, CN= and FN=. There was less progressive movement of cells on CN= than on FN=, as shown in imaging through the 24-hour time-course of experiments (Figure 8A, 8B) and by "HT plots" of cell migration (Figure 8C, 8D). Cell morphology was observed after setup and in time-lapse video images. Cells were rounded immediately after loading into the docking area at the start of each experiment (0-hr panels in Figures 8A, 8B). Cells quickly

flattened as they attached to the substrate and aligned in the docking area, next to the barrier with the migration channel. Flattening was particularly notable in cells migrating on the FN= substrate. Some cells divided and their cytoplasm expanded before they moved entered the cell-migration channel by passing under the narrow opening in the barrier, producing extensions and/or moving the entire cell body into the channel. On FN=, cells also displayed long cytoplasmic extensions reaching toward the other side of the channel and at different angles to the length of the migration channel, making contact with the cytoplasmic extensions and/or cell bodies of other myoblasts.

HT plots illustrate the time-course of cell migration through various bins across a migration channel; the time at which cells moved into a particular bin is depicted as the timepoint (on the x-axis) at which the curve for that bin, rises above zero (on the y-axis). Cell position was tracked according to the location of the cell nucleus during movement. Overall, HT plots show cell progress across a migration channel as sequential waves of cells tracked through their sequential movements into each bin over time. Figure 8C, 8D show plots for bins 2-5, with curves representing bins 6-10 omitted for clarity. Complete HT plots for the same two experiments, that show the proportions of cells in all 10 bins, are presented in Supplementary Figure S1 at https://doi.org/10.5203/FK2/Y1KK0O [147]. Progressive movement is shown by significant time-dependent changes in the frequency distribution of cells across bins of the channel (Chi-square, $p<0.001$ for both CN= and FN=). Few cells moved further than bin 5 (144 µm) on CN=, while many moved into bin 8 (192 µm) or further on FN=. All comparisons between the two substrates for cell distributions in the same bin were significantly different for bins 3-10 (Chi-square, $p<0.01$). From direct observations, cells moved from bin 1 toward bin 10, although some could move part way across the channel and either stop in that bin or move backward to a previous bin, and then resume movement toward bin 10. These movements were consistent with the up- or downward changes in curves of the HT plots denoting cell proportion in each bin.

3.5.2 Haptotaxis on opposing gradients of CN-FN and FN-CN

Potentially competitive effects of CN and FN substrates on myoblast migration were evaluated by generating opposing gradients of CN and FN across the microfluidic migration channel. Gradient configurations were verified as stable using densitometry tracings of fluorescence intensity from rhodamine-labeled FN and FITC-conjugated CN in the channels at the beginning and the end of the experiment (Figure 9A, 9B). Representative time-lapse videos of C2C12 myoblasts migrating on each of the four substrates are available in Supplementary Figure

S2A-F at https://doi.org/10.5203/FK2/Y1KK0O [147].

Initial observations of cell movement were considered using HT plots for cells in two representative channels and suggested different distributions of migrating cells on the two opposing-gradient substrates, CN-FN vs. FN-CN. Tracked by the position of their nucleus, cells migrating on CN-FN progressed from high CN all the way to bin 10 in the highest FN concentration over 24 hr. By 10-12 hr. on CN-FN, cells were present in the first 5 bins (Figure 10A only shows the distribution of cells in bins 2-5, for clarity). Tracking the same cells by their leading (front) edge (Figure 10B) shows cells were somewhat polarized as they moved toward FN, as the cell leading edges reached bins 3, 4 or 5 from 3, 7 or 4 hr. before the nuclei in this single channel (comparing Figure 10B to 10A).

The HT plot for the nuclei or cells migrating in a channel coated with the FN-CN opposing-gradient substrate, shows that cell nuclei did not enter bin entered bin 2 about 2 hr. later than on CN-FN, and only entered bin 3 at 14 hr. compared with 6 hr. on CN-FN (Figure 10C vs. 10A). In the channel of FN-CN, the leading edges of cells reached bins 3 and 4, 4 and 6 hr. earlier than the nuclei (comparing Figure 10D to 10C) and moved only as far as bin 7 (192 µm) by the end of the 24-hr experiment. HT plots for the same two experiments represented in Figure 10 are provided as Supplementary Figure S3 and show the proportions of cells in bins 2-10 at https://doi.org/10.5203/FK2/Y1KK0O [147]. These comparisons suggested cells might be polarized during migration, possibly more on FN-CN than CN-FN, as leading edge of cells moved further into the channel than cell bodies, and cell bodies were only observed up to bin 7 over 24 hr.

3.5.3 Derivative plot analysis of haptotaxis on 4 substrates

Derivative plot analyses confirmed earlier observations that cells moved into a bin (positive change in cell proportion) and out of a bin (negative change in cell proportion) within migration channels over time. Thus, each bin demonstrated both positive and negative peaks in the proportion of cells located there for the 24-hr experiment. Cell migration speed was determined from the time (on the x-axis) of the first maximum (TTP+) and first minimum (TTP-) values on the curve for cells in waves 1 and 2, respectively, to reach a particular bin. A representative derivative plot (Figure 11A) shows cell movement represented as initial increases and later decreases in the proportion of cells (y-axis) in bins 2 (48 µm) and 6 (144 µm, the mid-channel bin) for an experiment on FN=, where cells were tracked by the position of their nucleus.

Derivative-plot analysis from each experiment was derived from data in the respective HT

plot (Figure 11A) before TTPs of waves 1 and 2 were compiled from multiple experiments to assess substrate effects on migration speed. Migration speed in bin 2 at 10 hr. (Figure 11B, 11C) did not vary significantly by substrate for cells in either wave 1 or wave 2. However, in bin 6 in the middle of the channel, cells migrated slower (larger TTP values) on FN-CN than other substrates. There was no movement in bin 6 on either CN= or CN-FN in either wave 1 or 2 at 10 hr. At 24 hr., migration speed again did not differ on the different substrates in bin 2, although migration in wave 1 on the opposing gradients tended to be faster (i.e., smaller TTP values) than on the two uniform substrates (Figure 11D). At bin 6, however, there was no wave 2 of cells on CN-FN, while movement by cells in wave 2 on FN-CN was faster than on CN= (ANOVA $p=0.03$, Tukey's test $p<0.01$) (Figure 11E). Migration speed tended to be slower (i.e., larger TTP) at bin 6 than at bin 2 at 24 hr. (compare 11E vs. 11D).

There were generally more cells moving on uniform CN= and FN= than on opposing gradient substrates in bin 2 at 10 and 24 hr. although the within-group variability was greater on the uniform substrates (Figures 11F-I). Absence of bulk-cell movement in bin 6 at 10 hr. on CN= and CN-FN indicated cells on those substrates had not entered the bin. At 24 hr., bulk-cell movement at bin 6 was significantly higher on FN= than on other substrates in both waves 1 and 2 (Figure 4I). While fewer cells reached bin 6 than bin 2 in migration on CN-FN, the complete lack of wave 2 in bin 6 on CN-FN at either 10 or 24 hr. (Figures 11C, 11E) demonstrated that once cells reached the higher-FN aspect of a migration channel, they stayed there.

Since migration speed varied in the 2 waves of migration and in bin 6, by substrate, the net distance cells migrated under different conditions was assessed. Net migration distance was calculated for every cell within the migration channel at 10 and 24 hr. of the experiments. Net migration distance differed significantly by substrate (ANOVA, $p<0.0001$, a total of 372 cells tracked) (Figure 11J). Cells moved a greater distance on FN= and FN-CN than CN= or CN-FN (Tukey's tests, $p<0.001$). At 10 hours myoblasts on FN= had traveled more than twice as far across the 240-μm channel compared to cells moving on CN=. Cells also moved almost twice as far when migrating on FN-CN compared to cells migrating on CN-FN, as cells moved more in bulk on FN-CN at 10 hr. and did not move on CN-FN in bin 6 at that time. At 24 hr., net migration distance was also greater on FN= than on all other substrates (Tukey's tests, $0.01<p<0.05$). The maximum-to-minimum range of datasets was greater on uniform substrates (Figure 11F-I) possibly due to

reduced directional guidance on an artificially imposed pure substrate *in vitro*, in the absence of a substrate-gradient configuration, as would be expected *in vivo*.

Haptotaxis experiments demonstrated that myoblast motility showed haptotaxis responses to substrate cues, and further showed that the impact of an opposing-gradient substrate on cell migration was complex: regardless of the time of cell movement (wave 1 or wave 2) in the region of the substrate overlap (including bin 6), the response was distinctive from cell responses to either of the uniform haptotaxis substrates. Comparisons of uniform vs. opposing-gradient substrates suggested that the substrate that cells first encountered when moving into the migration channel (e.g., CN on both CN= and CN-FN, and FN on both FN= and FN-CN) influenced the net distance they traveled.

3.5.4 Shape factor

Since comparisons of cell position by tracking nuclei vs. leading edges suggested the possibility of cell polarity on opposing-gradient substrates, cell configuration was further investigated. Real-time observations suggested cells elongated more on CN when they were moving from FN-CN than in channels where they were migrating on the inverse opposing-gradient substrate, CN-FN (Figures 12A, B). These changes in cell morphology occurred while cell bodies occupied bins close to the loading dock, when the relative proportion of FN was low in the CN-FN substrate, approximately 20-30% of the substrate, as estimated from relative fluorescence intensity in the opposing-gradient substrates (Figure 9B). Shape factor was measured for cells in the migration channel in 5 independent experiments. For cells migrating from FN-CN, SF was significantly larger, indicating the cells were more elongated than those migrating on the inverse substrate, from CN-FN (t-test, $p<0.05$).

3.5.5 Chemotaxis on a uniform substrate

Potential interaction of a chemotaxin with a uniform substrate, either CN= or FN= were first evaluated by examining effects of various configurations of HGF (uniform, or a shallow or steep gradient across the channel vs. the control without HGF) on myoblast migration using the microfluidic D3 chip.

Densitometry studies of FITC-dextran fluorescence intensity over time established that HGF gradients were stable, since the gradient slope did not decay for at least 5 hours (Figure 13). During observations of cells and their movement, any HGF gradient was refreshed at 5 hours and 10 hours, to maintain stability overnight. While some HGF conditions showed no movement

within the first 5 hours of gradient stability, most showed cell migration into and past the middle of the migration channel (bin 6) by 10 hours. Migration speed, net migration distance, and bulk-cell movement were evaluated at 10 and 24 hours to study cell-migration responses to combinations of HGF-chemotaxis and substrate haptotaxis.

In the presence of HGF, myoblasts moving on uniform substrate again showed two (or more) waves of migration through bins 2 and 6 over time. However, in the presence of HGF, migration speed, net migration distance, and bulk-cell movement differed between CN= and FN= substrates (Figures 14 and 15, respectively).

3.5.6 Fibronectin substrate

Migration speed by cells in wave 1 moving on FN= through bin 2 at 10 hr was more rapid in a steep HGF gradient than without HGF, or in a shallow gradient of HGF; migration speed of cells moving in wave 2 did not vary by HGF condition (Figure 14A). At bin 6 on FN= (Figure 14B), there was no migration in either direction for cells moving in a shallow HGF gradient or uniform HGF (ANOVA, $p=0.0002$ wave 1; $p=0.00007$ wave 2).

Net migration distance on FN= (Figure 14C) was less in uniform HGF than without HGF or in a steep HGF gradient (ANOVA $p<0.0001$, Tukey's tests $p=0.001$), possibly as HGF has a potent unidirectional influence. Bulk-cell movement in both waves 1 and 2 at 10 hr. in bin 2 (Figure 14D) was also affected by the HGF conditions. Cells moved more in bulk in a shallow HGF gradient than in control medium or uniform HGF (ANOVA $p=0.05$, Tukey's tests $p<0.05$). Bulk-cell movement by wave 2 at bin 2 and 10 hr. was lowest in uniform HGF than in control medium or either HGF gradient (ANOVA $p=0.04$, Tukey's tests, $0.01<p<0.05$). Bulk-cell movement at bin 6 at 10 hr. showed similar effects of HGF, being larger on a steep gradient than in control conditions in both wave 1 and wave 2, although at much lower levels (ANOVA, $p=0.004$ wave 1, $p<0.01$ wave 2, Tukey's tests $0.006<p<0.05$) (Figure 14E).

At 24 hrs., migration speed in bin 2 was not affected by HGF conditions (Figure 14F), while at bin 6 speed was slower in wave 2 in uniform HGF than in a shallow HGF gradient (ANOVA $p=0.05$, Tukey's $p<0.05$) (Figure 14G). Net migration distance did not vary by HGF condition at 24 hrs. (Figure 14H). Bulk-cell movement in both migration waves varied greatly at 24 hr. in bins 2 and 6 (Figures 14I, 14J).

Overall, on a uniform substrate of FN, cells moving in either wave 1 or 2 at bin 6 either did not move at 10 hr. or moved (or tended to move) more slowly at 24 hr. in uniform HGF than in a

shallow HGF gradient. This slowing by uniform HGF on a FN= substrate, resulted in a small net migration distance after 10 hours compared to other HGF conditions. By 24 hr., cells migrating on FN= in uniform HGF had "caught up" with cells in the other HGF conditions, and since wave 2 movement was small in uniform HGF at 24 hr., net migration distance at 24 hr. did not differ among groups.

3.5.7 Collagen substrate

Cell migration behavior on a CN= substrate was significantly different from that on FN=. Although HGF conditions did not affect the 10-hr migration speed in bin 2 (Figure 15A), cells notably did not move at all, in bin 6 at 10 hr. (Figure 15B). Net migration distance on CN= was therefore low over the first 10 hours (Figure 15C), which differed markedly from the influence of HGF on FN= (compare with Figure 14). Bulk-cell movement through bin 2 at 10 hr. was not affected by HGF conditions in either wave 1 or 2 (Figure 15D). However, in bin 6 (Figure 15E) cells moved more as a population in the steep HGF gradient than in the three other conditions for both wave 1 and wave 2 (ANOVAs, $p \leq 0.0003$, Tukey's tests $0.001 < p < 0.01$).

At 24 hr., migration speed by cells in wave 1 was much slower in bin 6 than in bin 2 (ANOVA $p < 0.01$), although speed in both bins was not affected by HGF conditions. Net migration distance was greater in a steep HGF gradient and in uniform HGF than in the control channel (ANOVA, $p=0.006$, Tukey's tests $p=0.05$ and $p=0.014$, respectively). Bulk-cell movement did not vary significantly in either bin 2 or bin 6 at 24 hr.

Overall, on a uniform substrate of CN, cells essentially stopped moving by 10 hr. into bin 6 and only moved slowly into bin 6 at 24 hr. As a result, net migration distance was lower than on FN=, and increased only marginally between 10 and 24 hr. in either a steep HGF gradient or uniform HGF. Differences in cell movement were also noted as a large drop in bulk-cell movement: only 50% (10 hr.) or 10% as many (24 hr.) cells moved in bin 6 as in bin 2. Few cells were moving at 24 hr. particularly in a shallow HGF gradient.

Experiments on uniform substrates demonstrated that myoblast motility showed chemotaxis responses to soluble HGF cues in the medium that differed between the two uniform substrates, (FN= vs. CN=) and was also influenced by the form of HGF (uniform vs. shallow vs. steep gradients) in the medium across the channel. Migration speed differed between the low and steep HGF gradients in the first wave of cells entering at bin 2 on FN= but not CN=. However, migration speed in both gradients slowed between 10 and 24 hr. (greater TTP) during cell

movement in wave 1 through bin 6 for FN= and CN= and during cell movement in wave 2 for FN=. Cell migration behavior again showed different responses to haptotaxis cues from uniform CN= and FN= substrates in the control channel, without the influence of HGF during migration.

3.5.8 Chemotaxis on a haptotaxis gradient

Since cells moved differently on opposing-gradients than on uniform substrates (Figure 11) and also displayed substrate-dependent migration behaviors (speed, net distance, cell-bulk movement) on uniform substrates when moving in different HGF conditions (Figures 14 and 15), interactions between opposing-gradient substrates and HGF-chemotaxis were investigated. The influence of HGF was assessed by comparing migration in two HGF conditions, uniform HGF vs. a shallow HGF gradient, both with a concentration of 2.5 ng/ml at bin 10. The hypothesis was that cell migration behavior (speed, net distance, population movement) would differ based on the configuration of a chemotaxis stimulus (uniform vs. gradient) and the pattern of an opposing-gradient substrate (i.e., whether cells moved from high CN in bin 1 close to the loading dock toward high FN at bin 10 on the opposite side of the migration channel, or in the inverse pattern).

In gradient HGF at bin 2 at 10 hr., migration by cells in wave 2 was slower (larger TTP value) than migration by wave 1 when moving on FN-CN. By comparison in uniform HGF, migration speed did not differ between substrates for cells in either wave 1 or wave 2. Cells did not move into bin 6 at 10 hr. in the shallow HGF gradient, and in uniform HGF where there was some movement, migration speed did not differ between substrates (Figure 16B). At 10 hr. in bin 2, bulk-cell movement by wave 2 in the shallow HGF gradient was smaller on CN-FN than FN-CN; in uniform HGF, movement by wave 1 was less on CN-FN than on FN-CN (Figure 16C). In bin 6 at 10 hr., only cells on CN-FN in uniform HGF showed any movement (Figure 16D).

At 24 hr. in bin 2 in the shallow HGF gradient, the migration speed of wave 2 was slower than for wave 1 on FN-CN, whereas in uniform HGF, cells moving in wave 2 were slower than wave 1 when migrating on the inverse opposing-gradient substrate, CN-FN. (Figure 16E). Migration by wave 1 at bin 6 at 24 hr. in the shallow HGF gradient was faster on FN-CN than on CN-FN (Figure 16F). At 24 hr., bulk-cell migration by wave 1 was higher on FN-CN than on CN-FN in bin 2 and at a smaller scale in bin 6 (Figures 16G, 16H). Net migration distance in the shallow HGF gradient at 10 hr. was greater on FN-CN than on CN-FN, as more cells had moved into the channel and reached bin 6 by that time. By comparison, net migration distance did not differ in the two opposing-gradient substrates in uniform HGF at 10 hr., or in either gradient or

uniform HGF at 24 hr. (Figure 16I).

Compared to cells migrating without any HGF (Figure 11), HGF imposed distinctive chemotactic effects on cells migrating over opposing-gradient substrates depending on whether it was uniform or in a shallow gradient. In bin 2 at 24 hr., either a shallow HGF gradient or uniform HGF resulted in a slower migration speed by cells in wave 1 on CN-FN (t-tests $0.01<p<0.05$; compare Figures 16E and 11D). At 24 hr., migration speed by cells in wave 1 was also slowed by a shallow HGF gradient compared to migration without HGF, while migration speed by cells in wave 2 moving on FN-CN was accelerated in a shallow gradient but slowed in uniform HGF compared to the control (no HGF) condition (t-tests $0.01<p<0.05$; compare Figures 16F vs. 11E). Whereas at 24 hr., there was no wave 2 of cells moving in bin 6 on CN-FN without HGF, both the shallow HGF gradient and uniform HGF stimulated movement by a second wave of cells in the same bin at the same time. Those cells migrating on CN-FN reached bin 6 under the influence of HGF is likely due to the chemotactic effects on bulk-cell movement earlier in the channel in bin 2. A shallow HGF gradient advanced bulk-cell movement in bin 2, as waves 1 and 2 both had more cells moving on both opposing-gradient substrates in bin 2 at 10 hr. Uniform HGF also had a chemotactic effect on bulk-cell movement in waves 1 and 2 although only on FN-CN (t-tests, $0.01<p<0.05$, compare Figures 16C and 11F).

Therefore, opposing-gradient substrates imposed complex influences on migration that were influenced further by chemotaxis to HGF, and that additional influence by HGF was dependent on the shallow-gradient vs. uniform configuration of HGF in the channel.

3.6 Figures

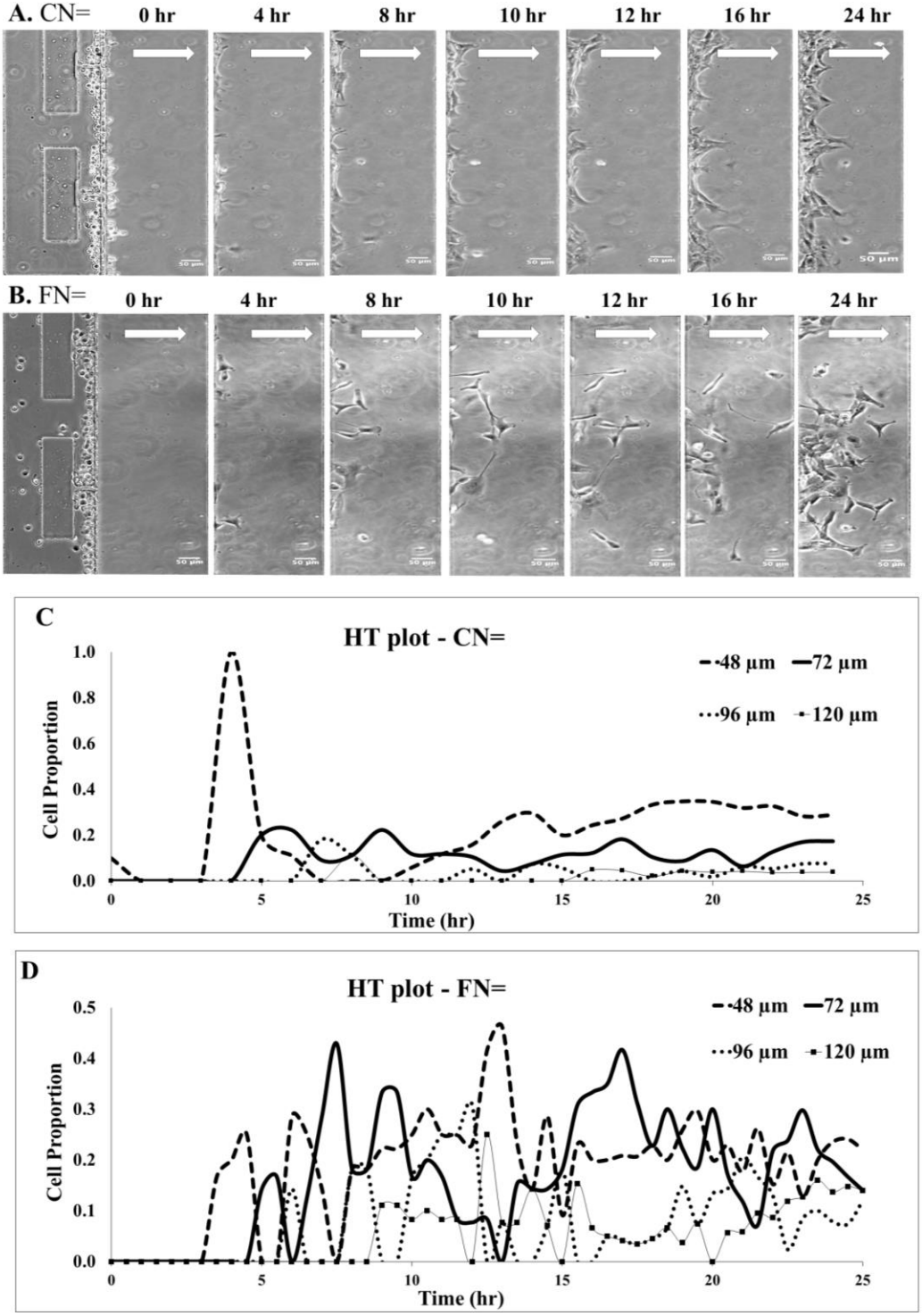

Figure 8. C2C12 myoblast migration and histogram-by-time (HT) plots of haptotaxis experiments on a uniform substrate. Images (A, B) and HT plots (C,D) of representative 24-hr

experiments on uniform collagen (CN=; A,C from one experiment) and uniform fibronectin (FN=; B,D from one experiment). Cells were loaded into the docking area (the left half of 0-hr panel) and moved into the migration channel (direction indicated by white arrows) during an experiment (at 0, 4, 8, 10, 12, 16, and 24 hr.). A and B. Cells appeared to move further into the channel and as a larger population when migrating on a substrate of FN= than on CN=. C and D. HT plots of myoblast migration on CN= (C) or FN= (D) across the 240-µm migration channel. Images of the channel were divided into 10 bins for analysis using NIH ImageJ. The proportion of cells in each bin (y-axes, note different scales) is plotted over 24 hr. (x-axis). Position of each cell was tracked by the nucleus, as cells travelled in a wave into bin 2 (48 µm), then bin 3 (72 µm), bin 4 (96 µm), etc. Curves for some bins show multiple waves of cells during movement across the migration channel. Cell distribution across bins changed over time for CN= (Chi-square (df=198)=174.3; $p<0.001$) and FN= (Chi-square (df=216)=147.1; $p<0.001$) in comparisons across 10 bins. The proportion of cells in each bin from bins 3-10 was greater on FN= than in the same bin and timepoint for cells migrating on CN= (Chi-square (df=24), $p<0.01$, for each comparison). The total number of cells tracked was 50 (A,C) and 52 (B,D). HT plots show bins 1-5 for clarity; complete HT plots of all 10 bins from these two experiments are presented in Supplementary Figure S1 at https://doi.org/10.5203/FK2/Y1KK0O [147].

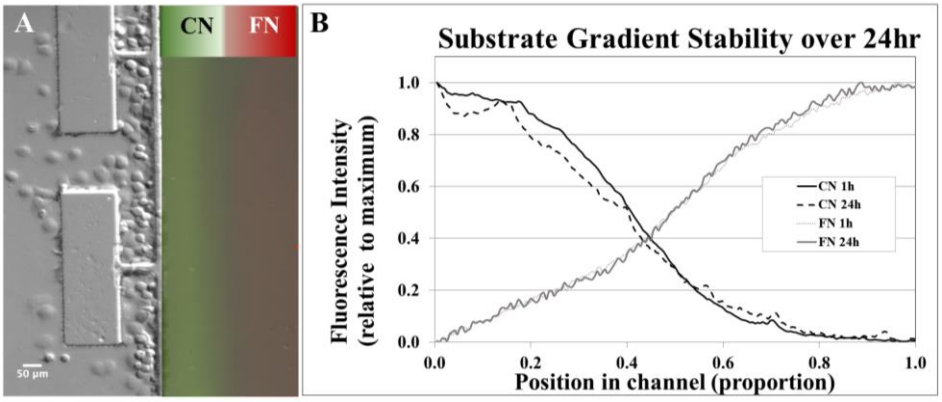

Figure 9. Haptotaxis-gradient experiment on C2C12 myoblasts. A. A representative image of the cell-docking area (left) beside a cell-migration channel (right) which is coated with FITC-labeled CN and rhodamine-labeled FN using gravity flow to form an opposing-gradient substrate. Green and red fluorescence signals meet in mid-channel. B. The fluorescence intensity of each of the green (CN) and red (FN) signals across the channel at 1 hr and after 24 hr of an experiment.

Fluorescence intensity is plotted relative to the maximum fluorescence for each curve. Both FN and CN gradients were stable over 24 hr., at the end of an experiment. Time-lapse videos of cell migration on CN=, FN=, CN-FN, and FN-CN are provided in Supplementary Figure S2 at https://doi.org/10.5203/FK2/Y1KK0O [147].

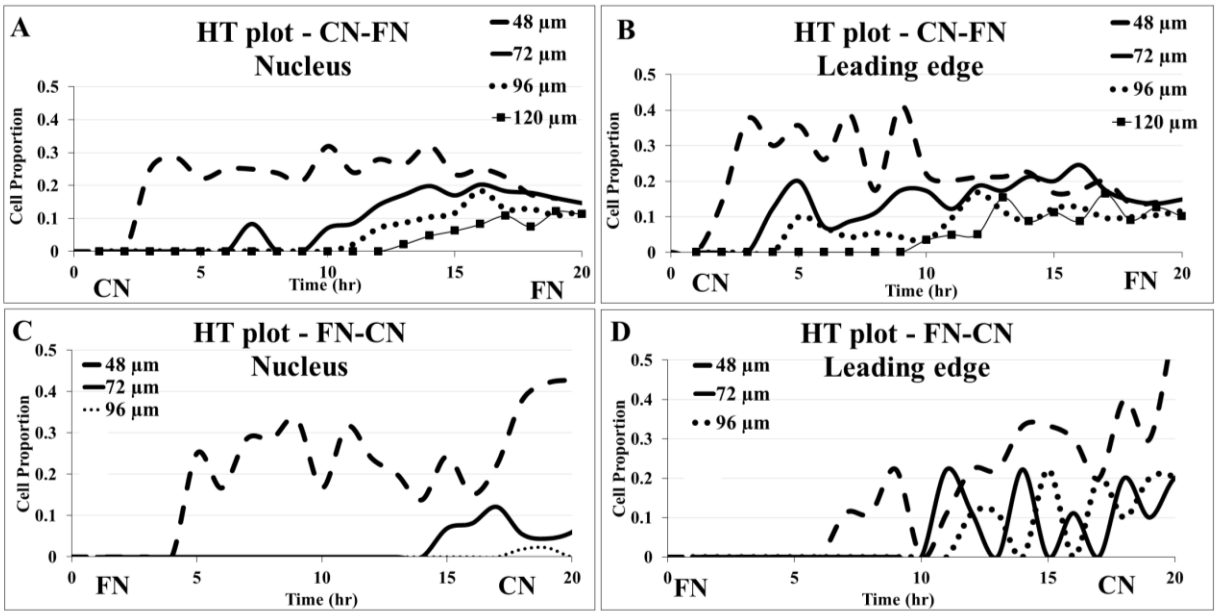

Figure 10. Histogram-by-time (HT) plots of C2C12 cells tracked during migration on opposing-gradient substrates of CN and FN over time. The proportion of cells in different 24-µm subdivisions (bins) of the migration channel (y-axis) is plotted against time (x-axis), tracking cells by the position of their nucleus (A, C) or leading edge (B, D) on CN-FN (A,B) and a second channel on FN-CN (C,D) in the same experiment. A. HT plot for nuclei in cells migrating in bins 2 (48 µm), 3 (72 µm), 4 (96 µm) and 5 (120 µm) from CN toward FN (CN-FN substrate). Each curve represents the proportion of cells in a particular bin; the plot illustrates cells progress in waves across a channel, as cell proportion increases (cells moving into a bin) and decrease (cells moving out of a bin). B. Cell tracking of the same experiment as A, with cells tracked at their leading (front) edge. C. HT plot of cells migrating through bins 2-4 (48 µm to 96 µm) from FN to CN (FN-CN substrate), with cells tracked by the position of their nucleus. Most cell bodies moved only as far as bin 2 (48 µm) by the end of the experiment. D. Cell tracking of the same experiment as in C, with cells tracked at their leading edge. Comparing leading-edge and nuclear tracking (A vs. B, and C vs. D) suggests cells elongated during migration, possibly more on FN-CN than CN-

FN, as cell leading edges were observed bins earlier than cell nuclei (not significant for either comparison). Proportions of cells in each bin over time are not plotted further than bin 5 (A,B) or bin 4 (C,D) for clarity and as proportions were near or equal to zero in higher bins. HT plots of cells moving across the width of the migration channel from these two experiments, are presented in Supplementary Figure S3 at https://doi.org/10.5203/FK2/Y1KK0O [147].

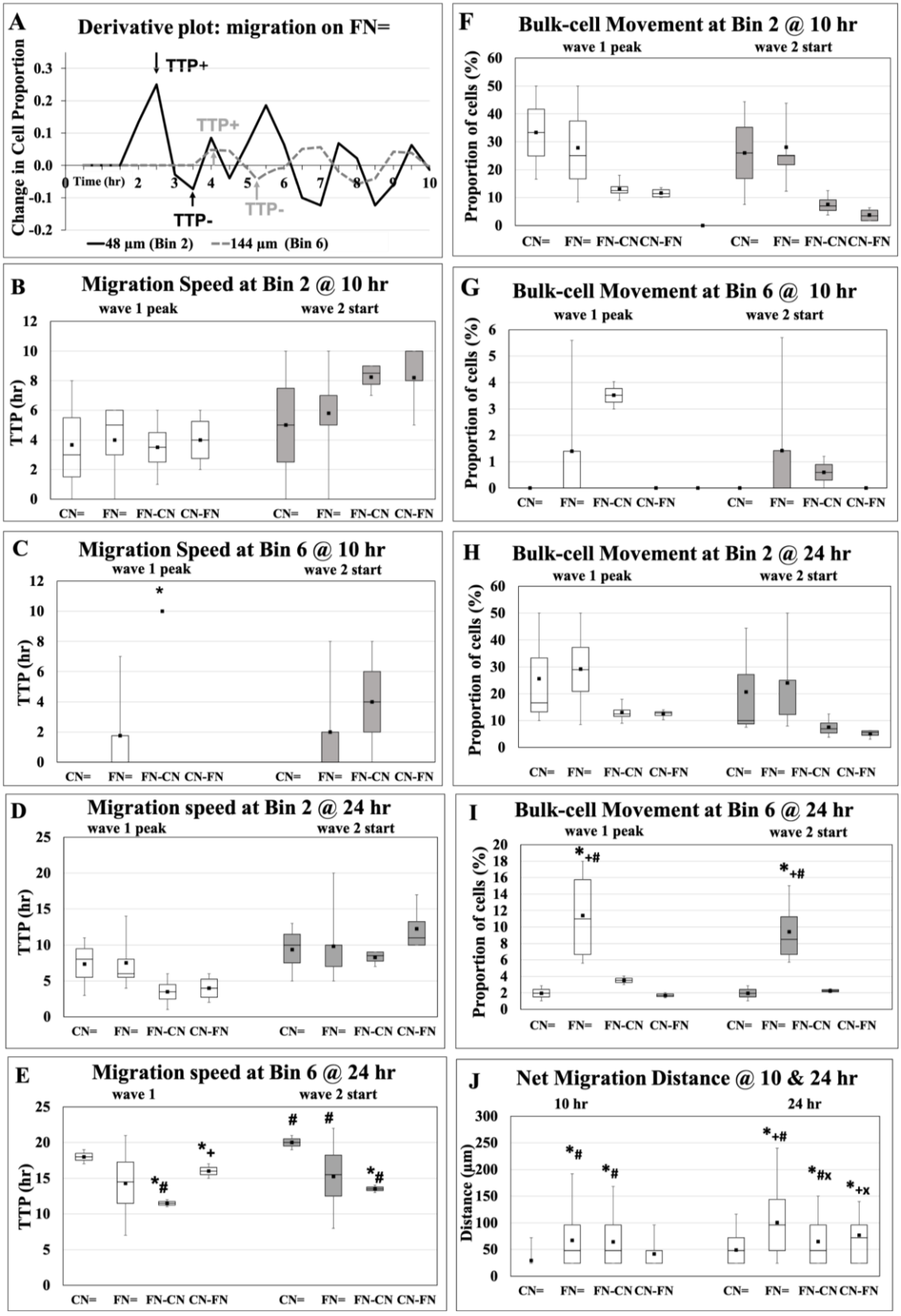
A
Derivative plot: migration on FN=
Change in Cell Proportion
TTP+
TTP+
TTP-
TTP-
Time (hr)
48 µm (Bin 2)
144 µm (Bin 6)
B
Migration Speed at Bin 2 @ 10 hr
wave 1 peak
wave 2 start
TTP (hr)
C
Migration Speed at Bin 6 @ 10 hr
D
Migration speed at Bin 2 @ 24 hr
E
Migration speed at Bin 6 @ 24 hr
wave 1
F
Bulk-cell Movement at Bin 2 @ 10 hr
Proportion of cells (%)
G
Bulk-cell Movement at Bin 6 @ 10 hr
H
Bulk-cell Movement at Bin 2 @ 24 hr
I
Bulk-cell Movement at Bin 6 @ 24 hr
J
Net Migration Distance @ 10 & 24 hr
10 hr
24 hr
Distance (µm)
CN=
FN=
FN-CN
CN-FN

Figure 11. C2C12 myoblast haptotaxis on CN, FN, and opposing-gradient substrates, tracked on the cell nucleus. A. A representative derivative plot shows the feature of waves in cell migration over time (here on FN=) in plots during early ingress into the channel (bin 2, 48 μm, black line) and at the mid-channel position (bin 6, 144 μm, dashed grey line). The first peak (TTP+) and trough (TTP-) of changes in cell proportion identify the times of peak migration in wave 1, and the start of the second wave into the same bin, respectively over 24 hr. B-J. Box-whisker plots of the mean (box), maximum, minimum, third and first quartile (upper and lower borders of box), and median (line through the box) of migration parameters: speed at 10 hr. (B,C) and 24 hr. (D,E), bulk-cell movement at 10 hr. (F,G) and 24 hr. (H,I), and net migration distance at 10 and 24 hr. (J) through bin 2 (B,D,F,H) and bin 6 (C,E,G,I) from cells migrating on uniform (=) collagen (CN=), fibronectin (FN=), and the two opposing-substrate gradients FN-CN, and CN-FN. Cell in wave 1 are shown as white boxes; cells migrating in wave 2 are shown as grey boxes. Data derive from 2-5 independent experiments. B. Migration speed at bin 2 did not vary by substrate for migration of cells in wave 1 or at the start of wave 2. C. At 10 hr. in bin 6, wave 1 migration speed was faster (smaller TTP) on FN-CN than on other substrates (Tukey's tests, $p<0.01$) while migration speed at the start of wave 2 did not vary by substrate. Note that for groups without data, there were no cells moving in or inside a bin. D. Migration speed at bin 2 at 24 hr. shows no changes with different substrate conditions, for cells in either wave 1 or at the start of wave 2. E. Migration speed in waves 1 and 2 at bin 6 at 24 hr., varied markedly by substrate (ANOVA, $p=0.003$); CN-FN showed no wave 2 of cell movement into bin 6 (Tukey's tests, $0.005<p<0.05$). F-I. Bulk-cell movement in waves 1 and 2 for cells moving in bin 2 (F,H) did not differ by substrate for either wave (ANOVA, $p=0.23$ and $p=0.13$, respectively). In bin 6, bulk-cell migration in wave 1 in bin 6 tended to vary by substrate at 10 and 24 hr. (ANOVA, $p=0.087$, $p=0.12$, respectively). Cells moved as a larger population in wave 2 in bin 6 on FN= than on CN-FN (ANOVA $p=0.012$, Tukey's test, $p<0.05$). A smaller proportion of cells (roughly 10-fold fewer) reached bin 6, the mid-channel bin, than reached bin 2 (compare y-axis values F vs. G, H vs. I). J. Net migration distance per cell over 10 and 24 hr., both differed among substrates (ANOVA, $p<0.0001$) and was greater at 10 hr. on FN= and FN-CN than on CN= or CN-FN (Tukey's tests, $p=0.001$). At 24 hr., net migration distance was smaller on CN= than for other substrates. Symbols indicate significant difference from CN= (*), FN= (x), FN-CN (+), or CN-FN (#).

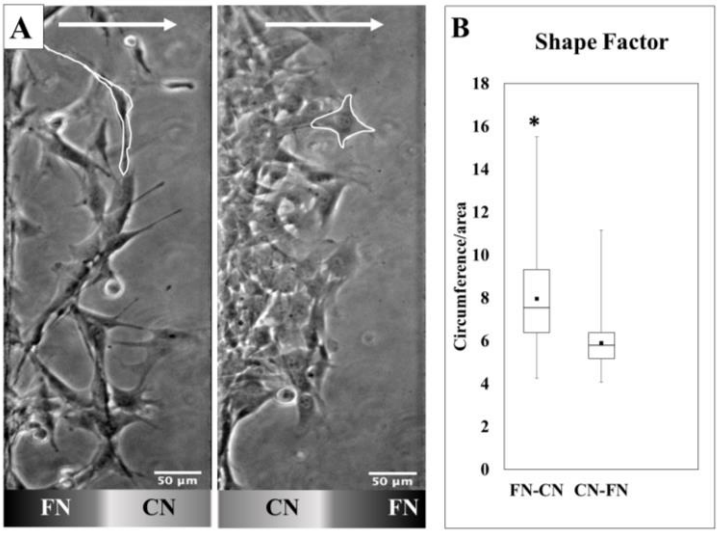

Figure 12. C2C12 cell morphology and shape factor on different opposing-gradient substrates in the absence of HGF. A. The image shows the full width of two migration channels from a single representative experiment in a D3 microfluidic chip. Channels were coated with opposing-gradient substrates of FN-CN (left) or CN-FN (right) as indicated by the graduated grey scales below each image. Cells entered a channel in the direction indicated by the white arrow, from bin 1 to bin 10. Cells are elongated toward the region of CN substrate in the opposing-gradient FN-CN substrate (left), beginning when the substrate was >80% FN (see Figure 2B). By comparison, cells are smaller and more rounded in the channel with CN-FN substrate during migration toward increasing FN (right) even though the substrate was only approximately 30% FN. Representative cells in each panel are outlined in white. B. Box-whisker plot comparing shape factor measured at 10 hr., from cells in migration channels coated with CN-FN and FN-CN. Shape factor was higher (more elongated) when migrating on FN-CN (n=145) than on CN-FN (n=155) (t-test, $p<0.01$). Symbol (***)** indicates significant difference from CN-FN. Data derive from 5 independent experiments for each condition. HGF was not present in the medium of these two migration channels.

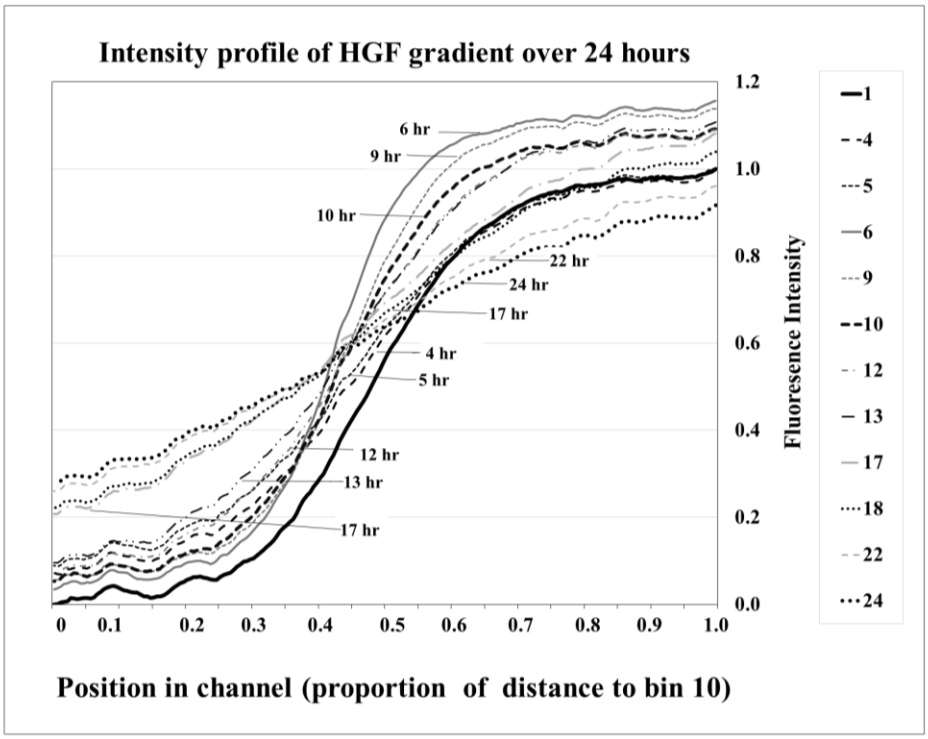

Figure 13. Profile of an HGF during a 24-hr chemotaxis experiment on C2C12 myoblasts. The intensity profile of an HGF gradient (relative to maximum intensity at 1 hr.) over the 24-hr time-course of a representative experiment (legend for time appears to the left of the plot). Fluorescence intensity was plotted from left (bin 1) to right (bin 10) by position in the channel (proportion of channel width, x-axis). The HGF gradient generated by flow in the migration channels of a D3 chip microfluidic device was highly stable for over 5 hours. Adjustments to flow in the migration channel at 5 hr. and 10 hr. were used to maintain gradient stability overnight and until 24 hr.

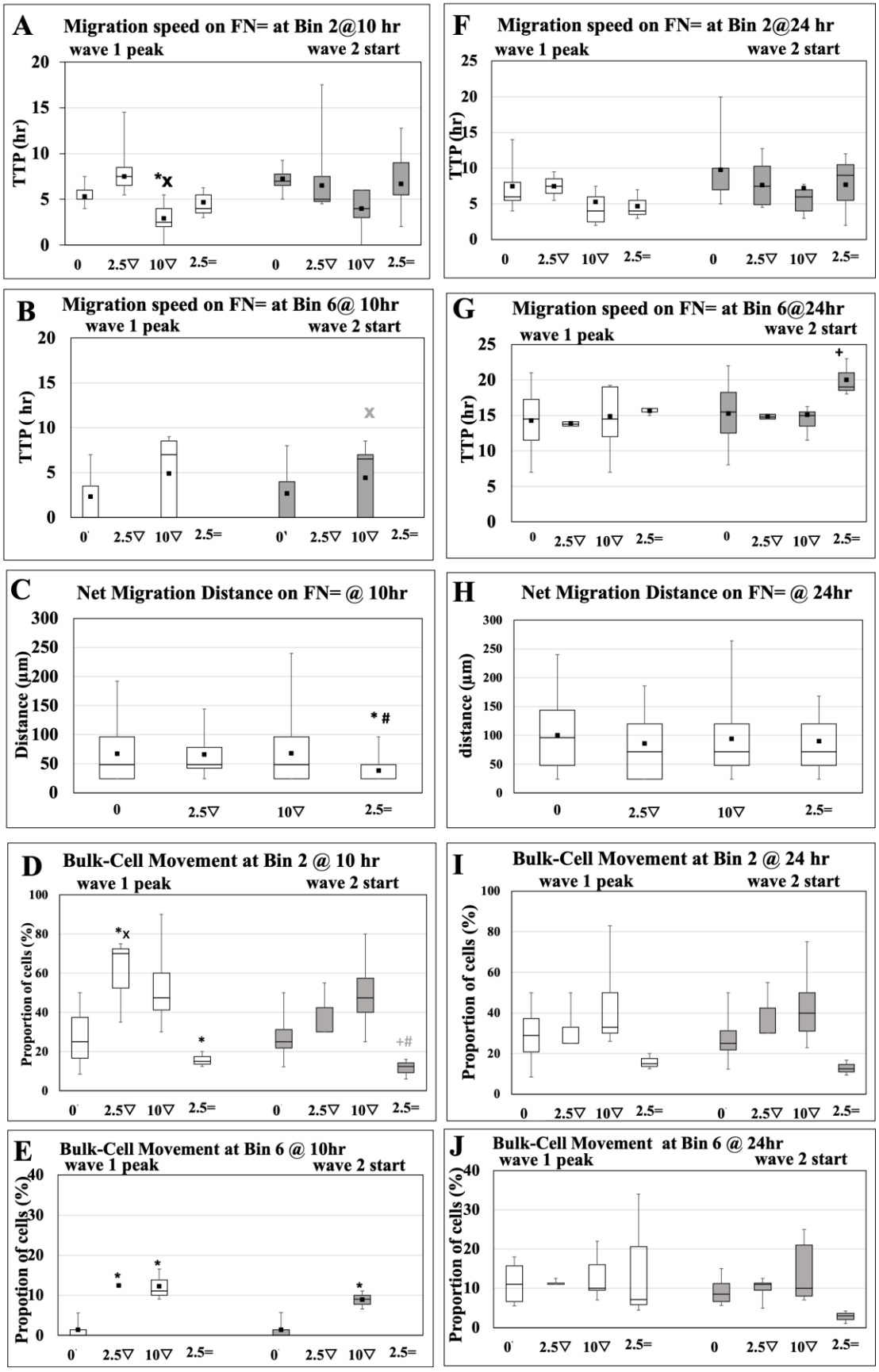
A
Migration speed on FN= at Bin 2@10 hr
wave 1 peak
wave 2 start
TTP (hr)
0 2.5▽ 10▽ 2.5= 0 2.5▽ 10▽ 2.5=
F
Migration speed on FN= at Bin 2@24 hr
wave 1 peak
wave 2 start
TTP (hr)
0 2.5▽ 10▽ 2.5= 0 2.5▽ 10▽ 2.5=
B
Migration speed on FN= at Bin 6@ 10hr
wave 1 peak
wave 2 start
TTP (hr)
0' 2.5▽ 10▽ 2.5= 0' 2.5▽ 10▽ 2.5=
G
Migration speed on FN= at Bin 6@24hr
wave 1 peak
wave 2 start
TTP (hr)
0 2.5▽ 10▽ 2.5= 0 2.5▽ 10▽ 2.5=
C
Net Migration Distance on FN= @ 10hr
Distance (µm)
0 2.5▽ 10▽ 2.5=
H
Net Migration Distance on FN= @ 24hr
distance (µm)
0 2.5▽ 10▽ 2.5=
D
Bulk-Cell Movement at Bin 2 @ 10 hr
wave 1 peak
wave 2 start
Proportion of cells (%)
0' 2.5▽ 10▽ 2.5= 0 2.5▽ 10▽ 2.5=
I
Bulk-Cell Movement at Bin 2 @ 24 hr
wave 1 peak
wave 2 start
Proportion of cells (%)
0 2.5▽ 10▽ 2.5= 0' 2.5▽ 10▽ 2.5=
E
Bulk-Cell Movement at Bin 6 @ 10hr
wave 1 peak
wave 2 start
Propotion of cells (%)
0' 2.5▽ 10▽ 2.5= 0' 2.5▽ 10▽ 2.5=
J
Bulk-Cell Movement at Bin 6 @ 24hr
wave 1 peak
wave 2 start
Proportion of cells (%)
0' 2.5▽ 10▽ 2.5= 0 2.5▽ 10▽ 2.5=

Figure 14. C2C12 cell experiments on HGF chemotaxis on a uniform FN substrate. Box-whisker plots of cell-migration speed (A,B,F,G), bulk-cell movement (C,D, H,I), and net migration distance (E,J) for cells migrating on FN= within a channel containing 2.5-10 ng/ml HGF, applied either uniformly (2.5=), as a shallow gradient (2.5▽) or a steep gradient (10▽) across the channel. A channel without HGF (0) served as the control. Plots show results for cells migrating through bin 2 (A,C,F,H) and bin 6 (B,D,G,I) over the first 10 hr. (A-E) or 24 hr. (F-J), in wave 1 (white boxes) and wave 2 (grey boxes). Data derive from 3-5 independent experiments. A. Migration speed in bin 2 on FN= at 10 hr. was faster (smaller TTP) than in control and the shallow HGF gradient in wave 1 (ANOVA, $p=0.04$, Tukey's tests, $p<0.05$). B. There was no cell migration on FN= in bin 6 at 10 hr. under a shallow HGF gradient (2.5▽) in either wave 1 or wave 2. Migration speed of cells in wave 1 tended strongly to be faster (earlier) in the steep HGF gradient (10▽) than in uniform HGF (2.5=) (Tukey's test, $p=0.07$, symbol is grey). C. Net migration distance at 10 hr. of cells moving on FN= in uniform HGF (2.5=) was less than for cells in the control channel (0 HGF) and in the steep HGF gradient (10▽) (ANOVA $p<0.00001$, Tukey's tests, both $p=0.001$). D&E. Bulk-cell movements, calculated as the proportion of cells moving in bin 2 (D) and bin 6 (E) in each of wave 1 and wave 2. In bin 2 on FN= at 10 hr., bulk-cell movement in wave 1 was greater in a shallow HGF gradient than in control or uniform HGF (ANOVA, $p<0.05$, Tukey's tests, $p<0.05$). Bulk-cell movement in wave 2 in 2.5= showed a strong tendency to be greater than in shallow or steep HGF gradients than in uniform HGF (ANOVA, $p=0.07$, symbols are grey). E. In bin 6 at 10 hr., bulk-cell movement in wave 1 and 2 varied by HGF condition (ANOVAs, $p=0.003$ and $p=0.0008$, respectively). A higher proportion of cells moved in wave 1 in bin 6 in a shallow or steep HGF gradient than in the control channel (Tukey's tests, $p=0.006$, $p=0.01$, respectively). Bulk-cell movement in wave 2 was higher in the steep gradient than in the control channel, and was absent in the shallow gradient or uniform HGF. F. At 24 hr. in bin 2, migration speed did not vary by condition in either wave 1 or wave 2. G. In bin 6 at 24 hr., migration speed was higher in uniform HGF than in the shallow HGF gradient (ANOVA $p<0.01$, Tukey's test, $p<0.01$). H. Net migration distance at 24 hr. did not differ in different HGF conditions. H&I. Bulk-cell movement did not vary with HGF conditions in the channel in either bin 2 or bin 6 at 24 hr. on FN=. Symbols indicate significant difference from: control (*), 2.5▽ (+), 10▽ (#), or 2.5= (x).

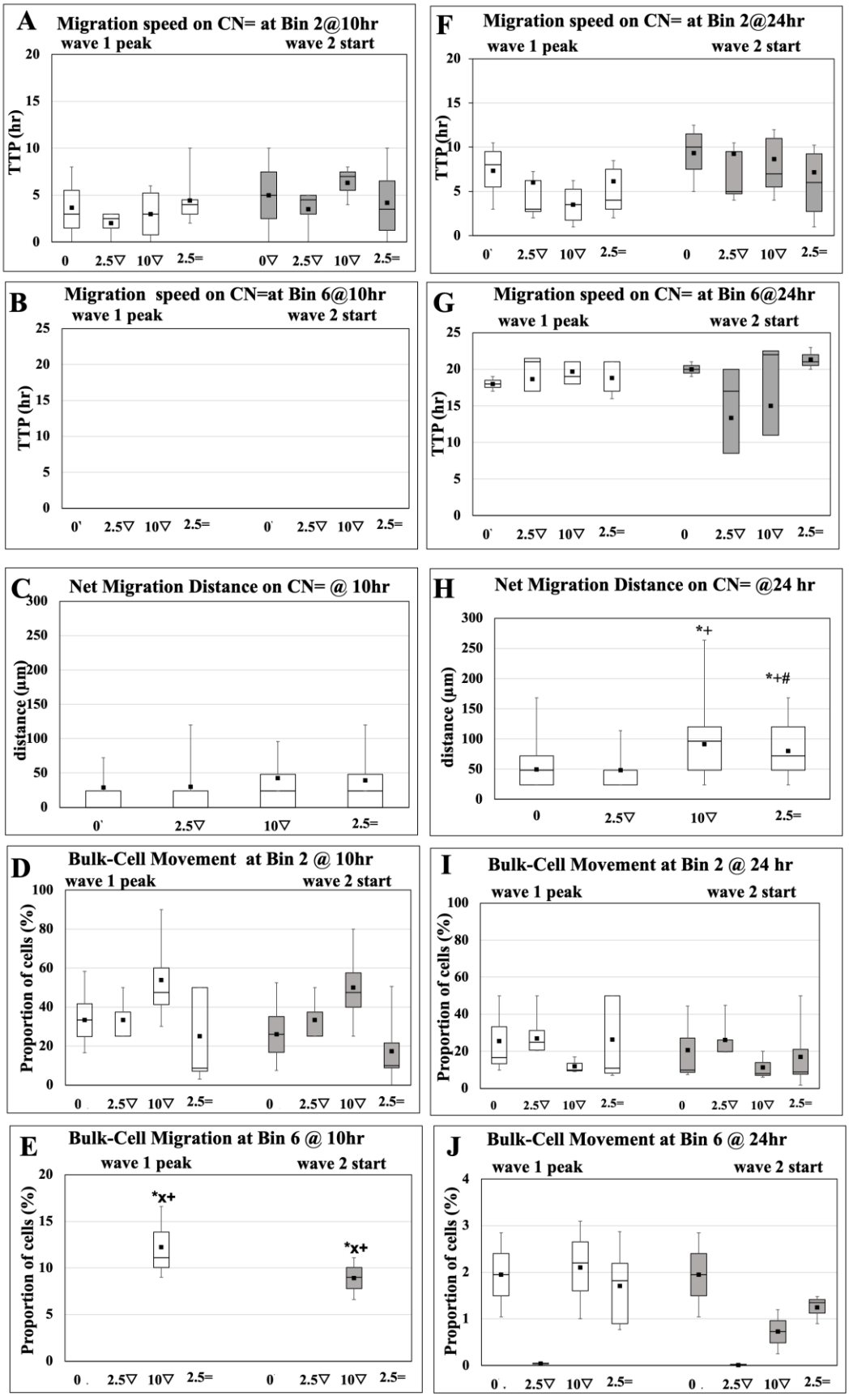
A
Migration speed on CN= at Bin 2@10hr
wave 1 peak
wave 2 start
TTP (hr)
0 2.5▽ 10▽ 2.5= 0▽ 2.5▽ 10▽ 2.5=
F
Migration speed on CN= at Bin 2@24hr
wave 1 peak
wave 2 start
TTP (hr)
0 2.5▽ 10▽ 2.5= 0 2.5▽ 10▽ 2.5=
B
Migration speed on CN=at Bin 6@10hr
wave 1 peak
wave 2 start
TTP (hr)
0 2.5▽ 10▽ 2.5= 0 2.5▽ 10▽ 2.5=
G
Migration speed on CN= at Bin 6@24hr
wave 1 peak
wave 2 start
TTP (hr)
0 2.5▽ 10▽ 2.5= 0 2.5▽ 10▽ 2.5=
C
Net Migration Distance on CN= @ 10hr
distance (µm)
0 2.5▽ 10▽ 2.5=
H
Net Migration Distance on CN= @24 hr
distance (µm)
*+
*+#
0 2.5▽ 10▽ 2.5=
D
Bulk-Cell Movement at Bin 2 @ 10hr
wave 1 peak
wave 2 start
Proportion of cells (%)
0 2.5▽ 10▽ 2.5= 0 2.5▽ 10▽ 2.5=
I
Bulk-Cell Movement at Bin 2 @ 24 hr
wave 1 peak
wave 2 start
Proportion of cells (%)
0 2.5▽ 10▽ 2.5= 0 2.5▽ 10▽ 2.5=
E
Bulk-Cell Migration at Bin 6 @ 10hr
wave 1 peak
wave 2 start
Proportion of cells (%)
*x+
*x+
0 2.5▽ 10▽ 2.5= 0 2.5▽ 10▽ 2.5=
J
Bulk-Cell Movement at Bin 6 @ 24hr
wave 1 peak
wave 2 start
Proportion of cells (%)
0 2.5▽ 10▽ 2.5= 0 2.5▽ 10▽ 2.5=

Figure 15. C2C12 myoblast chemotaxis stimulated by HGF on a uniform CN substrate. Box-whisker plots of cell-migration speed (A,B,F,G), bulk-cell movement (C,D, H,I), and net migration distance (E,J) for cells migrating on CN= within a channel containing 2.5-10 ng/ml HGF, applied either uniformly (2.5=), as a shallow gradient (2.5▽) or a steep gradient (10▽) across the channel. A migration channel without HGF (0) served as the control. Plots show results for cells migrating through bin 2 (A,C,F,H) and bin 6 (B,D,G,I) over the first 10 hr. (A-E) or 24 hr. (F-J), in wave 1 (white boxes) and wave 2 (grey boxes). Data derive from 3-5 independent experiments. A&B. In bin 2 (A) and bin 6 (B) at 10 hr., HGF conditions did not affect migration speeds for wave 1 or wave 2. There was no migration into bin 6 on CN= at 10 hr. C. Net migration distance traveled by cells up to 10 hrs., was not affected by HGF conditions. D&E. Bulk-cell migration in bin 2 at 10 hr. was not affected by HGF conditions. In bin 6 at 10 hr., ~12% of the cell population had progressed to bin 6. As there was no cell movement in the control channel, a shallow HGF gradient, or uniform HGF, bulk-cell migration was greater in the steep gradient for waves 1 and 2 than in other HGF conditions (ANOVAs, $p<0.001$, Tukey's tests $p<0.001$). At 24 hr., (F-J) cell migration speeds in bin 2 (F) and bin 6 (G) were not affected by HGF conditions. H. By 24 hr., net migration distance was greater in the steep HGF gradient and uniform HGF than in control and shallow-gradient conditions (Tukey's tests, $0.01<p<0.05$). I&J. Bulk-cell movement on CN= for cells moving in either wave 1 or wave 2 was not affected by HGF conditions at either bin 2 (I) or bin 6 (J). Symbols indicate significant difference from: control (*), 2.5▽ (+), 10▽ (#), or 2.5= (x).

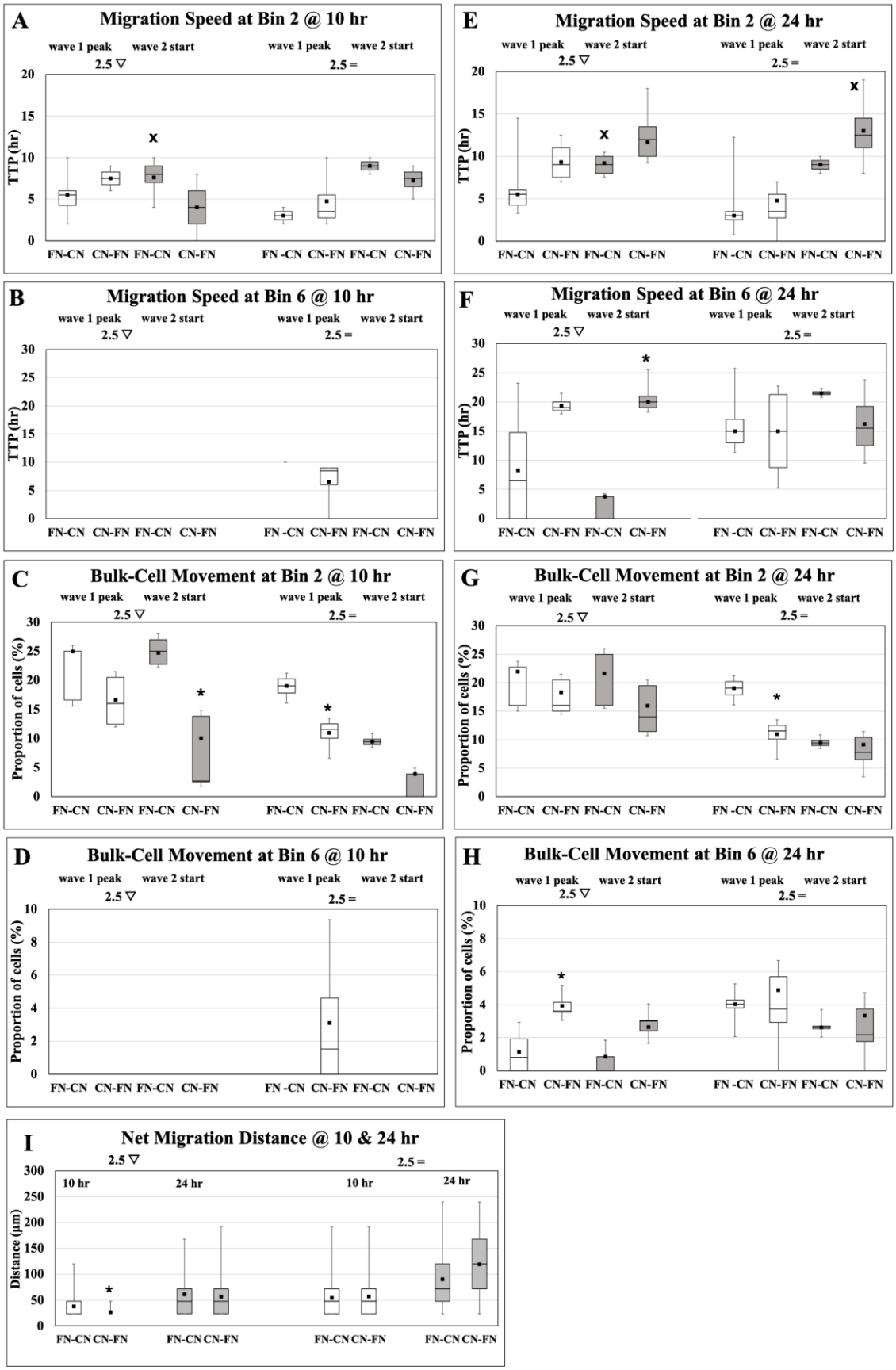
A
Migration Speed at Bin 2 @ 10 hr
wave 1 peak
wave 2 start
2.5 ▽
2.5 =
TTP (hr)
FN-CN CN-FN FN-CN CN-FN FN -CN CN-FN FN-CN CN-FN
E
Migration Speed at Bin 2 @ 24 hr
B
Migration Speed at Bin 6 @ 10 hr
F
Migration Speed at Bin 6 @ 24 hr
C
Bulk-Cell Movement at Bin 2 @ 10 hr
Proportion of cells (%)
G
Bulk-Cell Movement at Bin 2 @ 24 hr
D
Bulk-Cell Movement at Bin 6 @ 10 hr
H
Bulk-Cell Movement at Bin 6 @ 24 hr
I
Net Migration Distance @ 10 & 24 hr
10 hr
24 hr
Distance (µm)
FN-CN CN-FN

Figure 16. C2C12 cell migration responses to uniform and gradient HGF conditions in combination with opposing-gradient substrates. Box-whisker plots of cell-migration speed (A,B,E,F), bulk-cell movement (C,D,G,H), and net migration distance (I) for cells migrating on opposing-gradient substrates FN-CN or CN-FN in wave 1 and wave 2 in either a shallow HGF gradient (maximum at 2.5 ng/ml in bin 10) or uniform HGF (2.5 ng/ml). Plots show results for cells migrating through bin 2 (A,C,E,G) and bin 6 (B,D,F,H) over the first 10 hr. (A-D) or 24 hr. (E-H). Cells moving in wave 1 are shown as white boxes; cells migrating in wave 2 are shown as grey boxes. Data derive from 2-5 (shallow HGF gradient) and 2-7 (uniform HGF) independent experiments. A. In bin 2 at 10 hr., migration speed for cells in wave 2 on FN-CN in a shallow HGF gradient was slower (larger TTP) than for cells in wave 1 (paired t-test, $p<0.01$). B. Bin 6 at 10 hr. showed no migration in a shallow HGF gradient, and speed did not differ by direction or substrate in uniform HGF. C. Bulk-cell movement for cells in wave 1 was smaller on CN-FN than on FN-CN in uniform HGF in the wave 1 (t-test, $p=0.02$). Bulk-cell movement for cells in wave 2 at 10 hr. in bin 2 was smaller on CN-FN than on FN-CN in a shallow HGF gradient (t-test, $p=0.05$). D. There was no bulk-cell movement in bin 6 except for movement of wave 1 in uniform HGF on CN-FN. E. Migration speed on FN-CN in a shallow HGF gradient in bin 2 at 24 hr. was slower for cells in wave 2 than for cells in wave 1 (paired t-test, $p=0.006$). In uniform HGF on CN-FN, migration by wave 2 was slower than for wave 1 ($p=0.05$). F. Migration speed in bin 6 at 24 hr. for cells in wave 2 was slower on CN-FN than on FN-CN ($p<0.05$). G. Bulk-cell movement in bin 2 at 24 hr. was less on CN-FN in uniform HGF (t-test, $p<0.007$). H. Bulk-cell movement in CN-FN was higher than on FN-CN in the shallow HGF gradient (t-test, $p=0.05$). I. Net migration distance was smaller on CN-FN than FN-CN for cells in wave 2 (t-test, $p<0.01$). Symbols indicate significant difference with FN-CN in the same direction (*) or from movement of cells in wave 1 on the same substrate (x).

3.7 Discussion

Our findings provide novel insights into interactions of previously reported dose-dependent, chemokine-driven responses (to HGF) and substrate composition including opposing-substrate gradients, in guiding the timing, wave-form, and net distance of migratory responses by myoblasts. Key findings were that: FN was a more potent and positive haptotaxis signal to myoblast migration than CN; chemotaxis signaling by HGF was modified by substrate composition and the configuration of HGF concentrations across a migration channel; cell

morphology changed with the pattern or directionality of opposing-substrate gradients; and migration behavior was further modified by combined effects of haptotaxis and chemotaxis depending on timing, cell position in the channel, and the configurations of overlying HGF and underlying substrate gradients. Measures of net migration distance and bulk-cell movement corroborated findings of HGF and substrate effects on migration speed for two waves of cell migration, and also showed that cell migration will stop under particular conditions extant in the migration channel. These findings highlight the value of microfluidic approaches to studying myoblast migration behavior, as the control and stability of chemokine and/or substrate configurations can be confirmed by measurements over time. Microfluidic experiments thus serve as a more effective model of *in vivo* conditions during tissue damage and repair than typical *in vitro* experiments on cultures of dispersed cells or isolated muscle fibers. Time-dependent changes in the distribution of cell populations using histogram-time (HT) plots were further analyzed using derivative plots to track migration speeds by the first two waves of cells as they moved through two bins that were sampled as representative behavior early after entry into the channel (bin 2) and mid-way across the channel (bin 6). Migration behavior was also examined at two time points (10 and 24 hr), selected to provide two fairly long intervals for cells to move (10 then 14 hours). The times were selected to accommodate set-up time at the start of day 1 in these long experiments, such that each interval provided many data points for tracking cell movement. Finally, the dual approach to measuring cell migration by tracking cell position by its nucleus vs. its leading edge on cellular extensions, revealed that morphological observations are important to interpreting cell behavior on opposing-gradient substrates, and strongly suggest a role for cell-shape changes including filopodial processes, that have a role in myoblast migration.

Haptotaxis experiments demonstrated that by 24 hr., FN was more potent as a haptotactic stimulus of migration behavior than CN. Cells moved into the middle of a migration channel faster, moved more as a population, and traveled a greater net distance when moving on a uniform substrate of FN than of CN. Novel experiments of haptotaxis on opposing-gradient substrates, where cells traveled from CN into increasing FN (or inversely, on FN into increasing CN concentrations), showed these unique substrates influenced cell morphology. Cells were significantly more elongated in moving from FN-CN (larger shape factor) than those moving from CN-FN. In addition, results showed that the initial substrate encountered by cells entering into the migration channel influenced the net distance that cells migrated. Cells traveled further into the

channel on FN= and FN-CN than on CN= and CN-FN. Such patterning of behavior by an early experience of C2C12 cells suggests individual cells may provide signals or leave clues for other cells. that shape the haptotaxis response of the myoblast population. Such patterning may have important implications in research to select strategies that could promote muscle regeneration and advance tissue engineering approaches that could replace large-volume muscle loss.

Chemotaxis experiments showed that HGF is a significant chemotaxin for C2C12 myoblasts migrating on CN or FN. The format of HGF configuration in the medium, either uniform or as a shallow or steep gradient, also influences migration behavior. Importantly, on uniform FN, cells only progressed to the middle of the migration channel by 10 hr. in a steep HGF gradient or the control condition (0 HGF). By comparison, on uniform CN, no cells progressed to the middle of the channel by 10 hr. and migration speed at 24 hr. was generally slower in mid-channel on CN than FN.

Results also showed that a gradient of HGF is a different chemokine stimulus than uniform HGF to myoblast migration. A gradient of HGF concentrations seemed to sensitize myoblasts to migrate faster or slower into the migration channel (bin 2 at 10 hr.) at a lower concentration of the chemotaxin when cells are moving on a uniform substrate of CN= than FN= (Figure 7A vs. 8A). The impact of gradient vs. uniform HGF was noted even though cells showed slower mid-channel migration speed at 24 hr. on CN= than on FN=. The speed of wave 1 moving in bin 2 at 10 hr. was faster on the steep than shallow HGF gradient on FN= but did not differ between the two HGF gradients on CN= (measured at the same time and position in the channel). While many experiments in this report considered movement of a cell population, termed bulk-cell movement, future studies of individual cells will be important in characterizing changes in gene expression, cell by cell, after tracking behavior of each cell through various chemo- and haptotaxis experiments. As the HGF receptor, c-met is expressed in both activated, migratory myoblasts and in quiescent satellite cells before activation [148], downstream pathways involving Wnt signaling [149-151] and for example, potential cell-level changes in migration behavior with aging [152] should also be accessible to experimentation using microfluidics. More detailed study of myoblast behavior during the intriguing waves of migration (resolved in derivative plots), from wave 1 to wave 2 (including the intervening interval when the population of cells in that bin was decreasing) could reveal time-points for focused study of differential increases or decreases in gene or protein expression under specific conditions.

Novel experiments combining haptotaxis and chemotaxis stimuli identified further details of myoblast migration in an environment of complex substrate interactions influenced by a chemokine. The opposing-gradient substrate of CN-FN without HGF prevented cells moving at all (neither wave 1 or wave 2 appeared) in the mid-channel bin (bin 6) at 10 hr. By contrast, the inverse opposing-gradient substrate, FN-CN (also without HGF) initially induced a fast wave 1 of cells and slowed cells moving in wave 2 in bin 6 at 10 hr. Later at 24 hr. without HGF, wave 1 migration speed at 24 hr. was faster on FN-CN than CN-FN and wave 2 was still absent. In combination experiments by comparison, migration speed differed in the two waves of cell movement (wave 1 vs. wave 2) only for FN-CN at 10 hr. at bin 2 in the shallow HGF gradient. In the presence of uniform HGF, migration speed (wave 1 and wave 2) on the two opposing-gradient substrates did not differ. It was fascinating that the speed of wave 2 moving in bin 2 at 10 hr. tended to be faster on CN-FN than on FN-CN in the shallow HGF gradient, because bin 2 in the chemokine gradient (according to Figure 6) had only 10% of a maximum 2.5 ng/ml concentration of HGF. By contrast, in uniform chemokine of 2.5 ng/ml HGF throughout the channel, the migration speed of wave 2 was nearly identical between the two opposing-gradient substrates. Comparisons of bulk-cell migration at 10 hr. and 24 hr., and migration speed in bin 2 and 6 at 24 hr. revealed further examples of interactions between the directional pattern of the opposing-substrate gradients and the configuration of HGF concentrations, remembering that the uniform and shallow HGF gradients shared the same HGF concentration at bin 10 (2.5 ng/ml). These comparisons are interpreted as showing that subtle distinctions in concentration(s) of haptotaxis substrate and a chemokine, including gradients in both substrate and chemokine within the local environment are detected by cells during migration.

The observation that cells in wave 2 moved more as a population (larger bulk-cell movement) in the shallow HGF gradient than in uniform HGF (bin 2 at 10 hr.) on both opposing-gradient substrates, suggests that the configuration of HGF acting as a chemokine may also affect other attributes of myoblast behavior. For example, the heterogeneous expression heterogeneity among myoblasts of the HGF receptor, c-met, may be narrower, to give more uniform response, or expanded to provide a wider range of responses across a population of cells. A rising concentration of HGF is known first to stimulate (at low HGF) and then inhibit (at high HGF) satellite cell activation [153]. This is an intriguing “dual effect” of a single protein HGF [154] that acts as a ligand for a high-affinity receptor that is an early immediate gene in satellite cell activation

from quiescence [133]. C-met is known as a potent "motogenic" (and mitogenic) receptor [155]. Since HGF effects are mediated by binding to c-met receptors on satellite cells and myoblasts, a dose-dependent effect of high HGF to decrease migration speed by C2C12 myoblast was expected. Surprisingly, a steep HGF gradient (e.g., on FN= in Figure 7A) increased migration speed (lower TTP) more than both a shallow HGF gradient or uniform HGF. Cells migrating on CN= did not show the same impact of the chemokine gradient or concentration. It is also fascinating that myoblasts (and differentiated muscle fibers) also express and release HGF, particularly during mechanical muscle activity and after injury [156-161]. A large population of cells that is actively migrating would therefore, also be adding endogenously produced HGF to the migration channel, augmenting whatever HGF is present exogenously. Depending on the time-course of experiments, the proportion of cells in a migration wave, and the speed of migration by a cell wave, net migration distance, migration speed or the magnitude of that or subsequent wave of cells would thus be modified by two sources of HGF. The regulation of these responses by precise HGF concentrations over time will be fascinating to unravel.

Earlier migration studies of activated satellite cells moving on myofibers in culture demonstrated their migration was more rapid and direct (with a straighter path) in the presence of HGF [138]. It is not known whether an HGF gradient would have similar effects on migration behavior of myoblasts on differentiated muscle cells or myotubes in a microfluidic device or on fibers *in vivo*. Whether or how the composition of ECM proteins might change along a fiber (possibly through gradients of CN, FN and other proteins) is not clear. However, the concurrent influences of an opposing-substrate gradient and a shallow HGF gradient in present experiments, produced the opposite effect and cells did not demonstrate a faster or more direct migration. This may be an attribute of the above-noted dual effect of HGF that results in one effect at high level and a different effect at low concentrations. Studies of mass myoblast cultures previously showed that 10 ng/ml HGF accelerated myotube formation from myoblasts, a differentiation effect that was decreased at 2 ng/ml of HGF [162]. A previous chemotaxis study of cultured adult rat skeletal myoblasts derived from satellite cells, showed that only two growth factors, HGF and transforming growth factor-beta, stimulated positive chemotactic responses on cell migration between 1-10 ng/ml of HGF [142]. Thus, while HGF is already known to have complex effects on myoblast migration and activity (e.g., proliferation after activation of satellite cells), current findings that chemokine configuration, substrate composition, cell morphology, and substrate patterning all

interact, adds a further level of intricacy to our understanding of myoblast motility.

Technical limitations of the present experiments prevented the more mechanistic, molecular studies needed to fully reveal the basis of the haptotaxis-chemotaxis interactions observed here. Cells could not be imaged at high resolution due to device thickness, which precluded use of vital staining methods to track subcellular molecular movements over time. Use of powerful, modern tools to tag molecules with fluorescent vital stains requires real-time or frequent imaging with ultraviolet light (UV), which causes severe cell damage over a lengthy experiment. However, present findings can now be used to focus future experiments on particular molecules, time intervals, situations, or structures of interest, so their design can better accommodate frequent exposures for live-cell imaging. High- or ultrastructural resolution of myoblast extensions during migration would also be of interest. Extensions were especially notable in cells travelling from FN into CN on the opposing-gradient substrate, and appeared to show cells sensing the microenvironment ahead (further into the channel where the CN concentration increased) rather than behind (back toward higher concentrations of FN).

Understanding the function and mechanisms of cell extensions, likely involving up- and down-regulation of receptor expression and membrane density during migration, could help determine how structural modifications of cell shape, membrane configuration, and protein expression are so quickly synchronized to enable myoblast detection of substrate composition and apparently other myoblasts in the immediate and proximate microenvironments. Changes in cell shape by extension of pseudopodia during cell-cell interactions were reported in relation to the migration behavior of activated muscle satellite cells on muscle fibers in culture [163]. In that situation, extensions gave direct evidence of cells actively exploring the microenvironment and communicating with one another (either cells of the same lineage or even two daughter cells of a single precursor). Structurally, the extremely thin cellular extensions observed during myoblast responses to the FN-CN opposing-substrate gradient resemble the cellular connections that form between activated satellite cells and their underlying fibers; those processes were found to include tunnelling nanotubes [164]. It is not known whether similar structures are involved in myoblast migration behavior in the absence of fibers. However, the potential significance of a shape-factor index of cellular receptivity (to particular cues such as increasing or decreasing concentrations of a given protein in the substrate and/or other cells) during migration, was suggested by current findings. Studies of cell-wave proportions over time in HT plots of cells tracked by their nucleus

and their leading edge and confirmed by use of derivative plots, revealed migration speed was faster on uniform FN and toward a high FN concentration on the CN-FN substrate than on uniform CN or FN-CN. Future research on cell-cell communication during migration will benefit from observing aspects of cytoskeletal organization, flexibility, remodeling, and nuclear position that are ideally enabled by real-time tracking. The impact of genetically altered cytoskeletal proteins would also help explore the significance of cell-shape changes during migration.

Microfluidic devices such as the D3 chip employed here, allow exquisitely fine regulation of the shape of gradients produced under flow. Such devices are major improvements over pipette-based methods, Dunn or Boyden chambers, and Transwell plates for studying chemotaxis [165]. This is especially true considering the complex shape of gradients in regenerating tissue *in vivo* [166], as gradients are likely to be multiple and changing rapidly over time as a mixture of cells moves through a local region. The stability of chemokine gradients established in a device is also important. In the current device, for example, the migration-channel gradient was stable for at least 6 hours. Previous studies from this lab used different devices including those where gradients generated by flow were stable for only a few hours. For example, a ladder-chamber device was used to study neutrophil migration and established a steady-state gradient in 2D and in a 3D gel for up to 60 minutes [167]. A gradient stable for 24 hours was established in a 3-layer PDMS device without the need for fluid flow [168].

For studies of myoblasts migrating in a gradient that aim to model complex tissue conditions *in vivo*, it is critical to establish a chemotaxis gradient, as cells will respond by both positive and negative chemotaxis to topographical cues in their microenvironment. That environment is far more complex than a chemokine concentration in medium and/or a homogeneous substrate, such as presented in typical culture studies. Microfluidic devices are often made in-house (including by this laboratory) using optical and soft lithography [145,169], and their use provides additional control of the ECM composition of the substrate in the cell-migration channel [165]. The capacity to control both haptotaxis and chemotaxis stimuli is a valuable resource to migration-biology research. For example, an FN substrate and Wnt chemokines have a pivotal role in shaping planar cell-polarity during satellite cell proliferation [170] and cell elongation-extension [171]. High-resolution studies of myoblast interactions with other cells in a regenerating muscle [172] could benefit by use of microfluidic devices. As another example, HGF is released by anti-inflammatory M2-macrophages and induces myoblasts to release Semaphorin 3A (Sema3A),

a repellent chemotaxin to neurites [173,174]. Since Sema3A is considered important in coordinating reinnervation and capillary formation during muscle repair and wound healing [138,174,175], new designs for microfluidic devices (including thinner base materials to enable high-resolution imaging) may reveal further complexities of cell-cell interactions during *in vitro* modeling, such as during neuromuscular junction formation [65-67].

Results of the present study extend our current characterization of myoblast responses to an HGF gradient by demonstrating that migration behavior and cell morphology are a net result of interactions between the nature of the substrate and the nature of HGF-chemokine exposure. To our knowledge, the only other report of combined effects of haptotaxis and chemotaxis examined myoblast migration on an FN substrate in medium containing platelet-derived growth factor using a Boyden chamber [176].

Myoblasts elongated on CN and were more mobile on FN. Such distinctive roles could feasibly modulate the speed or outcome of muscle regeneration. That myoblasts responded later to CN and had more bulk-cell motility on FN is consistent with the sequence of connective tissue protein synthesis in muscle repair: FN and CN-3 are produced before CN-1 [177]. All three proteins are critical in wound healing, exemplified by: fibroblast trapping with FN, flexibility properties of CN-3, and the end-tensile strength of CN-1. FN, laminin, CNs 4 and 5, and collagenase are all within the basement membrane around muscle fibers [178,179]. CN-1 is also essential to stimulation by decorin, an antifibrotic agent [180], and it may interact with decorin during myoblast responses to a chemokine gradient or opposing-gradient substrates such as CN-FN and FN-CN. Devices designed to simplify use of vital stains for specific molecules without the need for UV illumination, and allow the collection of particular cells under observation during an experiment would be ideal in studying cell physiology, although challenging to devise.

While cells appeared to "prefer" FN over CN for migration in current experiments, the presence of HGF in the migration channel clearly influenced the direction and speed of migration; cells seemed to "choose" among optional trajectories. Potential differences in cell shape, the rapidity of changes in direction (in a second-derivative plot), or cell behavior relative to substrate concentration at other bins (3-5 and 7-10) may also be influenced by HGF configuration. However, migration behavior was more dynamic in response to the combination of chemotaxis and haptotaxis signals. First, both the presence and patterning or directionality of an opposing-substrate gradient across a migration channel, changed the net distance of cell migration. Second and

complementary, both the presence and the slope of the HGF gradient affected migration speed. Since migration distance and speed would both affect net formation of muscle fibers in regeneration, application of findings may help develop an effective muscle patch for therapeutics by improving guidance to myoblasts migrating into 3D scaffolds engineered with multi-substrate gradients.

Substrate composition, stiffness, compliance, density, and topography, all influence cell migration in 2D, as reported for endothelial cells [181], fibroblasts [166], and myoblasts[165]. For effective skeletal muscle tissue engineering, experiments will need to determine an optimal substrate combination to promote myoblast migration and extension then fusion into myotubes and then subsequently guides some myoblasts to become quiescent satellite cells to support engineered tissue to adapt and remodel once implanted *in vivo*. Such experiments are technically challenging. Muscle-derived stem cells grown on CN-1 respond by making other ECM proteins, and at the same time, CN-1 inhibits expression of growth factors and ECM proteins that promote myoblast proliferation and growth; this occurs independent of mechanical factors [182]. Present findings predict that a mixture of CN-1 and FN in the substrate will promote C2C12 myoblast migration in an HGF gradient, since cell migratory responses to FN are regulated by combining FN and CN-1 [183].

Both chemotaxis and haptotaxis affect myoblast migration and morphology in muscle tissue development and repair [184]. Differential effects of an HGF gradient on myoblast migration depending on uniform vs. opposing-substrate gradients, even in a shallow HGF gradient add further detail to our understanding of cell-migration behavior. The influences of free-edge (empty) space and collective cell-cell interactions in epithelial cell migration [185,186] may play additional roles in migration of myoblasts (derived from mesoderm). The current study, therefore, addressed a major gap in our knowledge of myoblast migration and may advance our capacity to promote wound healing in normal muscle and regeneration in disease conditions such as dystrophin deficiency, where myoblast regulation is disrupted [88,132,133].

4. Influence of natural substrate on myotube formation and behavior on microfluidic platforms – Results-2

4.1 Abstract

Natural extracellular matrices made from cultured cells or tissues, are tissue and cell specific, and critical in tissue engineering and cellular applications. This study focused on the effects of a more naturally produced substrate, made by myotubes differentiated within a device channel, on migration and proliferation (haptotaxis) of a second set of cells (set2) loaded into the device. First, four different microfluidic devices were designed with pillars in either an offset pattern or aligned rows along the channel to investigate the myotube formation. C2C12 cells preloaded with Hoechst stain to label DNA (set1 cells), were loaded into device channels in medium with 2% serum to induce differentiation. Results showed that in devices with aligned rows, cells were more concentrated toward pillars, and their distance from a pillar was smaller than for cells in devices with offset rows of pillars. An average of 20-30 set2 cells was tracked over 10 hours, by image capture every 2 hours in the 3 or 4 channels of each device. Results were compiled in Excel and analyzed by multi-way ANOVAs using Jamovi software. Minimum distance to a pillar occurred rapidly, at day 0 for all four devices and increased over time. After allowing set-1 cells to differentiate for 5 days, prestained set-2 cells were loaded. The nucleus position of set2 cells was categorized as located nearest to one of four places in the migration channel: the nucleus of a set1 cell, an extension of a set-1 cell, a pillar, or the device-channel wall. Results showed that a 3-channel device with offset rows of pillars was best able to lead set1 cells to form and align myotubes in the channel and then attract the most set-2 cells to nuclei of those set1 cells. Since cellular proximity is critical to myotube formation and set-2 cells were closer to the set1 nuclei than to device pillars over 10 hours imaging. Differences in flow rate among the four devices suggest that the pillars' orientation, channel dimensions, and initial velocity are factors that influenced behavioral variations among set1 cells from the time of loading to the end of the 5-day differentiation period. Devices with three channels either without pillar, offset rows or aligned rows of pillar showed the highest flow rate in comparison with 4 channel devices. The flow time was also highest in 3 channel devices specially in the device with offset rows of pillars. The velocity was smaller in 3 channel devices with offset rows of pillars; cells had more time to settle down and attach to the substrate in 3 channels mainly in 3 channel devices with offset rows of pillars. Further study of cellular taxis should provide clues to identifying a device that would best

create a muscle by promoting muscle fiber growth (by fusion of set2 to set1 cells) or in the longer term, induce set2 cells to become quiescent satellite (stem) cells.

4.2 Introduction

Myoblasts use multiple cues to guide their migration during muscle regeneration, including those included in two key processes: chemotaxis, the influence of soluble molecules in the cell environment, and haptotaxis, the influence of the substrate on cell behaviour. Different cell behaviors, including, substrate binding, proliferation, migration, and differentiation occurs due to cell and extracellular matrix substrate (ECM) interactions[187]. ECM is composed of water, proteins especially fibrous proteins such as fibronectin (FN) and collagen (CN)[59], and polysaccharides which are remodeled continuously[58].

ECM as a critical non-cellular organizer of tissues, is an essential reservoir for fluids and growth factors[188], and shows topologically unique features across different tissues as a result of development and cell-cell communication[59]. FN is a key multifunctional protein in the ECM[187], and is essential in connecting neighboring cells through fibrils in both linear and branched mesh-works[188]. Observing the interactions of myoblasts with a natural FN-containing ECM on *in vitro* over time through phases of myotube differentiation and comparing that to behavior on an applied FN substrate required a device that the flow rate, myotube formation, and coating interactions can be studied overtime.

Previous research in this laboratory, investigated the effects of chemotaxis and haptotaxis signals on muscle cell migration using a D3 microfluidic chip[3,80]. That microfluidic device has a cell-docking area and 3 channels in which chemotaxis and haptotaxis gradients are created and cell behavior can be visualized over time. For 5 days or longer, migration speed and distance could be tracked in response to changes in substrates of collagen, fibronectin, and the direction of a collagen:fibronectin (CN-FN or FN-CN) gradient. Similarly, the cellular responses to the chemotaxin, hepatocyte growth factor, were followed. However, with the ultimate goal of that tissue-engineering approach directed to making muscle tissue, the device had a significant limitation. Over time, the cells that were loaded into the D3 chip, proliferated and blocked the docking area; this blockage prevented any further loading of a second set of cells that would enable the study of their migration upon a substrate formed by differentiated myotubes and the ECM they produced in the device. This opened the need to develop new devices without a docking area, specifically so a second set of cells could be loaded without any blockage. Such new devices could

allow cell behavior to be visualized in an environment that might encourage myotube formation and behavior.

In low-serum media, skeletal myoblasts typically differentiate, cluster and align, and then fuse into myotubes; this occurs *in vivo* in development and regeneration[86,87], in culture[189], as well as in channels and patterned substrates of a variety of PDMS-based microfluidic devices[89]. Indeed, myoblasts migrate to regions of high density in cultures of dispersed non-fused muscle cells and also toward fused myotubes in a standard culture[90]; these findings are consistent with observations that small muscle wounds heal quickly in comparison to large-volume muscle injuries. However, it is not known how a differentiated myotube by itself, can slow or overwhelm the extent of myoblast migration sufficient to trigger the return of a myoblast to the quiescent state as a stem cell in the satellite-cell position on a newly repaired fiber in a muscle *in vivo*, after injury.

This study was designed to investigate whether and how, the channel-design pattern influences cell morphology and alignment during myotube formation (by set 1 cells) and how device design affects the behavior of a second set of cells seeded after set-1 cells differentiate. Specifically, we were interested in 1) how a natural ECM substrate made by differentiated myotubes will affect the migration (haptotaxis) and morphology of a second set of cells loaded into the device channel; 2) how the presence of pillars in a channel creates turbulence that impacts flow rate; and 3) the time- and substrate-dependence of pillar and flow influence on cell migration, cell morphology, and myotube differentiation within the channels.

4.3 Materials and Methods

4.3.1 Cell preparation

C2C12 mouse myoblasts (cat. no. CRL-1772, RRID: CVCL_0188, American Type Culture Collection, Manassas, VA) were cultured in Falcon flasks (50 mL, VWR Fisher, Mississauga, ON, Canada) for up to 20 passages in high-glucose growth medium containing Dulbecco's modified Eagle's medium (11965092, Thermo Fisher Scientific, Grand Island, NY), 10% fetal bovine serum (FBS, SH3039603, Thermo Fisher), and 1% penicillin streptomycin (CA45000-652 PS, VWR, South Logan, UT) under 5% CO2 at 37°C and 95% relative humidity. Cells were detached from flasks using trypsin and counted. Because cell density influenced morphology and migration behavior (low cell density limited cell-cell contact, essentially prevented mobility, and led to cell detachment), a standard 1,000 myoblasts were seeded into each cell-loading port in a microfluidic device[3] (From paper #1). After cells reached almost 50% confluency, growth medium was

switched with differentiation medium with 2% FBS for 5 days. At day 5 of differentiation set 2 cells which were labeled with Hoechst (H3570, Invitrogen, Life Technologies, Waltham, MA, USA) were loaded to the device on top of set 1 cell with growth medium and imaged over 10 hours.

4.3.2 Microfluidic devices

Four different microfluidic devices were designed and fabricated with pillars in different patterns of diamonds (offset rows) or squares (aligned rows) to first investigate the formation of myotubes in the device. Standard photolithography and soft lithography were employed to fabricate the device in one-layer with flow channels 50- 60 μm thickness, modified from previous reports[3,80], to allow movement of the large C2C12 myoblasts. Microfluidic channels were coated with ECM substrate only fibronectin and C2C12 cells were seeded in the device (106 cells/mL of medium), loading 1 μL of cell suspension per port.

4.4 Data analysis

Three to four independent experiments were used to study each condition. Each experiment examined 2-3 conditions as the devices had either 3 or 4 channels. Devices 1 (D1) and D2 had individual inlets and outlets, therefore, the channels in those devices were considered to represent 3 independent experiments (separate flow channels and groups of cells). By comparison, D3 and D4 had 4 channels opening from a single inlet and ending at 2 outlets, and were considered to represent 2 separate experiments, as the flow through those two devices could be controlled for each pair of channels flowing to an outlet.

Channel dimensions were identified using tools in AutoCAD software[190] before calculations of flow. Data (reported as nucleus position, cell angle, cell area, angle of proximity, and distance to pillar) were plotted as box-whisker plots showing values for the mean, median, maximum, minimum, and first and third quartiles. For clarity, the whiskers are not representative of standard error of the mean or standard deviation; they designate the span of the dataset from third quartile to the maximum value (upper whisker) and from the first quartile down to the minimum value (lower whisker) in the dataset. Changes in nucleus position and cell morphology were evaluated using analysis of variance (ANOVA). Results were considered significant at a probability of $P<0.05$ or $P<0.001$.

4.5 Results

Variables were measured devices with 3 or 4 channels that were designed to differ in their length, width, inlets, outlets, and pillar configuration (Figure 17.). Table 1 shows the design differences, measurements, flow rates, velocities, and flow times of four different devices. D1 and D2 had 3 channels with individual inlets and outlets and either offset rows or aligned rows of pillars. D3 and D4 were composed of one inlet and 2 outlets and had either offset or aligned rows of pillars. Channel length and width were same in each D1 and D2, D3 and D4, the differences are the pillar arrangements. Considering flow rate in a device without any pillars in both types of devices, the flow rate was highest in 3-channel devices without pillars compared to those with pillars;4-channel devices without pillars had a higher flow rate compared to 4-channel devices with pillars. The flow calculation was based on Poiseuille's law [191,192], where flow is considered laminar since the channel dimensions were so small and the presence and pattern of pillars could only change the flow direction. Devices were considered as 3 parts, including A, B, and C, with B as the main channel with pillars; as a control condition, part B was also considered without pillars, similar to other parts of the channel. The control condition was required for comparison of the velocity, flow rate and flow time across devices. Resistance was calculated in each region by considering the respective width of channels in their different parts, and the sum of resistance for each part was used as the total resistance in calculating the flow. The calculated flow rate was therefore, the same through entire channels, due to flow continuity. Velocity and flow rates were measured in each region.

Therefore, dimensions and calculations were taken in each of the 3 parts of a channel, channel A, channel B, and channel C. Part A of a channel was set as the path in a microfluidic device from the inlet to part B of the channel. Part B of a channel was set as the wider path in a device containing the pillars. Part C of the channel was set as the path in a device from part B of the channel to the outlet. Note that because microfluidic devices were symmetrical, the flow was symmetrical. The length of part A in each channel was assumed to be identical for all channels of a 4-channel device and corresponded to the four-part Bs of the four channels connected to the same outlet.

Resistance (R) was calculated as $R = 12\mu L/(wh^3(1-0.63h/w))$, where w, h, and L were the dimensions of the three channels shown in figure 18. Dynamic viscosity μ is taken as 0.93 cP or 0.00093 Pa-s, referred from work by C. Poon and colleagues in 2020[193]. Resistances were then

summed for the effective resistance for the entire path in the device, so the flow Q can be calculated. The pressure is taken as $\Delta P = \rho g \Delta h$, where ρ is the density of the DMEM, g is gravity, and Δh is the height difference between DMEM in the inlet and outlet. The flow rate is taken as $Q = \Delta P/R$ for three devices, one with no pillars, one with a square pillar pattern in channel part B, and one with a diamond pillar pattern in channel part B, respectively. The velocity is taken as $V = Q/A$ for each channel for three models, one with no pillars, one with a square pillar pattern in channel B, and one with a diamond pillar pattern in channel B, respectively. The flow time is taken as $t = d/V$ for each channel for three devices, one with no pillars, one with a square pillar pattern in channel B, and one with a diamond pillar pattern in channel B, respectively. The time value is the sum of the times, t, in each of the respective channels, and is considered as the time that one DMEM particle takes to reach the outlet from the inlet, given the pressure ΔP.

Measurement details for each device are shown in Figure 18 A-D. Channel width was greater for devices with 3 channels than for those with 4 channels, and 3-channel devices had separate channels whereas 4-channel devices had channels connected in pairs, to two different outlets with all four channels sharing a single, general inlet (TYP= μm).

4.5.1 Choosing a device suitable for myotube formation

Four different microfluidic devices were designed and fabricated with pillars in different patterns of diamonds (offset rows) or squares (aligned rows) to first investigate the formation of myotubes in the device. C2C12 cells were preloaded during culture with the vital Hoechst stain to label their DNA, and a small number of cells was loaded 24 hr. later into device channels through the inlet ports using medium with 2% serum to induce their differentiation into myotubes. preliminary runs of this experiment captured images every 1 hr., to observe the process of cell behavior during development of differentiated cells and myotubes. From images of the fixed/stained cells within migration channels, the angle of proximity (of a cell to a pillar), cell angle (longitudinally in the migration channel), cell area, and distance of the cell nucleus to the nearest pillar were measured (Figure. 19). Most set-1 cells were observed at this stage (after 5 days in differentiation medium) as containing one or two myonuclei. Due to density of cells, it was typically difficult to tell if cells had 3 or more nuclei. However, sarcomeres were observed in device channels of set-1 cells after 5 days differentiation.

A second set of cells was loaded into each of the devices containing differentiated C2C12 cells at differentiation-day 5 of the first set of cells, based on well-established timelines for

myoblast differentiation *in vitro*[194]. In the device, channels were photographed every 2 hr. for 10 hrs., to track the migration behavior of these second-set cells in the channels. Channels at this time contained a mixture of differentiated myocytes and myotubes (from set 1), plus newly loaded myoblasts. To analyze the behavior of the second set of cells, the nucleus position of these cells was categorized as located in one of four places in a migration channel: nearest to the nucleus of a cell in the first set of cells, nearest to an extension of a cell in the first set of cells, nearest a pillar or nearest the channel wall of the device. Among all this information the device that was best able to promote formation and alignment of myotubes in the channel (from set-1 cells) and to best attract the most set-2 cells to locate proximate to set-1 cells (and possibly fuse to them or could in the longer term, become a quiescent satellite cell) was identified.

4.5.2 Set-1 cell configuration in four devices

Myoblasts migratory behavior in four devices across the channels on FN substrate over 5 days was mostly significant in cell area and distance to pillar as shown in figures bellow. Angle of proximity plots over device illustrates that minimum and maximum angle of proximity belongs to device 4. Time (the factor, day) had a significant effect ($p=0.050$, $df=3$, ANOVA) on the localization of cells within devices, with significant post hoc differences between day 1 and day 5 ($p=0.053$, Tukey's) and a trend between day 1 and day 3 ($p=0.066$, Tukey's). In addition, distribution graphs showed cells in device 1 had a more normal distribution in their localization compare to cells in other devices. As well, the angle-of-proximity distribution was more variable for devices 2 and 4, possibly due to the higher number of pillars or the aligned (square) pattern of pillars in those two devices (Figure 20). Results of these analyses of the first set of cells showed that in devices with aligned rows, cells were more concentrated toward pillars and the distance to pillar was smaller in comparison to the first set of cells in devices with offset rows of pillars. Consistently across devices, the minimum distance to pillar was recorded at day 0 and increased over time.

After 5 days of differentiation by set-1 cells, labeled set-2 cells were added to the devices through inlet ports. The position of nuclei of set-2 cells with respect to set-1 cells was measured every 2 hr. for 10 hours after seeding. Overall, the most notable observation was that set-2 cells tended to get closer to the nuclei or pillars at the time of seeding and over 10 hours. The proportion of cells set-2 cells closest to nuclei of set-1 cells was higher at 2 hr. and then declined over time.

However, that proportion remained higher than the proportion that was measured closes to a pillar or a wall of any device, or to an extension of a set-1 cell (Figure 21).

In Device 2, there was a higher proportion of cells closest to a pillar than to a set-1 cell nucleus Over 10 hr. of imaging, set-2 cells were initially furthest from a device wall and migrated further toward a device pillar or a set-1 cell nucleus during the experiments, with a fluctuation of the proportion localized nearest to set-1 cell nuclei. In D3, the proportion of set-2 cell nuclei in closest proximity to a device pillar or a set-1 cell nucleus was essentially the same at 0 hr. and over time, set-2 cells positioned closer to a set-1 cell nucleus than to a device pillar.

4.6 Figures

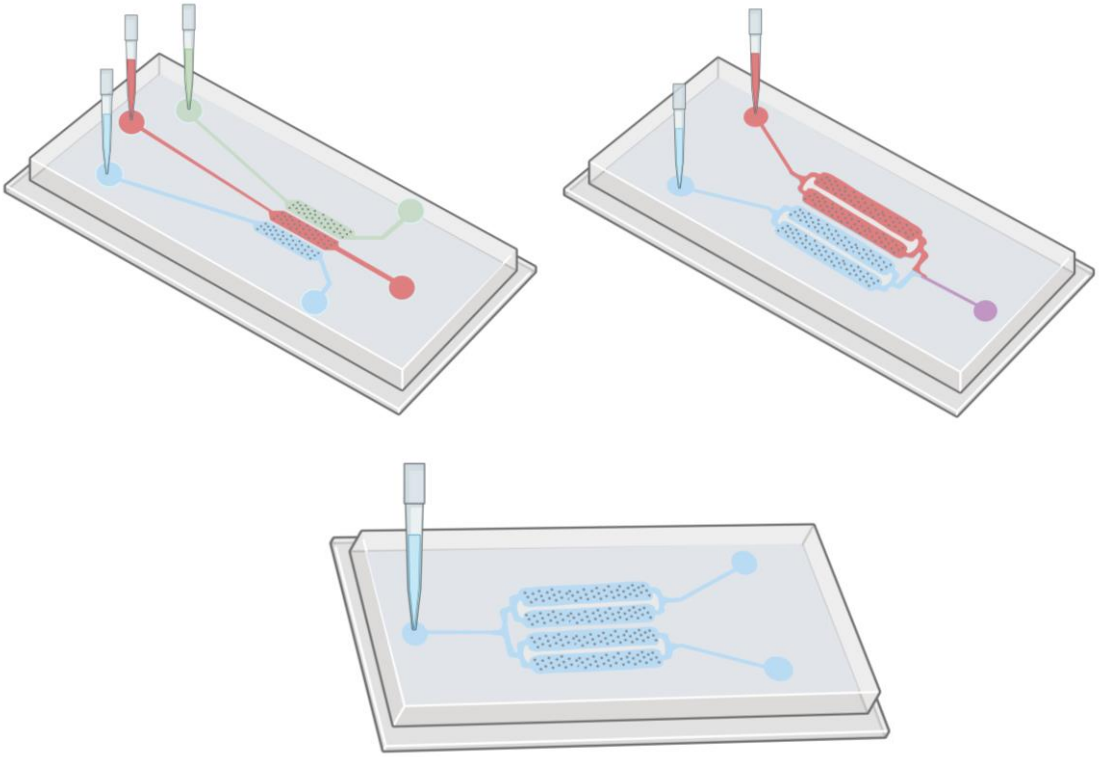

Figure 17. Schematic of a pillared device. Devices 1 and 2 (top left) have 3 individual channels, inlets, and outlets. Devices 3 and 4 have 4 channels connected via 1 inlet and 2 outlets (bottom). If the medium in devices 3 and 4 was inserted from the outlet ports, it would only be mixed at the inlet port (top right). Original artwork by Z. Rovei Miab, 2021.

Table 1. Measurements of design features and flow rate, velocity, and transit time in the 4 microfluidic devices. Device channels were designed to vary in channel length and width, as well as the distance between the pillars and their configuration within the channel. Devices (D) 1 and 2 had 3 channels and devices 3 and 4 had 4 channels. Devices 1 and 3 had offset rows of pillars in a diamond configuration (seen from above), while devices 2 and 4 had aligned rows of pillars.

Device		**D1**	**D2**	**D3**	**D4**	**control**	**control**
# Channels		3	**3**	**4**	**4**	**3**	**4**
Pillar design		Offset rows	Aligned rows	offset rows	aligned rows	none	none
Channel Length	A	8000 µm	8000 µm	1970 µm	1970 µm	8000 µm	1970 µm
	B	1100 µm	1100 µm	800 µm	800 µm	1100 µm	800 µm
	C	4000 µm	4000 µm	2400 µm	2400 µm	4000 µm	2400 µm
Channel Width	A	100 µm	100 µm	60 µm	60 µm	100 µm	60 µm
	B	300 µm	300 µm	200 µm	200 µm	300 µm	200 µm
	C	100 µm	100 µm	60 µm	60 µm	100 µm	60 µm
Inter-pillar distance - diagonal		57 µm	57 µm	36 µm	36 µm	NA	NA
Inter-pillar distance-transverse		100 µm	40 µm	80 µm	30 µm	NA	NA
Flow rate (µl/s)		0.00301	0.00303	0.00289	0.00291	0.00309	0.00297
Velocity (µm/s)		V_A=602.55	V_A= 606.32	V_A= 965.62	V_A= 972.18	V_A= 618.40	V_A= 992.63
		V_B=200.85	V_B= 202.10	V_B= 289.68	V_B= 291.65	V_B= 206.13	V_B= 297.78
		V_C=602.55	V_C=618.40	V_C= 965.62	V_C= 972.18	V_C= 618.40	V_C= 992.63
Time (total) (S)		27.30	25.23	9.08	8.06	24.7	7.89

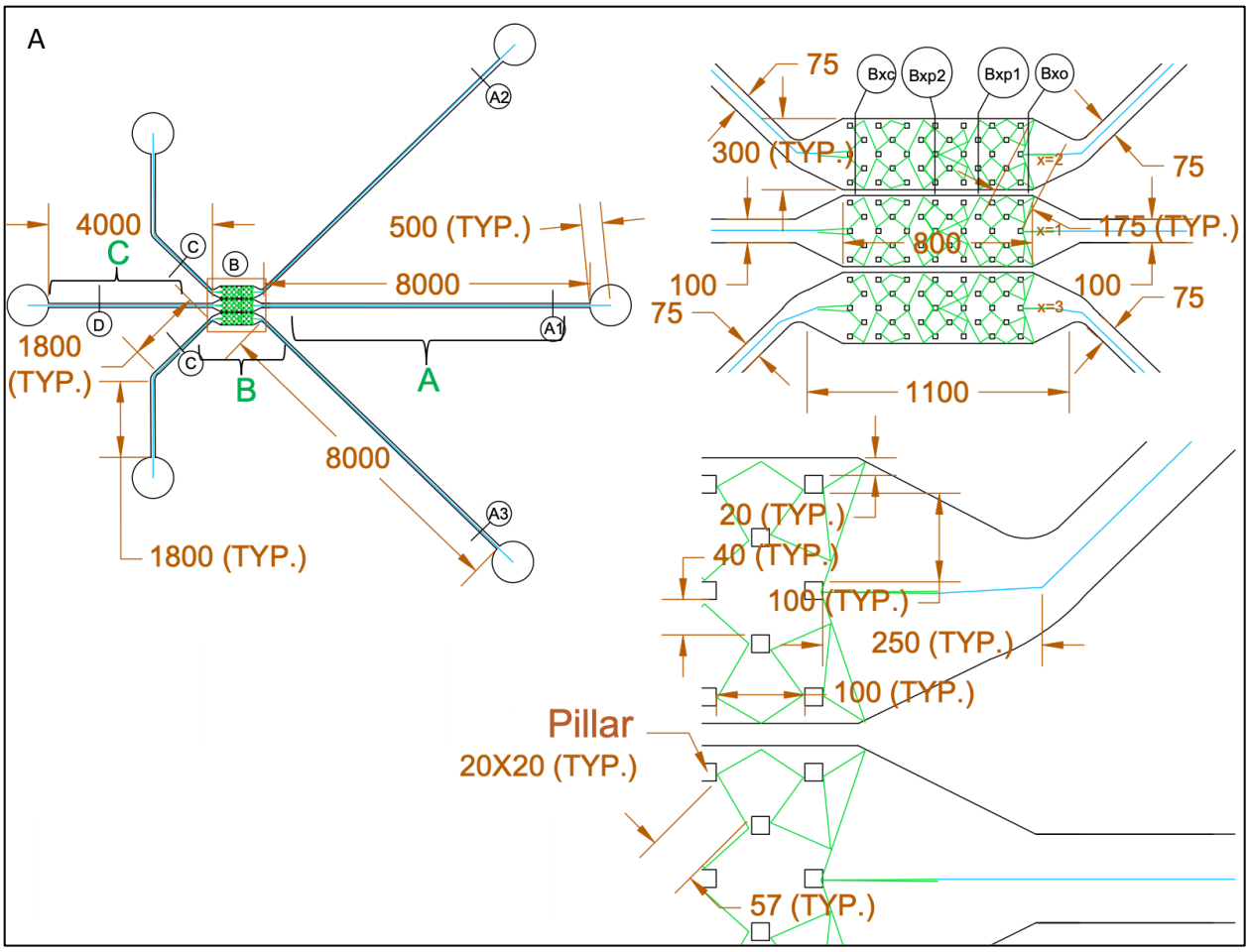
A
A2
A3
A1
4000
C
D
C
B
C
B
A
8000
500 (TYP.)
1800
(TYP.)
1800 (TYP.)
8000
75
Bxo
Bxp2
Bxp1
Bxo
300 (TYP.)
x=2
75
x=1
175 (TYP.)
800
100
75
x=3
100
75
1100
20 (TYP.)
40 (TYP.)
100 (TYP.)
250 (TYP.)
100 (TYP.)
Pillar
20X20 (TYP.)
57 (TYP.)

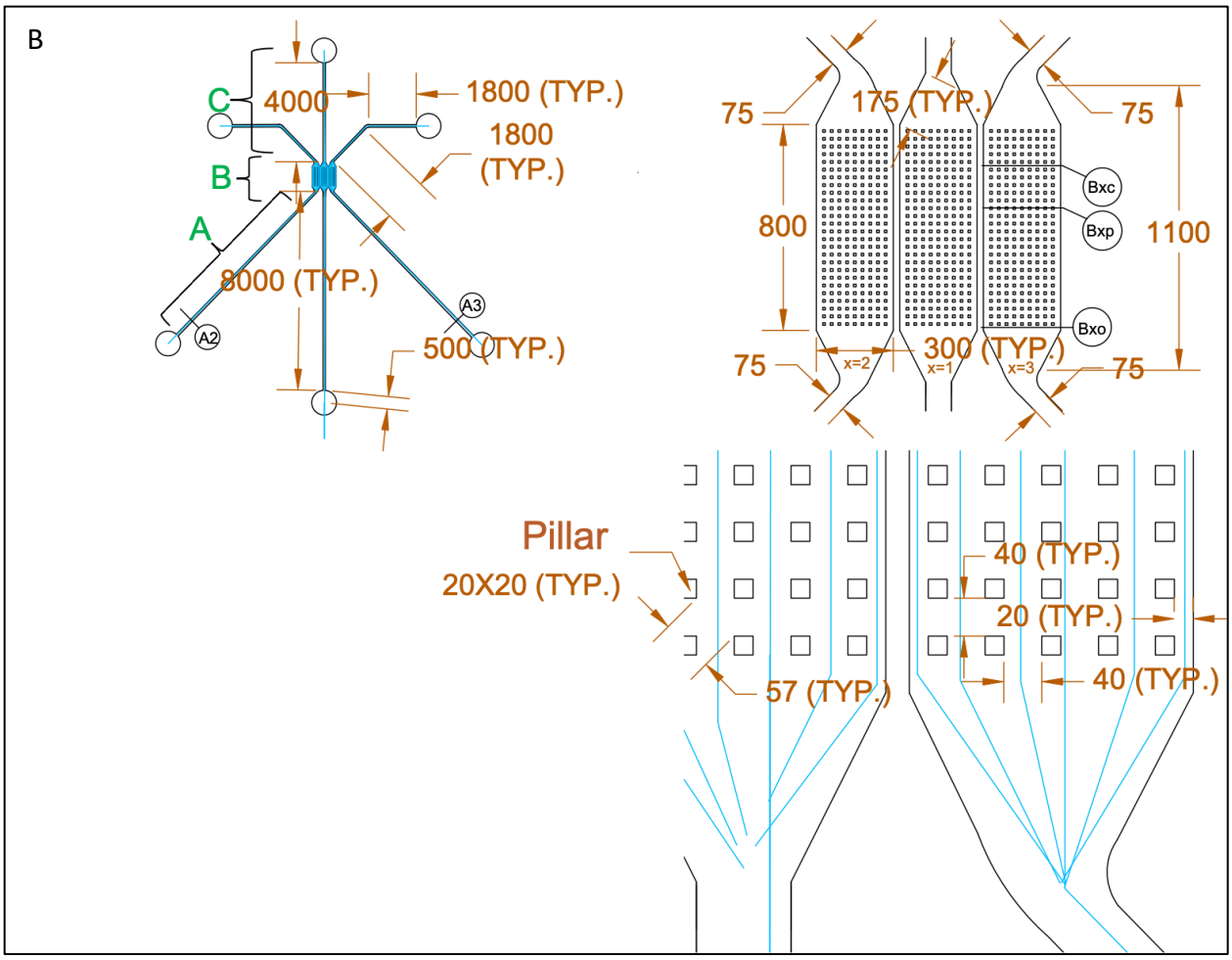
B
C
4000
1800 (TYP.)
1800
(TYP.)
B
A
8000 (TYP.)
A3
A2
500 (TYP.)
75
175 (TYP.)
75
800
1100
Bxc
Bxp
Bxo
75
x=2
300 (TYP.)
x=1
x=3
75
Pillar
20X20 (TYP.)
40 (TYP.)
20 (TYP.)
57 (TYP.)
40 (TYP.)

C

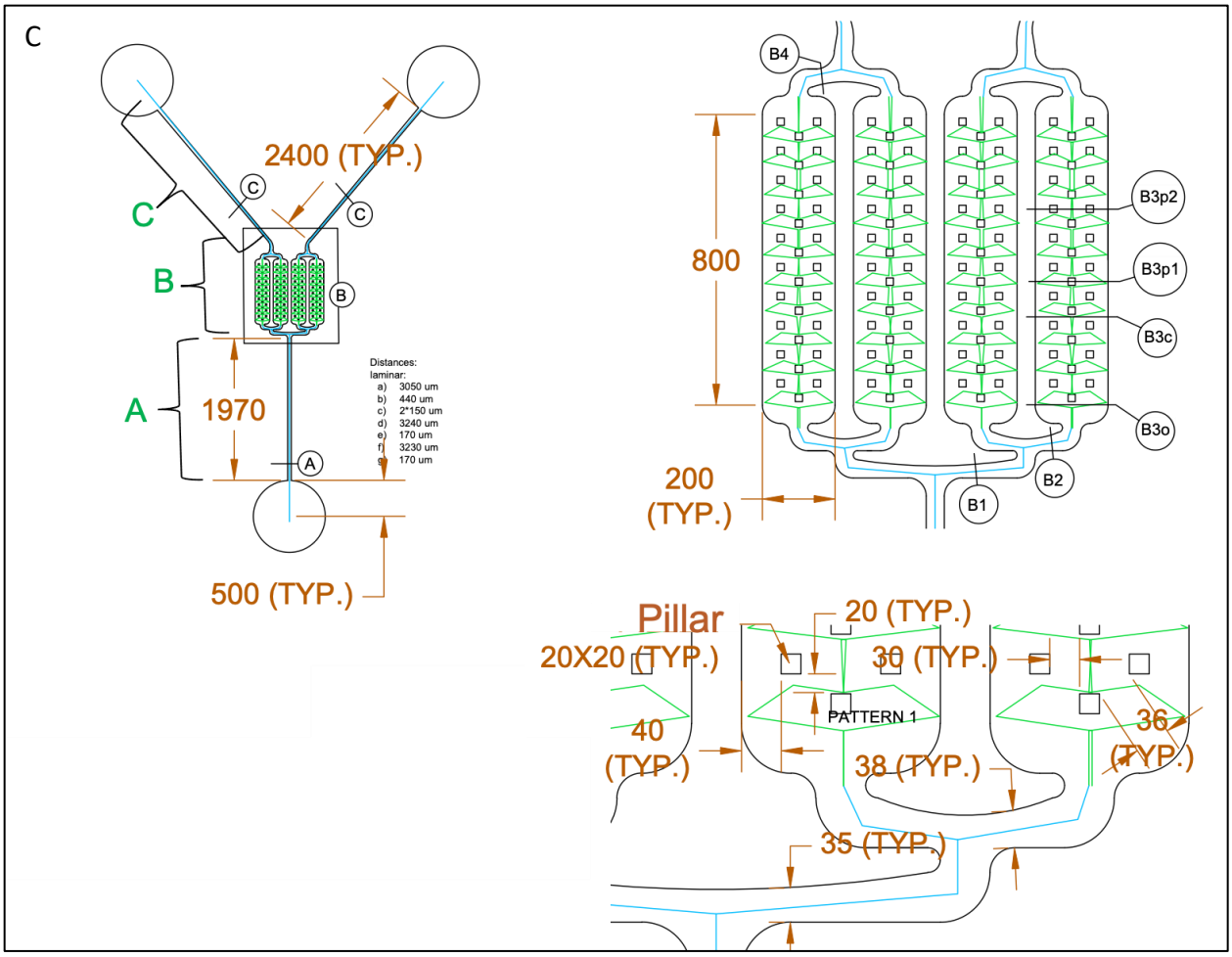
2400 (TYP.)
C
C
C
B
B
A
1970
A
Distances:
laminar:
a) 3050 um
b) 440 um
c) 2*150 um
d) 3240 um
e) 170 um
f) 3230 um
g) 170 um
500 (TYP.)
B4
800
B3p2
B3p1
B3c
B3o
B2
B1
200
(TYP.)
Pillar
20X20 (TYP.)
20 (TYP.)
30 (TYP.)
PATTERN 1
40
(TYP.)
38 (TYP.)
36
(TYP.)
35 (TYP.)

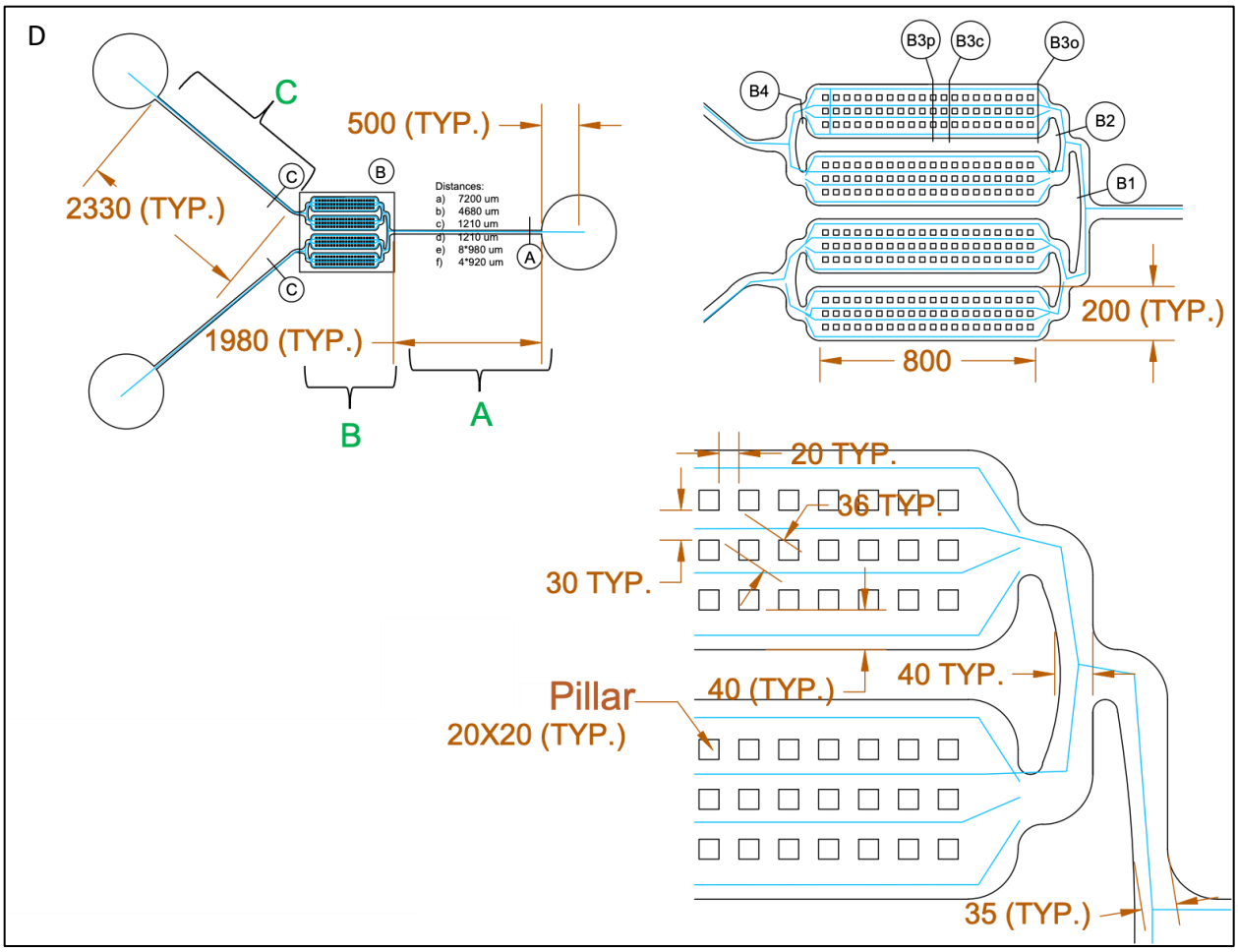

Figure 18. Channel measurements in four different devices, as made using AutoCAD software. A) D1 has 3 independent channels, each with a unique inlet and outlet, and each containing offset rows of pillars. Green lines show how medium flows through the channel going around the pillars. B) D2 is composed of 3 independent channels, each with a separate inlet and outlet, and aligned rows of pillars. Blue lines show how the medium flows through a channel going around pillars. C) D3 is made of 4 channels connected to one inlet and flowing out to one of two outlets, and offset rows of pillars. Each pair of channels is independent from the other pair, sharing the same inlet but having two different outlet ports. Green lines show how medium flows through the channel. D) D4 has 4 channels connected to one inlet and flowing out through one of the two outlets and aligned rows of pillars. Blue lines show how medium flows through the channel going through the pillars (TYP= µm). Original artwork by Z. Rovei Miab, 2021.

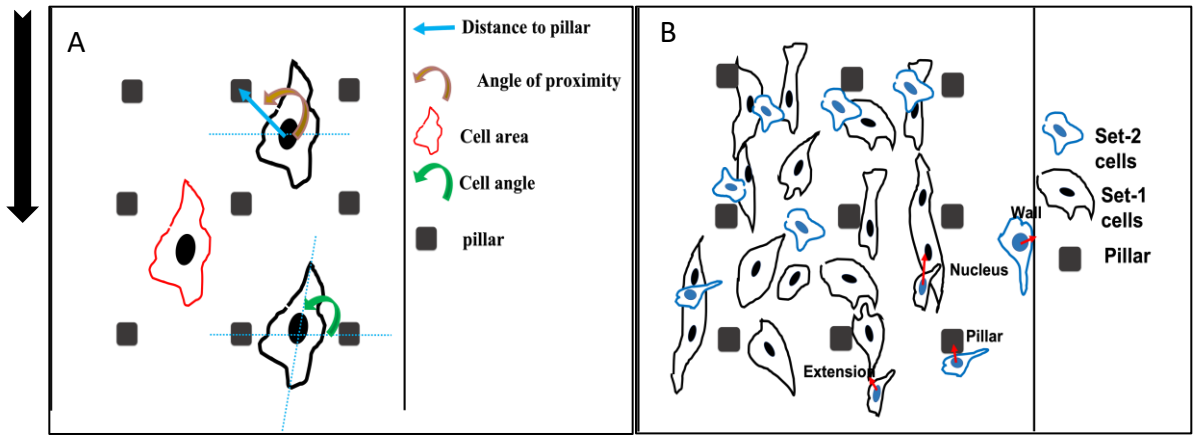

Figure 19. Orientation to measurements of set-1 and set-2 cells within a device. A) Schematic of cells in a device channel showing the details of measuring cell area, cell angle (angle subtended from a line between the longest chord of a cell elongated in the channel and the transverse diameter of the channel), the distance to pillar, and the angle of proximity (angle subtended from a line between a cell nucleus and the nearest pillar to the transverse diameter of the channel) for set-1 cells and set-2 cells was measured over 10 hours. B) Schematic of cells in a device channel. The position of set-2 cell nuclei (nuclei were pre-loaded with Hoechst dye) was measured as their proximity to the nearest set-1 cell nucleus, in different devices over time (with significant differences determined statistically at $p<0.01$ or $p<0.05$). Note, while set-1 cells were differentiated and there were multinucleated myotubes demonstrating sarcomeres in various device channels and experiments, the set-1 cells were typically mononucleated and likely differentiated myocytes. Original artwork by Z. Rovei Miab, 2021.

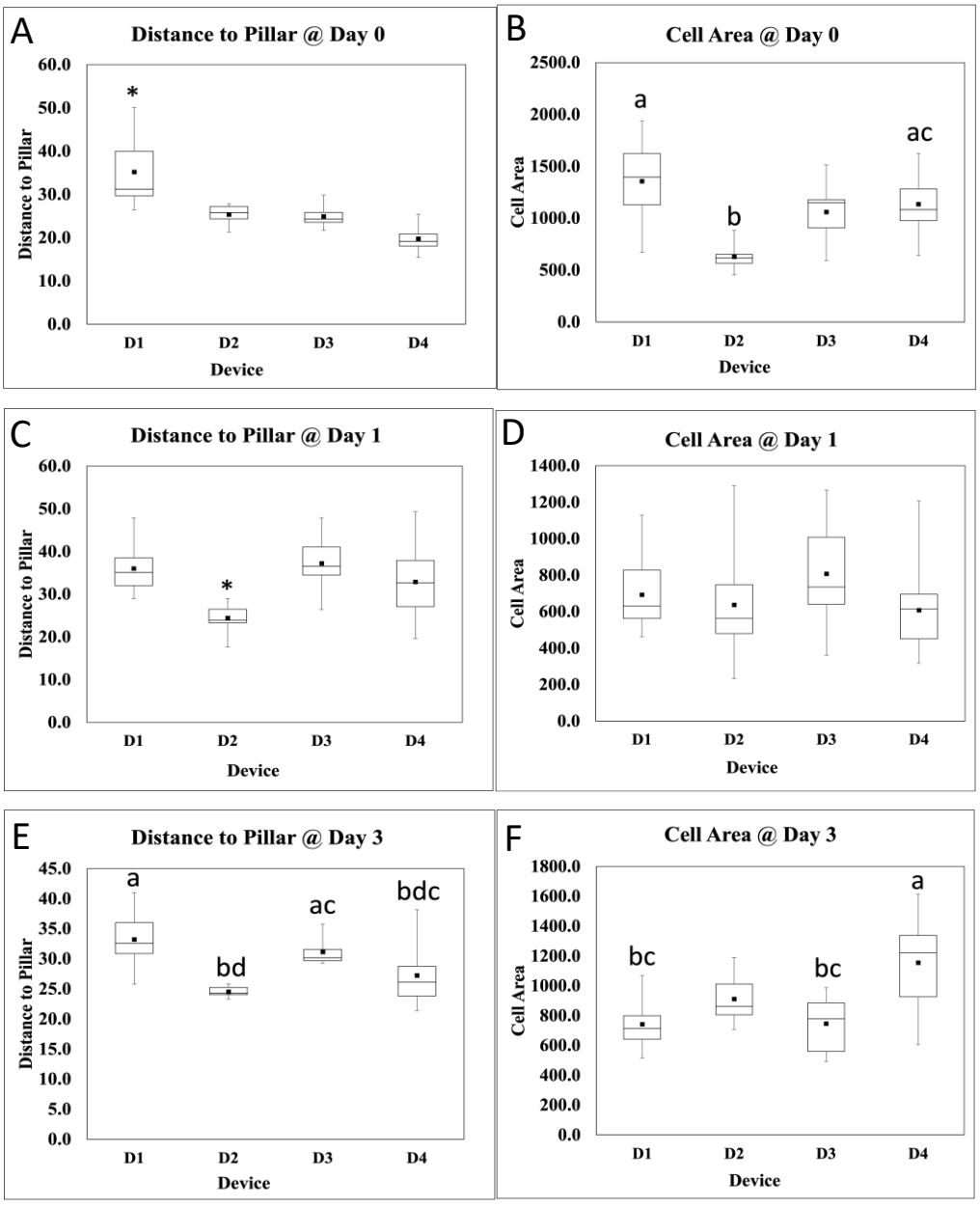
A
Distance to Pillar @ Day 0
Distance to Pillar
60.0
50.0
40.0
30.0
20.0
10.0
0.0
*
D1
D2
D3
D4
Device
B
Cell Area @ Day 0
Cell Area
2500.0
2000.0
1500.0
1000.0
500.0
0.0
a
b
ac
D1
D2
D3
D4
Device
C
Distance to Pillar @ Day 1
Distance to Pillar
60.0
50.0
40.0
30.0
20.0
10.0
0.0
*
D1
D2
D3
D4
Device
D
Cell Area @ Day 1
Cell Area
1400.0
1200.0
1000.0
800.0
600.0
400.0
200.0
0.0
D1
D2
D3
D4
Device
E
Distance to Pillar @ Day 3
Distance to Pillar
45.0
40.0
35.0
30.0
25.0
20.0
15.0
10.0
5.0
0.0
a
bd
ac
bdc
D1
D2
D3
D4
Device
F
Cell Area @ Day 3
Cell Area
1800.0
1600.0
1400.0
1200.0
1000.0
800.0
600.0
400.0
200.0
0.0
bc
bc
a
D1
D2
D3
D4
Device

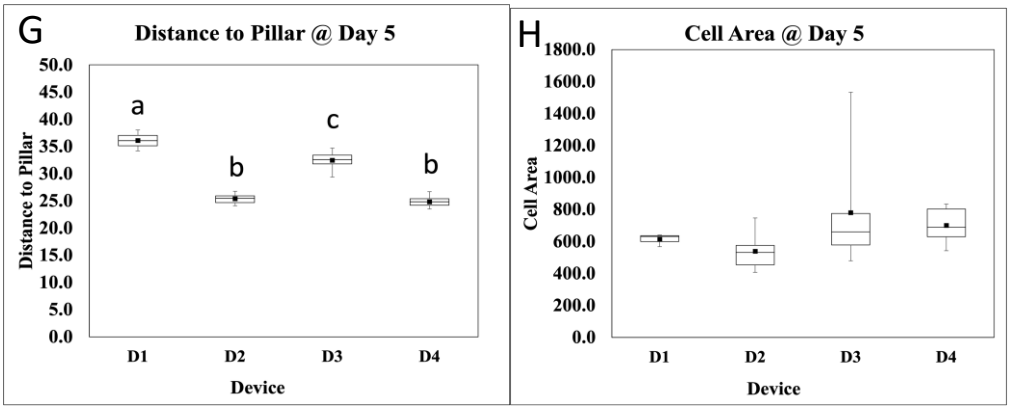

Figure 20. Distance-to-pillar and cell-area plots of set-1 C2C12 cells over time and across device. Images were captured at day 0, 1, 3, and 5 of differentiation on FN substrate. Data derive from 3-6 independent experiments. Different letters over the boxes indicate significant post hoc differences by Tukey's test. (A, B) Distance-to-pillar measurements at day 0 differed significantly between the 4 devices ($p=0.004$, $df1=3$, $df2=12.1$, ANOVA). The largest changes were between device (D) 1 and the other 3 devices. Cells were further from pillars in D1 compared to D2 ($p=0.009$), D3 ($p=0.003$), and D4 ($p<0.001$) (post hoc Tukey's test). Cell area at day 0 also differed significantly across devices ($p=0.001$, $df1=3$, $df2=12.4$, ANOVA), with pairwise differences between D1 and D2 ($p=0.003$, Tukey's) and D2 and D4 ($p=0.032$, Tukey's). (C, D) At day 1, the distance-to-pillar between 4 devices was significant with $p<0.001$. Tukey shows that D1 and D2 with $p<0.001$, D2 and D3 with $p<0.001$, and D2 and D4 with $p=0.002$ have the most significant changes. Cell area at day 1 did not differ across devices ($p=0.135$). (E, F) At day 3, distance-to-pillar differed across devices ($p<0.001$, $df1=3$, $df2=11.6$ ANOVA); there were pairwise differences between D1 and D2 ($p=0.004$), D1 and D4 ($p=0.045$), and D2 and D3 ($p=0.024$). Cell area also differed across devices (ANOVA, $p<0.001$). G &H. At day 5, distance-to-pillar is still different across devices (ANOVA, $df=3$, $p<0.001$), with pairwise differences (by Tukey's tests) between D1 and D2 ($p<0.001$), D1 and D3 ($p=0.003$), D1 and D4 ($p<0.001$), D2 and D3 ($p<0.001$), and D3 and D4 ($p<0.001$).

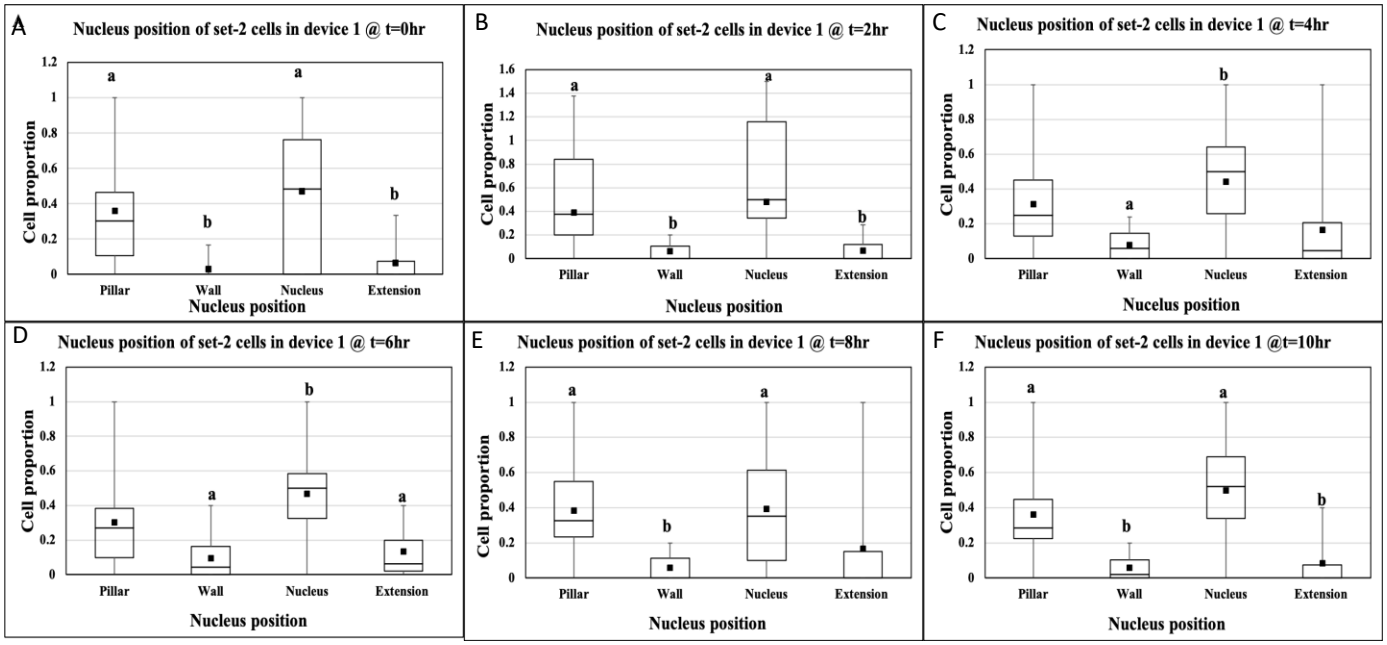

Figure 21. Device1, the proportion of total set-2 cells in a device channel observed with nucleus closest to device pillar, device wall, a differentiated set-1 cell nucleus, or a differentiated set-1 cell extension. Cell position was measured every 2 hr. for 10 hr. Data derive from 3-6 independent experiments. Different letters above boxes indicate significant post hoc differences between groups (Tukey's tests). The proportion of set-2 cell nuclei differed among the four index positions (two from the device, and two from set-1 cells), and set-2 cells were consistently positioned closest (although with a broader range) to a pillar or to a set-1 cell nucleus than to a wall or the extension of a set-1 cell throughout an experiment. A) At t=0 hr., more set-2 cells were positioned closest to a pillar than to a device wall or set-1 cell extension ($p<0.05$), and closer to a set-1 cell nucleus than a device wall and closer to a set-1 cell nucleus than a set-1 cell extension ($p<0.01$). B) At t=2 hr., set-2 cells were localized closer to a device pillar than a device wall or a set-1 cell extension (($p<0.05$), and closer to a set-1 cell nucleus than a device wall or a set-1 cell extension ($p<0.01$(=). C) At t=4 hr., set-2 cells were closer to a set-1 cell nucleus than to a device wall ($p<0.05$), and were closer to the device wall or a set-1 cell extension than at 0 and 2 hr. D) At t=6 hr., the proportion of set-2 cells was higher closest to a set-1 cell nucleus than to a device wall or a set-1 cell extension ($p<0.01$). E) At t=8 hr., the proportion of set-2 cells was generally closer to the extension of a set-1 cell than at earlier times. The proportion of set-2 cells was higher closest to a set-1 cell nucleus or a device pillar than to a device wall ($p<0.05$). F) At t= 10 hr., the proportion of set-2 cells closest to a device wall or a set-1 cell extension declines such

that set-2 cells are closest to a device pillar than a device wall and closest to a device pillar than a set-1-extension ($p<0.05$) and closest to a set-1 cell nucleus than either a device wall or a set-1 cell extension ($p<0.01$).

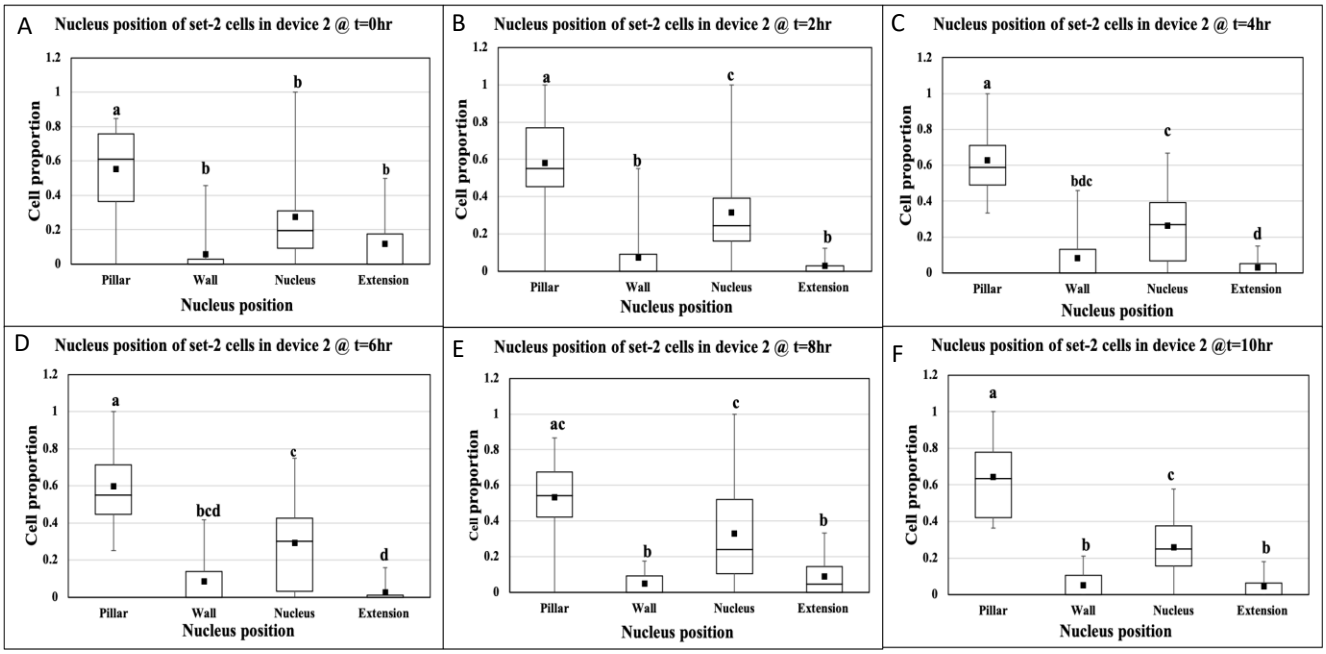

Figure 22. Device2, the proportion of total set-2 cells in a device channel observed with nucleus closest to device pillar, device wall, a differentiated set-1 cell nucleus, or a differentiated set-1 cell extension. Cell position was measured every 2 hr. for 10 hr. Data derive from 3-6 independent experiments. Different letters above boxes indicate significant post hoc differences between groups (Tukey's tests). The proportion of set-2 cell nuclei differed among the four index positions (two from the device, and two from set-1 cells), and set-2 cells were consistently positioned closest (although with a broader range) to a pillar or to a set-1 cell nucleus than to a wall or the extension of a set-1 cell throughout an experiment. A) At t=0hr, more set-2 cells were positioned closet to a device pillar than device wall, set-1 cell extension ($p<0.01$), and set-1 cell nucleus ($p<0.05$). B) At t=2hr., set-2 cells were localized closer to a device pillar than a device wall or a set-1 cell extension ($p<0.01$) and closer to device pillar than set 1-cell nucleus ($p<0.05$). C) At t=4 hr., set 2 cells were closer to the device pillar, than device wall, and set 1-cell nucleus and extension ($p<0.01$). D) At t=6 hr., the proportion of set-2 cells was higher closet to the device pillar than device wall and set-1 cell extension and nucleus ($P<0.01$) and has the highest proportion compare to the last 6 hours. E) At t=8 hr. set-2 cells were positioned closet to device pillar than device wall and set-1 cell extension ($P<0.01$) and localized closer to set-1 cell nucleus

than set-1 cells extension and device pillar ($p<0.05$). F) at t=10 hr., set-2 cell proportion is higher closer to device pillar than device wall, set-1 cell nucleus and extension ($p<0.01$).

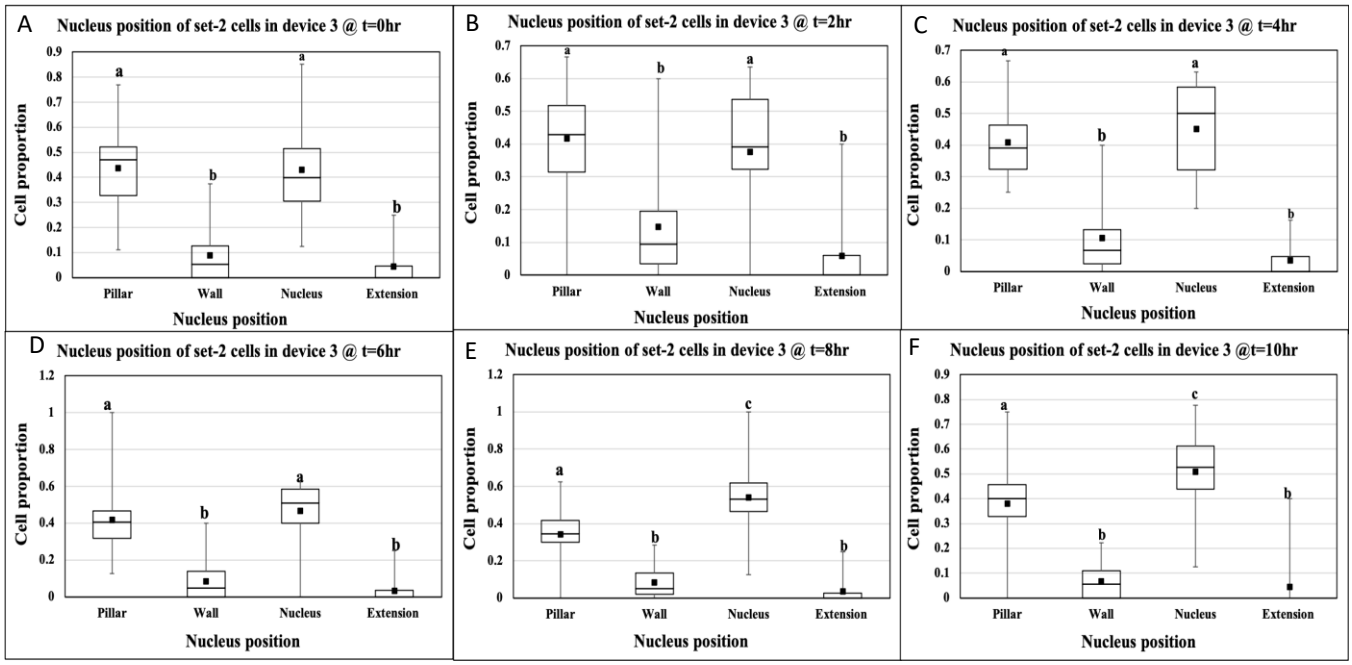

Figure 23. Device3, the proportion of total set-2 cells in a device channel observed with nucleus closest to device pillar, device wall, a differentiated set-1 cell nucleus, or a differentiated set-1 cell extension. Cell position was measured every 2 hr. for 10 hr. Data derive from 3-6 independent experiments. Different letters above boxes indicate significant post hoc differences between groups (Tukey's tests). The proportion of set-2 cell nuclei differed among the four index positions (two from the device, and two from set-1 cells), and set-2 cells were consistently positioned closest (although with a broader range) to a pillar or to a set-1 cell nucleus than to a wall or the extension of a set-1 cell throughout an experiment. A) At t=0 hr., more set-2 cells were positioned closet to a device pillar than device wall and set-1 cell extension and closer to set-1 cell nucleus than device wall and set-1 cell extension ($p<0.01$). B) At t=2 hr., set-2 cells were closer to a device pillar than device wall and set-1 cell extension and closer to set-1 cell nucleus than device wall and set-1 cell extension ($p<0.01$). higher set-2 cells were closer a device wall than last 2 hours. C) At t=4hr., set-2 cells were localized closer to a device pillar than device wall and set-1 cell extension and closer to set-1 cell nucleus than device wall and set-1 cell extension ($p<0.01$). Set-2 cell proportion is positioned higher closer to set-1 cell nucleus than

device pillar compares to last 4 hours and will continue the same trend. D) At t=6hr., set-2 cells were closer to a device pillar than device wall and set-1 cell extension and closer to set-1 cell nucleus than device wall and set-1 cell extension ($p<0.01$). E) At t=8hr., set- cells were positioned closer to set-1 cell nuclei than device pillar, or wall, and set-1 cell extension ($p<0.01$). F) At t=10 hr., set-2 cells were closer to set-1 cell nuclei than a device pillar ($P<0.05$) and closer to set-1 cell nuclei than a device wall and set-1 cell extension ($P<0.01$).

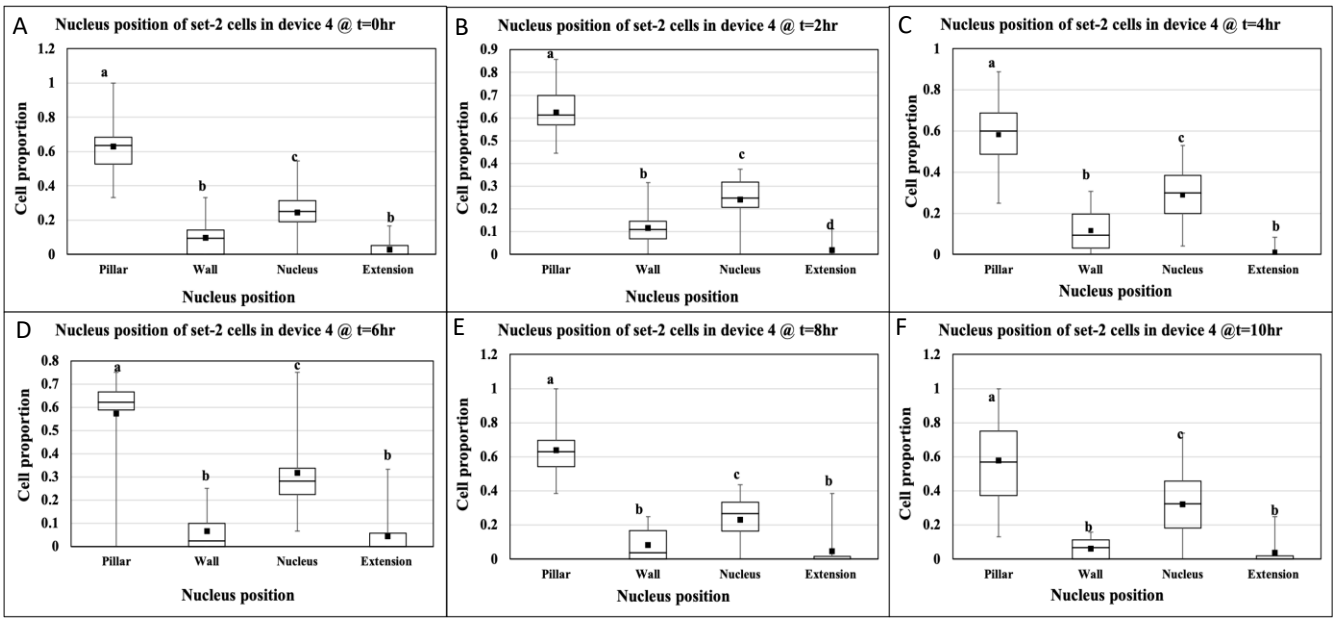

Figure 24. Device 4, the proportion of set-2 cells in device 4, with their nucleus positioned closest to a device pillar or wall, or a set-1 cell nucleus or extension, over time. Cell position was measured every 2 hr. for 10 hr. Data derive from 3-6 independent experiments. Different letters above boxes indicate significant post hoc differences between groups (Tukey's tests). The proportion of set-2 cell nuclei differed among the four index positions (two from the device, and two from set-1 cells), and set-2 cells were consistently positioned closest (although with a broader range) to a pillar or to a set-1 cell nucleus than to a wall or the extension of a set-1 cell throughout an experiment. A) At t=0hr., set-2 cells were settled closet to the device pillar than set-1 cell nucleus, device wall, and set-1 cell extension ($p<0.01$). B) At t=2hr, set-2 cells were localized closet to device pillar than set-1 cell nucleus or extension, and device wall ($P<0.01$), there is higher cell proportion closer to device wall than set-1 cell extension ($p<0.05$). C) At t=4 hr., set-2 cells were positioned closer to device pillar than device wall, and also set-1 cell nucleus and extension ($p<0.01$). D) At t=6, set- 2 cells were localized closet to device pillar than device wall, and also

set-1 cell nucleus and extension ($p<0.01$). E) At t=8, set-2 cells were settled closer to device pillar than set-1 cell nucleus or extension, and device wall ($p<0.01$), and nucleus-wall with $p<0.05$, and closets to set-1 cell nucleus than device wall ($P<0.05$). F) At t=10hr., set-2 cells were located closer to device pillar than set-1 cell nucleus or extension, and device wall ($p<0.01$).

4.7 Discussion

Four new microfluidic devices designed with different pillar patterns, were fabricated by photolithography to test the impact of device design on myoblast migration on a natural substrate produced by an initial set of cells that had attached, migrated, and differentiated in the device. The overall objective of this research was to select a device design that would best promote myotube formation with potential for use in tissue engineering toward muscle regeneration or muscle-patch studies to replace volumetric loss of muscle tissue. Interest in microfluidic devices has increased in the past 10 years due to their availability, minimal use of reagents, portability, and capacity for allowing visualization for long-term studies of living cells[195]. Experiments were designed to explore device-design features and myoblast migration behavior.

In general set-1 cells were monitored over 5 days from the day of seeding at day 0,1,3, and 5 to examine their migration behavior through different devices. Four different conditions were measured including distance to pillar, angle of proximity, cell area, and cell angle. Distance of set-1 cells to a pillar and the area of set-1 cells differed between the different devices. Set-1 cells were farther from the pillar most of the time in devices 1 and 3; therefore, set-2 cells would be closer to nuclei at these two types of devices with offset rows of pillar. The lowest transverse cell distance to pillars in device 2 and 4 with aligned rows of pillar could keep set-1 cells closer to the pillars and cells would have less freedom to make contact, interact, fuse and form myotubes. Cell area of set-1 cells also varied significantly over four devices over time. The highest cell area happened in device 1 at day 0 and dropped dramatically over 5 days of differentiation. At the end of day 5 of differentiation the highest cell area belonged to device 4 with aligned rows of pillars. While it was not possible to demonstrate that differentiated cells were multinucleated myotubes (3 or more nuclei in a single cell membrane), myotubes containing sarcomeres were present in device channels. Ideally, devices would have been stained for a cell-membrane protein such as dystrophin, so cell configuration could be observed at the end of each experiment, to confirm differentiation of set-1 cells and determine how far cells had differentiated toward myotube formation and

elongation. Without such confirmation, it is difficult to say for certain, whether set-2 cells were interacting with mature myotubes or differentiated myocytes. Since the state of the set-1 cells is presumed to have influenced their attractiveness to set-2 cell migration behavior, it may be that set-2 cells are more attracted towards myotubes in early than later differentiation. Myocytes and mature myotubes presumably have different (if overlapping) sets of proteins on their surfaces, given differences in the extent of differentiation and interaction with other types of cells if they are *in vivo*. Myoblasts (set-2 cells) will interact distinctly with more or less mature cells, even mononucleated cells in different states of differentiation and fusion. Thus, the current experimental system may be modeling an earlier set of interactions (i.e., myoblast-myocyte rather than myoblast-myotube) in the developmental or regenerative process. The uncertainty about the differentiation state of set-1 cells does constrain the interpretation of the current study.

In devices with aligned pillars (D2 and D4), set-2 cells accumulated closest to a device pillar than to the nucleus of a differentiated set-1 cell by 10 hr. By comparison, in devices with offset rows of pillars (D1 and D3), set-2 cells migrated to a position closest to a set-1 cell nucleus. In addition, the proportion of set-2 cells closest to a device wall did not differ significantly from the proportion closest to the extension of a set-1 cell in both offset and aligned rows of pillar devices and was consistently lower than that closest to a set-2 cell nucleus or a device pillar.

Findings are interpreted to indicate that devices with offset rows of pillars would guide the myoblasts to form the myotube faster as cells either set-1 or set-2 cells would be farther from the pillars and set-2 cells were closer to the nuclei of set-1 cells. This can help us to understand what the barriers are for forming a muscle patch in tissue engineering purposes. Having set-1 cells over a naturally formed FN substrate by means of differentiated set-1 cells can compensate the role of FN substrate to guide the cells in a same patter as FN coated substrate devices. Looking at the cytoskeleton of set-1and set-2 cells in different devices when set-2 was loaded over set-1 cells could help us to better understand the effects of substrates on myotube formation and alignment. This would be possible by live imaging and the thickness of the device didn't let us to have a high-quality image.

A number of reports have previously explored myoblast alignment within microscopic devices that vary in substrate and design. For example, using a microdevice in a biocompatible polymer, poly (lactic-co-glycolic acid, PLGA) melt-casted from a PDMS mold, the PLGA-based device was used to form microgrooves of various depths into the substrate for culturing C2C12

cells. Authors examined myoblast migration and proliferation[74]. In that study, C2C12 cells showed different alignment responses depending on the dimensions of the grooves in which they were cultured. Migration and alignment of C2C12 cells both were closely related to groove depth, since cells migrated to a certain height and aligned using their pseudopodia. The expression of filamentous actin, the cytoskeleton protein, was higher in aligned than non-aligned cells[74] likely due to the formation of large stress fibers. The 3D microgrooves also were able to induce cell proliferation, consistent with observations that proliferation is lower on a smooth substrate than on a grooved surface. The higher rate of proliferation may be due to the greater adhesion of cells on a rougher surface.

Three-dimensional (3D) configuration of the ECM, cell alignment, and tissue architecture are all important influences on migration by skeletal muscle cells. The early study of primary myoblasts *in vitro* on an early computerized cell-stretching system, also demonstrated alignment[73]. In another report, mesenchymal stem cells cultured on rough surfaces demonstrated a rapid upregulation of focal adhesion kinase which is expressed at a much lower level when cells are cultured on smooth surfaces. Similar studies were done by culturing muscle cells on a shear fluid substrate. Shear forces of the fluid movement on the aligned substrates were designed to explore whether fluid shear influences cell alignment behavior. In addition, the cues of the substrate and its geometric patterns and movement can direct cellular migration and were effective in guiding motility in endothelial cell cultures[76].

In 2010, Ahmed et al. studied the responses of different types of cells, including C2C12 cells, after plating on different ECM substrates and tracked their growth and motility responses to mechanical stimuli[77]. C2C12 cells oriented themselves perpendicular to the stretch direction on non-patterned surfaces, similar to a much earlier study[73] but showed irregular orientation or became realigned in parallel to the orientation of the micropatterned fibronectin substrate[77]. These studies were designed to help improve methods of engineering skeletal muscle tissue by culture of "bulk muscle grafts" that could replace large volumes of muscle lost through trauma or other injuries.

Comparing the devices used in this study, device pairs: D1 and D2, and D3 and D4, shared the same length, width, diagonal space, and inlet and outlet conditions; the only difference between those pairs of devices was the pillar arrangement in aligned (D2 and D4) or offset rows (D1 and D3). Device pairs also have similar inlet-outlet arrangements: D1 and D2 have 3 separate channels

with 3 independent inlets and outlets, while D3 and D4 have 4 channels connected by one inlet and two outlets. The pillar arrangements, and differences in inter-pillar distance in diagonal and longitudinal/transverse directions, decreased the calculated flow rate in part A of the channels to roughly 25%in part B of the channels containing the pillars, in both 3-and 4-channel devices. The presence of pillars also creates turbulence in the flow pathway, one of the main features that can impact the flow rate, illustrated by comparison with control (model) devices of the same measurements but without pillars. We hypothesized that the arrangement of device pillars and differences in flow rate would influence cell migration and differentiation within part B of the channels. In D3 and D4, devices with one inlet and two outlets, one of the outlets can be blocked by having medium in it and cells can flow in the other two channels with an open outlet, so in those devices, future experiments could be conducted with two control and two repeat experimental channels at one time, since flow rate is the same in each pair of channels connected with the same outlet.

The differences of calculated flow rate and velocity across the different devices with aligned and offset pillars, 3- and 4-channels, and including no-pillar controls, is small. This may result from consideration of the fluidic resistance which derives more from parts A and C of the channels, where there are no pillars. In 3-channel devices, flow rate without pillars is highest, as velocity is proportional to flow rate, and transit time through the device is inversely proportional to velocity, medium through the 3 channels with no pillar flow with the highest speed in shorter time than pillared 3 channel devices. However, results of our earlier research on myoblast haptotaxis and chemotaxis, showed that cells have difficulty settling on a substrate in a device with rapid flow, unimpeded by barriers such as pillars that may also restrict cell spread and attachment[2]. D1 with offset rows of pillars, had the lowest flow rate, only slightly different from the no-pillar control; still, that difference was sufficient to help cells settle down better than in D2 with aligned rows of pillars. Furthermore, set-2 cells in D1 were able to migrate and localize more proximate to the nuclei of set-1 cells, a condition that seems more conducive to cell fusion and myotube growth[196-200]. Based on this interpretation, D1 with a flow transit time that is higher by 2 seconds than D2 and 3 seconds higher than calculated flow time for 3-channel devices with no pillars. A similar situation can be considered for 4-channel devices: when there are no pillars, the flow rate is higher than in devices with pillars and therefore, the velocity of flow is highest, and the flow time is much shorter. The smallest flow rate and velocity in 4-channel devices belonged to D3 with

offset rows of pillars, as found for 3-channel devices. Thus, devices with aligned rows of pillars had higher flow rate and velocity compared to devices with offset rows of pillars, since the offset pattern exposes the medium to more surface area and causes turbulence that misdirects flow through the channel. To form a myotube in these devices, the expectation is that the nuclei of set-2 cells become closer to the nuclei of set-1 cells, and thus would show that cell nuclei during cell fusion events would get closer to each other to fuse and form a myotube. This behavior was the observed pattern in the devices that were examined, and reflected the inward migration of elongating, migratory myoblasts during regeneration *in vivo*[199], even though cell-cell fusion is often observed between extensions of two cells in close proximity *in vitro*. Therefore, it shows cells are forming myotube with set 2 and they are not just migrating over set 1 of cells. In devices with aligned rows cells get closer to the pillars, this can prohibit the cell fusion and delay myotube formation. But as offset rows devices show more freedom for myoblasts to communicate and fuse, the cell proportion is higher to the areas closer to the nuclei of set 1 cell. The aligned rows of pillars appear to support the migration of myoblasts more to the pillars as in D2; that apparent attraction may be due to the effects of cell proliferation and/or cell-cell contact, as if cells find a location conducive or supportive of cell-cell fusion.

5. *The roles of fibronectin-integrin interactions in C2C12 myoblast migration – Results-3*

5.1 Abstract

Previous experiments in devices that were precoated with a fibronectin substrate showed that fibronectin (FN) shortened the time to confluency of set-1 cells by about 2 days. Further studies were designed to explore the interaction of fibronectin with integrin to advance our understanding of the mechanism targeted by variations in device design that affect cell behavior or movement. Four different inhibitors or blockers were used to disrupt FN interaction and signaling through integrins (Intg). Two treatments were applied to set-1 cells after 5 days of differentiation: an RGD inhibitor ((Arg-Gly-Asp) peptide) of fibronectin binding to integrins, and CS1 peptide (in the type III connecting segment of FN), were examined for their impact on the immediate behavior of differentiated set-1 cells (myotubes), and on set-2 cells seeded over the differentiated set-1 cells. Two other treatments targeted fibronectin signaling in migration,

including a focal adhesion kinase (FAK) inhibitor and an anti-integrin blocking antibody, were applied to set-2 cells just prior to seeding onto differentiated set-1 cells. All treatments were applied in a device with offset rows of pillars that had previously shown the highest frequency of set-2 cells closest to the nuclei of set-1 cells, an important feature of myotube formation. The purpose of this study was to investigate how the FN binding and inhibitors would influence set-2 cell behavior on set-1 cells, comparing the behavior of cells on a naturally produced substrate or an applied FN coating or substrate. Results showed that anti-integrin and CS1 treatments had the greatest number of significant effects on set-2 cells on a naturally produced and coated FN substrate. In channels without an FN coating substrate, the naturally produced substrate was able to impose further impact on in addition to treatment effects. Treatments with RGD, CS1, FAK, and anti-Intg respectively, had the lowest to highest inhibitory and blocking impact on cell morphology, including cell alignment, positioning, cell area, and attachment. Further study of cellular taxis should provide clues to identifying a device that would best create a muscle by promoting muscle fiber growth by advancing fusion of set-2 to set-1 cells, and in the longer term, inducing set-2 cells to become quiescent satellite (stem) cells, so valuable in effective producing of muscle tissue by engineering and regeneration.

5.2 Introduction

In previous studies, microfluidic devices were investigated to determine C2C12 myoblast responses to a chemokine and to substrate composition[3]. Cell behavior was visualized for almost 5 days in conditions with or without chemokine and haptotaxis substrate gradients in the migration channel. Changes in gradients affected the direction and behavior of myoblasts during migration across the channel, and the haptotaxis substrate configuration modified myoblast chemotaxis responses to hepatocyte growth factor. Notably *in vivo*, the interaction of extracellular matrix substrate and growth factors within a region of injured muscle directly impacts myoblast migration, differentiation, and new fiber formation[201]. Considering the importance of substrate in myoblast migration, new devices that varied in substrate configuration and flow parameters were designed to determine which would best promote the myoblast alignment and myotube formation that are essential for engineering muscle tissue for use in treating injuries such as volumetric muscle loss.

Further investigation of channel design features in a microfluidic device, and the ability to compare the impact of a natural substrate produced by cells in the device channel with an applied FN coating in the channel, identified how one set of cells seeded to a device (set-1) influenced behavior of a subsequent population of cells (set-2) seeded into the device after set-1 had differentiated[202]. Those new devices were developed with aligned or offset pillars within the channels, such that offset pillars were twice as far from one another in horizontal and vertical directions than in devices with aligned pillars. These channel features affected flow and turbulence. Results showed that the device with the highest flow rate and the longest transit time for flow (due to turbulence induced by offset rows of pillars) also induced the highest alignment of set-1 cells along the vertical axis, parallel to the overall flow in the channel. Results evidenced that myotube formation, aside from substrate dependency, was also both flow- and time-dependent; moreover, myotube formation changed in the absence of a FN substrate in the devices, likely due to the interaction of FN with the integrins (Intg) used for cell attachment during migration.

Although the presence and concentration of collagen in relation to FN in the extracellular matrix (ECM) mediates myoblast migration behavior[3], cell migration in general, depends on FN-Intg interactions[101] through a highly complex pathway. FN and its receptor α5β1 integrin (Intg) are integral to processes in myoblast differentiation, fusion, and myotube formation, including cell spreading, contacts, migration, and proliferation[101].

FN is a high molecular weight glycoprotein composed of 12 type I, two type II, and 15-17 type III domains[203,204]. Of two immunologically identical FNs, one is secreted from the liver into plasma and the other is an almost-ubiquitous cell-surface protein with critical functions in development, cell adhesion, migration, homeostasis, organogenesis, shape, and wound healing. FN consists of 2 subunits connected by disulfide binds, and FN molecules must be assembled into larger fibrils within the ECM to be functionally effective[203,204]. To achieve this fibril formation, FN has 4 binding segments that help connect it to other FN molecules[205]. Segment $I_{1\text{-}5,}$ the assembly domain, is essential in FN-matrix assembly. A cell-binding domain $I_{9\text{-}10}$ contains the RGD sequence (Arg-Gly-Asp) and the cell-attachment site, via binding to $\alpha_5ß_1$ and $\alpha V ß_3$ Intg[206-208]. FN's connection with $\alpha_5ß_1$-Intg occurs through a synergy site, domain III_9. Other FN domains modulate binding to fibrin, collagen, fibulin-1, heparan, and syndecan[205,209].

The current study utilized a microfluidic device, with or without preparation by an overlay substrate of fibronectin (FN), given our report of the key role of haptotaxis substrates in myoblast

migration in a microfluidic device[3]. Here, we investigated the impact of applying inhibitors and blocking peptides of FN binding to integrin (Intg), including RGD peptide, a FAK inhibitor, CS1 peptide, and an anti-Intg antibody, on myoblast migration behavior. The purpose of this study was to investigate the impact of specific interference with the FN-Intg binding process and compare the behavior of cells differentiated for 5 days after being seeded in the device (set-1), with a second set of cells (set-2) seeded onto set-1. We were also interested in whether and how a natural ECM produced and distributed by differentiated myotubes from set-1 myoblasts, might compensate for the lack of FN substrate over time. Based on our previous findings[202], a particular device with offset rows of pillars, D1 from the earlier report, was selected for the experiments with inhibitors with or without FN.

Cell migration is well established as dependent on FN-Intg interaction[101]. Our initial observation and measurement of cell shape, cell area, cell angle (long axis of the cell in relation to the horizontal axis across channel), and angle of proximity (long axis of the cell in relation to the nearest pillar) suggest that these variables will change in the absence of various aspects of that FN-Intg interaction pathway.

FN and its receptor α5β1 integrin are intimately involved in myoblast differentiation, fusion, and the process of myotube formation, including cell spreading, contacts, migration, and proliferation stages[101]. Inhibitors were selected for the present research by tracing the complex signaling pathway of FN-Intg interaction that unfolds between the time one cell such as a myotube, makes FN, and when a second cell, a myoblast expressing Intg, reacts to that FN.

RGD peptide can block FN-Intg interactions through α5β1, αvβ1, αvβ3 Intgs; at t 0.9 mM of RGD peptide, blockage leads first to cell detachment and then cell death[101]. FN is comprised of four segments, including a connecting segment-1 peptide (CS1) that can be used to probe the activity of the type III segment of FN[126]. Adding 100 μg/ml CS1 to cell growth medium can block FN-α4β1 Intg binding interaction[101].The RGD and CS1 blockers of specific FN binding sites were applied to differentiated set-1 cells cultured in channels of the microfluidic device.

FAK (focal adhesion kinase) is localized in the cytosol and mediates signaling between Intg in the membrane and actin filaments inside the cell; thus FAK mediates the cellular responses to the FN-integrin binding and enables cell adhesion to a substrate[128]. FAK activity transduces FN-Intg binding signals into the formation of actin-filament bundles that shape the cell[128]. Indeed, any

blockage that affects Intg signaling can cause defective adhesion, and induce an aging phenotype in muscle stem cells[128].

Representative inhibitors of along the timeline of FN-Intg signaling were selected for the present exploration of the underlying mechanism involved in changes in myoblast alignment and myotube formation in a device with offset pillars, high flow and long flow time. Experiments using either a CS1 or an RGD peptide to block specific FN-Intg binding from the ligand side, were hypothesized to interfere in set-2 cell responses to FN, including FN made by set-1 cells and in an FN coating. CS1 and RGD peptides were applied to myotubes after 5 days of differentiation in the device. A specific blocking antibody to α5β1-Intg (anti-Intg) and a FAK inhibitor[126] were hypothesized to disrupt the receptor side of the FN-Intg binding and the responsiveness of set-2 cells to FN, again on the differentiated myotubes and any FN coating. Anti-Intg and FAK inhibitor were applied to set-2 cells prior to their loading into devices containing differentiated (and untreated) set-1 cells. By interrupting the signal transduction pathway at different steps, blockers and antibodies were used to establish the importance of each step in the myogenesis sequence where myoblast migration toward differentiated myotubes is essential. We hypothesized that after at least one of the above four treatments, set-2 cell migration toward nuclei of differentiated set-1 cells would be reduced in favor of device pillars as was the case for set-1 cells in the previous study, or set-1 cell extensions, and/or that set-2 cells would behave similar to undifferentiated set-1 cells when seeded on a fresh device. Such a finding would mean that signals from the natural substrate produced by set-1 myotubes had been blocked or interrupted by treatment.

5.3 Materials and Methods

5.3.1 Preparation of the microfluidic device

Devices were fabricated as reported[3] with offset rows of pillars using standard photolithography and lithography in one-layer with flow channels 50-60 μm in thickness[3,80], to allow movement of the large C2C12 myoblasts. Microfluidic channels were uncoated or coated with FN as reported[3].

5.3.2 Cell preparation

C2C12 mouse myoblasts (cat. no. CRL-1772, RRID: CVCL_0188, American Type Culture Collection, Manassas, VA) were cultured in Falcon flasks (50 mL, VWR Fisher, Mississauga, ON, Canada) for up to 20 passages in high-glucose growth medium containing Dulbecco's modified

Eagle's medium (11965092, ThermoFisher Scientific, Grand Island, NY), 10% fetal bovine serum (FBS, SH3039603, ThermoFisher), and 1% penicillin streptomycin (CA45000-652 PS, VWR, South Logan, UT) under 5% CO2 at 37°C and 95% relative humidity. Cells were detached from flasks using trypsin and counted. Since cell density influenced morphology and migration behavior (low cell density limited cell-cell contact, essentially prevented mobility, and led to cell detachment), set-1 cells were seeded in the device (106 cells/mL of medium), loading 1 µL of cell suspension per port[3]. Set-1 cells were imaged using a 10X objective by confocal microscopy every 2 hrs from 0-10 hr after seeding into the device channels, as reported[3,202].

After set-1 cells were 50% confluent in the three independent device channels, growth medium was switched to differentiation medium with 2% FBS for 5 days. At day 5 of differentiation, set-1 cells were treated (or not) with an inhibitor of FN-Intg binding, either RGD or CS1 peptide (see below), and imaged again, every 2 hr. from 0-10 hr.

Set-2 cells were pre-loaded with Hoechst (H3570, Invitrogen, Life Technologies, Waltham, MA), trypsinized from dishes, pelleted, and resuspended in growth medium before seeding into the device channels onto set-1 cells. Again, channels were imaged by confocal microscopy every 2 hr. from 0-10 hr.

5.3.3 Fibronectin-binding inhibitors

At day 5 of differentiation, set-1 cells in two channels were treated with 0.5 mM of RGD (Gly-Arg-Gly-Asp-Ser) (G4391, Millipore Sigma, Oakville, ON) for 5 mins, a time based on preliminary dose-response trials on C2C12 cells to prevent cell death and rapid detachment. One channel of set-1 cells was untreated with inhibitor and served as the independent control channel. After 5 mins, RGD was washed replaced by growth medium in the device. A separate 1-day culture of C2C12 cells (set-2 cells) was trypsinized, pelleted, resuspended in medium, and loaded into devices containing differentiated set-1 cells. With 5-6 repeat experiments, use of 3 independent channels (2 treated and one control), produced 10-12 experimental channels and 6 control channels per inhibitor/blocking treatment. In another set of experiments, set-1 cells were treated with 100 µg/ml fibronectin CS1 peptide (RP10838-1, GenScript, Piscataway, NJ) for a few minutes (again, based on preliminary dose-response experiments to minimize rapid detachment and cell death), and then switched to growth medium.

Two additional sets of experiments used only the control conditions for set-1 cells in untreated channels, described above. Here set-2 cells were loaded, with or without pretreatment

with either 7mM of FAK inhibitor 14 (SML0837, Sigma Millipore, Oakville, Ontario) for 30 mins, or 10 µg/ml recombinant monoclonal human anti-human $\alpha_5\beta_1$-Intg antibody[101] (blocking clone M200, LS-C821471-0.2, LsBio, Seattle, WA) for 30 mins, before preparation and loading onto set-1 cells at day 5 of differentiation (Figure 25).

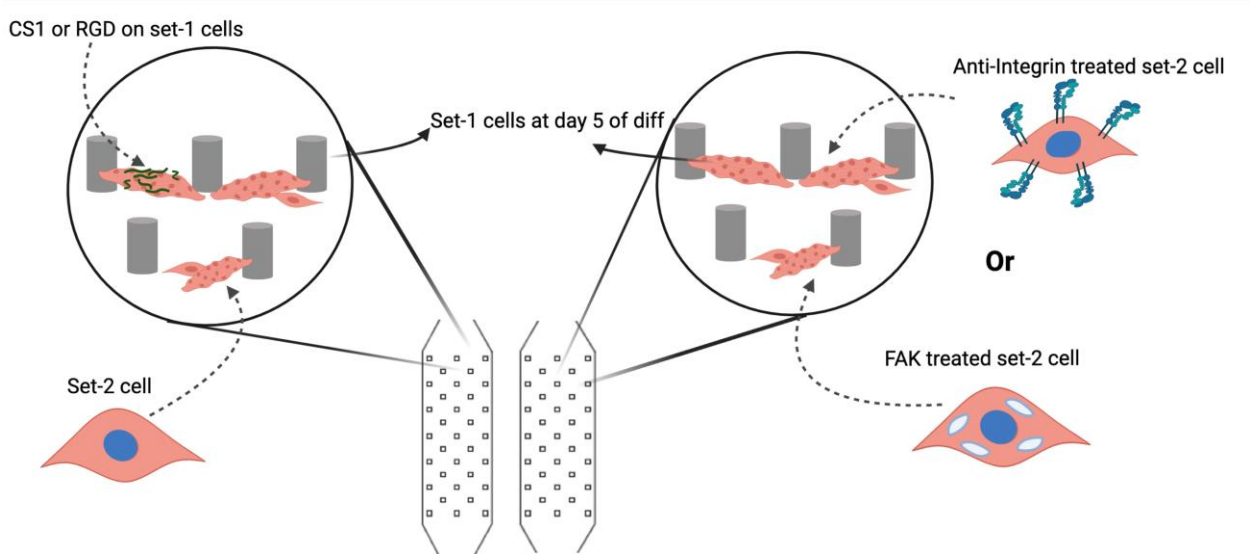

Figure 25. Treatment of set-1 and set-2 cells with peptides and inhibitors to inhibit FN-Intg interaction. Elongated set-1 cells (shown inside circles as dotted pink cells between grey device pillars) were treated with RGD or CS1 (wavy green lines) at day 5 of differentiation; set-2 cells were treated with either FAK or anti-Integrin after 24 hr. of culture and loaded on top of set-1 cells. Original artwork by Z. Rovei Miab, 2021.

5.4 Data analysis

Five to six independent replicates of the experiment were used to study each condition, each with 2 treated and 1 control channel of a device designed to have 3 independent channels. Both set-1 and set-2 cells in device channels were imaged by phase contrast at 10X using an inverted fluorescence confocal Nikon Ti-U microscope (Nikon Canada, Inc., Mississauga, ON, Canada) at 0,2,4,6,8, and 10 hr. after seeding into a device. Additionally, set-1 cells were imaged again and photographed at 0,2,4,6,8, and 10 hr. after treatment). Data were collected from images measured using NIH ImageJ. Every set-1 cell in a channel, almost 150 on average, was observed to identify the center of its nucleus (reported as nucleus position) and the distance (µm) of that nucleus to the nearest pillar in the channel. The cell area (μm^2) was measured as the footprint of the cell on the

floor of the device channel. The cell angle (angle between the long axis of a cell and the longitudinal direction of flow along the channel) and the angle of proximity (angle between a line from the cell nucleus to the nearest pillar and the long axis of the cell) were also measured.

Set-2 cells were identified by their blue fluorescent nuclei. For set-2 cells, the distance (μm) to the nearest pillar and the nearest set-1 cell nucleus were measured, as well as the angle of proximity, cell angle, and cell area. Finally, set-2 cells were categorized as being closest to one of four reference locations in a channel: a channel pillar or wall, or the nucleus or an extension of a set-1 cell. Distributions showed few (<10%) of all set-2 cells were localized closest to a wall or set-1 cell extension, so a nucleus: pillar (N:P) ratio was calculated as the ratio of the proportion of set-2 cells closest to a set-1 cell nucleus divided by the proportion closest to a channel pillar. The N:P ratio was used as a proxy measure that would decrease with increasing myotube formation. Note that there are no data for CS1 or RGD treatments for day 0 on set-1 cells as treatment was at day 5; this accounts for the comparison of set-1 cell behavior before (day 5) vs. after treatment (day 5, 0-10 hr.) with RGD or CS1 peptides.

Measures of the above parameters were compiled according to set of cells (set-1 or set-2), treatment condition (control or treatment with an inhibitor/blocker), time (day and 0-10 hr.), and substrate condition (with or without applied FN coating in the device) in Excel spreadsheets and variable means calculated for each channel. Channels were considered independent experiments as they each had separate inlet and outlet ports. Results were plotted as box-whisker plots showing mean, median, maximum, minimum values, and first and third quartile values. Changes in nucleus position and cell morphology were evaluated using analysis of variance (ANOVA) and *post hoc* Tukey's tests were used to determine pairwise differences, as appropriate. Results were considered significant at a probability of $p<0.05$.

Graphs were drawn using box-whisker plots as it is a convenient and standard method that shows the distribution of data by depicting the first and third quartiles, and the median, minimum, and maximum in addition to the mean. The extended lines out of the box are the whiskers; they show the range of data above and below the third and first quartiles, respectively. Box plots are, therefore, far more informative than bar graphs with error bars; for clarification, standard deviation and standard error of the mean are not plotted on box-whisker graphs.

5.5 Results

One of two blocking inhibitors, RGD and CS1, was applied to differentiated set-1 cells. Subsequent cell behavior was compared to the behavior of the same cells just before treatment on day 5, to explore the impact of treatment on migration behavior. Devices were either uncoated or pre-coated with FN. Figure 26 shows representative set-1 cells in device channels at day 5, and the same cells immediately after treatment with CS1 (or RGD) at day 5. By day 5, sarcomeres were observed within the myotubes present after differentiation. Results are reported by treatment; a summary of significant findings and probability values is presented in Table 2. Findings confirm the importance of FN substrate coating on cell differentiation, since many of the variables were significantly affected by the presence of FN, alone or in combination with treatment, time, or the set of cells being assessed. RGD or CS1 treatment had little, if any, impact on differentiated set-1 cells. RGD only had a significant effect on set-1 cell area through a treatment*coating interaction (Figure 27). Treatment with RGD increased cell area without FN and decreased it when set-1 cells were differentiated on an FN coating. There were similar coating effects on other variables, including cell distance to pillar (in the RGD experiments) and angle of proximity (in the CS1 experiments), without any significant influence of treatment or treatment*coating interactions.

The above before-versus-after experiments with RGD and CS1 treatment occurred prior to seeding Hoechst-loaded set-2 cells into device channels. Additional, parallel sets of experiments had identical seeding, day-1 imaging (at 0-10 hr.), and differentiation of set-1 cells in devices with or without FN pre-coating before seeding Hoechst-preloaded set-2 cells treated with either a FAK inhibitor or anti-Intg into device channels. All four treatments were examined for their effects on set-2 cell behavior. Results are reported by treatment, and a summary of significant findings and probability values is presented in Table 3. Figure 28 shows a representative device channel containing set-1 cells aligning and proliferating over time at day 0; after 5 days, set-2 cells were visualized in the same experiment channel at various time points during their migration and alignment within the device channel containing differentiated set-1 cells.

To assess the effect of RGD, which inhibits the engagement of FN with RGD-binding integrins, differentiated set-1 cells were treated with RGD peptide. Comparisons of behavior by set-2 vs. set-1 cells, both at day 0 (right after being loaded into devices) showed differences in the cell angle (Figure 29) and cell area (Figure 30). A summary of the comparisons between set-1 and set-2 cells for all treatments is presented in Table 3. RGD treatment significantly decreased cell

angle in a complex interaction with FN coating and time (p=0.037). In graphs, there are no data at 0 hr. for set-1 without FN coating, as cell attachment to the glass substrate was delayed for up to 2 hr. for that treatment.

Effects of treatment with CS1, which interferes with integrin dimers binding to FN, were determined by comparing the behavior of set-2 and set-1 cells over the 10 hours after their loading into devices. Data are missing for 0 hr. in the no-FN substrate, due to delayed cell attachment to the uncoated glass substrate of the device, itself, until 2 hr. of culture. Angle of proximity (Figure 31) was significantly decreased by CS1 treatment (p=0.013), and there was also a significant treatment*coating interaction (p=0.038) in that the angle of proximity was higher without FN than with an applied FN substrate coating in the device. CS1 treatment also decreased the measured distance to pillar (p=0.017) (Figure 32) whereas cell angle (Figure 33) and cell area (Figure 34) were affected by conditions other than treatment with CS1. Distance to pillar was smaller for set-2 cells compared to set-1 cells.

The relative positioning of set-2 cells on set-1 cells was also examined by calculating the nucleus:pillar (N:P) ratio (Figure 35). CS1 treatment and FN substrate had a significant interaction effect to decrease the N:P ratio (p=0.031). There was a smaller proportion of set-2 cells closer to a set-1 cell nucleus than to a device pillar at 0 hours, with or without FN substrate. However, by 10 hours, the ratio had fluctuated among groups and was lowest without FN substrate and without CS1 treatment. CS1 appeared to somewhat delay an overall reduction in N:P ratio over time.

Set-2 cells were treated with FAK inhibitor to determine the impact on cell behavior of blocking the final step in the pathway that links FN-integrin binding to cell adhesion. There were no treatment-specific effects of FAK inhibitor on the angle of proximity (Figure 36), the distance to pillar (Figure 37), or the cell angle (Figure 38). There were significant effects of coating and an interaction between coating and set of cells for the angle of proximity and cell angle. In graphs, there are no data at 0 hr. for set-1 without FN coating, as cell attachment to the glass substrate was delayed for up to 2 hr. There are also no data for FAK-inhibitor or anti-Intg treatments for day 0 on set-1 cells (with or without FN) as treatment was on set-2 cells before seeding on set-1 cells at day 5; this accounts for the comparison of set-1 cell behavior before (day 0) vs. after treatment (day 5, 0-10 hr.) with FAK or anti-Intg inhibitors. Angle of proximity was generally larger in set-2 cells in the absence of an FN substrate. Angle of proximity was highest at 8 hours of treatment

in the absence of FN substrate precoating and then decreased. Cell angle was smallest at 4 hour and fluctuated for set-2 cells either with or without an FN substrate.

Both FAK-inhibitor treatment and FN coating significantly affected cell area. Cell area for set-2 cells was smaller overall compared to that for set-1 cells, likely because set-2 cells have less freedom to spread. Cell area was dramatically reduced by FAK-inhibitor treatment ($p=0.007$) and further reduced in a significant interaction with FN coating ($p=0.026$), such that by 10 hours, cell area was larger for FAK-inhibitor treated cells in the absence of FN substrate compared to cells without FAK inhibitor in the presence of FN coating. Generally, cell area was smaller right after seeding into device channels and increased over 10 hours, likely through cell growth. Therefore, FAK inhibitor in the absence of an FN substrate resulted in increased cell area in set-2 cells 10 hours after seeding onto differentiated set-1 cells.

The relative positioning of set-2 cells after loading on set-1 cells was tested by calculating the N:P ratio (Figure 39). N:P ratio decreased over time ($p=0.014$) and was higher on an FN substrate than in the absence of FN precoating.

Anti-Intg treatment was applied to set-2 cells to determine the impact of blocking integrin, the FN receptors themselves, thereby preventing cells from binding with FN. Treatment with anti-Intg had no treatment-specific effect on angle of proximity (Figure 40), although it was higher in set-2 than set-1 cells due to coating effects. However, anti-Intg treatment significantly affected the measured distance to pillar (Figure 41): while set-2 cells were closer to pillars than set-1 cells, a significant interaction between treatment and coating produced a small decrease in distance to pillar in the absence of FN coating. Overall, set-2 cells were closer to a pillar than set-1 cells under control conditions (no treatment or coating). Cell angle and cell area (Figure 42) was not affected by anti-Intg treatment, itself. However, cell area was larger in set-1 cells compared to set-2 cells, especially for set-1 cells seeded on an FN substrate. In control conditions, cell area gradually increased over time. A treatment*coating interaction raised set-2 cell area compared to the control condition, but again, set-1 cells had the largest cell area, possibly due to having more freedom for cell spreading.

The nucleus:pillar (N:P) ratio (Figure 43) was significantly reduced by anti-Intg treatment of set-2 cells ($p=0.013$). The N:P ratio was initially highest under control conditions (without FN or treatment), and by 10 hours the set-2 cells in control channels had the lowest N:P ratio among all the groups.

5.6 Figures

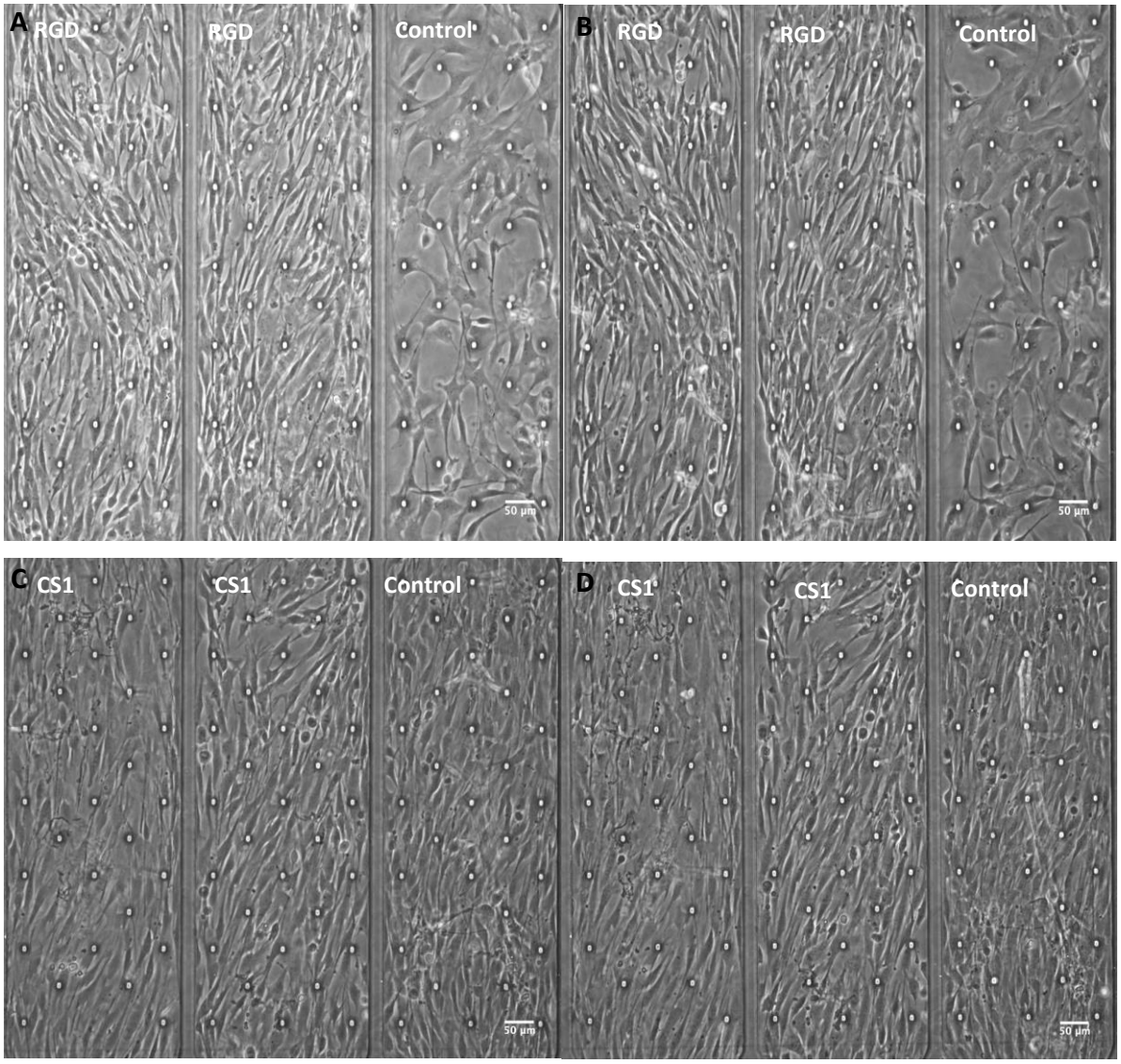

Figure 26. Representative independent experiments in the 3 channels of a microfluidic device containing set-1 cells at day 5 with FN coating substrate. From the outset, two channels were identified for treatment with either RGD or CS1 as indicated, and the third channel was untreated and served as a parallel control experiment. A and B show the same cells before (A) and just after (B) RGD treatment (time 0 hr.) in the two left-hand channels. C and D show the same cells before (C) and immediately after (B) CS1 treatment (time 0 hr.) in the two left-hand channels.

Table 2. Table of significant findings from analysis of variance tests (df=1) on effects of RGD and CS1 treatments applied separately to differentiated set-1 C2C12 cells. Cell angle, angle of proximity, cell area, and distance to pillar were compared at times 0-10 hr. after treatment applied to differentiated set-1 cells to the same cell imaged at day 0 (0-10 hr.) immediately after seeding into the device channel, for the effects of treatment, FN coating, time, and interaction effects.

Treatment	**Variable**	**Significant effects (p value)** • ***Tukey's comparisons (p value)***
RGD	distance to pillar	coating (p=0.005)
	cell area	coating (p=0.008) treatment*coating (p=0.033)
CS1	angle of proximity	coating (p<0.001) • *FN-CS1 vs. noFN-noCS1(p=0.027)* • *FN-noCS1 vs. noFN-noCS1(p=0.032)*
	cell area	coating (p<0.001) • *FN-CS1 vs. noFN-noCS1(p=0.005)* • *noFN-CS1 vs. FN-noCS1(p=0.005)* • *FN-noCS1 vs. noFN-noCS1(p<0.001)*

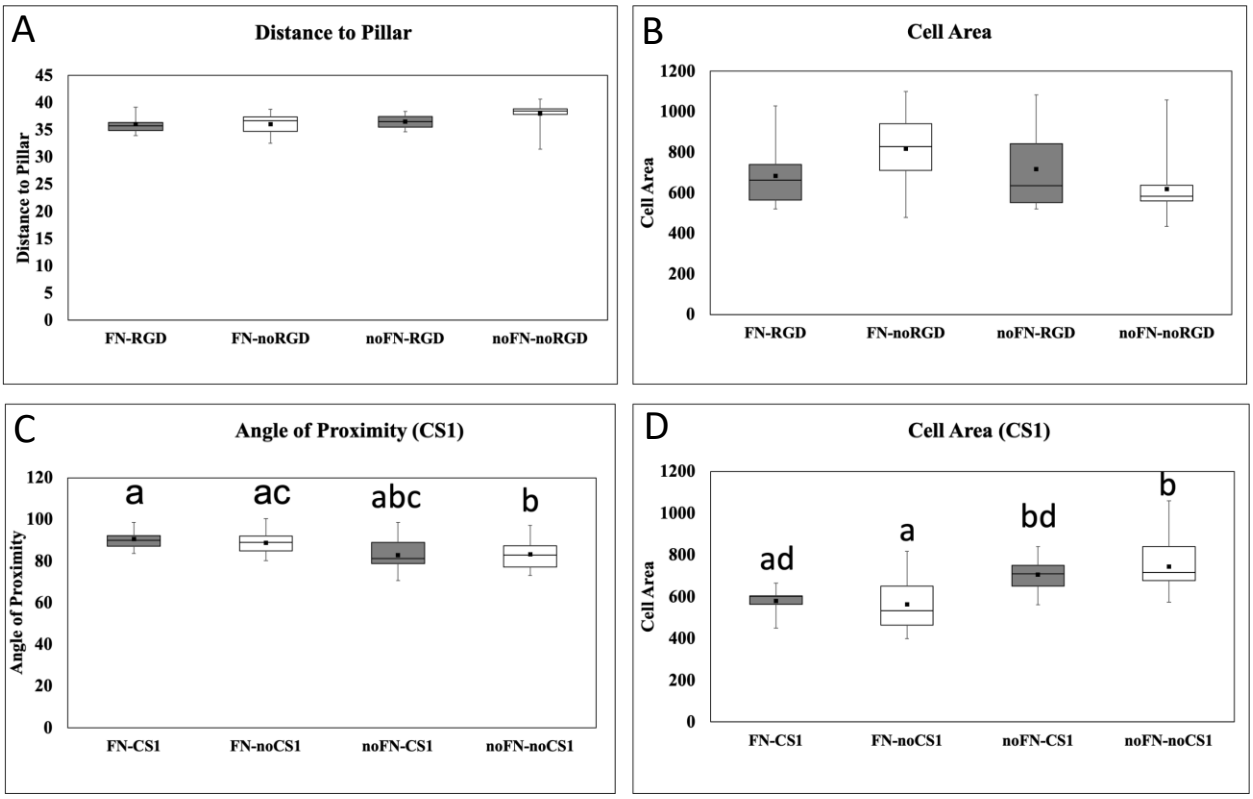

Figure 27. Effects of RGD or CS1 treatment on set-1 cells. Images were captured at day 5 of differentiation in devices with or without an applied FN substrate before and after treatment with RGD (A, B) or CS1 (C, D). Data derive from 5-6 independent experiments. (A) Distance-to-pillar showed a significant effect of FN coating measured at day 5 before and after treatment with RGD differed significantly because of FN coating ($p=0.005$, df=1, ANOVA) it was decreased. (B) Cell area at day 5 also showed a significant effect of FN coating differed significantly after treatment with RGD, due to effects of FN coating ($p=0.008$, df=1, ANOVA) and a coating*treatment interaction ($p=0.033$, df=1, ANOVA). RGD treatment reduced the cell area on FN while it increased the cell area on noFN substrate. (C) At day 5, the angle of proximity changed due to effects of FN coating ($p<0.001$). Angle of proximity increased due to CS1 treatment on FN substrate, in addition CS1 could slightly increase the angle of proximity on noFN substrate. (D) Cell area at day 5 differed due to significant effect of FN coating ($p<0.001$). While CS1 tended to reduce the cell area on both FN and noFN substrates, there was only a significant effect of FN coating on cell area, rather than a specific effect of CS1 treatment Different letters over the boxes indicate significant post hoc differences by Tukey's test.

Table 3. Significantly different behavior of set-2 cells compared to set-1 cells, from analysis of variance tests (df=1) on experiments with 4 inhibitors RGD, CS1, anti-integrin (anti-Ing), and FAK inhibitor. Set-2 cells were loaded on differentiated set-1 myotubes. Effects of treatment, FN coating, time from seeding into the device (every 2 hr for10 hr), and interactions are listed.

Treatment	Variable	Significant effects (ANOVA p value)
RGD peptide	cell angle	**treatment***coating*time (p=0.037)
	cell area	coating (p<0.001) set of cells (p<0.001) time (p<0.001) coating*set of cells (p<0.001)
CS1 peptide	angle of proximity	**treatment** (p=0.013) coating (p<0.001) **treatment***coating (p=0.038)
	distance to pillar	**treatment** (p=0.017)
	cell angle	set of cells (p<0.001)
	cell area	coating (p<0.001) set of cells (p<0.001) time (p<0.001) coating*set of cells (p<0.001) set of cells*time (p<0.001)
	N:P ratio	**treatment***coating (p=0.031)
FAK inhibitor	angle of proximity	coating*set of cells (p=0.002)
	distance to pillar	coating (p=0.046)
	cell angle	coating (p<0.001) set of cells (p=0.001)
	cell area	**treatment** (p=0.007) coating (p<0.001) set of cells (p<0.001) time (p<0.001) **treatment***coating (p=0.026) coating*set of cells (p<0.001)
	N:P ratio	time (p=0.014)
Anti-Intg	angle of proximity	coating (p=0.013) set of cells (p=0.029)
	distance to pillar	**treatment***coating (p=0.023) coating*set of cells (p<0.001)
	cell angle	set of cells (p=0.002)
	cell area	coating (p<0.001) set of cells (p<0.001) time (p<0.001) coating*set of cells (p=0.002) coating*time (p<0.001) set of cells*time (p<0.001) coating*set of cells*time (p<0.001)
	N:P ratio	**treatment** (p=0.013) time (p=0.037)

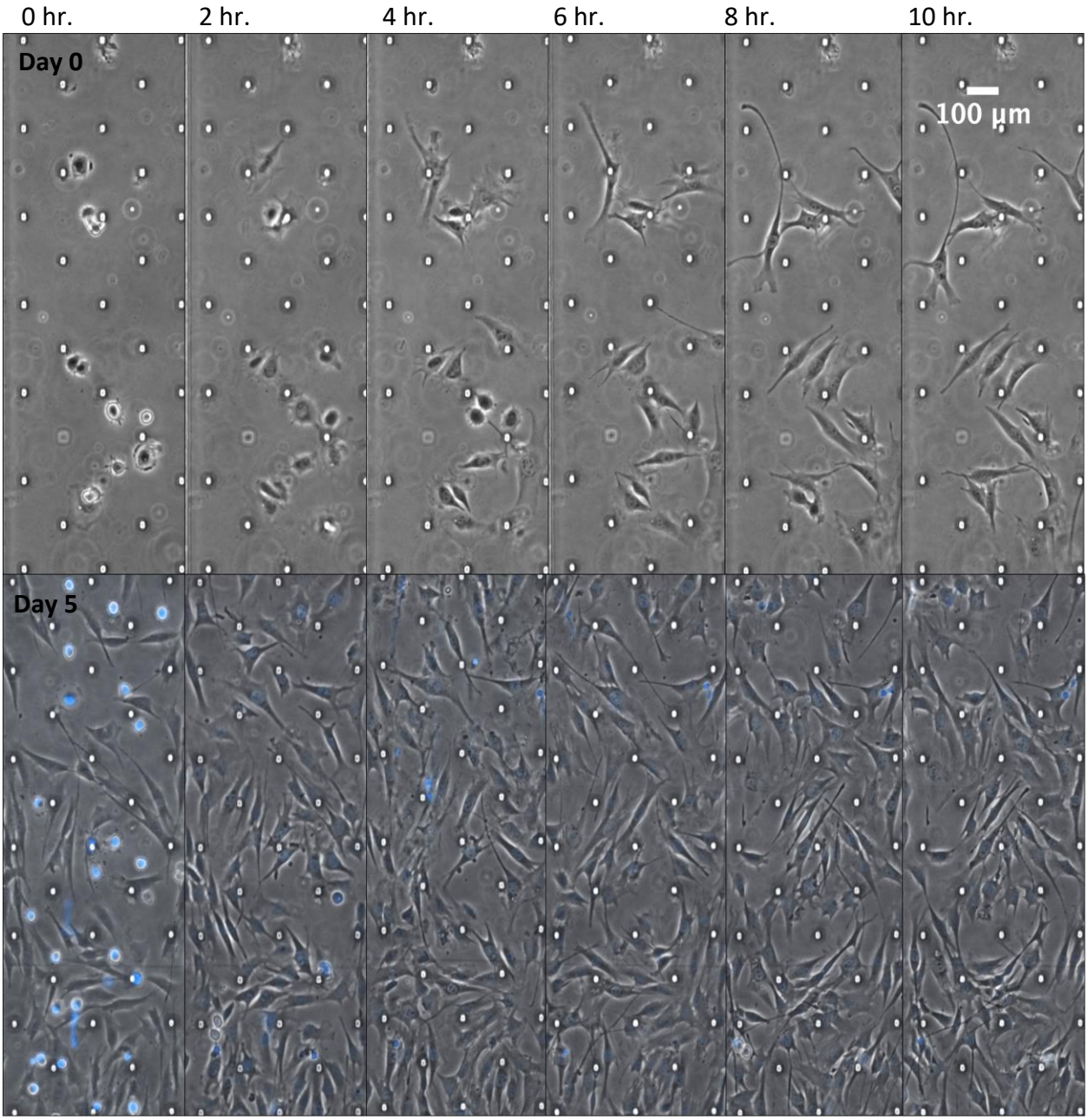

Figure 28. Set-1 cells (top row) at day 0 and set 2 cells (bottom row) seeded onto day-5 differentiated set-1 cells. Offset rows of pillars appear as shiny white dots in a diamond-shaped array. Set-1 cells (top row) migrate, proliferate, and align within the channels over the first 10 hr. after seeding. Rounded set-2 cells (with blue nuclei from pre-loading with Hoechst dye) are seeded on top of differentiated set-1 cells after 5 days of differentiation. Images show set-2 cells begin to elongate after 2 hr., and then find alignment within the channel.

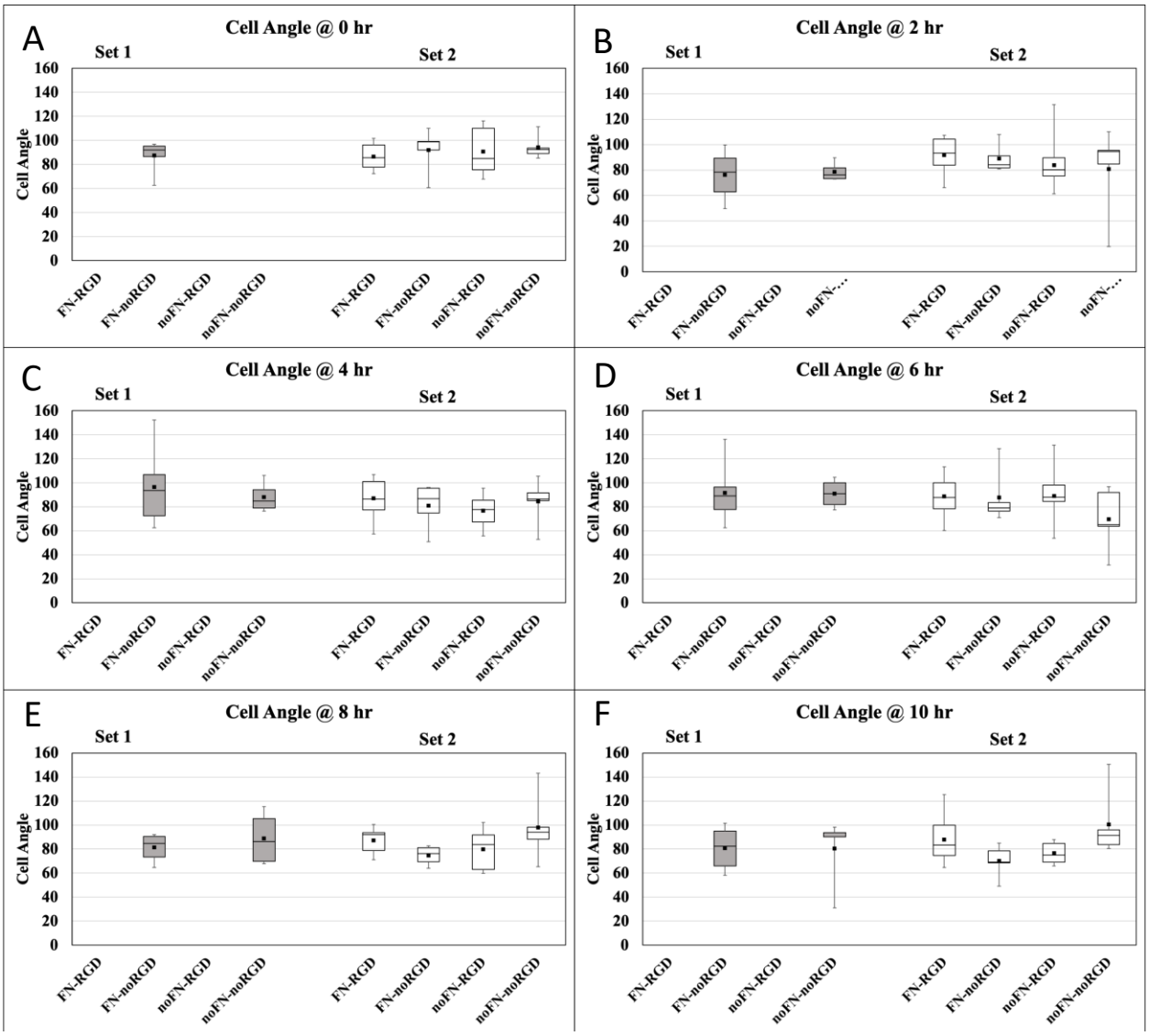

Figure 29. Cell angle for set-1 and set-2 cells over 10 hours, in RGD experiments. Cell angle was measured every 2 hr. for 10 hr. for set-1 cells at day 0 of seeding and set-2 cells at day 0 after loading onto differentiated set-1 cells. An RGD treatment*coating*time interaction consistently reduced the cell angle measured for set-2 cells compared to set-1 cells, but pairwise differences were not significant. At the beginning of treatment RGD could increase the cell angle on noFN substrate, and control condition (noFN-noRGD) had the lowest cell angle. After 10 hr., RGD decreased the cell angle on noFN substrate to be lower than in the control condition.

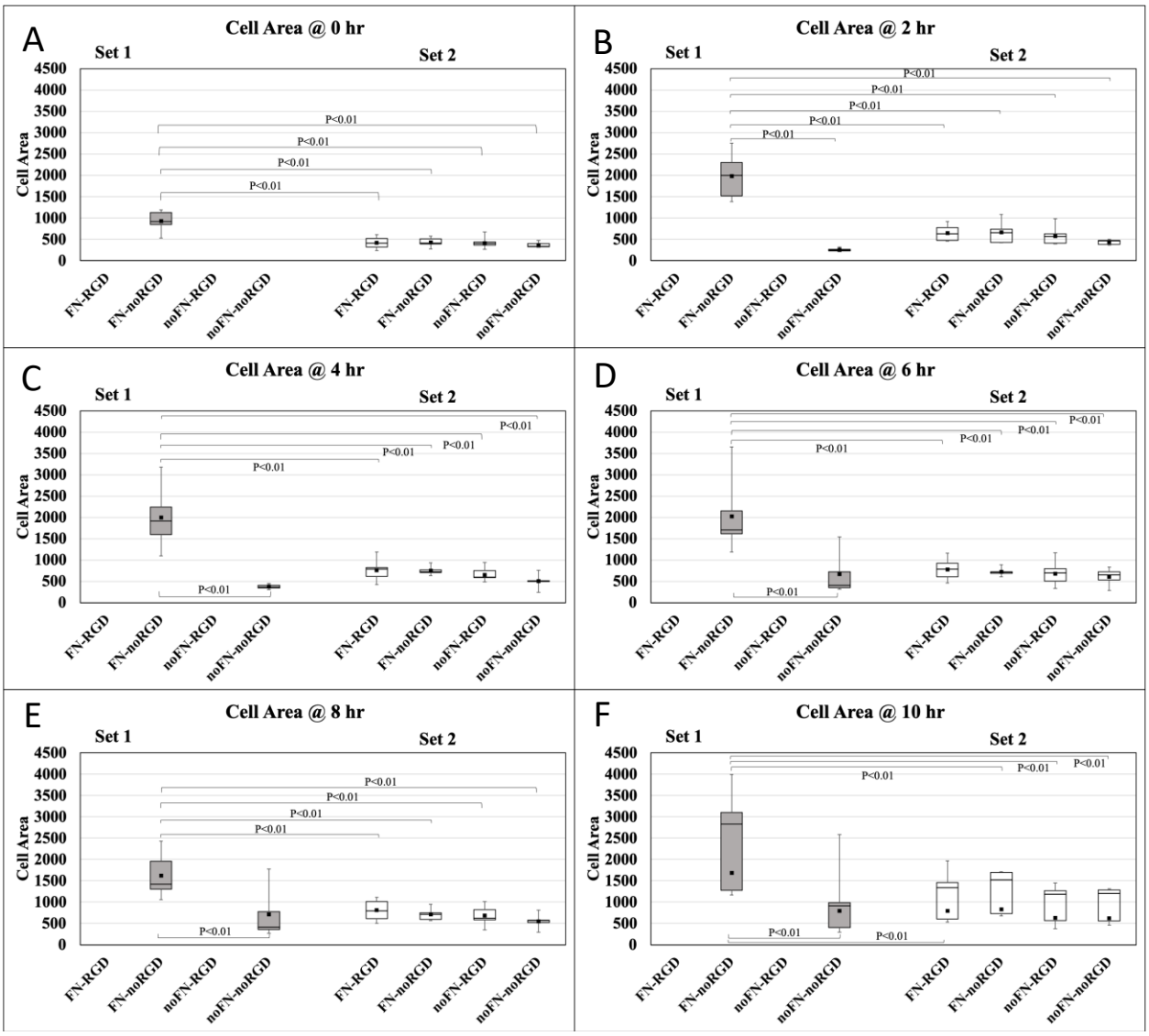

Figure 30. Cell area for set-1 and set-2 cells over 10 hours, in RGD experiments. Cell area was measured every 2 hr. for 10 hr. for set-1 cells at day 0 of seeding and set 2 cells at day 0 of loading onto differentiated set-1 cells. FN treatment effects consistently reduced the cell area measured for set-2 cells compared to set-1 cells. Differences were significant at $p<0.01$; df=4 at 0 hr. and df=5 from 2-10 hrs. There were significant effects of both coating and time on cell area in set-2 cells compared to set-1 cells. Cell area was lowest under control conditions until 10 hr. when the interaction of coating*time*set of cells was able to compensate such that the cell area in the noFN-RGD condition did not differ from the control. Lines indicate significant difference (by Tukey's tests).

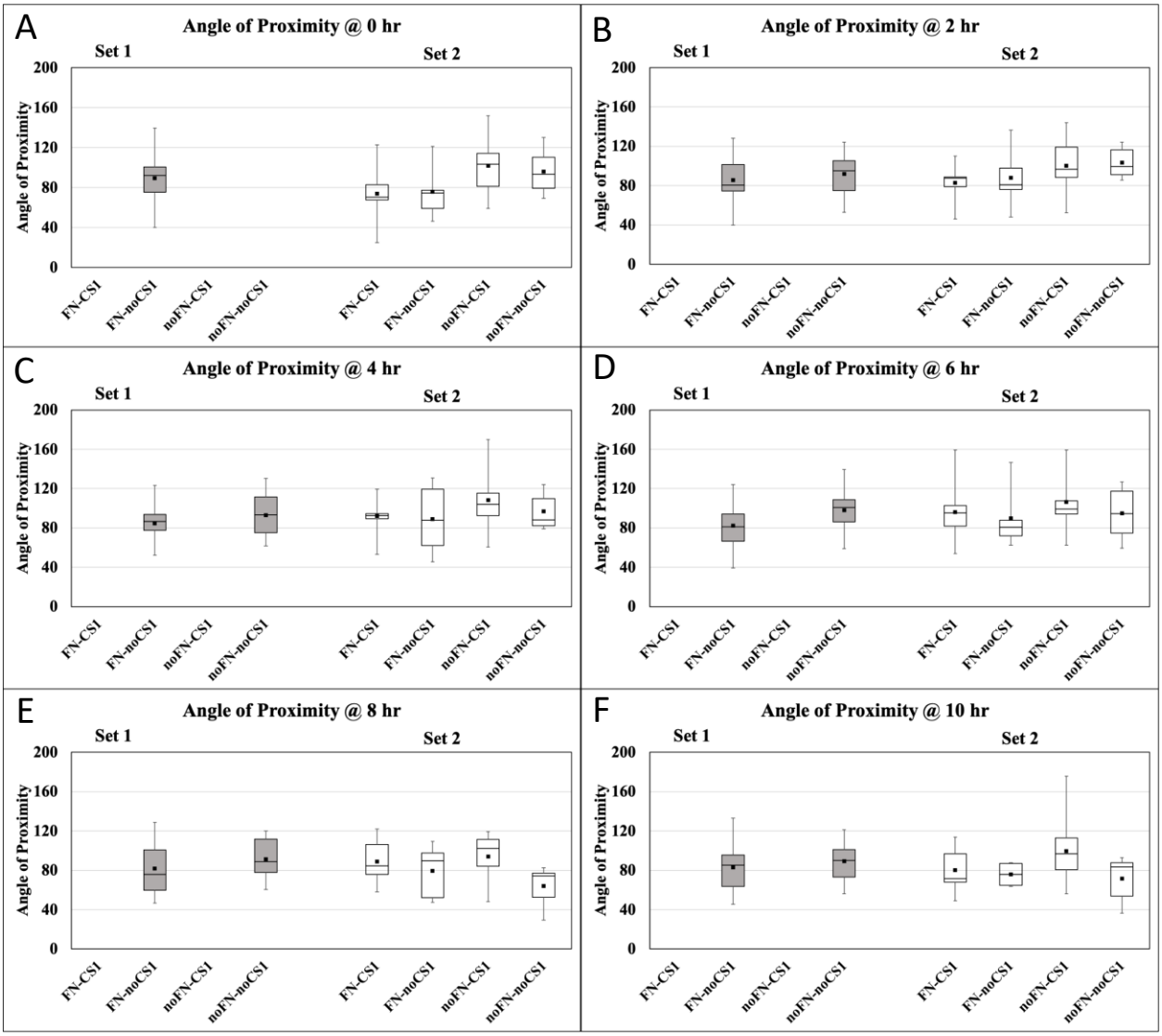

Figure 31. Angle of proximity for set-1 and set-2 cells over 10 hours, in CS1 experiments. Angle of proximity was measured every 2 hr. for 10 hr. for set-1 cells at day 0 of seeding and set 2 cells at day 0 of loading onto differentiated set-1 cells. CS1 treatment, FN coating and their interaction gradually fluctuated the angle of proximity measured for set-2 cells compared to set-1 cells, but pairwise differences were not significant.

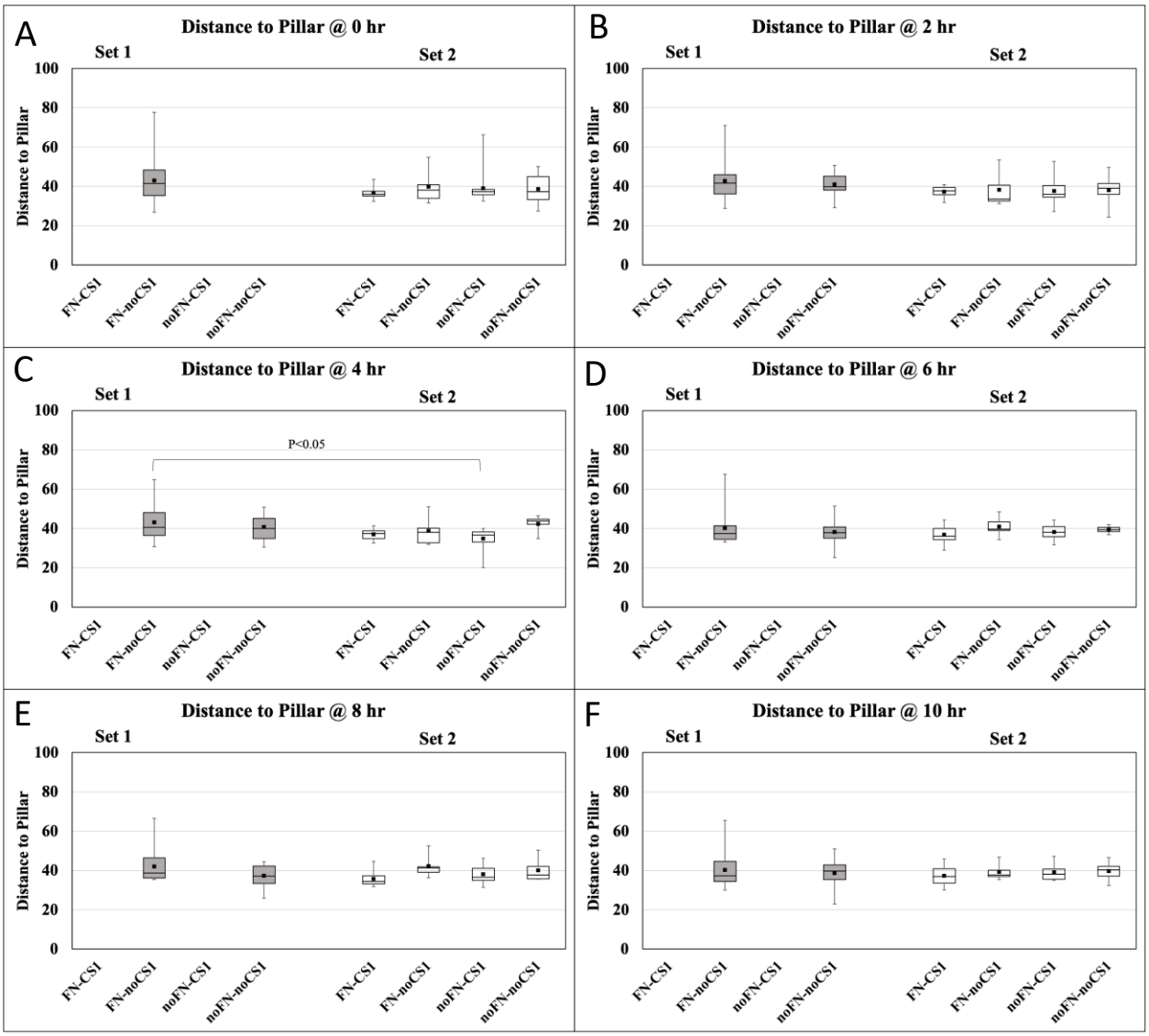

Figure 32. Distance to pillar for set-1 and set-2 cells over 10 hours, in CS1 experiments. Distance to pillar was measured every 2 hr. for 10 hr. for set-1 cells at day 0 of seeding and set-2 cells at day 0 of loading onto differentiated set-1 cells. CS1 treatment consistently reduced the distance to pillar measured for set-2 cells compared to set-1 cells (treatment effect), and distance to pillar was higher on FN than the noFN substrate (interaction effects). Pairwise differences were not significant except at 4 hr. of treatment; line indicates significant difference ($p=0.03$, $df=5$) (by Tukey's tests, $p<0.05$) from FN-noCS1 vs noFN-CS1 between set-1 and set-2 of cells.

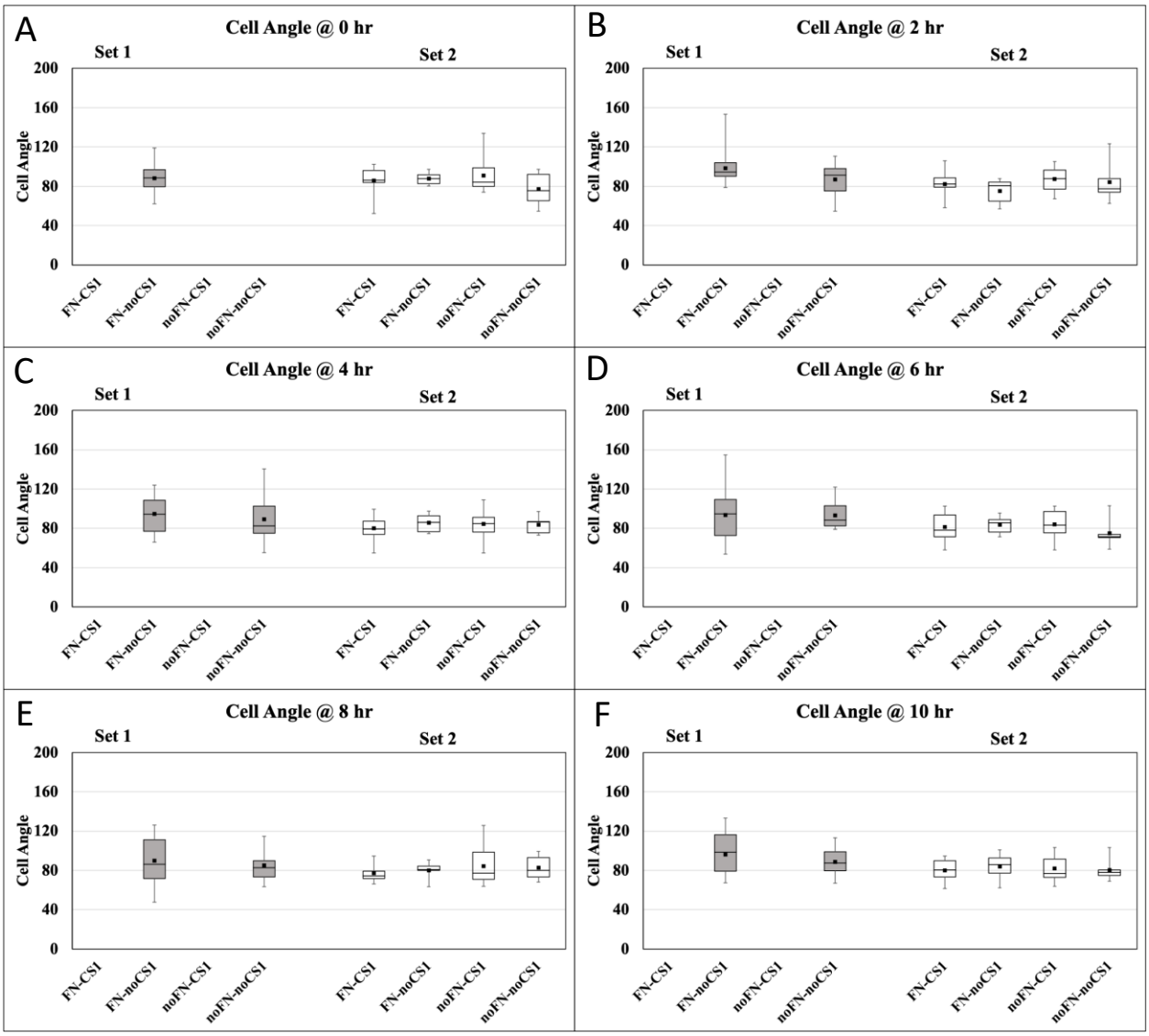

Figure 33. Cell angle for set-1 and set-2 cells over 10 hours, in CS1 experiments. Cell angle was measured every 2 hr. for 10 hr. for set-1 cells at day 0 of seeding and set 2 cells at day 0 of loading onto differentiated set-1 cells. Pairwise differences were not significant, except at 2 hr. of treatment (df=5, p=0.03), Tukey's tests don't show any significant changes between two groups. At the beginning and end of 10 hr. control condition (noFN-noCS1) has the smallest cell angle compared to set-1 and other conditions between set-2 cells.

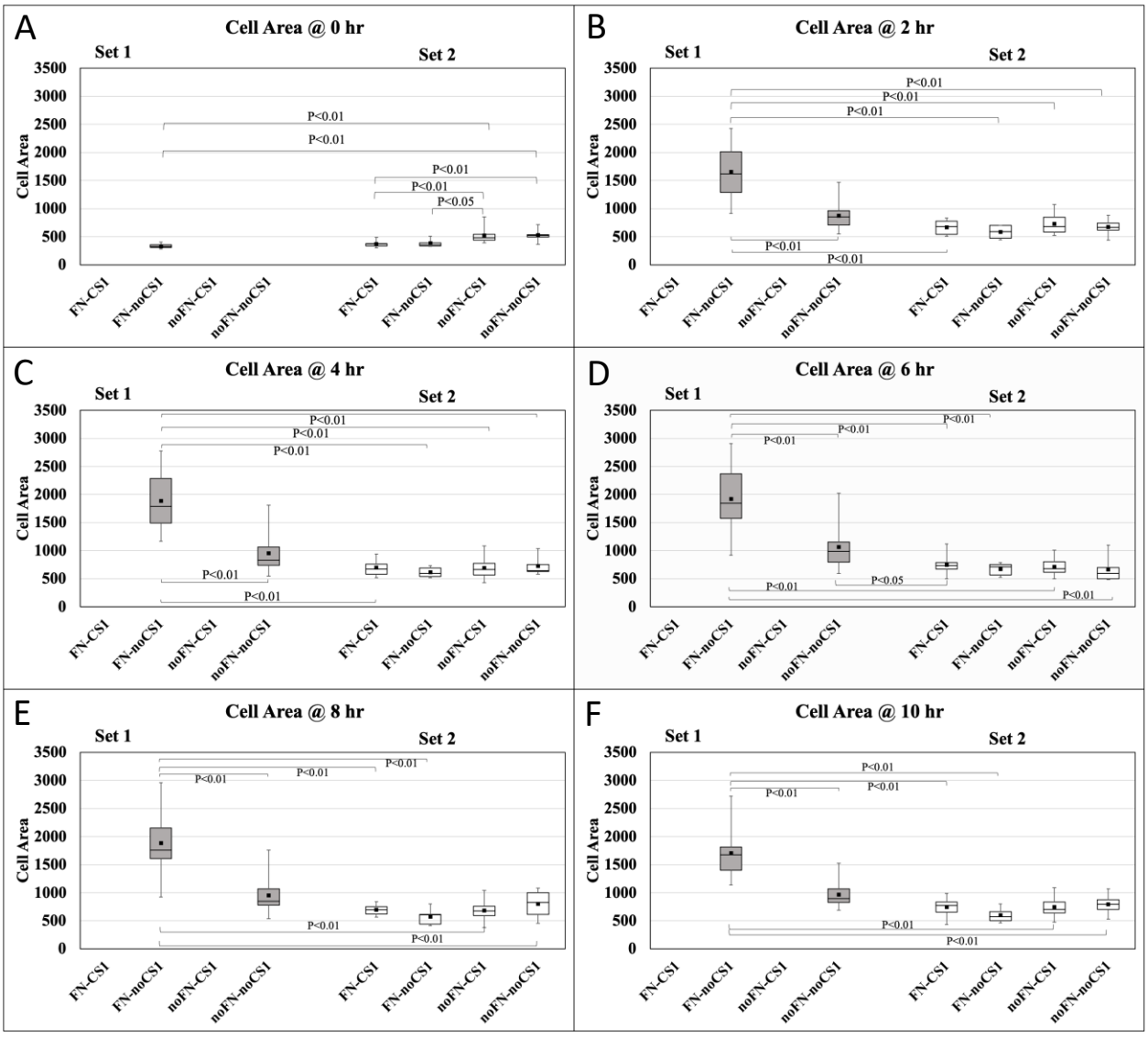

Figure 34. Cell area for set-1 and set-2 cells over 10 hours, in CS1 experiments. Cell area was measured every 2 hr. for 10 hr. for set-1 cells at day 0 of seeding and set 2 cells at day 0 of loading onto differentiated set-1 cells. Set-1 cells on FN substrate had the largest cell area; in general, in set-2 cells, cell area was bigger on noFN substrate.CS1 treatment had no significant effect on cell area changes between set-1 and set-2 cells. Coating over time reduced the cell area measured for set-2 cells compared to set-1 cells, as shown in the graph. Pairwise differences were significant at $p<0.01$, df=4 at 0 hr. and df=5 from 2-10 hrs. Lines indicate significant difference between set-1 and set-2 cells (by Tukey's tests, $p<0.01$ and $p<0.05$) as shown.

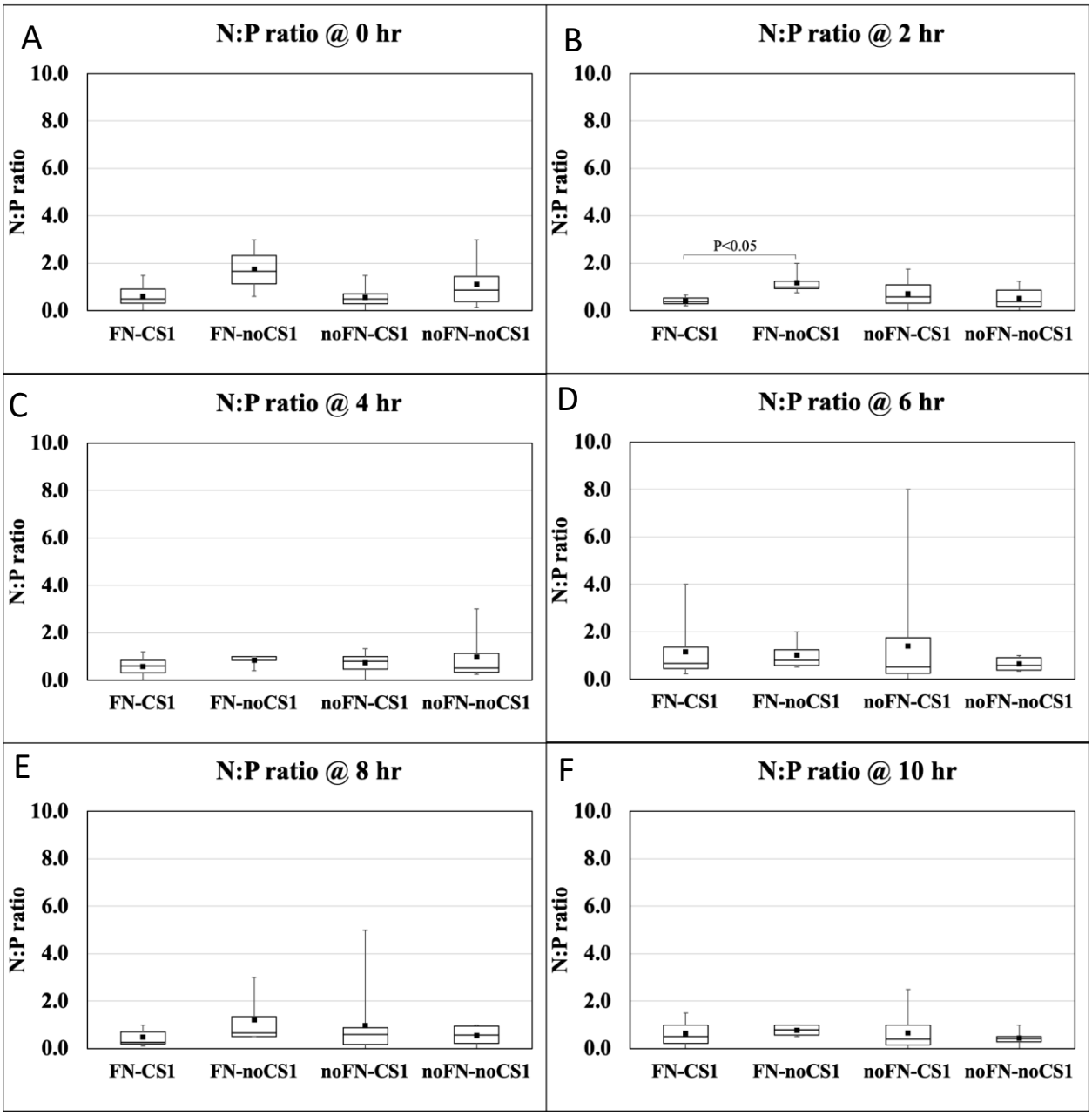

Figure 35. Nucleus:pillar (N:P) ratio for set-1 and set-2 cells over 10 hours, in CS1 experiments. A treatment*coating interaction had significant effects on the position of set-2 cells over 10 hr. (p=0.031). Initially at time 0, set-2 cells were closer to the nuclei than to the pillars (higher N:P ratio) without CS1 treatment on either FN or noFN substrate. Over time, N:P ratio fluctuations in the N:P ratio resulted in fewer and smaller differences across groups. By 10 hrs., the N:P ratio was lowest without either FN or CS1 treatment, meaning that after CS1 treatment, set-2 cells got closer to the pillar. There were no significant Tukey's comparisons between group pairs except at 0 hr. (df=3, $p<0.05$, no significances in Tukey's) and at 2 hr. (df=3, $p=0.05$; Tukey,

p<0.05). CS1 treatment on FN substrate after 2 hours could reduce the N:P ratio by moving set-2 cells closer to the device pillar than nuclei of set-1 cells.

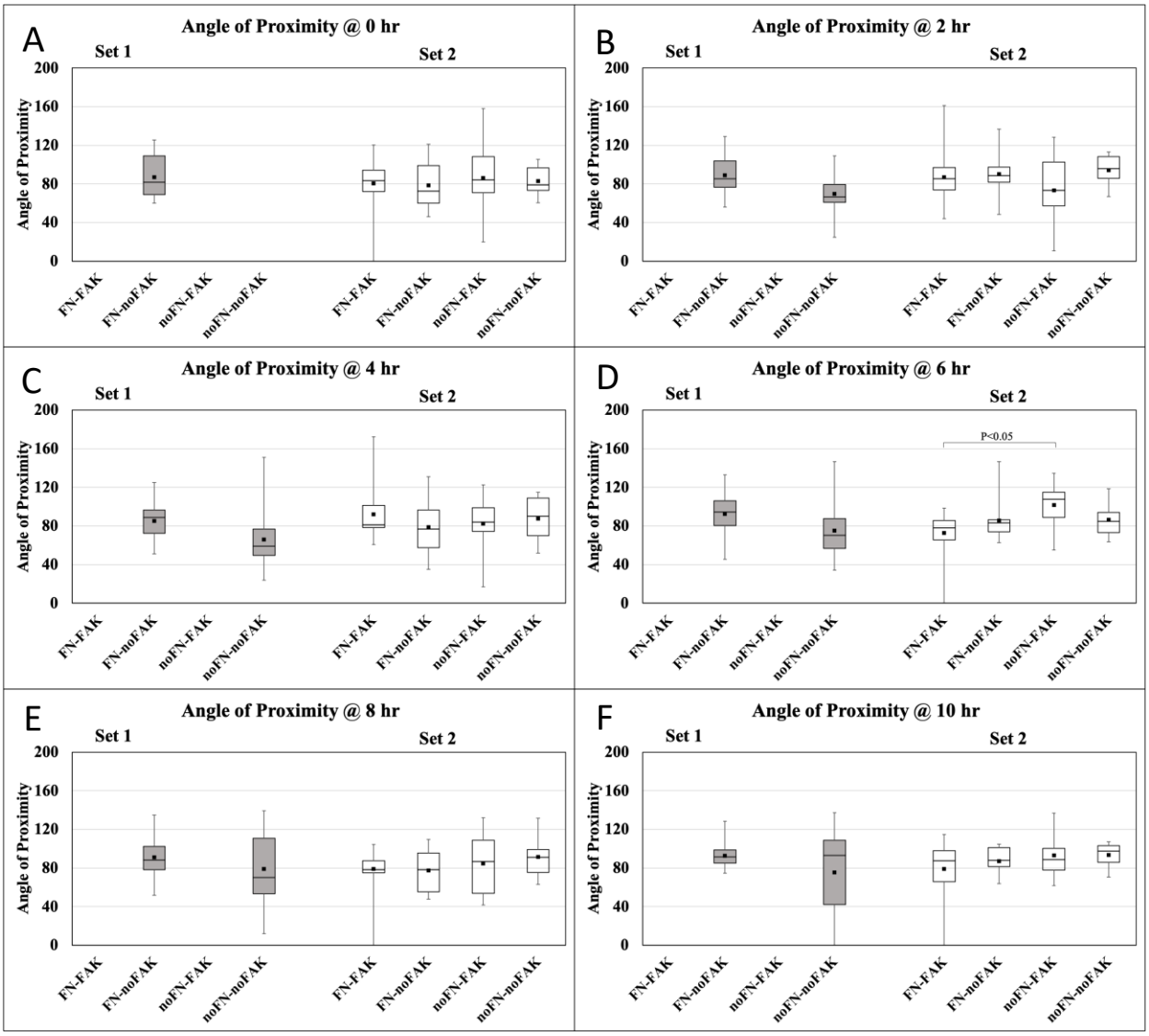

Figure 36. Angle of proximity for set-1 and set-2 cells over 10 hours, in FAK inhibitor (FAK) experiments. Angle of proximity was measured every 2 hr. for 10 hr. for set-1 cells at day 0 of seeding and set 2 cells at day 0 of loading onto differentiated set-1 cells. Coating increased the angle of proximity measured for set-2 cells compared to set-1 cells in overall. Differences were only significant at 6 hr. of treatment (p=0.03, df=5). Line indicates significant pairwise difference (by Tukey's tests) between groups with FAK-inhibitor treatment on set- 2 cells in device channels

with and without applied FN substrate, such that after 6 hr., FAK-inhibitor treatment increased the angle of proximity in the absence of an FN substrate.

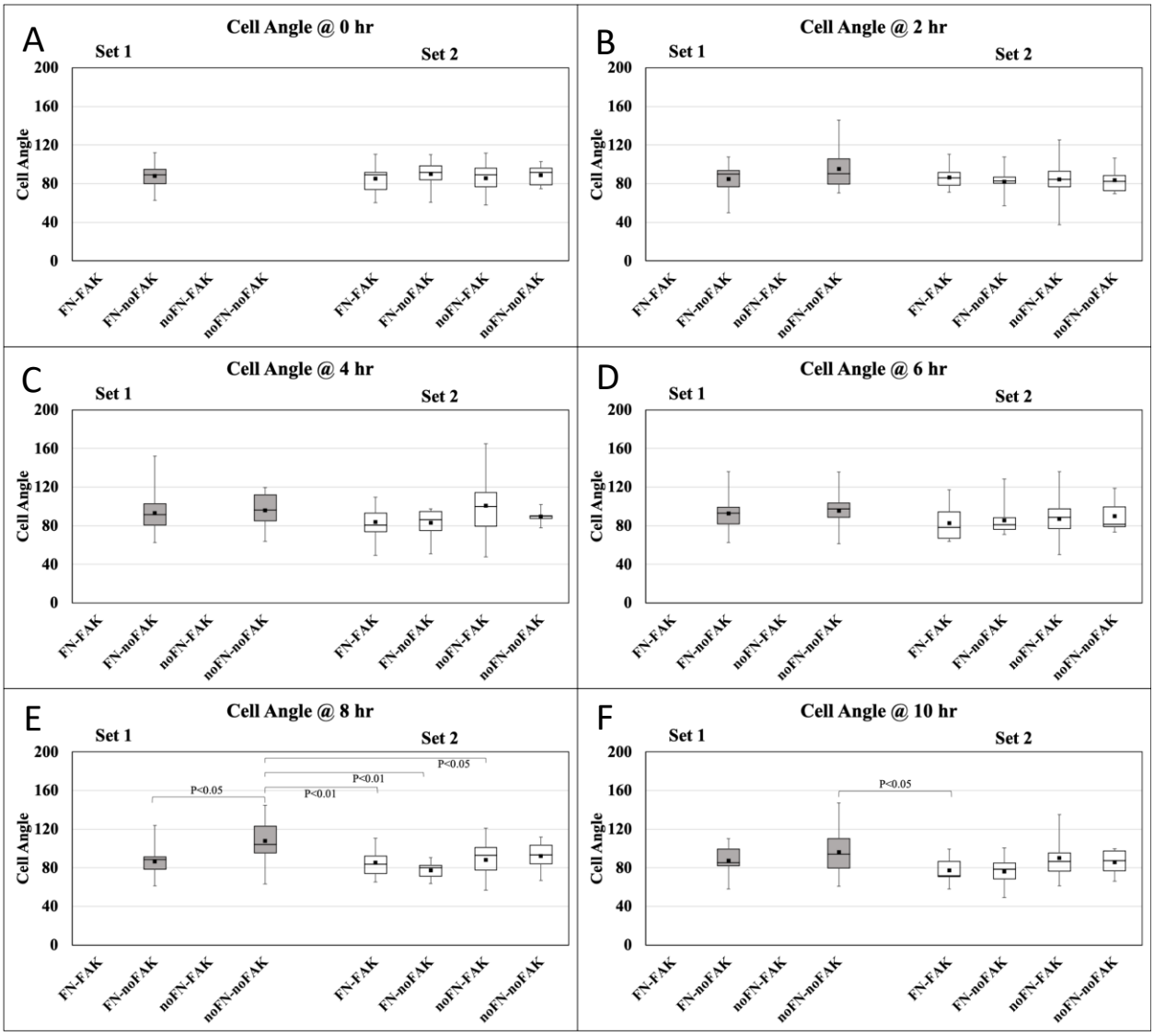

Figure 37. Cell angle for set-1 and set-2 cells over 10 hours, in FAK inhibitor (FAK) experiments. Cell angle was measured every 2 hr. for 10 hr. for set-1 cells at day 0 of seeding and set 2 cells at day 0 of loading onto differentiated set-1 cells. FN coating gradually, reduced the cell angle measured for set-2 cells compared to set-1 cells. Differences were significant at 8 hr. of treatment between set-1 and set-2 cells ($p=0.001$, $df=5$), and at 10 hr. ($p=0.04$, $df=5$), showing that both coating and FAK-inhibitor treatment could reduce set-2 cell angle significantly only after 8 hr. of treatment.

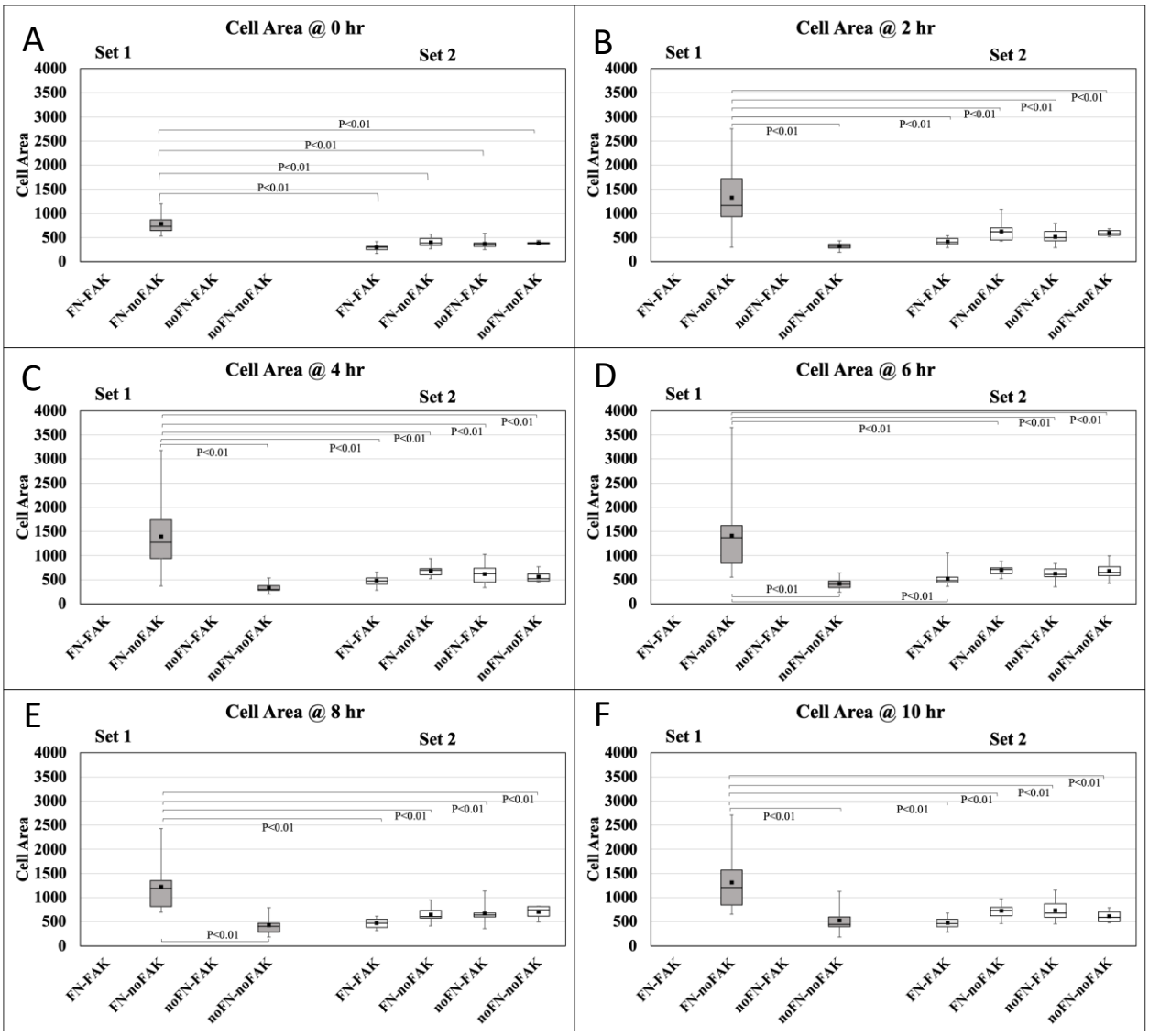

Figure 38. Cell area for set-1 and set-2 cells over 10 hours, in FAK inhibitor (FAK) experiments. Cell area was measured every 2 hr. for 10 hr. for set-1 cells at day 0 of seeding and set 2 cells at day 0 of loading onto differentiated set-1 cells. FAK-inhibitor treatment and FN coating both dramatically reduced the cell area measured for set-2 cells compared to set-1 cells, especially in the presence of FN substrate coating in the device channel, as shown in the graphs. Differences were significant at $p<0.01$, df=4 for 0 hr. and df= 5 from 2-10 hr.

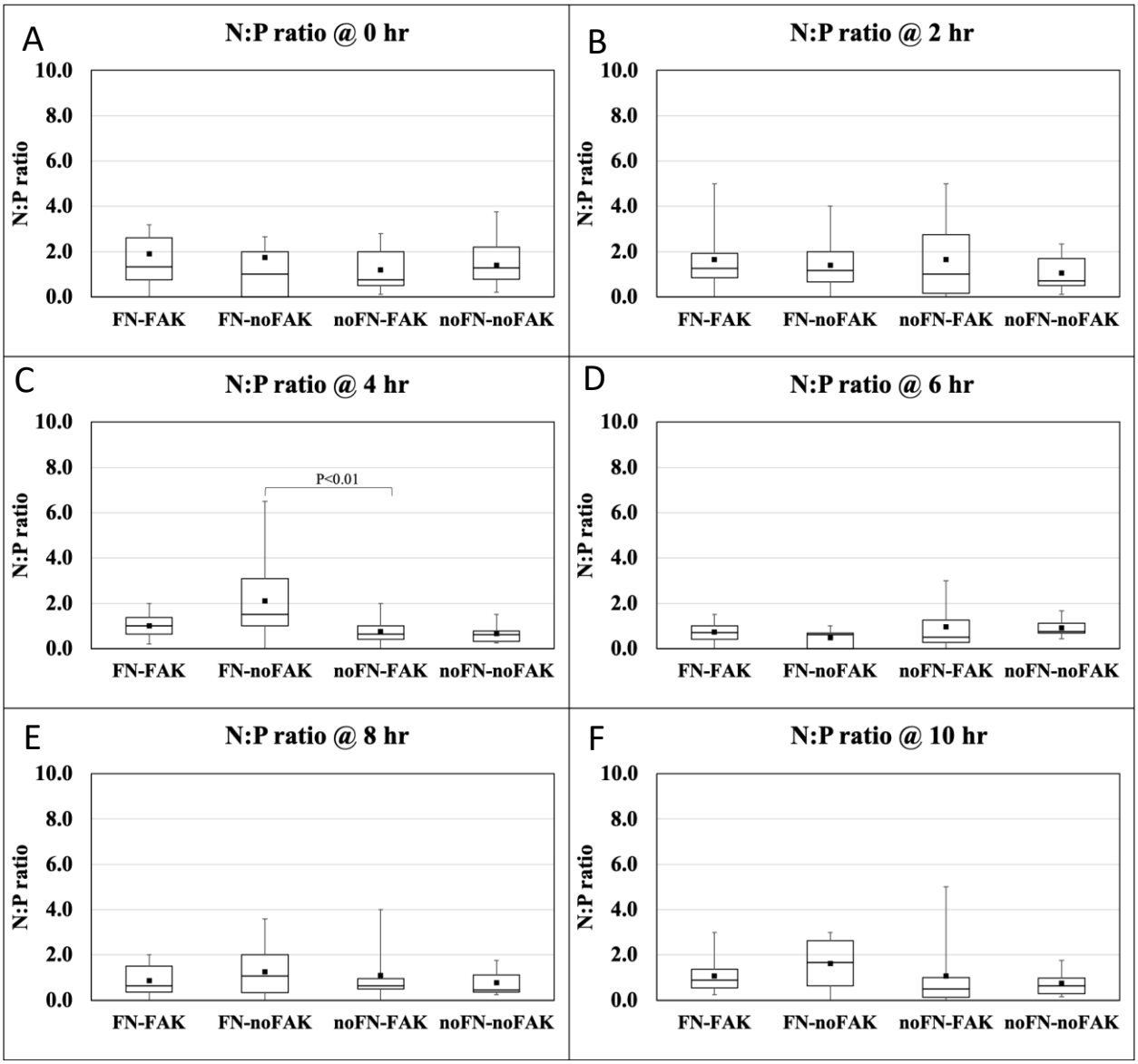

Figure 39. Nucleus:pillar (N:P) ratio for set-1 and set-2 cells over 10 hours, in FAK inhibitor (FAK) experiments. The position of set-2 cells was significantly affected over time, as N:P ratio decreased (p=0.014) and tended to be lower in the absence of an FN substrate. By the end of 10 hr., there was a greater proportion of set-2 cells closer to the nuclei of set-1 cells than device pillars, when cells were seeded on a substrate of FN; FAK-inhibitor treatment did not allow set-2 cells to be attracted to the nuclei of set-1 cells. There were no significant Tukey's pairwise comparisons except at 4hr after treatment (p=0.022, df=3), as shown by the line in the 4-hr graph.

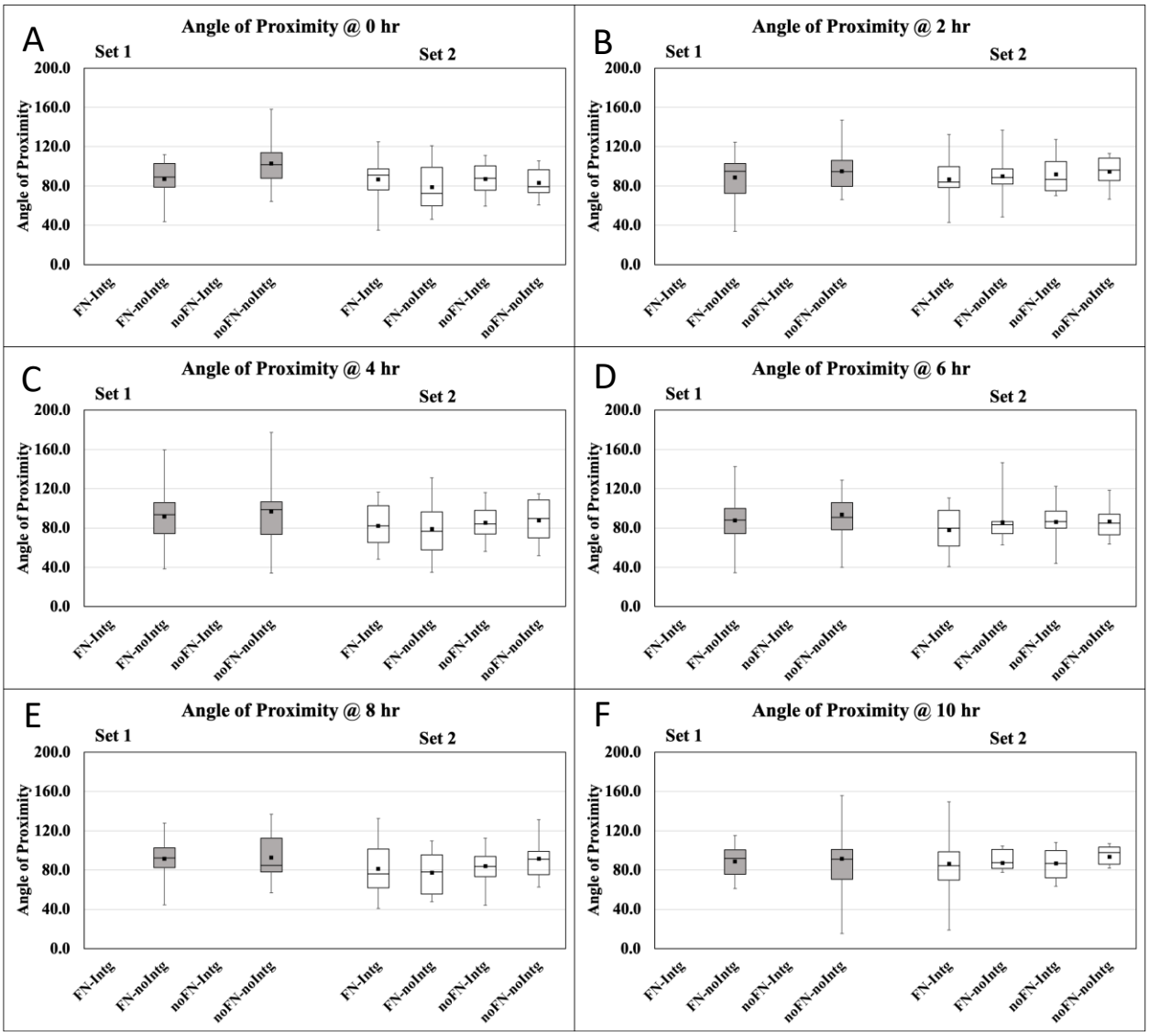

Figure 40. Angle of proximity for set-1 and set-2 cells over 10 hours, in anti-Integrin antibody (Intg) experiments. Angle of proximity was measured every 2 hr. for 10 hr. for set-1 cells at day 0 of seeding and set-2 cells at day 0 of loading onto differentiated set-1 cells. There was no significant effect of Anti-Intg (in graphs, groups are labeled "Intg") on the angle of proximity. Although there was a trend to between-group changes based on effects of FN coating, there were no significant pairwise differences between groups.

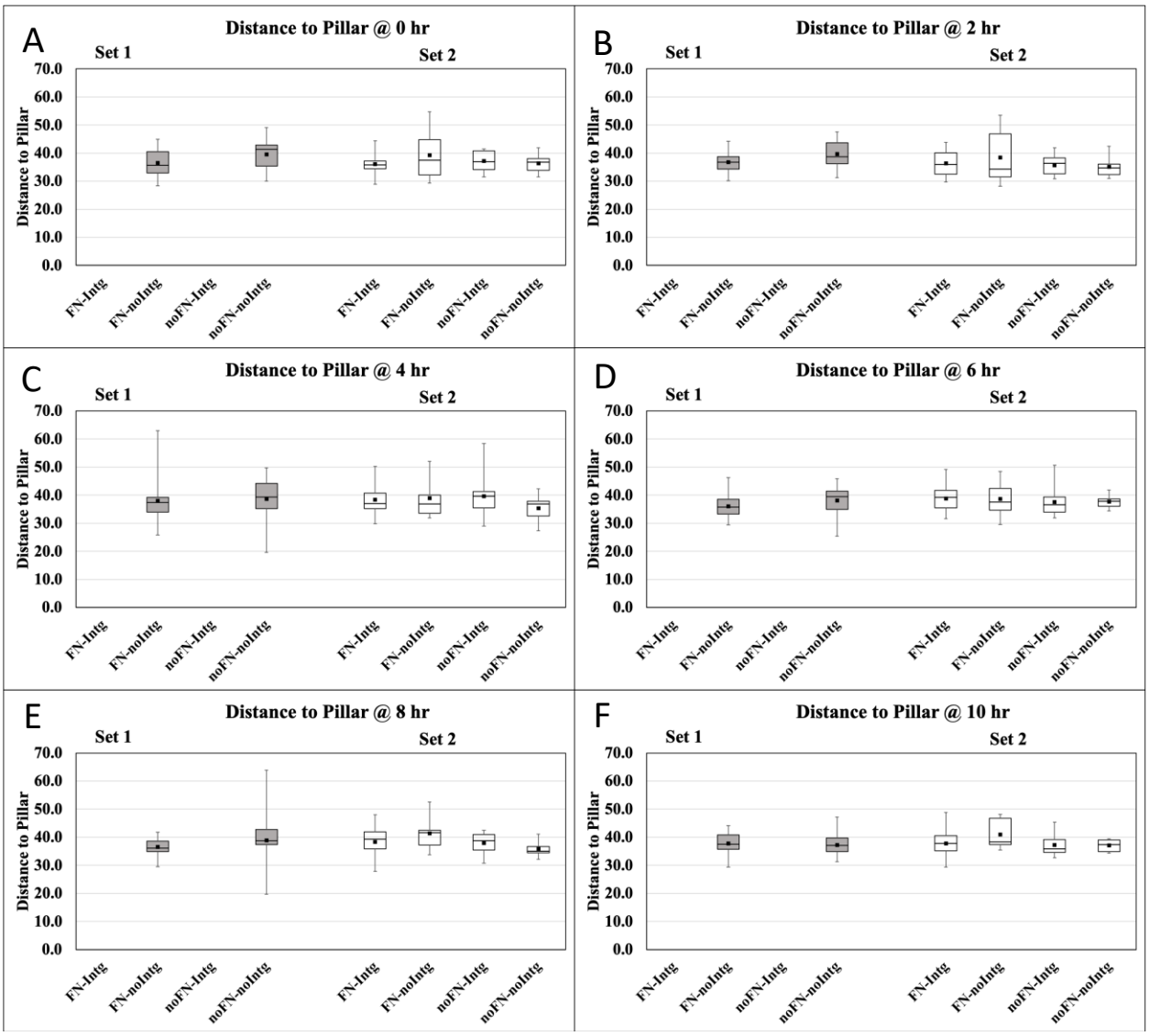

Figure 41. Distance to pillar for set-1 and set-2 cells over 10 hours, in anti-integrin antibody (Intg) experiments. Distance to pillar was measured every 2 hr. for 10 hr. for set-1 cells at day 0 of seeding and set-2 cells at day 0 of loading onto differentiated set-1 cells. Treatment with anti-Intg (in graph, "Intg") subtly reduced distance to pillar measured for set-2 cells, with some compensation by FN substrate coating due to a treatment*coating interaction (p=0.023). However, pairwise differences by Tukey's tests were not significant.

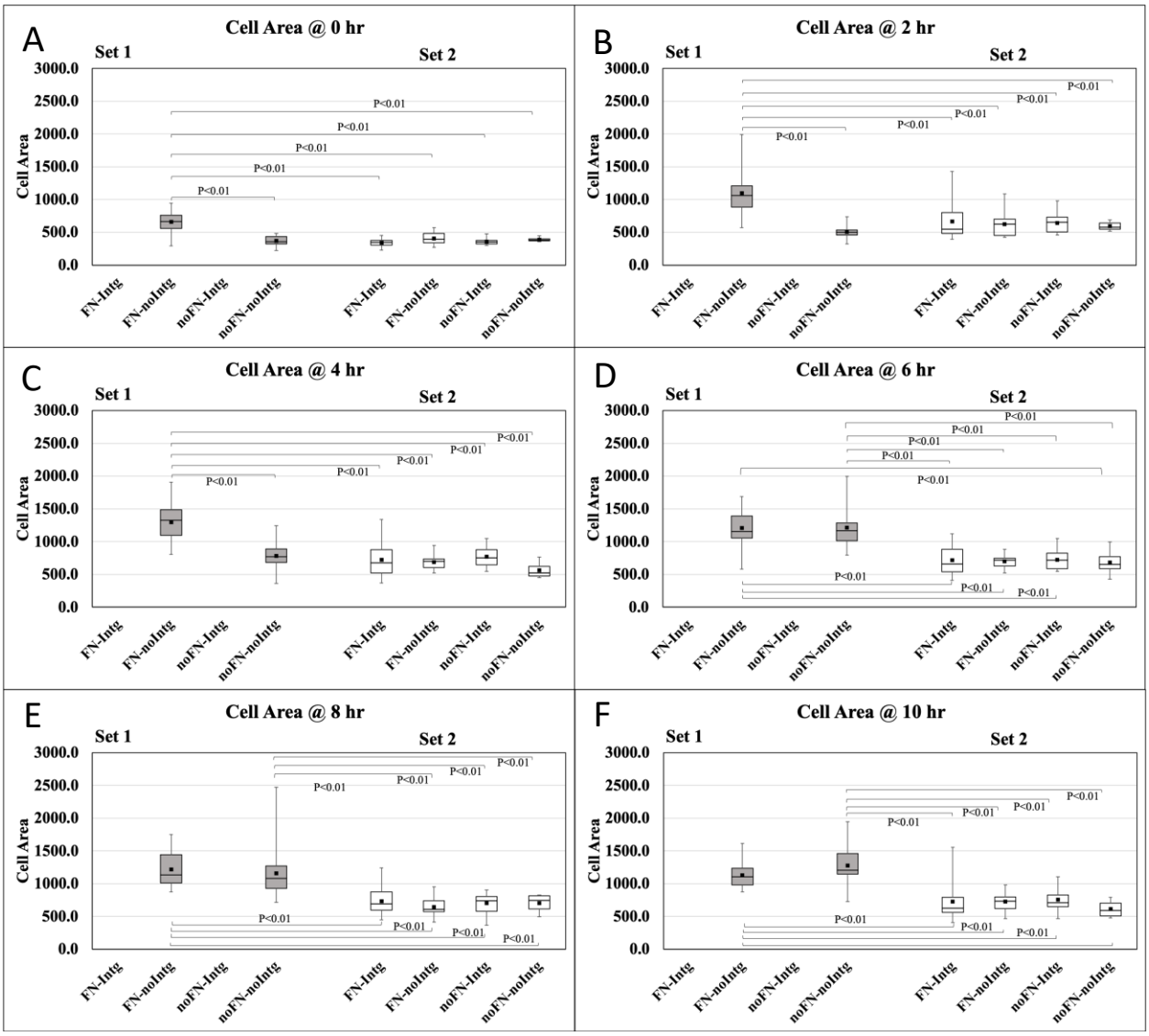

Figure 42. Cell area for set-1 and set-2 cells over 10 hours, in anti-Integrin antibody (Intg) experiments. Cell area was measured every 2 hr. for 10 hr. for set-1 cells at day 0 of seeding and set 2 cells at day 0 of loading onto differentiated set-1 cells. Cell area for set-2 cells was dramatically decreased by the presence of an FN coating compared to set-1 cells. Differences were significant at $p<0.01$. Lines indicate significant difference of pairwise comparisons (by Tukey's tests) between set-1 and set-2 cells over time.

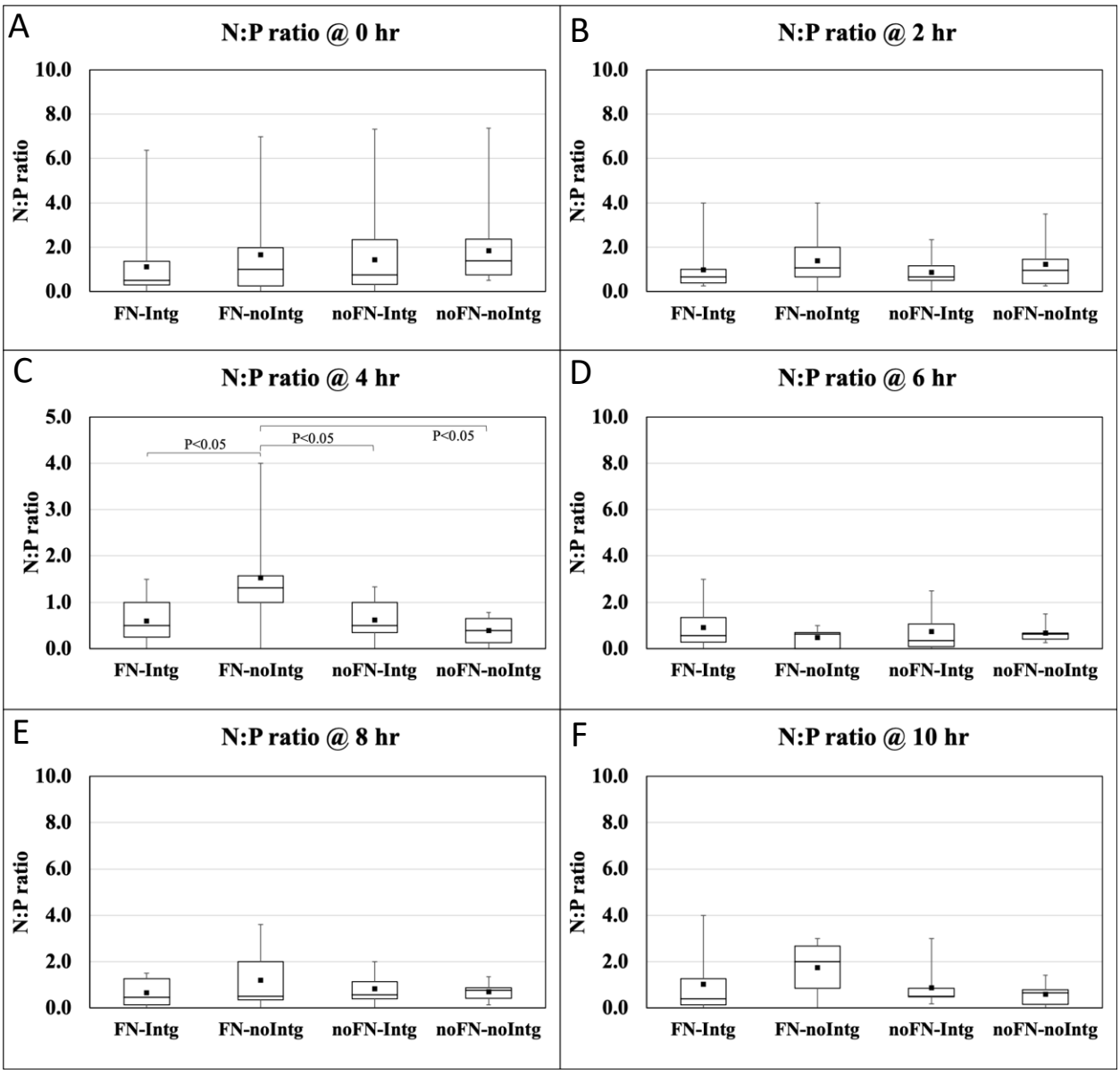

Figure 43. Nucleus:pillar (N:P) ratio for set-1 and set-2 cells over 10 hours, in anti-integrin antibody (Intg) experiments. Both treatment (p=0.013) and time (p=0.037) had significant effects on the position of set-2 cells. The N:P ratio was reduced by Anti-Intg treatment ("Intg" in graphs) and increased over time as cells became more closely aligned with set-1 cell nuclei than with device pillars. There were no significant Tukey's comparisons between groups.

5.7 Discussion

Experiments were conducted to investigate four steps in the interaction processes between myoblasts or myotubes and fibronectin in the ECM that have direct impact on FN-Intg signaling, a process that is critical in cell adhesion, and defective in an aging phenotype in muscle cells. Overall, the presence of FN coating was highly influential to cell behavior during all four treatments, particularly for FAK-inhibitor and anti-Intg treatments of set-2 cells. Treatment, on its own or in an interaction effect, always reduced the magnitude of a particular variable used to assess cell behavior, including cell angle (RGD), angle of proximity (CS1, also in interaction with FN coating), distance to pillar (CS1, anti-Intg in interaction with FN), cell area (FAK inhibitor, also in interaction with FN), and N:P ratio (CS1 in interaction with FN, anti-Intg). There were also time-dependent changes in cell angle (in interaction with FN and RGD), cell area (RGD, CS1, FAK inhibitor, and anti-Intg, and in interaction with FN, set of cells, and FN*set for anti-Intg), and N:P ratio (anti-Intg and FAK inhibitor). Set-2 cells typically behaved differently than set-1 cells in their cell area (RGD, CS1, FAK, anti-Intg), cell angle (CS1, FAK inhibitor, anti-Intg), angle of proximity (FAK inhibitor in interaction with FN, anti-Intg), and distance to pillar (anti-Intg). Results are interpreted as a gradual increase from RGD to CS1 to FAK to anti-Intg, in the severity of impact by the blocking or inhibitory treatment effects on cell alignment, positioning, and/or area of attachment.

Initial observations during experiments showed that set-1 cells continued to move in the channels even after set-2 cells were added. Set-1 and set-2 cells could each move and displace other set of cells in the 10-hr window of imaging and analysis of set-2 cells. Sometimes a set-2 cell moved around a pillar, in and among the set-1 cells that were in close proximity. As well, the larger set-1 cells (multi-nucleated myotubes) moved much less than myoblasts, although their nuclei were still moving internally, and other set-1 cells could still be fusing into the myotubes throughout the period of observation, illustrating the highly dynamic process of myogenesis.

The first set of cells typically filled 60-70% of the channel area by day 5, and occasionally the channel appeared completely filled with cells. That observation of filled or nearly filled channels suggests that the second set of cells was moving between the first set of cells and would have been influenced by contact inhibition. Alternatively, set-2 cells were also fusing with differentiated set-1 cells, as would be likely with positioning toward set-1 cell nuclei. While the presence of sarcomeric myotubes could be established by staining fixed cells for proteins such as

myosin, troponin, desmin, or filamentous actin, sarcomeres were observed in large multinucleated myotubes viewed under by phase-contrast imaging at day five of differentiation. The area of the channel occupied by set-1 cells could not be completely controlled so it would fall within a narrow range, as cells may or may not settle rapidly upon seeding. Set-1 cells also continued to proliferate, at least while in growth medium before being switched to low-serum medium at day 1 to promote differentiation. However, the control for consistency is there: the same number of cells was loaded, and cells were maintained in the same conditions and for the same time in each device and across all experiments. Even in a regular tissue culture dish, the exact proportion of fused cells is extremely hard to determine with certainty and will never reach 100%, since all cells can be subject to differentiation conditions (due to 2% FBS in the medium) and may still not fuse[210]. Even in high-serum medium (25% FBS plus 10% horse serum), differentiation and myotube formation will still occur *in vitro,* since proliferation, differentiation are independently regulated[189]. As well, even *in vivo*, not all differentiated myocytes injected into damaged muscle will fuse into myotubes during regeneration (up to 30%), and can stay in between the new fibers for a long time as so-called "muscle reserve cells" that are MyoD-negative and Pax7-positive cells with potential for at least partial function in myogenic repair after a later injury[210-212]. Normal muscle also contains a population of CD146-positive interstitial muscle progenitor cells that are different from satellite cells but can function as muscle precursors[213]. Normally there is contact inhibition[214-216], so cells that are packed together will naturally stop dividing and differentiate and/or fuse. However, if the serum level is high, then cells typically keep proliferating longer, and they might get smaller and smaller without differentiating.

Binding of fibronectin to its membrane receptor, integrin, is critical to cell adhesion, migration, growth, and differentiation. The effects of applying inhibitors and peptide blockers of FN-Intg binding on myoblast migration behavior were investigated through experiments with RGD, which inhibits the engagement of FN with RGD-binding integrins; CS1, which interferes with integrin dimers binding to FN; with FAK inhibitor, to determine the impact on cell behavior after seeding, of blocking the final step in the pathway that links FN-integrin binding to cell adhesion; and with anti-Intg, to determine the impact of blocking integrin, the FN receptors specifically on set-2 cells, from binding with FN. All these treatments were applied to compare the behavior of set-2 and set-1 cells at their respective day 0 timepoint, right after seeding into the device channels. Another interest was to observe whether the natural ECM, containing FN and

produced and distributed by differentiated myotubes from set-1 myoblasts, could compensate for the lack of an applied FN coating as the substrate, over time.

Among the four treatments, treating set-1 cells with CS1 directly impacted set-2 cell behavior by interrupting fibronectin-α4β1 integrin binding interaction. The distance of set-2 cells to a pillar, their angle of proximity, and the positioning of set-2 cells in relation to the nuclei of set-1 cells (the N:P ratio) were all affected by CS1 treatment, and all these variables were reduced in magnitude compared to the measurements for set-1 cells. This finding showed that CS1 treatment influenced set-2 cell behavior by disrupting the activity of the type III segment of FN more than the disruptions attributable to the effects of the other treatment on integrin itself from antibody blocking treatment, interference with the RGD-binding receptor sites, and blocking integrin-dimer binding to fibronectin.

CS1 and RGD peptides are both segments of FN type III, and they are in the cell-binding domain of FN. The LDV motif is the key cell-binding sequence of the CS1 peptide. LDV is the cell adhesion motif by which fibronectin binds to integrin α4β1[124,217]. FN binds to the receptor, integrin, through both RGD and LDV-type tripeptides[218]. Since these two important binding sites are positioned in the III_9 site of FN, it was assumed that loading either of RGD and CS1 on set-1 cells which have already made FN ligand, would have similar direct effects to disrupt FN itself and subsequently would influence FN-integrin ligand-receptor binding by set-2 cells. In these experiments, most of the significant effects of RGD and CS1 treatments were on cell angle, angle of proximity, distance to pillar and N:P ratio. However, CS1 treatment by itself, only affected the angle of proximity and distance to pillar variables, although significant treatment interactions with FN coating and time influenced set-2 cell behavior. CS1 treatment alone reduced the distance to pillar in set-2 cells, resulting in more set-2 cells closer to a pillar than without treatment; this accounted for the parallel decrease in the N:P ratio, the relative of proportions of set-2 cells closest to a set-1 cell nucleus or to a pillar, during the interaction of treatment with the FN coating substrate. All these changes from CS1 treatment and fewer from RGD treatment, suggest that interrupting RGD-dependent FN binding to Intg did not interrupt the cell binding behavior up to the point of detaching cells from the substrate; these results are interpreted to mean that RGD has dose-dependent effects that differ from CS1 treatment. CS1 treatment affected more variables compared to treatment with RGD peptide, anti-Intg antibody, or FAK inhibitor.

FAK-inhibitor and anti-Intg treatments had significant effects on a different set of variables (cell area, distance to pillar, N:P ratio) than RGD and CS1 (cell angle, angle of proximity, distance to pillar, N:P ratio). This differential effect related to distinctive impact by the two pairs of treatments on myoblast morphology and behavior; the difference clearly shows the importance of understanding which parts of FN-binding segments are interrupted by each treatment. FAK, for example, is located on the cytoplasmic side of the mechanism of cell-attachment to the ECM, and is activated when force is generated through actomyosin fibers that are attached to the FAK complex[219]. Activation of FAK has significant effects on myoblast differentiation, muscle fiber formation, and fiber size. Integrin, the FN receptors, including α5β1 integrin, are localized close to FAK in the attachment complex, and both are critical in cell attachment[219]. Current experiments involved treatment by one of the two types of inhibition: FAK inhibition and blocking α5β1-Intg on set-2 cells, and set-2 cells reacted in almost the same way to both these treatments[219].

We hypothesized that FAK inhibitor and anti-Intg would behave in a similar way and interrupt the binding of integrin, the FN receptors on set-2 cells to an FN substrate. Most of the significant effects of anti-Intg were on the N:P ratio, which was reduced by anti-Intg treatment, inducing the cells to move toward device pillars more than toward the nuclei of set-1 cells. Treatment with FAK inhibitor also affected cell attachment, seen as significant interaction of FAK inhibitor with FN coating on set-2 cell area. While set-2 cells were attached, their distance to set-1 cell nuclei, and reduced cell area after FAK inhibition means they didn't spread as freely throughout set-1 cells in the device as they did in the absence of FAK inhibition. The treatment*coating interaction also reduced the distance to pillar measured for set-2 cells in comparison that measured for set-1 cells, which seems similar to the lower distance to pillar measured after anti-Intg treatment of set-2 cells. These results, therefore, agree with the observation that N:P ratio was reduced in set-2 cells when more set-2 cells were positioned closer to device pillars than to nuclei of set-1 cells. FAK is the kinase enzyme that activates focal adhesion (FA) signaling; the inhibition of FAK in these experiments was very likely partial rather than complete, otherwise the cells would not have retained any adhesion to the device substrate. FAs change in size and distribution over time during cell attachment, typically in response to substrate deformations or applied mechanical stress. Thus, it can be anticipated that FAK mutations or exposure to a toxin that inactivates FAK activity would have an impact on muscle cell adhesion and migration, as those changes would likely change the size of FAs, decrease the

cell-migration speed, and loosen adhesion to the substrate. Notably in this research, only the enzymatic activity of FAK was inhibited; over time, or with higher concentrations of inhibitor, cells would likely detach from the substrate after FA sites got too small to support adhesion.

The most important proxy variable for myotube formation is N:P ratio as it illustrates how fusion into myotubes is happening and how well myoblasts are able to find one to differentiate, fuse and form myotubes in the device. Most of the changes were due to significant effects of the FN coating, which was prominent in demonstrating the impact of FAK inhibitor and anti-Intg treatments. Considering all the treatments, only anti-Intg by itself was able to disrupt the N:P ratio, probably since it had the general effect to block integrin binding with any kind of FN. Aside from the FN-Intg-binding pathway, N-cadherin, ß-catenin, and NCAM are also critical in cell differentiation, forming myotubes, and are the primary mechanism for cell-cell adhesion and attachment in skeletal muscle cells[220,221]. For the present experiments, it was anticipated that all the treatments would influence at least one of the parameters of cell morphology and alignment that were measured in current experiments, given the importance of the ECM dimension in muscle development[222]. However, results also showed that the interaction of cellular morphology and alignment with FN is functionally critical in cell behavior including myotube formation.

There were significant effects of time after seeding cells into the device, and the set of cells affected, varied for the different treatments. Set-2 and set-1 cells behaved differently, showing changes in cell area or both cell area and cell angle, when set-1 cells were treated with CS1 or RGD, respectively. More variables were affected when set-2 cells were treated with FAK inhibitor or anti-Intg, which caused set-2 cells to behave differently than set-1 cells in angle of proximity, cell angle, cell area, and distance to pillar. This comparison, showing a more generalized impact by affecting more variables, after FAK or anti-Intg than after CS1 or RGD, is interpreted to mean that interrupting integrin-binding segments on set-1 cells (CS1, RGD) changed the behavior of set-2 cells sufficiently to disrupt their pattern of cell differentiation, a cell cycle-dependent change in migration[223], and cell fusion into myotubes than was seen for set-1 cells before those treatments were applied. Thus, CS1 and RGD treatments seemed to delay the further augmentation of myotubes by the fusion of set-2 cells. Confirming this possibility would require longer study of set-2 cells in the device, to observe the localization of their fluorescent nuclei.

Cell angle, the alignment of the long axis of cells with the horizontal (transverse) axis of the channel perpendicular to flow, was only affected by treatment in interactions. Treatment

interacted with coating (for FAK inhibitor), both coating and time (for RGD), or the set of cells (for anti-Intg and CS1). These differences and interactions are interpreted to mean that myoblast alignment was interrupted more by disturbing the FAK and RGD integrin-binding receptors than blocking all Intg binding (with anti-Intg) or CS1-mediated binding. Myoblast alignment would be critical in myotube formation, since myotubes orient parallel to each other in forming muscle fibers *in vivo*[224]. The ability to regulate flow rate and velocity within devices through changes in design (described in Results chapter 2 in this thesis, and highlighted in[63]), and the well-established sensitivity of myoblasts and myotubes to mechanical perturbations and surface topography at a cell-structural and molecular level[73,194,225,226], suggest the importance of assessing cell alignment parameters in tissue engineering approaches, well before the measurable outcome of prominent myotube or fiber alignment within engineered muscle tissue in a device. That mechanical gradients at the nano-scale level across the cell-membrane surface, have been explored through a FN-based mechanical sensor[227] speaks volumes to the complexity of important interactions of cell morphology and alignment with cell functions such as migration.

In summary anti-Intg experiments have outlined the importance of cell-cell interaction and binding in FN-Intg interaction through its effect on the N:P ratio alone, and on the distance to pillar variable in an interaction with the FN coating. This showed that cells interrupted with an anti-Intg binding inhibitor were not as close to each other at their nuclei and preferred to stay closer to the device pillars; this impact would also interrupt cell connectivity and fusion. The ECM not only connects myoblasts together, it also guides them in their migration procedure. Cell angle, the transverse orientation of cells in the channel, was affected and reduced by RGD treatment in interaction with the FN coating and time. None of the treatments had treatment-specific effects on cell orientation, except RGD in interaction with other factors. One of the important concerns in muscle formation is how myotubes can align with each other; a proxy measure for this feature only interrupted by RGD treatment. This shows that RGD is important in cell alignment in addition to its role in cell binding to a substrate. Cell area measurement encompassed variables related to the attachment and the spreading of cells, and in part, was a reflection of how much freedom cells have in the channel to spread. Cell area was only affected in being reduced after FAK-inhibitor treatment. FAK is positioned inside the myoblast cytoplasm and is important in cell attachment, since an impediment to cell attachment will have direct influence on cell cycle, growth, differentiation and finally cell fusion, the critical step for myotube formation. The angle of

proximity, the angular alignment of cells with a pillar that is in line with the direction of flow, was only affected through a reduction directly by CS1 treatment and also in an interaction of CS1 with the FN coating. A reduction in this angle of proximity means that cells were aligning across the direction of flow, which would change the directional movement of myoblasts and make their alignment more random than without the treatment, which would in turn reduce the myotube formation.

It was also shown that α7β1, integrin receptor's dimers enhancement could promote cell proliferation, and adhesion to laminin, differentiation, and resistance to apoptosis without any changes in gene expression. This is the result of settlement of dystrophin-glycoprotein complex. Therefore, increasing integrin in skeletal muscle can be a treatment for muscular dystrophy[228]. In comparison with previous findings, myogenic differentiation factor 1, myogenin, myogenic factor 6, myosin heavy chain expressions were blocked by silencing α7, and myoblast fusion was inhibited. This was followed by increasing in expression of connexin 43, which regulates cell death, proliferation, and differentiation, and decreasing in expression of M-cadherin, as a mediator in cell-cell interaction. This demonstrates the regulatory role of α7β1 signaling via connexin 43 and M-cadherin in myoblasts interactions[229].

One of the most interesting findings was that expectations were not all confirmed. For instance, I expected to find that CS1 and RGD had similar effects on the measured variables since they were both applied to set-1 cells and both acted on FN. And I expected that FAK inhibitor and anti-Integrin would also have similar effects as they were both applied to set-2 cells and acted on the action end of the pathway, directly on other proteins and signaling inside the cells. However, results were surprising, in that neither CS1 and RGD or FAK inhibitor and anti-Integrin showed matching effects (see Tables 2 and 3 in Chapter 5). This illustrates the unique features of each part of molecular structures and their importance in shaping the ultimate function of a molecule, as well as the distinctive regulation of each step of a signaling pathway from FN-Intg binding to FA activity and the cellular response.

This research has added new details of the role of different parts of the FN-Intg binding pathway and shown how various blockers and inhibitors were able to change cell shape, alignment, and migration during the formation of myotubes. Visualizing those parameters at the scale of single cells provided a powerful advantage in considering myoblast behavior, and thus can be used to advantage research that is directed to modify and improve the engineering platforms used to

promote cell-cell interaction in myoblast differentiation and myotube formation. In future research toward muscle tissue engineering, sharper focus on the various steps in this FN-Intg signaling pathway and their interaction with cell differentiation over time, should provide new advances in the goal of forming better myotubes in a tissue that can be used to replace muscle loss in a large area of tissue injury.

6. Overall discussion

This thesis research was conducted in three distinct parts. Early findings in this thesis, provided novel understanding of a chemokine (hepatocyte growth factor, HGF) and substrate haptotaxis in controlling the myoblast migratory behavior. **Chapter 3, the first results chapter**, showed that fibronectin (FN) in the substrate of migrating myoblasts provides a more positive haptotaxis signal than collagen (CN). I also found that the effect of HGF in chemotaxis signaling could be modified by interaction with substrate composition and showed the dose dependency of HGF chemotaxis. Looking at haptotaxis and chemotaxis individually, as well as their interactions through experiments that controlled the slope of the soluble HGF gradient was one of the challenges to that research. Another limitation (actually throughout the research of this thesis) was the length of time cells could be observed. Cells were imaged for the analysis of their behavior, and longer-term exposure to UV required to excite the fluorochromes used to examine the substrate composition over time or the cell cytoskeleton in real time, would have had an impact on myoblast migration and growth, as well as cell viability as UV illumination induced cell apoptosis. In addition, it would have been ideal in that first study, to be able to estimate the flow and pressure of the growth medium and to be able to control the flow rate more accurately over time. Being technically able to study myoblasts for a longer time period while varying conditions of chemotaxis and haptotaxis under closer controls of temperature, humidity, and CO_2 in the microscope chamber would offer yet another perspective on cell migration behavior, since it is likely that repeated transferring of the device in and out of the incubator induced at least some fluctuations in the temperature, CO_2 and humidity. I was also interested in being able to analyze the cell cytoskeleton over the time when cells were exposed to the solid and soluble gradients in order to observe the internal changes in myoblasts during their movement. Such experiments were not possible in a regular culture flask, so access to using the microfluidics technology was pivotal in these studies. Unfortunately, the preliminary experiments using live-cell labeling of actin filaments by transient transfection, produced too transient a signal and the device design precluded high-resolution imaging. The alternative approach, to fix cells at different time points after a treatment, and stain for markers of cell differentiation or gene expression at those intervals, would have precluded the study of single cells over time, while adding valuable information on the activities of myoblasts and the myotubes differentiated at 5 days after seeding into devices.

The contribution of fibronectin as a substrate for cell growth, proliferation, migration, and differentiation is clearly not negligible, having been demonstrated conclusively by results of all three Results chapters of this thesis. However, a combination of fibronectin with laminin would likely further change findings on some of the variables of migration that were measured to assess the behavior of myoblasts[194]. A 1:1 ratio of applied laminin:FN would likely affect migration speed, angle of proximity, cell angle, cell area, and distance from set-1 nucleus. Presumably, as laminin has a significant contribution in cell attachment, shape, differentiation, and movement, a 1:1 laminin:FN substrate would be anticipated to increase cell area and attachment in comparison to fibronectin alone.

In my research, the behavior of a cell population, rather than only observing the behavior of single cells, was also a consideration. However, since many researchers are looking at single-cell behavior, further extension of current findings from the first Results chapter, will need to await future research on hapto- and chemotaxis. Each single cell has its discrete behavior and structure, and each aspect is regulated through both discrete and overlapping signaling pathways in the niche of that particular cell; those signaling pathways are important in cell-cell communication, development, and gene expression. Hepatocyte growth factor (HGF) is a potent mitogenic and motogenic ligand to the c-met receptors that are expressed by myoblasts, and changes in HGF concentration are known to influence on myoblast migratory behavior; unfortunately, the impact of HGF was not investigated in myoblasts seeded onto differentiated myotubes, or by any *in vivo* studies that might have addressed the issues of chemotaxis and cell behavior. Development of a new microfluidic device that would allow cells to be exposed to various concentrations of HGF while migrating on opposing solid gradients of ECM, and then the culture of those cells into differentiation, would provide opportunity for direct observation of myotube-formation behavior in real time. If I were to repeat the experiments in the D3 chip and produce a soluble HGF gradient over a CN:FN during myoblast differentiation, I would expect to observe myotubes that formed and elongated toward the fibronectin under a shallow HGF gradient .

It would also be attractive to examine the effects of combining other soluble gradients on myoblasts, since HGF is only one of many growth factors, hormones, and myokines presented in normal muscle or an area of muscle injury. For example, it would be useful to examine the impact of transforming growth factor-ß along with HGF, on myoblast migration behavior or to combine myoblasts with other types of cells in co-culture in a device under such a combined influence.

Molecular studies available through vital approaches such as transfection by strongly GFP-expressing plasmids, would allow us to observe the interaction of chemokines on myoblasts during migration in real time, with specific experimental time points to limit UV exposure.

There were also other methods that could have enhanced the research presented in this thesis that were not possible due to technical difficulties in imaging and in particular due to the thickness of the glass floor of the device and the device itself. For example, live-cell imaging with fluorescence markers would have been useful for studying the molecular behavior in detail in single cells, although their application would still bring challenges from UV exposure to damage the myoblasts. In neuro-muscular studies where muscle-nerve connections are established and the signaling effects of each cell type on the cellular behavior, the interactions of those two types of cells can be examined *in vitro* using a microfluidic platform. Such research would allow further study of nuclear positioning during cell migration, differentiation, and myotube formation, in response to changes in synapse formation between axon terminals and myotubes. It would also be interesting to input mechanical stretching on the substrate of myoblasts while they are differentiating and forming myotubes in a device, in addition to imposing gradients. That type of complex experiment would allow us to investigate the effect of mechanical and chemical signals on the patterning and timing of myotube formation, since the mechanistic basis of set-2 cells migrating toward nuclei of differentiated set-1 cells is not yet understood.

Chapter 4, the second study of microfluidic devices in this thesis, showed it was possible to create patterns in the substrate platform that would guide myoblasts during their migration, alignment, fusion, and myotube formation. I was able to define some of the important parameters that could be used in future to better form muscle fibers in tissue engineering. Microfluidic devices with pillar patterns were designed and fabricated to study the effect of the substrate pattern in forming myotubes. I was also interested in seeing which device characteristics, particularly the specific flow rate and flow time, might influence myoblast behavior. It would be also fascinating to determine the effect of loading more than two sets of cells at different times, much like cells produced by ongoing cycles of proliferation in a regenerating muscle, on the initial few sets of cells that had already been established and differentiated within a device. Alternatively, it would be interesting to load different types of cells, especially including macrophages and/or epithelial cells along with myoblasts, since macrophages produce HGF[24], and also are fusogenic[230], and definitely are important in muscle tissue regeneration from injury.

In my second study, four devices with offset or aligned rows of pillars, and either three (independent) or four (in independent pairs) channels were designed and fabricated. Those devices were aimed to study how the pillar alignment was able to influence cell behavior including alignment toward myotube formation, and how pillar alignment would interact with a FN coating substrate, but not directly looking at myotube formation. The experiments in that second results chapter involved three-channel and four-channel devices, both with either offset or aligned rows of pillars, distributed transversely across the channels. The different devices also differed in their number of channels, inlets, outlets, channel width and interpillar distances. Devices with three channels had three independent outlets and inlets, while four-channel devices had 4 channels and shared 2 outlets and one inlet. C2C12 cells were loaded in each device on a FN substrate and differentiated for five days before set-2 cells were loaded over the set-1 cells. Set-2 cells had their DNA live stained with Hoechst so they could be distinguished from set-1 cells. The location in device channels of set-2 cells was then tracked and compared to the location of set-1-cells after their initial seeding, to see how cells behaved on the FN coated substrate or on a substrate that developed naturally from the set-1 cells. I also studied how the pillar arrangement influenced myoblast alignment toward myotube formation. In devices with aligned rows of pillars, set-2 cells were located closer to a device pillar while in devices with offset rows of pillars, set-2 cells were positioned closer to the nuclei of set-1 cells.

In that study, myoblasts were observed to interact with each other while growing and differentiating, then fuse and form myotubes; observations showed that cells were interacting more easily in devices with offset rows of pillars, as they could “find” the nuclei of previously differentiated set-1 cells. Various measures of cell morphology were developed, assessed and compared between the two sets of cells, to study variables including cell area, cell angle, distance to pillar, and angle of proximity that I considered important in tracking cell behavior. Again, with the thickness of the device, observing changes in the cell cytoskeleton that I had hoped to visualize through vital staining using LifeAct™ technology, were not possible, as the staining was too transient to persist through culture, and the device design precluded high-resolution imaging. A device with thinner substrate, and capability to transfect cells for longer-term vital imaging of the cell cytoskeleton, plus expression of myogenin, the presence of sarcomeric myosin, and other markers of cell maturation, would be ideal for enabling details of cell structure over time during differentiation in a microfluidic device.

Velocity, flow rate, and flow time were calculated based on Poiseuille's law on created laminar flow. Small differences were observed between three-channel devices simulated with no pillars, offset rows, and aligned rows of pillars. Flow rate and flow time in devices 1 and 2 were higher as the device channels were wider. However, velocity was lower in three-channel devices and the highest velocity was found under the simulated control conditions (no pillars) in a four-channel device. In general, control conditions with no pillars resulted in the highest velocity compared to other devices with pillars, meaning that the speed of fluid going through the channels was higher in the absence of any interruption in the fluid stream, as would be expected. Among four different devices, device 1 with offset rows of pillars and the lowest flow rate, even though only slightly different than the no-pillar control, was able to help the cells settle down on the substrate and spread better than device 2 which had aligned rows of pillars. Migration and positioning of set-2 cells closer to the nuclei of set-1 cells was also more effective in device 1. This led to my selection of device 1 for further studies of cell migration behavior during differentiation toward cell fusion and myotube formation using two sets of cells.

A coating substrate of FN, an important protein that binds to the receptor, integrin in the cell membrane, was established as important in cell migration behavior in the first and second parts of this thesis project. **Chapter 5, the third set of experiments**, focused on the impact of interrupting the binding of FN to integrin, through blockers and inhibitors of FN-integrin signaling. This approach was designed to allow comparison of myoblast positioning, differentiation, and fusion on a naturally coated substrate with or without an additional applied FN substrate coating. In this final set of experiments, FN-Intg binding sites were interrupted by treating set-1 cells with RGD or CS1 at day 5 of differentiation or treating set-2 cells with either a FAK inhibitor or an anti-Intg antibody prior to seeding into the device. Set-1 cells were loaded in the device following protocols from results chapter 2, and at day 5 of differentiation, either RGD or CS1 peptide was added to the device to inhibit integrin-dimer bindings to FN. In other experiments, set-2 cells were treated with FAK inhibitor to investigate the impact of blocking the final step in the pathway that links to FN-integrin receptors in order to observe effects on cell morphology and behavior. Set-2 cells were also treated with anti-Intg to study the impact of blocking the receptors, integrin on set-2 cells from binding with FN. After treatment, set-2 cells were loaded over set-1 cells and imaged over 10 hours. Cell area, angle of proximity, cell angle, and distance to pillar were measured once again, and compared between the two sets of cells. A subset of the treatments induced significant

changes on their own, and there were other changes related to the effects of time, set of cells, the presence of applied FN coating, and the interaction of these parameters with treatment. Those effects varied among the different treatments.

Most of the significant changes in behavior between the two sets of cells occurred due to effects of FN coating, which agrees with the findings of the previous research in this thesis and well-established effects of FN on cell migration[3,202]. However, treatment effects of CS1 and anti-α5β1 Intg antibody were strong, showing the importance of FN binding to integrin dimers and the overall function of integrin, the FN receptors, respectively. Knowing that cell-cell interaction is critical in cell growth, proliferation and differentiation, anti-Intg was able to narrow the distance at which set-2 cells positioned in relation to a device pillar; this resulted in cells being closer to pillar rather than to a nucleus of a set-1 cell, a position that would disrupt the potential for cell-cell interaction and delay or impede their fusion into myotubes.

The orientation of the cells was also measured using a cell-angle calculation; the cell angle of set-2 cells was affected only with RGD-peptide treatment of set-1 cells. The whole cell attachment process leads to cell spreading; in these experiments, the measurement of cell area was influenced by treatment with a highly specific inhibitor of intracellular FAK which was applied to set-2 cells before they were loaded onto differentiated set-1 cells. By comparison, treatment with CS1 peptide applied directly to differentiated set-1 cells measurably reduced the angle of proximity (to pillars) of set-2 cells, the angle being in line with the flow direction.

These results, showing significant changes in migration behavior and morphology between set-1 and set-2 cells, demonstrated that there are several important steps in the FN-Intg binding pathway that directly influence the process of myoblasts forming myotubes, early muscle fibers. Mutations in many ECM proteins are known to cause myopathies, so it is highly likely that changes in the expression of various matrix proteins will be involved in each stage of myoblast migration toward differentiation and fusion to myotubes. Experiments here and elsewhere, with FN highlighted that these processes can be altered by subtle changes that have different effects on FN-Intg signaling pathways and could likely cause fiber malformation that would reduce the effective level of contraction and strength in muscle.

6.1. Summary

The main findings of this thesis research project are summarized as follows:

1. Fibronectin (FN) created more positive haptotaxis signal than collagen (CN) in the substrate while myoblast migratory behavior was studying.
2. Chemotaxis signaling effects of HGF, while being dose dependent, were modified by substate composition interaction, including FN and CN.
3. Pillar arrangement in the substrate platform in four different microfluidic devices was able to guide migration of myoblasts, their alignments, fusion, and myotube formation.
4. C2C12 cells were able to interact more in devices with offset rows of pillars, as they could locate the nuclei of previously differentiated set-1 cells.
5. Both set of cells migrated and were positioned better in device 1 with offset rows of pillars with the lowest flow rate; therefore, device 1 was chosen for further cell fusion and myotube formation studies.
6. Interruption of the fibronectin-integrin binding sites, either treating set-1 or set-2 cells with inhibitors or antibodies, caused significant behavioral changes between set-1 and set-2 cells.
7. Treatment with anti-Intg on set-2 cells before loading on differentiated set-1 cells, disrupted variables used to assess cell-cell interaction among myoblasts, and delayed myoblast fusion.
8. RGD peptide treatment of differentiated set-1 cells had impact on cell orientation, a feature that is critical in fusion and myotube formation.
9. FAK-inhibitor treatment of set-2 cells, applied before loading cells onto differentiated set-1 cells, influenced myoblast spreading and attachment.
10. CS1 treatment of differentiated set-1 cells caused myoblasts to align more randomly, an effect that would reduce myotube formation.

6.1. Future research and conclusion

While cell population and bulk cell movements were the main focus in the whole research in microfluidic devices, individual cell studies will be critical in studying and characterizing gene expression specially in chemo-hapto experiments, by considering the expression c-met receptors in both migratory and quiescent satellite cells. In another set of the experiments despite being

interested in flow rate, flow time of the migratory myoblasts, it would be fascinating to observe the migratory behavior, characteristics, and cycle of proliferation of more than two-set of cells at different time points and their effects on cell differentiation and fusion in muscle. Loading macrophages and/or epithelial cells with myoblasts specially that HGF is also produced by macrophages would be important in muscle regeneration studies. While having set-2 cells loaded on set- 1 cells as a naturally formed FN substrate, looking at the cytoskeleton of both set of cells would give us better understanding of myoblasts alignment and myotube formation by live imaging. In the last set of experiments in this research project, four steps in the interaction process between fibronectin, myoblasts, and myotubes in the ECM with direct impact on FN-Intg signaling were investigated, while this research needs a sharper focus on the various steps in FN-Intg signaling pathway which can be helpful in forming better myotubes in a tissue.

The main observations from research findings in Chapter 3 were that FN is a more potent haptotaxis signal on myoblast migration compared to CN and that HGF chemotaxis signaling was modified by substrate composition. These findings pull together the main idea that cell migration and morphology are developed through a combination of factors in the environment, and changing those factors has potential to promote the wound healing and speed up the muscle regeneration.

The main ideas from research findings in Chapter 4 were that the design of pillar-patterned devices can direct cells toward fusion and myotube formation and that it was important to examine the interaction of myoblasts with the naturally produced substrate from set-1 cells in studying the behavior of set-2 cells. One of the four new devices, the one with offset rows of pillars and the lowest flow rate and velocity was better at promoting cell fusion and myotube formation. From this, I conclude that myoblasts not only migrate around earlier-formed myotubes, they detect signals in the substrate and soluble environment that promote their fusion to those myotubes, which will augment the myotube size. This idea suggests that the substrate used in tissue engineering may be manipulated over time, to improve the formation of micro-muscle patches; that formation would help overcome the current challenges in muscle tissue engineering for treatment of volumetric muscle loss.

Finally, the main ideas from Chapter 5 showed that the novel device selected on the basis of previous findings, was able to help examine another important aspect of the current challenges to muscle tissue engineering: cell-ECM interactions. Inhibiting and interrupting the connections between FN and its receptor, integrin. Interrupting integrin $\alpha 5\beta 1$ dimers, the FN receptor on set-2

cells had more potent effects on the distance of set-2 cells to the nuclei of set-1 cells, an effect that would reduce the myotube formation. Thus, activating the receptor before exposing set-2 cells to the differentiated myotubes already in the device, could be used to increase the chance of cell-cell fusion and myotube formation.

It is hoped that the results of this thesis research will lead to further improvements in muscle-tissue engineering, so that volumetric muscle loss and even use of micro-muscle patches to treat smaller injuries in patients with physiological or immunological challenges to muscle regeneration, will be feasible sooner than later.

7. References

1 Relaix, F. & Zammit, P. S. Satellite cells are essential for skeletal muscle regeneration: the cell on the edge returns centre stage. *Development* **139**, 2845-2856 (2012).

2 Roveimiab, Z., Lin, F. & Anderson, J. E. Emerging development of microfluidics-based approaches to improve studies of muscle cell migration. *Tissue Engineering Part B: Reviews* **25**, 30-45 (2019).

3 Roveimiab, Z., Lin, F. & Anderson, J. E. Traction and attraction: Haptotaxis substrates collagen and fibronectin interact with chemotaxis by HGF to regulate myoblast migration in a microfluidic device. *American Journal of Physiology-Cell Physiology* **319**, C75-C92 (2020).

4 Wolf, K. *et al.* Multi-step pericellular proteolysis controls the transition from individual to collective cancer cell invasion. *Nature cell biology* **9**, 893 (2007).

5 Achilleos, A. & Trainor, P. A. Neural crest stem cells: discovery, properties and potential for therapy. *Cell Research* **22**, 288-304, doi:10.1038/cr.2012.11 (2012).

6 Shakhova, O. & Sommer, L. in *StemBook [internet]* (Harvard Stem Cell Institute, 2010).

7 Shi, X. & Garry, D. J. Muscle stem cells in development, regeneration, and disease. *Genes & development* **20**, 1692-1708 (2006).

8 Seale, P., Asakura, A. & Rudnicki, M. A. The potential of muscle stem cells. *Developmental cell* **1**, 333-342 (2001).

9 Aman, A. & Piotrowski, T. Cell migration during morphogenesis. *Developmental Biology* **341**, 20-33, doi:10.1016/j.ydbio.2009.11.014 (2010).

10 Ridley, A. J. *et al.* Cell migration: integrating signals from front to back. *Science* **302**, 1704-1709 (2003).

11 Friedl, P. & Wolf, K. Plasticity of cell migration: a multiscale tuning model. *Journal of Cell Biology* **188**, 11-19 (2010).

12 Ananthakrishnan, R. & Ehrlicher, A. The forces behind cell movement. *International journal of biological sciences* **3**, 303 (2007).

13 Li, R. & Gundersen, G. G. Beyond polymer polarity: how the cytoskeleton builds a polarized cell. *Nature Reviews Molecular Cell Biology* **9**, 860-873, doi:10.1038/nrm2522 (2008).

14 Fletcher, D. A. & Mullins, R. D. Cell mechanics and the cytoskeleton. *Nature* **463**, 485 (2010).

15 Lowery, J., Kuczmarski, E. R., Herrmann, H. & Goldman, R. D. Intermediate filaments play a pivotal role in regulating cell architecture and function. *Journal of Biological Chemistry* **290**, 17145-17153 (2015).

16 Tsai, F.-C., Kuo, G.-H., Chang, S.-W. & Tsai, P.-J. Ca2+ signaling in cytoskeletal reorganization, cell migration, and cancer metastasis. *BioMed research international* **2015** (2015).

17 Gm, C. *The Cell: A Molecular Approach.Structure and Organization of Actin Filaments*. 2nd edn, (2000).

18 Gerthoffer, W. T. Mechanisms of vascular smooth muscle cell migration. *Circulation Research* **100**, 607-621, doi:10.1161/01.RES.0000258492.96097.47 (2007).

19 Peyton, S. R. & Putnam, A. J. Extracellular matrix rigidity governs smooth muscle cell motility in a biphasic fashion. *Journal of cellular physiology* **204**, 198-209 (2005).
20 van Velthoven, C. T., de Morree, A., Egner, I. M., Brett, J. O. & Rando, T. A. Transcriptional profiling of quiescent muscle stem cells in vivo. *Cell reports* **21**, 1994-2004 (2017).
21 Wozniak, A. C., Kong, J., Bock, E., Pilipowicz, O. & Anderson, J. E. Signaling satellite-cell activation in skeletal muscle: markers, models, stretch, and potential alternate pathways. *Muscle & Nerve: Official Journal of the American Association of Electrodiagnostic Medicine* **31**, 283-300 (2005).
22 Leiter, J. R. & Anderson, J. E. Satellite cells are increasingly refractory to activation by nitric oxide and stretch in aged mouse-muscle cultures. *The international journal of biochemistry & cell biology* **42**, 132-136 (2010).
23 Saini, J., McPhee, J. S., Al-Dabbagh, S., Stewart, C. E. & Al-Shanti, N. Regenerative function of immune system: Modulation of muscle stem cells. *Ageing research reviews* **27**, 67-76 (2016).
24 Sakaguchi, S. *et al.* Implication of anti-inflammatory macrophages in regenerative moto-neuritogenesis: promotion of myoblast migration and neural chemorepellent semaphorin 3A expression in injured muscle. *The international journal of biochemistry & cell biology* **54**, 272-285 (2014).
25 Anderson, J. E. in *Growth Factors and Cytokines in Skeletal Muscle Development, Growth, Regeneration and Disease* 1-25 (Springer, 2016).
26 Anderson, J. E. *et al.* The role of semaphorin3A in myogenic regeneration and the formation of functional neuromuscular junctions on new fibres. *Biological Reviews* **92**, 1389-1405 (2017).
27 Siegel, A. L., Atchison, K., Fisher, K. E., Davis, G. E. & Cornelison, D. 3D timelapse analysis of muscle satellite cell motility. *Stem cells* **27**, 2527-2538 (2009).
28 Tatsumi, R. *et al.* Possible implication of satellite cells in regenerative motoneuritogenesis: HGF upregulates neural chemorepellent Sema3A during myogenic differentiation. *American Journal of Physiology-Cell Physiology* **297**, C238-C252 (2009).
29 Anderson, J. & Pilipowicz, O. Activation of muscle satellite cells in single-fiber cultures. *Nitric Oxide* **7**, 36-41 (2002).
30 Péault, B. *et al.* Stem and progenitor cells in skeletal muscle development, maintenance, and therapy. *Molecular therapy* **15**, 867-877 (2007).
31 Chen, X. & Li, Y. Role of matrix metalloproteinases in skeletal muscle: migration, differentiation, regeneration and fibrosis. *Cell adhesion & migration* **3**, 337-341, doi:10.4161/cam.3.4.9338 (2009).
32 Elster, J. L. *et al.* Skeletal muscle satellite cell migration to injured tissue measured with 111 In-oxine and high-resolution SPECT imaging. *Journal of muscle research and cell motility* **34**, 417-427 (2013).
33 Wozniak, A. C. & Anderson, J. E. Single-fiber isolation and maintenance of satellite cell quiescence. *Biochem.Cell Biol.* **83**, 674-676, doi:10.1139/o05-046 (2005).
34 Wozniak, A. C. *et al.* C-met expression and mechanical activation of satellite cells on cultured muscle fibers. *J Histochem Cytochem* **51**, 1437-1445, doi:10.1177/002215540305101104 (2003).

35 Yin, H., Price, F. & Rudnicki, M. A. Satellite cells and the muscle stem cell niche. *Physiological reviews* **93**, 23-67 (2013).
36 Liu, X. & Ma, P. X. Polymeric scaffolds for bone tissue engineering. *Annals of biomedical engineering* **32**, 477-486 (2004).
37 Pashneh-Tala, S., MacNeil, S. & Claeyssens, F. The tissue-engineered vascular graft—past, present, and future. *Tissue Engineering Part B: Reviews* **22**, 68-100 (2015).
38 Sakuragawa, N., Yoshikawa, H. & Sasaki, M. Amniotic tissue transplantation: clinical and biochemical evaluations for some lysosomal storage diseases. *Brain and Development* **14**, 7-11 (1992).
39 Arnold, L. *et al.* Inflammatory monocytes recruited after skeletal muscle injury switch into antiinflammatory macrophages to support myogenesis. *Journal of Experimental Medicine* **204**, 1057-1069 (2007).
40 Sciorati, C., Rigamonti, E., Manfredi, A. & Rovere-Querini, P. Cell death, clearance and immunity in the skeletal muscle. *Cell death and differentiation* **23**, 927 (2016).
41 Das, S. *et al.* Innervation: the missing link for biofabricated tissues and organs. *NPJ Regenerative medicine* **5**, 1-19 (2020).
42 Martin, N. R. *et al.* Neuromuscular junction formation in tissue-engineered skeletal muscle augments contractile function and improves cytoskeletal organization. *Tissue Engineering Part A* **21**, 2595-2604 (2015).
43 Bach, A., Beier, J., Stern-Staeter, J. & Horch, R. Skeletal muscle tissue engineering. *Journal of cellular and molecular medicine* **8**, 413-422 (2004).
44 Nelson, R. D., Quie, P. G. & Simmons, R. L. Chemotaxis Under Agarose : A New and Simple Method for Measuring Chemotaxis and Spontaneous Migration of Human Polymorphonuclear Leukocytes and Monocytes Information about subscribing to The Journal of Immunology is online at : CHEMOTAXIS UNDER AGAROSE. (2013).
45 Falk, W. A 48-well micro chemotaxis assembly for rapid and accurate measurement of leukocyte migration. *Journal oflmmunological Methods* **33**, 239-247 (1980).
46 Kramer, N. *et al.* In vitro cell migration and invasion assays. *Mutation Research/Reviews in Mutation Research* **752**, 10-24 (2013).
47 Nyffeler, J. *et al.* Design of a high-Throughput human neural crest cell migration assay to indicate potential developmental toxicants. *Altex* **34**, 75-94, doi:10.14573/altex.1605031 (2017).
48 Rodriguez-Menocal, L., Shareef, S., Salgado, M., Shabbir, A. & Van Badiavas, E. Role of whole bone marrow, whole bone marrow cultured cells, and mesenchymal stem cells in chronic wound healing. *Stem Cell Research & Therapy* **6**, 24-24, doi:10.1186/s13287-015-0001-9 (2015).
49 Ratnayake, D. *et al.* Macrophages provide a transient muscle stem cell niche via NAMPT secretion. *Nature* **591**, 281-287 (2021).
50 Christoffersson, J. *et al.* A cardiac cell outgrowth assay for evaluating drug compounds using a cardiac spheroid-on-a-chip device. *Bioengineering* **5**, 36 (2018).
51 Keenan, T. M. & Folch, A. Biomolecular gradients in cell culture systems. *Lab Chip* **8**, 34-57, doi:10.1039/B711887B (2008).

52 Boyden, S. The chemotactic effect of mixtures of antibody and antigen on polymorphonuclear leucocytes. *The Journal of experimental medicine* **115**, 453-466 (1962).
53 Toetsch, S., Olwell, P., Prina-Mello, A. & Volkov, Y. The evolution of chemotaxis assays from static models to physiologically relevant platforms. *Integrative Biology* **1**, 170-181 (2009).
54 Gundersen, R. & Barrett, J. Neuronal chemotaxis: chick dorsal-root axons turn toward high concentrations of nerve growth factor. *Science* **206**, 1079-1080 (1979).
55 Araque, A., Parpura, V., Sanzgiri, R. P. & Haydon, P. G. Tripartite synapses: glia, the unacknowledged partner. *Trends in neurosciences* **22**, 208-215 (1999).
56 Servant, G. *et al.* Polarization of chemoattractant receptor signaling during neutrophil chemotaxis. *Science* **287**, 1037-1040 (2000).
57 Cornish, S. M., Bugera, E. M., Duhamel, T. A., Peeler, J. D. & Anderson, J. E. A focused review of myokines as a potential contributor to muscle hypertrophy from resistance-based exercise. *European Journal of Applied Physiology*, 1-19 (2020).
58 Bosman, F. T. & Stamenkovic, I. Functional structure and composition of the extracellular matrix. *The Journal of Pathology: A Journal of the Pathological Society of Great Britain and Ireland* **200**, 423-428 (2003).
59 Frantz, C., Stewart, K. M. & Weaver, V. M. The extracellular matrix at a glance. *Journal of cell science* **123**, 4195-4200 (2010).
60 Mecham, R. *The extracellular matrix: an overview*. (Springer Science & Business Media, 2011).
61 Warrick, J. W., Young, E. W. K., Schmuck, E. G., Saupe, K. W. & Beebe, D. J. High-content adhesion assay to address limited cell samples. *Integrative Biology* **5**, 720-720, doi:10.1039/c3ib20224k (2013).
62 Imanaka-Yoshida, K., Hiroe, M. & Yoshida, T. Interaction between cell and extracellular matrix in heart disease: Multiple roles of tenascin-C in tissue remodeling. *Histology and Histopathology* **19**, 517-525, doi:10.14670/HH-19.517 (2004).
63 Sackmann, E. K., Fulton, A. L. & Beebe, D. J. The present and future role of microfluidics in biomedical research. *Nature* **507**, 181-189, doi:10.1038/nature13118 (2014).
64 Roman, H. N., Juncker, D. & Lauzon, A. M. A microfluidic chamber to study the dynamics of muscle-contraction-specific molecular interactions. *Analytical Chemistry* **87**, 2582-2587, doi:10.1021/ac503963r (2015).
65 Taylor, A. M. *et al.* A microfluidic culture platform for CNS axonal injury, regeneration and transport. *Nat Methods* **8**, 599-605, doi:10.1038/nmeth777 (2005).
66 Southam, K. A., King, A. E., Blizzard, C. A., McCormack, G. H. & Dickson, T. C. Microfluidic primary culture model of the lower motor neuron-neuromuscular junction circuit. *J Neurosci Methods* **218**, 164-169, doi:10.1016/j.jneumeth.2013.06.002 (2013).
67 Zahavi, E. E. *et al.* A compartmentalized microfluidic neuromuscular co-culture system reveals spatial aspects of GDNF functions. *J Cell Sci* **128**, 1241-1252, doi:10.1242/jcs.167544 (2015).
68 Wadhawan, N. *et al.* Growth and positioning of adipose-derived stem cells in microfluidic devices. *Lab Chip* **12**, 4829-4834 (2012).

69 Wu, H., Xiong, W. C. & Mei, L. To build a synapse: signaling pathways in neuromuscular junction assembly. *Development* **137**, 1017-1033, doi:10.1242/dev.038711 (2010).
70 Figallo, E. *et al.* Micro-bioreactor array for controlling cellular microenvironments. *Lab on a Chip* **7**, 710-710, doi:10.1039/b700063d (2007).
71 Burattini, S. *et al.* C2C12 murine myoblasts as a model of skeletal muscle development: Morpho-functional characterization. *European Journal of Histochemistry* **48**, 223-233, doi:10.4081/891 (2004).
72 Morgan, J. T. *et al.* Integration of basal topographic cues and apical shear stress in vascular endothelial cells. *Biomaterials* **33**, 4126-4135 (2012).
73 Anderson, J., Carvalho, R., Yen, E. & Scott, J. Measurement of strain in cultured bone and fetal muscle and lung cells. *In vitro cellular & developmental biology*, 183-186 (1993).
74 Gao, H., Cao, X., Dong, H., Fu, X. & Wang, Y. Influence of 3D Microgrooves on C2C12 Cell Proliferation, Migration, Alignment, F-actin Protein Expression and Gene Expression. *Journal of Materials Science and Technology* **32**, 901-908, doi:10.1016/j.jmst.2016.01.011 (2016).
75 Wozniak, A. C. & Anderson, J. E. The dynamics of the nitric oxide release-transient from stretched muscle cells. *Int.J.Biochem.Cell Biol.* **41**, 625-631 (2009).
76 Andalib, M. N., Dzenis, Y., Donahue, H. J. & Lim, J. Y. Biomimetic substrate control of cellular mechanotransduction. *Biomaterials Research* **20**, 11-11, doi:10.1186/s40824-016-0059-1 (2016).
77 Ahmed, W. W. *et al.* Myoblast morphology and organization on biochemically micro-patterned hydrogel coatings under cyclic mechanical strain. *Biomaterials* **31**, 250-258 (2010).
78 Shimizu, K. *et al.* Microfluidic devices for construction of contractile skeletal muscle microtissues. *Journal of bioscience and bioengineering* **119**, 212-216 (2015).
79 Nagamine, K. *et al.* Contractile skeletal muscle cells cultured with a conducting soft wire for effective, selective stimulation. *Scientific reports* **8**, 1-9 (2018).
80 Yang, K. *et al.* Fibroblast growth factor 23 weakens chemotaxis of human blood neutrophils in microfluidic devices. *Sci Rep* **7**, 3100 (2017).
81 Aldridge, G. M., Podrebarac, D. M., Greenough, W. T. & Weiler, I. J. The use of total protein stains as loading controls: an alternative to high-abundance single-protein controls in semi-quantitative immunoblotting. *J.Neurosci.Methods* **172**, 250-254 (2008).
82 Giulitti, S., Magrofuoco, E., Prevedello, L. & Elvassore, N. Optimal periodic perfusion strategy for robust long-term microfluidic cell culture. *Lab on a Chip* **13**, 4430-4430, doi:10.1039/c3lc50643f (2013).
83 Futai, N., Gu, W., Song, J. W. & Takayama, S. Handheld recirculation system and customized media for microfluidic cell culture. *Lab Chip* **6**, 149-154, doi:10.1039/B510901A (2006).
84 Gu, W., Zhu, X., Futai, N., Cho, B. S. & Takayama, S. Computerized microfluidic cell culture using elastomeric channels and Braille displays. *Proceedings of the National Academy of Sciences* **101**, 15861-15866 (2004).
85 Almodóvar, J. *et al.* Spatial patterning of BMP-2 and BMP-7 on biopolymeric films and the guidance of muscle cell fate. *Biomaterials* **35**, 3975-3985, doi:10.1016/j.biomaterials.2014.01.012 (2014).

86 Janke, A., Upadhaya, R., Snow, W. M. & Anderson, J. E. A new look at cytoskeletal NOS-1 and β-dystroglycan changes in developing muscle and brain in control and mdx dystrophic mice. *Developmental Dynamics* **242**, 1369-1381, doi:10.1002/dvdy.24031 (2013).
87 McIntosh, L. M., Pernitsky, A. N. & Anderson, J. E. The effects of altered metabolism (hypothyroidism) on muscle repair in the mdx dystrophic mouse. *Muscle Nerve* **17**, 444-453 (1994).
88 Yablonka-Reuveni, Z. & Anderson, J. E. Satellite cells from dystrophic (Mdx) mice display accelerated differentiation in primary cultures and in isolated myofibers. *Dev.Dyn.* **235**, 203-212 (2006).
89 Bian, W. & Bursac, N. Engineered skeletal muscle tissue networks with controllable architecture. *Biomaterials* **30**, 1401-1412 (2009).
90 Chazaud, B., Christov, C., Gherardi, R. K. & Barlovatz-Meimon, G. In vitro evaluation of human muscle satellite cell migration prior to fusion into myotubes. *J Muscle Res Cell Motil.* **19**, 931-936 (1998).
91 Chehrehasa, F., Meedeniya, A. C., Dwyer, P., Abrahamsen, G. & Mackay-Sim, A. EdU, a new thymidine analogue for labelling proliferating cells in the nervous system. *J Neurosci Methods* **177**, 122-130 (2009).
92 Uzel, S. G. *et al.* Microfluidic device for the formation of optically excitable, three-dimensional, compartmentalized motor units. *Science advances* **2**, e1501429 (2016).
93 Quarta, M. *et al.* An artificial niche preserves the quiescence of muscle stem cells and enhances their therapeutic efficacy. *Nature biotechnology* **34**, 752-759 (2016).
94 Huang, N. F., Lee, R. J. & Li, S. Engineering of aligned skeletal muscle by micropatterning. *American journal of translational research* **2**, 43 (2010).
95 Tourovskaia, A., Figueroa-Masot, X. & Folch, A. Long-term microfluidic cultures of myotube microarrays for high-throughput focal stimulation. *Nature protocols* **1**, 1092 (2006).
96 Bentzinger, C. F., Wang, Y. X. & Rudnicki, M. A. Building muscle: molecular regulation of myogenesis. *Cold Spring Harbor perspectives in biology* **4**, a008342 (2012).
97 Brand-Saberi, B. B. O., Eric. in *Essential Current Concepts in Stem Cell Biology* 77-98 (Springer, Switzerland, 2020).
98 Megeney, L. A., Kablar, B., Garrett, K., Anderson, J. E. & Rudnicki, M. A. MyoD is required for myogenic stem cell function in adult skeletal muscle. *Genes & development* **10**, 1173-1183 (1996).
99 Sabourin, L. A. & Rudnicki, M. A. The molecular regulation of myogenesis. *Clinical genetics* **57**, 16-25 (2000).
100 Lian, Y.-L. *et al.* PIP3 depletion rescues myoblast fusion defects in human rhabdomyosarcoma cells. *Journal of Cell Science* **133** (2020).
101 Vaz, R., Martins, G. G., Thorsteinsdóttir, S. & Rodrigues, G. Fibronectin promotes migration, alignment and fusion in an in vitro myoblast cell model. *Cell and tissue research* **348**, 569-578 (2012).
102 Brack, A. S., Conboy, I. M., Conboy, M. J., Shen, J. & Rando, T. A. A temporal switch from notch to Wnt signaling in muscle stem cells is necessary for normal adult myogenesis. *Cell stem cell* **2**, 50-59 (2008).

103 Doukas, J. *et al.* Delivery of FGF genes to wound repair cells enhances arteriogenesis and myogenesis in skeletal muscle. *Molecular Therapy* **5**, 517-527 (2002).
104 Zammit, P. S. Function of the myogenic regulatory factors Myf5, MyoD, Myogenin and MRF4 in skeletal muscle, satellite cells and regenerative myogenesis. *Semin Cell Dev Biol* **72**, 19-32, doi:10.1016/j.semcdb.2017.11.011 (2017).
105 Hernández-Hernández, J. M., García-González, E. G., Brun, C. E. & Rudnicki, M. A. in *Seminars in cell & developmental biology.* 10-18 (Elsevier).
106 Asfour, H. A., Allouh, M. Z. & Said, R. S. Myogenic regulatory factors: The orchestrators of myogenesis after 30 years of discovery. *Experimental Biology and Medicine* **243**, 118-128 (2018).
107 Cadot, B., Gache, V. & E.R., G. Moving and positioning the nucleus in skeletal muscle - one step at a time. *Nucleus* **6**, 373-381, doi:10.1080/19491034.2015.1090073 (2015).
108 Petrany, M. J. & Millay, D. P. Cell Fusion: Merging Membranes and Making Muscle. *Trends in cell biology* (2019).
109 Zhang, H. *et al.* Human myotube formation is determined by MyoD–Myomixer/Myomaker axis. *Science Advances* **6**, eabc4062 (2020).
110 Kang, J.-S. *et al.* Netrins and neogenin promote myotube formation. *The Journal of cell biology* **167**, 493-504 (2004).
111 Zhang, M. & McLennan, I. S. During secondary myotube formation, primary myotubes preferentially absorb new nuclei at their ends. *Developmental Dynamics* **204**, 168-177 (1995).
112 Stromer, M. Invited Review The cytoskeleton in skeletal, cardiac and smooth muscle cells. *Histol Histopathol* **13**, 283-291 (1998).
113 Henderson, C. A., Gomez, C. G., Novak, S. M., Mi-Mi, L. & Gregorio, C. C. Overview of the muscle cytoskeleton. *Comprehensive Physiology* **7**, 891-944 (2011).
114 Guerin, C. M. & Kramer, S. G. Cytoskeletal remodeling during myotube assembly and guidance: coordinating the actin and microtubule networks. *Communicative & integrative biology* **2**, 452-457 (2009).
115 Peckham, M. Engineering a multi-nucleated myotube, the role of the actin cytoskeleton. *Journal of microscopy* **231**, 486-493 (2008).
116 J.R., S. & J.W., L. Development of the vertebrate neuromuscular junction. *Annual review of neuroscience* **22**, 389–442, doi:10.1146/annurev.neuro.22.1.389 (1999).
117 Zong, Y. & Jin, R. Structural mechanisms of the agrin-LRP4-MuSK signaling pathway in neuromuscular junction differentiation. *Cell Mol Life Sci* **70**, 3077-3088, doi:10.1007/s00018-012-1209-9 (2013).
118 Roman, W. & Gomes, E. R. Nuclear positioning in skeletal muscle. *Semin Cell Dev Biol* **82**, 51-56, doi:10.1016/j.semcdb.2017.11.005 (2018).
119 Grady, R. M., Starr, D. A., Ackerman, G. L., Sanes, J. R. & Han, M. Syne proteins anchor muscle nuclei at the neuromuscular junction. *Proc Natl Acad Sci U S A* **102**, 4359-4364, doi:10.1073/pnas.0500711102 (2005).
120 Das, M., Rumsey, J. W., Bhargava, N., Stancescu, M. & Hickman, J. J. A defined long-term in vitro tissue engineered model of neuromuscular junctions. *Biomaterials* **31**, 4880-4888, doi:10.1016/j.biomaterials.2010.02.055 (2010).

121 Das, M. *et al.* Embryonic motoneuron-skeletal muscle co-culture in a defined system. *Neuroscience* **146**, 481-488, doi:10.1016/j.neuroscience.2007.01.068 (2007).
122 Das, M., Wilson, K., Molnar, P. & Hickman, J. J. Differentiation of skeletal muscle and integration of myotubes with silicon microstructures using serum-free medium and a synthetic silane substrate. *Nat Protoc* **2**, 1795-1801, doi:10.1038/nprot.2007.229 (2007).
123 Guo, X., Gonzalez, M., Stancescu, M., Vandenburgh, H. H. & Hickman, J. J. Neuromuscular junction formation between human stem cell-derived motoneurons and human skeletal muscle in a defined system. *Biomaterials* **32**, 9602-9611, doi:10.1016/j.biomaterials.2011.09.014 (2011).
124 Johansson, S., Svineng, G., Wennerberg, K., Armulik, A. & Lohikangas, L. Fibronectin-integrin interactions. *Front Biosci* **2**, d126-d146 (1997).
125 Yamada, K. M. Fibronectin peptides in cell migration and wound repair. *The Journal of clinical investigation* **105**, 1507-1509 (2000).
126 Szekanecz, Z., Humphries, M. J. & Ager, A. Lymphocyte adhesion to high endothelium is mediated by two beta 1 integrin receptors for fibronectin, alpha 4 beta 1 and alpha 5 beta 1. *Journal of cell science* **101**, 885-894 (1992).
127 Bachman, H., Nicosia, J., Dysart, M. & Barker, T. H. Utilizing fibronectin integrin-binding specificity to control cellular responses. *Advances in wound care* **4**, 501-511 (2015).
128 Lukjanenko, L. *et al.* Loss of fibronectin from the aged stem cell niche affects the regenerative capacity of skeletal muscle in mice. *Nature medicine* **22**, 897-905 (2016).
129 Ponik, S. M. & Pavalko, F. M. Formation of focal adhesions on fibronectin promotes fluid shear stress induction of COX-2 and PGE2 release in MC3T3-E1 osteoblasts. *Journal of Applied Physiology* **97**, 135-142 (2004).
130 Anderson, J. E. A role for nitric oxide in muscle repair: nitric oxide-mediated activation of muscle satellite cells. *Mol.Biol.Cell* **11**, 1859-1874, doi:10.1091/mbc.11.5.1859 (2000).
131 Anderson, J. & Pilipowicz, O. Activation of muscle satellite cells in single-fiber cultures. *Nitric.Oxide.* **7**, 36-41, doi:https://doi.org/10.1016/S1089-8603(02)00011-3 (2002).
132 Wozniak, A. C. *et al.* C-met expression and mechanical activation of satellite cells on cultured muscle fibers. *J.Histochem.Cytochem.* **51**, 1437-1445, doi:10.1177/002215540305101104 (2003).
133 Wozniak, A. C. & Anderson, J. E. Nitric oxide-dependence of satellite stem cell activation and quiescence on normal skeletal muscle fibers. *Dev.Dyn.* **236**, 240-250 (2007).
134 von, M. J., Chang, N. C., Bentzinger, C. F. & Rudnicki, M. A. Wnt signaling in myogenesis. *Trends Cell Biol.* **22**, 602-609 (2012).
135 Dhawan, J. & Rando, T. A. Stem cells in postnatal myogenesis: molecular mechanisms of satellite cell quiescence, activation and replenishment. *Trends Cell Biol.* **15**, 666-673 (2005).
136 Almodóvar, J. *et al.* Spatial patterning of BMP-2 and BMP-7 on biopolymeric films and the guidance of muscle cell fate. *Biomaterials* **35**, 3975-3985 (2014).
137 Garrett, K. L. & Anderson, J. E. Colocalization of bFGF and the myogenic regulatory gene myogenin in dystrophic mdx muscle precursors and young myotubes in vivo. *Dev.Biol.* **169**, 596-608 (1995).

138 Siegel, A. L., Atchison, K., Fisher, K. E., Davis, G. E. & Cornelison, D. D. W. 3D timelapse analysis of muscle satellite cell motility. *Stem Cells* **27**, 2527-2538, doi:10.1002/stem.178 (2009).
139 Otto, A., Collins-Hooper, H., Patel, A., Dash, P. R. & Patel, K. Adult skeletal muscle stem cell migration is mediated by a blebbing/amoeboid mechanism. *Rejuvenation Res* **14**, 249-260, doi:10.1089/rej.2010.1151 (2011).
140 Cheng, S.-Y. *et al.* A hydrogel-based microfluidic device for the studies of directed cell migration. *Lab Chip* **7**, 763-769 (2007).
141 MacNearney, D. Nanocontact Printing of Proteins on Physiologically Soft Substrates to Study Cell Haptotaxis. *Langmuir* **32**, 13525−13533, doi:10.1021 (2016).
142 Bischoff, R. Chemotaxis of skeletal muscle satellite cells. *Dev.Dyn.* **208**, 505-515 (1997).
143 Péault, B. *et al.* Stem and progenitor cells in skeletal muscle development, maintenance, and therapy. *Mol Ther* **15**, 867-877 (2007).
144 Doyle, A. D., Petrie, R. J., Kutys, M. L. & Yamada, K. M. Dimensions in cell migration. *Curr Opin Cell Biol* **25**, 642-649 (2013).
145 Volpatti, L. R. & Yetisen, A. K. Commercialization of microfluidic devices. *Trends Biotechnol* **32**, 347-350 (2014).
146 DiMilla, P. A., Stone, J. A., Quinn, J. A., Albelda, S. M. & Lauffenburger, D. A. Maximal migration of human smooth muscle cells on fibronectin and type IV collagen occurs at an intermediate attachment strength. *J Cell Biol* **122**, 729-737 (1993).
147 Anderson, J. E. Anderson, Judy, 2020, "Replication Data for: Supplementary Figures", https://doi.org/10.5203/FK2/Y1KK0O, University of Manitoba, V1 doi:https://doi.org/10.5203/FK2/Y1KK0O (2020).
148 Cornelison, D. & Wold, B. Single-cell analysis of regulatory gene expression in quiescent and activated mouse skeletal muscle satellite cells. *Dev Biol* **191**, 270-283 (1997).
149 Brack, A. S. *et al.* Increased Wnt signaling during aging alters muscle stem cell fate and increases fibrosis. *Science* **317**, 807-810 (2007).
150 Brack, A. S., Conboy, I. M., Conboy, M. J., Shen, J. & Rando, T. A. A temporal switch from notch to Wnt signaling in muscle stem cells is necessary for normal adult myogenesis. *Cell Stem Cell* **2**, 50-59, doi:10.1016/j.stem.2007.10.006 (2008).
151 Brack, A. S. *et al.* BCL9 is an essential component of canonical Wnt signaling that mediates the differentiation of myogenic progenitors during muscle regeneration. *Dev.Biol.* **335**, 93-105 (2009).
152 Arthur, S. T. & Cooley, I. D. The effect of physiological stimuli on sarcopenia; impact of Notch and Wnt signaling on impaired aged skeletal muscle repair. *Int J Biol Sci* **8**, 731-760, doi:10.7150/ijbs.4262 (2012).
153 Yamada, M. *et al.* High concentrations of HGF inhibit skeletal muscle satellite cell proliferation in vitro by inducing expression of myostatin: a possible mechanism for reestablishing satellite cell quiescence in vivo. *Am.J.Physiol Cell Physiol* **298**, C465-C476 (2010).
154 Chazaud, B. Dual effect of HGF on satellite/myogenic cell quiescence. Focus on "High concentrations of HGF inhibit skeletal muscle satellite cell proliferation in vitro by inducing expression of myostatin: a possible mechanism for reestablishing satellite cell quiescence in vivo". *Am.J Physiol Cell Physiol* **298**, C448-C449 (2010).

155 Rong, S., Segal, S., Anver, M., Resau, J. H. & Vande Woude, G. F. Invasiveness and metastasis of NIH 3T3 cells induced by Met-hepatocyte growth factor/scatter factor autocrine stimulation. *Proc Natl Acad Sci U S A* **91**, 4731-4735, doi:10.1073/pnas.91.11.4731 (1994).
156 Tatsumi, R., Anderson, J. E., Nevoret, C. J., Halevy, O. & Allen, R. E. HGF/SF is present in normal adult skeletal muscle and is capable of activating satellite cells. *Dev.Biol.* **194**, 114-128, doi:10.1006/dbio.1997.8803 (1998).
157 Sheehan, S. M., Tatsumi, R., Temm-Grove, C. J. & Allen, R. E. HGF is an autocrine growth factor for skeletal muscle satellite cells in vitro. *Muscle Nerve* **23**, 239-245 (2000).
158 Tatsumi, R. *et al.* A role for calcium-calmodulin in regulating nitric oxide production during skeletal muscle satellite cell activation. *Am.J.Physiol Cell Physiol* **296**, C922-C929 (2009).
159 Tatsumi, R. Mechano-biology of skeletal muscle hypertrophy and regeneration: possible mechanism of stretch-induced activation of resident myogenic stem cells. *Anim Sci.J.* **81**, 11-20 (2010).
160 Hara, M. *et al.* Calcium influx through a possible coupling of cation channels impacts skeletal muscle satellite cell activation in response to mechanical stretch. *Am.J.Physiol Cell Physiol* **302**, C1741-C1750 (2012).
161 Anderson, J. E. Hepatocyte Growth Factor and Satellite Cell Activation. *Adv Exp Med Biol* **900**, 1-25, doi:10.1007/978-3-319-27511-6_1 (2016).
162 Walker, N., Kahamba, T., Woudberg, N., Goetsch, K. & Niesler, C. J. G. f. Dose-dependent modulation of myogenesis by HGF: implications for c-Met expression and downstream signalling pathways. *Growth Factors* **33**, 229-241 (2015).
163 Siegel, A. L., Atchison, K., Fisher, K. E., Davis, G. E. & Cornelison, D. D. 3D timelapse analysis of muscle satellite cell motility. *Stem Cells* **27**, 2527-2538 (2009).
164 Tavi, P. *et al.* Myogenic skeletal muscle satellite cells communicate by tunnelling nanotubes. *J Cell Physiol* **223**, 376-383 (2010).
165 Roveimiab, Z., Lin, F. & Anderson, J. Emerging development of microfluidic-based approaches to improve studies of muscle cell migration. *Tissue Eng. Part B: Rev.*, doi:10.1089 (2018).
166 Meyvantsson, I. & Beebe, D. Cell culture models in microfluidic systems. *Annu Rev Anal Chem* **1**, 423-449 (2008).
167 Saadi, W. *et al.* Generation of stable concentration gradients in 2D and 3D environments using a microfluidic ladder chamber. *Biomed Microdevices* **9**, 627-635 (2007).
168 Abhyankar, V. V., Lokuta, M. A., Huttenlocher, A. & Beebe, D. Characterization of a membrane-based gradient generator for use in cell-signaling studies. *Lab Chip* **6**, 389-393 (2006).
169 Wu, J. *et al.* A compact microfluidic system for cell migration studies. *Biomed. Microdevices* **16**, 521-528 (2014).
170 Bentzinger, C. F. *et al.* Fibronectin regulates Wnt7a signaling and satellite cell expansion. *Cell stem cell* **12**, 75-87 (2013).
171 Muñoz, R., Moreno, M., Oliva, C., Orbenes, C. & Larraín, J. Syndecan-4 regulates non-canonical Wnt signalling and is essential for convergent and extension movements in Xenopus embryos. *Nat Cell Biol* **8**, 492 (2006).

172 Wosczyna, M. N. & Rando, T. A. A muscle stem cell support group: Coordinated cellular responses in muscle regeneration. *Dev cell* **46**, 135-143 (2018).
173 Peyton, S. R., Kim, P. D., Ghajar, C. M., Seliktar, D. & Putnam, A. J. J. B. The effects of matrix stiffness and RhoA on the phenotypic plasticity of smooth muscle cells in a 3-D biosynthetic hydrogel system. *Biomaterials* **29**, 2597-2607 (2008).
174 Anderson, J. E. *et al.* The role of semaphorin3A in myogenic regeneration and the formation of functional neuromuscular junctions on new fibres. *Biol Rev* **92**, 1389-1405 (2017).
175 Tatsumi, R. *et al.* Possible implication of satellite cells in regenerative motoneuritogenesis: HGF upregulates neural chemorepellent Sema3A during myogenic differentiation. *Am.J.Physiol Cell Physiol* **297**, C238-C252, doi:10.1152/ajpcell.00161.2009 (2009).
176 Venkatasubramanian, K. & Solursh, M. Chemotactic behavior of myoblasts. *Dev Biol* **104**, 428-433 (1984).
177 Hurme, T., Kalimo, H., Sandberg, M., Lehto, M. & Vuorio, E. Localization of type I and III collagen and fibronectin production in injured gastrocnemius muscle. *Lab Invest* **64**, 76-84 (1991).
178 Sanes, J. R. Laminin, fibronectin, and collagen in synaptic and extrasynaptic portions of muscle fiber basement membrane. *J Cell Biol* **93**, 442-451 (1982).
179 Duance, V., Restall, D., Beard, H., Bourne, F. & Bailey, A. The location of three collagen types in skeletal muscle. *FEBS Lett* **79**, 248-252 (1977).
180 Goetsch, K., Kallmeyer, K. & Niesler, C. Decorin modulates collagen I-stimulated, but not fibronectin-stimulated, migration of C2C12 myoblasts. *Matrix Biol* **30**, 109-117 (2011).
181 Peyton, S. R. & Putnam, A. Extracellular matrix rigidity governs smooth muscle cell motility in a biphasic fashion. *J Cell Physiol* **204**, 198-209 (2005).
182 De Lisio, M., Jensen, T., Sukiennik, R. A., Huntsman, H. D. & Boppart, M. D. Substrate and strain alter the muscle-derived mesenchymal stem cell secretome to promote myogenesis. *Stem Cell Res Ther* **5**, 74 (2014).
183 Sottile, J. *et al.* Fibronectin-dependent collagen I deposition modulates the cell response to fibronectin. *Am J Physiol Cell Physiol* **293**, C1934-C1946 (2007).
184 Torrente, Y. *et al.* Tumor necrosis factor-α (TNF-α) stimulates chemotactic response in mouse myogenic cells. *Cell Transplant* **12**, 91-100 (2003).
185 Zhang, Y. *et al.* Collective cell migration has distinct directionality and speed dynamics. *Cell Mol Life Sci* **74**, 3841-3850, doi:10.1007/s00018-017-2553-6 (2017).
186 Rorth, P. Whence directionality: guidance mechanisms in solitary and collective cell migration. *Dev Cell* **20**, 9-18, doi:10.1016/j.devcel.2010.12.014 (2011).
187 Lee, E. J. *et al.* Identification of Novel FNIN2 and FNIN3 Fibronectin-Derived Peptides That Promote Cell Adhesion, Proliferation and Differentiation in Primary Cells and Stem Cells. *International Journal of Molecular Sciences* **22**, 3042 (2021).
188 Singh, P., Carraher, C. & Schwarzbauer, J. E. Assembly of fibronectin extracellular matrix. *Annual review of cell and developmental biology* **26**, 397-419 (2010).
189 Yablonka-Reuveni, Z. & Anderson, J. E. Satellite cells from dystrophic (mdx) mice display accelerated differentiation in primary cultures and in isolated myofibers. *Developmental*

dynamics: an official publication of the American Association of Anatomists **235**, 203-212 (2006).
190 Ayoib, A., Hashim, U., Thivina, V. & Nordin, N. Microfluidics photomask design using AutoCAD software for the application of DNA extraction in Lab-On-A-Chip biosensing devices. *eProceedings Chemistry* **3** (2017).
191 Beebe, D. J., Mensing, G. A. & Walker, G. M. Physics and applications of microfluidics in biology. *Annual review of biomedical engineering* **4**, 261-286 (2002).
192 Wu, J. *et al.* A passive mixing microfluidic urinary albumin chip for chronic kidney disease assessment. *ACS sensors* **3**, 2191-2197 (2018).
193 Poon, C. Measuring the density and viscosity of culture media for optimized computational fluid dynamics analysis of in vitro devices. *bioRxiv* (2020).
194 Li, E. W., McKee-Muir, O. C. & Gilbert, P. M. Cellular biomechanics in skeletal muscle regeneration. *Current topics in developmental biology* **126**, 125-176 (2018).
195 Andersson, H. & Van den Berg, A. Microfluidic devices for cellomics: a review. *Sensors and actuators B: Chemical* **92**, 315-325 (2003).
196 Bae, G.-U. *et al.* Regulation of myoblast motility and fusion by the CXCR4-associated sialomucin, CD164. *Journal of Biological Chemistry* **283**, 8301-8309 (2008).
197 Gardner, J. M. & Fambrough, D. M. Fibronectin expression during myogenesis. *The Journal of cell biology* **96**, 474-485 (1983).
198 Anderson, J. E. The satellite cell as a companion in skeletal muscle plasticity: currency, conveyance, clue, connector and colander. *Journal of Experimental Biology* **209**, 2276-2292 (2006).
199 McIntosh, L. M., Garrett, K. L., Megeney, L., Rudnicki, M. A. & Anderson, J. E. Regeneration and myogenic cell proliferation correlate with taurine levels in dystrophin- and MyoD-deficient muscles. *The Anatomical Record: An Official Publication of the American Association of Anatomists* **252**, 311-324 (1998).
200 Bischoff, R. & Holtzer, H. Mitosis and the processes of differentiation of myogenic cells in vitro. *The Journal of cell biology* **41**, 188-200 (1969).
201 Laumonier, T. & Menetrey, J. Muscle injuries and strategies for improving their repair. *Journal of experimental orthopaedics* **3**, 1-9 (2016).
202 Roveimiab, Z. Influence of natural substrate on myotube formation and behavior on microfluidic platforms. *Z Roveimiab, PhD Dissertation (draft), 2021.*
203 KOTELIANSKY, V. E. *et al.* A study of the structure of fibronectin. *European journal of biochemistry* **119**, 619-624 (1981).
204 Maurer, L. M., Ma, W. & Mosher, D. F. Dynamic structure of plasma fibronectin. *Critical reviews in biochemistry and molecular biology* **51**, 213-227 (2016).
205 Magnusson, M. K. & Mosher, D. F. Fibronectin: structure, assembly, and cardiovascular implications. *Arteriosclerosis, thrombosis, and vascular biology* **18**, 1363-1370 (1998).
206 Bachmann, M., Kukkurainen, S., Hytönen, V. P. & Wehrle-Haller, B. Cell adhesion by integrins. *Physiological reviews* **99**, 1655-1699 (2019).
207 Mould, A. P., Craig, S. E., Byron, S. K., Humphries, M. J. & Jowitt, T. A. Disruption of integrin–fibronectin complexes by allosteric but not ligand-mimetic inhibitors. *Biochemical Journal* **464**, 301-313 (2014).

208 Fogerty, F. J., Akiyama, S. K., Yamada, K. M. & Mosher, D. F. Inhibition of binding of fibronectin to matrix assembly sites by anti-integrin (alpha 5 beta 1) antibodies. *The Journal of cell biology* **111**, 699-708 (1990).
209 Hynes, R. O. *Fibronectins*. (Springer Science & Business Media, 2012).
210 Laumonier, T., Bermont, F., Hoffmeyer, P., Kindler, V. & Menetrey, J. Human myogenic reserve cells are quiescent stem cells that contribute to muscle regeneration after intramuscular transplantation in immunodeficient mice. *Scientific reports* **7**, 1-12 (2017).
211 Meng, J. *et al.* Human Skeletal Muscle–derived CD133+ Cells Form Functional Satellite Cells After Intramuscular Transplantation in Immunodeficient Host Mice. *Molecular Therapy* **22**, 1008-1017 (2014).
212 Baroffio, A. *et al.* Identification of self-renewing myoblasts in the progeny of single human muscle satellite cells. *Differentiation* **60**, 47-57 (1996).
213 Mierzejewski, B. *et al.* Mouse CD146+ muscle interstitial progenitor cells differ from satellite cells and present myogenic potential. *Stem cell research & therapy* **11**, 1-14 (2020).
214 Krauss, R. S. Regulation of promyogenic signal transduction by cell–cell contact and adhesion. *Experimental cell research* **316**, 3042-3049 (2010).
215 Krauss, R. S. *et al.* Close encounters: regulation of vertebrate skeletal myogenesis by cell-cell contact. *Journal of cell science* **118**, 2355-2362 (2005).
216 Arnold, L. L. *et al.* EphA7 promotes myogenic differentiation via cell-cell contact. *Elife* **9**, e53689 (2020).
217 MAKAREM, R. & HUMPHRIES, M. J. (Portland Press Ltd., 1991).
218 Adams, J. C., Chiquet-Ehrismann, R. & Tucker, R. P. The evolution of tenascins and fibronectin. *Cell adhesion & migration* **9**, 22-33 (2015).
219 Graham, Z. A., Gallagher, P. M. & Cardozo, C. P. Focal adhesion kinase and its role in skeletal muscle. *Journal of muscle research and cell motility* **36**, 305-315 (2015).
220 Charrasse, S., Meriane, M., Comunale, F., Blangy, A. & Gauthier-Rouvière, C. N-cadherin–dependent cell–cell contact regulates Rho GTPases and β-catenin localization in mouse C2C12 myoblasts. *Journal of Cell Biology* **158**, 953-965 (2002).
221 Lyons, G. E., Moore, R., Yahara, O., Buckingham, M. E. & Walsh, F. S. Expression of NCAM isoforms during skeletal myogenesis in the mouse embryo. *Developmental dynamics* **194**, 94-104 (1992).
222 Thorsteinsdóttir, S., Deries, M., Cachaço, A. S. & Bajanca, F. The extracellular matrix dimension of skeletal muscle development. *Developmental biology* **354**, 191-207 (2011).
223 Konagaya, Y. *et al.* Intravital imaging reveals cell cycle-dependent myogenic cell migration during muscle regeneration. *Cell Cycle* **19**, 3167-3181 (2020).
224 Takahashi, H., Shimizu, T., Nakayama, M., Yamato, M. & Okano, T. The use of anisotropic cell sheets to control orientation during the self-organization of 3D muscle tissue. *Biomaterials* **34**, 7372-7380 (2013).
225 Shen, Z. & Niethammer, P. A cellular sense of space and pressure. *Science* **370**, 295-296 (2020).
226 Brás-Pereira, C. & Moreno, E. Mechanical cell competition. *Current opinion in cell biology* **51**, 15-21 (2018).

227 Shiwarski, D. J. *et al.* Fibronectin-based nanomechanical biosensors to map 3D surface strains in live cells and tissue. *Nature communications* **11**, 1-15 (2020).
228 Liu, J., Burkin, D. J. & Kaufman, S. J. Increasing α7β1-integrin promotes muscle cell proliferation, adhesion, and resistance to apoptosis without changing gene expression. *American Journal of Physiology-Cell Physiology* **294**, C627-C640 (2008).
229 McClure, M. J., Ramey, A. N., Rashid, M., Boyan, B. D. & Schwartz, Z. Integrin-α7 signaling regulates connexin 43, M-cadherin, and myoblast fusion. *American Journal of Physiology-Cell Physiology* **316**, C876-C887 (2019).
230 Pajcini, K. V., Pomerantz, J. H., Alkan, O., Doyonnas, R. & Blau, H. M. Myoblasts and macrophages share molecular components that contribute to cell–cell fusion. *The Journal of cell biology* **180**, 1005-1019 (2008).